BLAST BRAIN INJURY RISK

A Dissertation

Presented to

the faculty of the School of Engineering and Applied Science

University of Virginia

In Partial Fulfillment

of the requirements for the Degree

Doctor of Philosophy

Biomedical Engineering

by

Karin A. Rafaels

December 2010

ABSTRACT

Exposures to blast can cause injuries in the brain. Limited studies have been performed to investigate the blast levels needed to induce blast brain injuries. This study examines the effects from an exposure to blast using a gyrencephalic animal model. The ferret was selected as the preferred model for blast brain injury when compared with rodents and rabbits for its brain structure and compatibility to the human brain and its size, ease of animal care, and wide availability. In this study, sixty-seven ferrets were used as blast specimens and three were used as controls.

The blast waves were generated with a shock tube at varying ranges of overpressures and durations, simulating blasts at standoffs of 2.5 to 20 m and charge sizes to approximately 800 kg. To isolate the blast exposure to the head, the abdomen and thorax were protected to blast levels that were an order of magnitude below pulmonary injury threshold conditions.

Physiological parameters, such as heart rate and respiration rate, sensory evoked potentials, and histology were all used to assess the incidence of brain injury. Bradycardia and apnea were present after the blast exposure, but would return to normal physiological values, if the specimen survived. Bradycardia and apnea also appeared to be duration dependent, in that at longer durations, lower pressures were needed to cause them. For durations less than 6 ms, bradycardia occurred in all specimens exposed to overpressures greater than 700 kPa. For durations less than 8.5 ms, apnea occurred in all specimens exposed to overpressures greater than 625 kPa. Blast overpressure levels greater than 700 kPa also resulted in at least a moderate hemorrhagic injury. Injury patterns seen during the tests suggested a mechanism of small displacement, but rapid

compression of the skull. Signal loss of the sensory evoked potentials was also related to the blast input conditions. VEP signal loss did not occur at overpressures lower than 700 kPa, and BAEP signal loss did not occur at overpressures lower than 400 kPa. Using the histological data, a correlation of the blast input to the injured axonal area was made. Severe blast exposure conditions had significantly injured axonal areas two orders of magnitude greater than nonblasted specimens.

Most importantly, injury risk functions were developed for risk of mild and moderate to severe meningeal bleeding, initial apnea, and evoked potential signal loss from the application of a blast shock. In addition, a risk assessment was developed for fatality using data from the current study combined with previous rabbit data. The fatality injury risk for brain was found to be more than twice the fatality injury risk for lungs at low positive phase durations. The blast level for 50% risk of mild brain bleeding was found to occur at similar overpressure values as the 50% risk of unprotected pulmonary injury onset.

APPROVAL SHEET

The dissertation is submitted in partial fulfillment

of the requirements for the degree of

Doctor of Philosophy

Biomedical Engineering

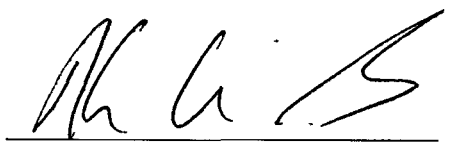

AUTHOR

This dissertation has been read and approved by the examining Committee:

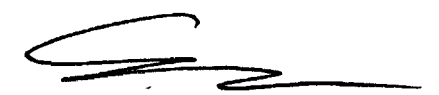

Dissertation advisor

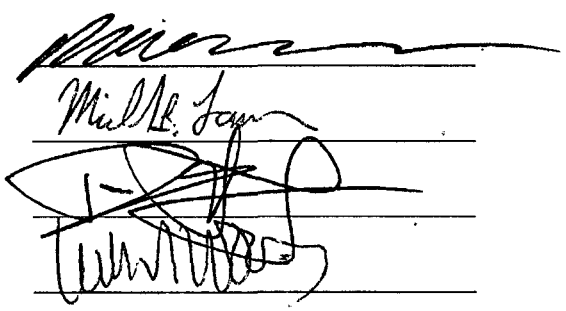

Accepted for the School of Engineering and Applied Science:

Dean, School of Engineering and
Applied Science

December 2010

ACKNOWLEDGEMENTS

This project was a massive undertaking, and there have been many people involved with helping me to tackle the issue of blast brain injury. First, thanks to Dale Bass for including me in every part of the research process from writing proposals, attending meetings, designing and running experiments, and evaluating and interpreting results. Without this experience early on in my graduate career, I would not have been able to run this final graduate project on blast brain injury nearly independently. He, as well as the other members of my examining committee; William Walker, Richard Kent, William Woods, and Michael Lawrence; also provided me with support, encouragement, insight and critique throughout the entire project. Thanks also to Sanford Feldman for guiding me through the animal protocol process, as well as teaching me how to work with research animals and providing me a crash course in veterinary sciences. I could not have performed all of the tests without the help of the Snyder vivarium staff, including Jim Weirich; the veterinary assistants, Jeremy Gatesman, Gina Wimer, and Kim Hellems; the mechanical whiz, Brian Overby; the medical tool encyclopedia, Thomas Gochenour; my eager and unpaid undergraduate researchers, Burcu Derkunt, Jon Foster, and Allison Mazur; and the occasional helping hands of Andrew Damon. None of the histological analysis would have been possible without the help of James Stone, who helped select the immunohistochemical stains, as well as taught me how to analyze and interpret the results. Without his guidance, I would have thrown all of the slides out in frustration. Moreover, Pat Pramoonjago and the rest of the Biorepository & Tissue Research Facility staff, as well as Fu Du and the staff at FD Neurotechnologies were all integral to the processing of brain tissue. Katie Lindstrom and Tom Cummings provided their much

appreciated pathology expertise when needed. Shayn Peirce granted me the gift of access to her confocal microscope and Liz Logsdon taught me how to use it, even in 25-inches of snow. John Shannon and Robert Bloodgood saved my life by providing me access to the digital slide scanner. Without their help, I would still be counting axons by hand and drawing pictures of histology slides. Matt Kindig, the MATLAB genius, helped me put together the semi-automatic axon quantification method, devoting countless hours of thought to making my MATLAB code better. Burcu Derkunt also helped to lighten the load of the quantification process by hand counting many axons herself, for which I am very appreciative. Mark Quigg played an integral role in the evoked potential portion of the study. He provided assistance in making a noisy, unreadable signal, into actual electrical activity recorded from brains, as well as in interpreting the resulting signals. Allison Mazur also helped to analyze the BAEP results. A big thanks to Tim Walilko, Greg Weiss, and Lee Ann Young at ARA for their support, guidance, expertise, and data acquisition during my entire graduate career, as well as to the rest of the staff at the Center for Applied Biomechanics and the Duke Injury and Orthopaedics Laboratory for their help throughout the years. A special thanks goes out to Robert Salzar who not only provided hands on and intellectual assistance whenever I needed it, but who was also willing to commiserate with me about testing, writing, or anything else.

I would like to thank my family for their love and support throughout my many years of school. Thanks to my brother, Nick, for his input on the statistics, my Mom for her late-night editing, and my Dad for always picking my brain and making me appreciate science and engineering. The rest of my extended family also deserves mention for their ever-present encouragement and support.

Finally, I would like to thank Meg Gerth for putting up with the many long days, late nights, and early mornings involved with the completion of a doctoral program. She was always available as springboard for ideas, a finder of solutions and a listener to the trials and tribulations I encountered along the way. She helped keep our house and lives in order when I had little time for such things and provided me with transportation when my car could not make it to the finish line. Not only did she keep me sane throughout this process, she also helped to proofread and edit the final paper. For all that and more, I am truly thankful.

TABLE OF CONTENTS

LIST OF FIGURES

LIST OF TABLES

LIST OF APPENDICES

LIST OF ABBREVIATIONS

4-HNE	4-Hydroxy-nonenal
ABC	avidin-biotin complex
ATP	adenosine triphosphatase
BABT	behind armor blunt trauma
BAEP	brainstem auditory evoked potential
CA	*Cornu Ammonis* (areas of hippocampus)
CNPase	2', 3'-cyclic nucleotide 3' phosphodiesterase
COX-2	cyclooxygenase
CSF	cerebrospinal fluid
CT	computed tomography
D	duration
DG	dentate gyrus
DNA	deoxyribonucleic acid
DTI	diffusion tensor imaging
ECG	electrocardiogram
EEG	electroencephalogram
ELISA	enzyme-linked immunosorbent assay
EM	electromagnetic
EMP	electromagnetic pulse
EP	evoked potential

FCC	Federal Communications Commission
FITC	fluorescein isothiocyanate
fMRI	functional magnetic resonance imaging
GAMBIT	Generalized Acceleration Model for Brain Injury Threshold
GFAP	glial fibrillary acidic protein
GSI	Gadd Severity Index
GSW	gunshot wound
H&E	hematoxylin and eosin
HE	high explosive
HIC	Head Injury Criterion
HIP	Head Impact Power
HMGB1	high-mobility group protein B1
Iba1	ionized calcium binding adaptor molecule 1
IHC	immunohistochemistry
ln	natural logarithm
LPB	leuco-patent blue
M107	155mm mortar round
MBP	myelin basic protein
MHC	major histocompatibility complex
MRI	magnetic resonance imaging
MVA	motor vehicle accident
N	negative wave component of VEP
NA	not available
NGS	normal goat serum
NPN	negative-positive-negative complex of VEP

NSE	neuron specific enolase
OVP	overpressure
P	pressure
P1, P2	positive components of VEP
P50	50% risk
PBS	phosphate buffered saline
PET	positron emission tomography
p-NFH	phosphorylated, heavy chain neurofilament subunit
PNP	positive-negative-positive complex of VEP
Pr	probability
PTSD	post-traumatic stress disorder
RGB	red, green, blue
TBI	traumatic brain injury
TNT	trinitrotoluene
TUNEL	terminal deoxy-nucleotidyl transferase dUTP nick end labeling
UCH-L1	ubiquitin carboxy-terminal hydrolase L1
VEP	visual evoked potential
β_0	parameter for regression
β_1	parameter for regression
β_2	parameter for regression
β-APP	beta-amyloid precursor protein

Chapter 1. INTRODUCTION

1.1 Statement of Problem

In current U.S. military conflicts, the use of improvised explosive devices (IEDs) and other explosives are a major threat and health concern for service members, as shown in Figure 1.1. In Iraq and Afghanistan, blasts are the primary initiating cause of injury to the head and neck for active duty military personnel (Owens 2008), as shown in Figure 1.2. Because of improved protective equipment and better access to medical care, a higher percentage of soldiers are surviving injuries that would have been fatal in previous wars (Goldberg 2010). Further, thoracic protection used in current conflicts allows the head/brain to be exposed to severe blasts that previously would have been fatal from pulmonary injury (e.g. Wood 2010). Additional epidemiological support for increased thoracic protection is shown by the greater percentage of injuries to the head and neck region in these conflicts than in World War II, Korea, and Vietnam. In current conflicts, injuries to the thorax are at their lowest (Owens 2008). At Walter Reed Army Medical Center, one of six medical center hubs of the United States Army, 32% of service members evacuated from the field had traumatic brain injury (TBI) (Meyer 2008). If soldiers whose wounds were not severe enough to require evacuation or whose injuries were not identified until after they completed their tours of duty were included, the total number of service members with evidence of brain injuries could be in the hundreds of thousands (Tanielian 2008).

Through many years of research from many different countries, there is little dispute that explosives can cause brain injury (e.g. Krohn 1941, Rafaels 2010b). Still to be determined are how these injuries might occur and at what explosive, or blast, level these

injuries begin to be observed. There are existing head injury criteria for low rate linear translation, rotational and translational energy transfer, and pure angular rotational criteria (Versace 1971, Newman 2000, Ommaya 1971); however, they may not be appropriate for blast loading (Lockhart 2010). A great need exists for a determination of threshold levels and injury risk for brain damage caused by blast exposure as a prerequisite to the development of protective equipment and to a better understanding of the injury mechanisms and the therapeutics of blast brain injury.

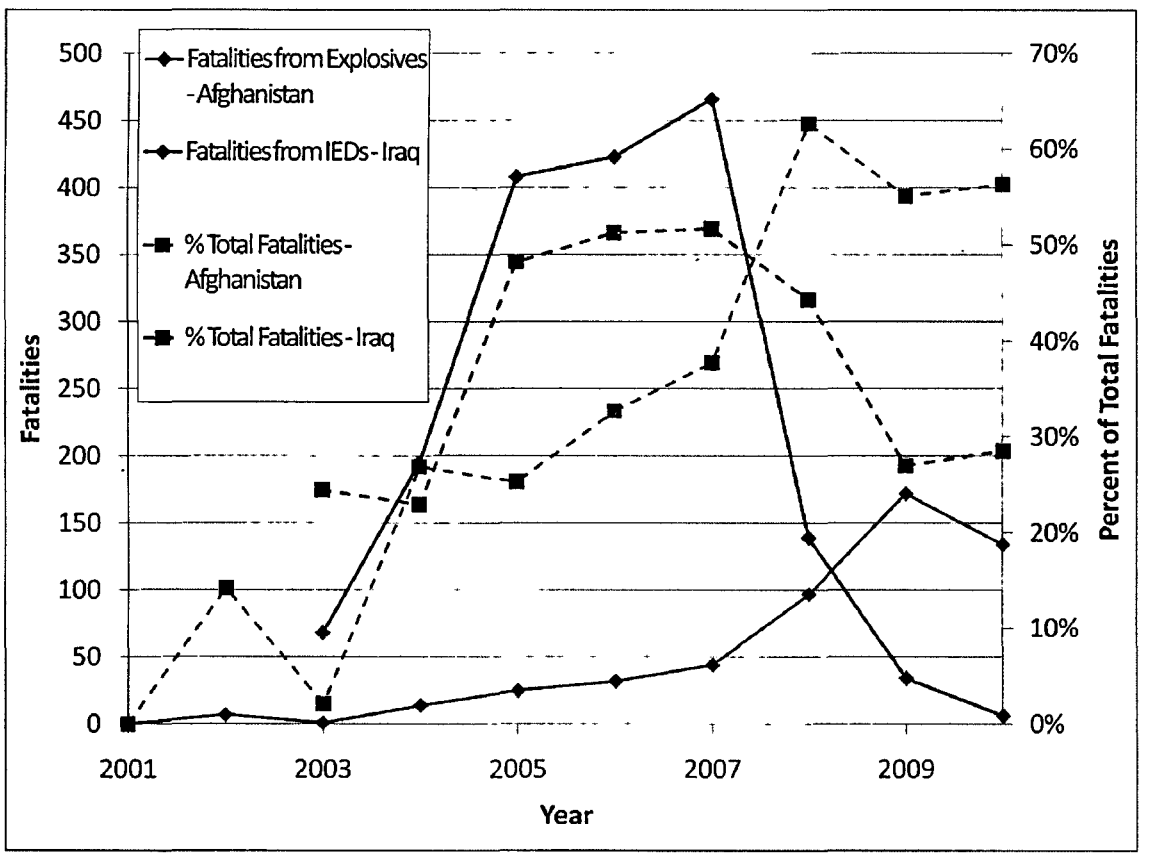

Figure 1.1. Marine Corps and Army Killed in Action. The statistics from Afghanistan range from 2001 to July 15, 2010 and include various forms of explosive threats, including IEDs. (www.brookings.edu/afghanistanindex) The statistics from Iraq range from March 2003 – June 2010, and only includes IED threats. (www.brookings.edu/iraqindex)

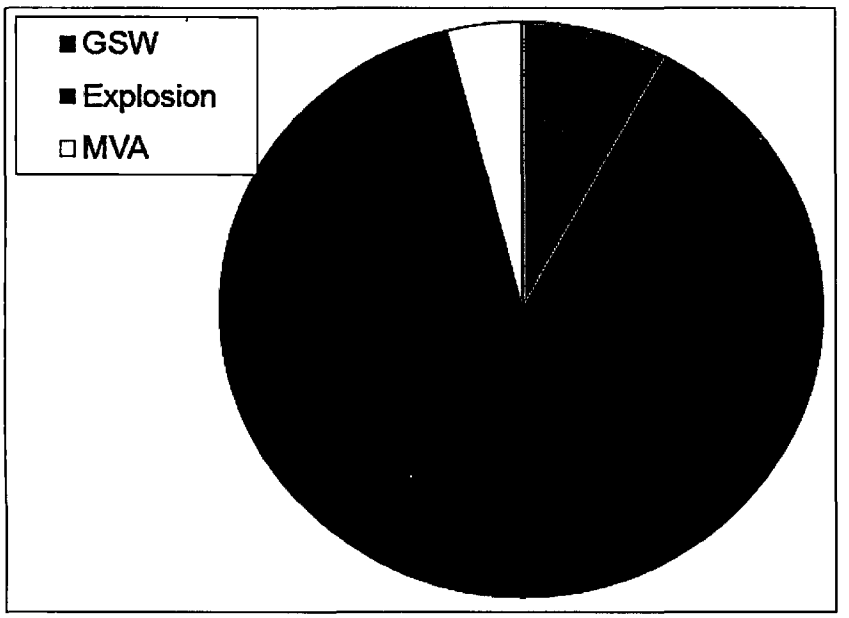

Figure 1.2. Cause of Injury for the Head and Neck in Iraq and Afghanistan. GSW = Gunshot Wound, MVA = Motor Vehicle Accident. (Owens 2008)

1.2 Background and Significance

Explosive weapons have been used as early as the 11th century by the Song Dynasty in China (Needham 1986) with the earliest high explosives being prepared in the 19th century (Graham 2003). With advances in explosive chemistry, detonation techniques, and transport and delivery of the explosive devices, these explosives have become highly effective weapons (Moyes 2009). As high explosives have high rates of death amongst people close to the blast and the capacity to damage surrounding infrastructure, they will likely continue to be a weapon of choice by both state and nonstate groups for many years to come (Moyes 2009). Consequently, gaining an understanding of the mechanisms and tolerances of blast injuries is imperative.

Injuries from explosive weapons, or blast injuries, are commonly separated into four categories (e.g. White 1963). The first of these is primary blast injury. Primary blast injuries are attributed to the direct effects of blast overpressure. Traditionally, the organs

that are most vulnerable to a primary blast injury are the air containing organs: lungs, bowel, and ears (Yelverton 1997). Recently, however, there has been a high prevalence of traumatic brain injury (TBI) associated with blasts in the conflicts in Iraq and Afghanistan (Kennedy 2007), whereas the prevalence of tympanic membrane rupture and blast lung injuries have been low (Ritenour 2010). Other types of blast injury include secondary blast injury attributed to the effects of penetrating trauma and the effects of projectiles and fragmentation; tertiary blast injury caused by the effects of structural and body translation; and quaternary (or miscellaneous) blast injury caused by burns, gases, inhalants, radiation exposure, or other effects not covered by the first three categories.

Primary blast injuries from simple, freefield blast waves (blast waves with a sharp rising peak overpressure followed by an exponential decay below zero and then back to baseline) have been studied for nearly a century with the efforts producing well accepted injury mechanisms (e.g. Hooker 1924, Hicks 2010). Although complex blast wave forms (blast exposures with multiple peaks and reflections) are encountered more often and produce more severe pulmonary injuries to humans (Axelsson 1996, Stuhmiller 1997, Gruss 2006), they are difficult to analyze and not well understood. To be able to understand and begin to assess the risk of blast brain injuries, only the simple, freefield blast case will be investigated.

Speculation on the occurrence of primary blast brain injuries began during World War I (e.g. Mott 1916), but experimental studies during and after the war (e.g. Hooker 1924) emphasized the vulnerability of the pulmonary system relative to the brain. Limited research into primary blast brain injuries began in earnest during World War II with studies on brain injury in experimental animals with protected thoraces and the

propagation of blast waves through the body with and without protection (Krohn 1941; Clemedson 1953, 1956a, 1956b). It was found that the majority of the blast waves seen inside the cranial vault were transmitted transcranially and that pulmonary lethality occurred at lower blast levels than brain fatalities.

More recently, experimental studies of primary blast brain injuries in animals have shown discernible effects at every level, from altered cellular and biochemical processes to changes in behavior at levels below pulmonary lethality. Behavioral changes after an exposure to nonlethal primary blast waves include a significant decline in active avoidance response performance (Cernak 2001b, Risling 2002); while pathological changes within the central nervous system have included neuronal degeneration, activated microglia and astrocytes, disruption of axonal transport, and increased nitric oxide generation (Moochhala 2004; Kaur 1995, 1997a, 1997b; Cernak 2001b; Saljo 2000, 2001, 2002a). Yet these studies used lissencephalic animal models, or animals with smooth surfaced brains. Lissencephalic animals have a proportionally thicker cortex and a smaller volume of white matter in relation to the total brain volume when compared to gyrencephalic, or convoluted brains (Hofman 1989). These differences may be of importance in blast brain injuries as the mechanical properties are different for the white and gray matter (Mehdizadeh 2008). Unfortunately, while providing valuable evidence of primary blast effects to the brain, these studies have not provided the systematic advances in our understanding of the blast overpressure input with injury output for a range of blast overpressures and durations.

Injury risk assessments and tolerances are a critical tool for guiding research into the injury mechanisms and designing protection against such injuries. These risk

assessments define a magnitude of loading which produces a specific type of injury severity and/or risk. There are existing head injury criteria for low rate linear translation (Versace 1971), rotational and translational energy transfer (Newman 2000), and pure angular rotational criteria (Ommaya 1971); however, they may not be appropriate for blast loading (Lockhart 2010). For blast, several injury risk functions have been determined for pulmonary blast injury (Bowen 1968, Dodd, 1990, Axelsson 1996, Stuhmiller 1997, Bass 2008) and for ear drum rupture (Richmond 1989). However, there are no studies of injury risk available for blast injuries to the brain, *where an injury tolerance or risk function is certainly needed* (Saljo 2000, Leung 2008, Moore 2008).

A clinical tool for diagnosing blast brain injury is also needed. No definitive selection criteria currently exist for diagnosing blast brain injury (Ling 2009). Many survivors of blast exposures may appear outwardly unscathed, but subsequently experience headaches; behavioral changes; and disturbances of vision, hearing, memory, and concentration (Trudeau 1998, Okie 2005, Murthy 1979, Hagerman 2008). A major difficulty in making a diagnosis with these common symptoms is that while they can be attributed to mild TBI, they are also associated with Post Traumatic Stress Disorder (PTSD) (Ling 2009). This overlap of symptoms, the high risk of the military population being exposed to a very stressful environment, and the likely comorbidity of mild TBI and PTSD make it difficult to diagnose organic TBI from a psychiatric disorder (Kennedy 2007).

More severe injuries resulting from a blast exposure include coma, subarachnoid and subdural hemorrhaging, diffuse cerebral edema and hyperemia, and vasospasm (Ling 2009, Abbott 1943, Murthy 1979). Diagnosis for the more severe injuries is often

complicated by patients presenting with many other serious injuries, such as penetration wounds, traumatic limb amputation, and hemorrhagic shock (Ling 2009). The correct diagnosis is important because it affects the treatment strategy, medical costs, and stigma associated with the disability.

One promising, relatively inexpensive, noninvasive clinical tool for blast brain injuries is electroencephalographic (EEG) measurements that measure the electrical activity of the brain. PTSD patients with a history of blast concussion have demonstrated significantly different EEG patterns when compared to PTSD patients that have no history of blast exposure (Trudeau 1998), perhaps suggesting a mild TBI. Post blast EEG changes are also well documented in patients not diagnosed as having PTSD (Cernak 1999b). These studies show that blast may affect the brain's normal electrical activity. However, EEGs have poor spatial resolution, are susceptible to noise and artifacts, and do not provide the brain sources for the potentials seen (Ellens 2009). On the other hand, sensory evoked potentials (EPs), specific techniques for measuring the brain's electrical activity, can reflect the neurophysiologic processing along the sensory pathways from sensation to primary sensory cortex (FitzGerald 2007). This technique is more sensitive and specific to neurophysiologic changes produced by traditional TBI than conventional EEG. Blast injured victims are often found with disturbances in vision and the auditory system (Sylvia 2001), likely disrupting the electrical activity in those sensory pathways. This proposal intends to examine the efficacy of visual and auditory evoked potentials as a clinical tool in diagnosing blast brain injuries.

1.3 Specific Aims

The specific aims are designed to provide a comprehensive assessment of the blast overpressure induced brain injuries in a ferret model:

1. Isolate blast overpressure exposure to the head. Although several different theories exist for the mechanism behind blast brain injuries, this study assesses the mechanism of blast brain injuries resulting from the pressure wave (which is the source for pulmonary injuries).

   A. The blast overpressure is separated from the other aspects of blast, i.e. Electromagnetic pulse (EMP), heat, and light, by using a shock tube to generate the blast overpressure.

   B. The blast overpressure is focused on the head to direct the injuries to the head/brain. Additionally, the rest of the body from the neck down is protected in a steel tube to prevent injuries to any other organs which may cause downstream effects on the brain.

   C. The head and neck is secured and fastened down to prevent motion which may cause acceleration/deceleration type injuries.

2. Correlate the blast overpressure with injury severity level. Threshold levels have not been assessed for brain damage caused by blast exposure. It is important to determine the blast overpressure levels that induce brain injury and the levels at which severe injuries can occur so that appropriate protection can be utilized to ensure mitigation of the injuries at those levels. Consequently, brain injury thresholds and injury severity risk are assessed.

   A. Various blast overpressures and durations are tested to determine the onset of brain injury and the different degrees of brain injury severity.

B. Necropsies and immunohistochemistry (IHC) for the β-amyloid precursor protein (β-APP), a marker for axonal injury, are performed to determine when brain injury occurs and to help determine severity.

C. A statistical regression analysis is executed on the resulting data to determine an injury threshold and injury risk function for blast brain injuries.

3. Correlate the immunohistochemistry results with a clinically applicable method for assessing blast brain injuries. Immunohistochemistry requires the cells from the tissue one is interested in examining. However, for the case of the brain, it is difficult to obtain samples of tissue in a living subject. Although IHC is an extremely powerful tool for determining injury, it may not be relevant in the clinical setting. Therefore, a clinically relevant technique is used to determine if a correlation exists between the IHC results and the clinically relevant technique.

A. The visual and auditory evoked potentials of the animal model are performed both before and after blast exposure.

B. The peaks, latencies, and separation of the evoked potentials are evaluated for differences between the pre and post exposures to determine any differences or effects.

C. Any differences noted in the evoked potentials are correlated to the IHC results for brain injury.

Blast brain injury has been called the signature wound of the military conflicts in Iraq and Afghanistan (Warden 2006). And as the number of blast casualties continues to increase, it becomes more imperative that we understand, treat, and protect against these

blast brain injuries. The goal was to focus on the most well accepted injury mechanism for blast brain injury (Specific Aim #1); to determine when injury occurs (Specific Aim #2); and to suggest a way to assess that injury in a clinical setting (Specific Aim #3).

Chapter 2. LITERATURE REVIEW

2.1 The Brain

2.1.1 Microanatomy of the Brain

Given that some structural damage in the brain may occur from blast, I outline the anatomy and physiology of the brain. The neuron, the cell type responsible for the majority of the electrical activity in the brain, can be distinguished from other cell types by its specialization for conduction of impulses, its great sensitivity to oxygen deprivation, its importance for many vital functions, and its inability to multiply (Liebman 1991). Neurons consist of a cell body, or soma, and long processes extending from the body as seen in Figure 2.1. There are two main kinds of processes: dendrites and axons. Dendrites receive impulses from other neurons and conduct them to the cell body. There are usually several projecting from the main cell body. Axons conduct the nerve impulses away and out to other neurons, muscles, or glands. Only one axon projects from the neuronal cell body,

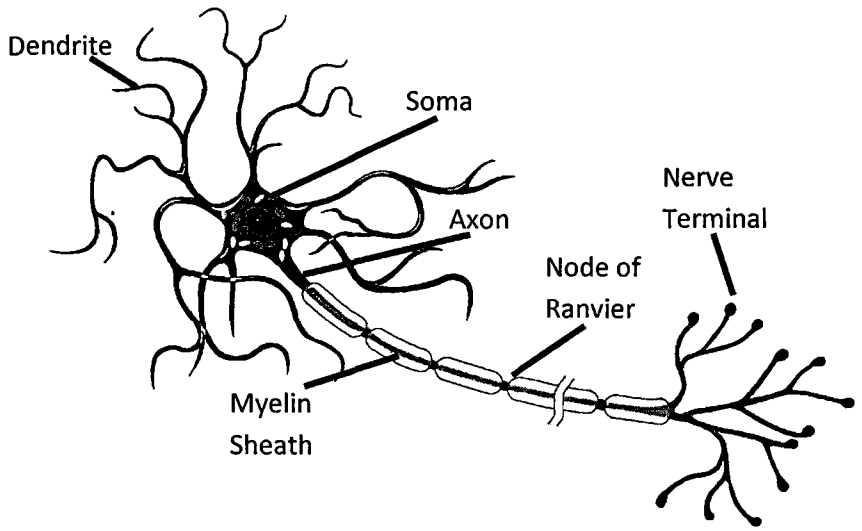

Figure 2.1. Basic structure of a neuron. Used with permission LifeART image copyright 1998 Lippincott Williams & Wilkins. All rights reserved.

Axons are typically thin and can extend for more than a meter. Because of its length, the neuron must use special axonal transport mechanisms to sustain its axon. The axoplasm, or cytoplasm in the axon, is packed with parallel arrays of microtubules and microfilaments that provide structural stability and a means to rapidly convey materials back and forth between the cell body and the axon terminus (Ransom 2003a). Since axons do not have ribosomes to produce proteins, they must rely on vesicles carrying proteins from the soma. The vesicles are carried down the axon along the microtubules by kinesin motors. However, if the microtubules become disrupted, the transport function is lost (Ransom 2003a). The protein, β-APP, used in the immunohistochemical analysis, uses this transport mechanism to travel along the axon. When the transport function is lost, β-APP can build up at the site of injury, and, when stained, can become visible under light microscopy.

To assist with flow of the electrical current along these lengthy projections, the axons of nearly all neurons in vertebrates are covered with a fatty white substance called myelin

(Withers 1992). The myelin sheath forms an insulating layer around the axons to reduce the loss of current to the surrounding tissue fluid during impulse conduction. However, the myelin sheath is interrupted at regular intervals, forming the nodes of Ranvier, so the nerve impulse can travel from node to node, increasing the speed of impulse propagation (Brodal 2004). These nodes of Ranvier can become areas of stress concentration when exposed to a mechanical load (Maxwell 1996). The myelin sheath is also responsible for the ability to identify regions in the central nervous tissue as white and gray matter. The white matter contains areas of myelinated nerve fibers, or axons, and the gray matter contains areas of cell bodies and dendrites. Although axons themselves have diameters on the order of several microns, we can visualize the white and gray matter macroscopically because the nerve pathways are made up of fascicles, or bundles, which in turn are made up of many hundreds of axons (Liebman 1991). Because of the differences in structure of the white and gray matter, it is not surprising that the mechanical properties are different for the white and gray matter (Mehdizadeh 2008).

The nervous system also has supporting cells called glial cells. Glial cells are typically grouped into three categories: microglia, the macrophages of the nervous system; oligodendrocytes, which form the myelin sheaths around the axons; and astrocytes, which provide support to the neurons and help create the blood brain barrier (Liebman 1991). Biomarkers for these cell types can indicate an injury to the brain tissue.

2.1.2 Macroanatomy of the Brain

Inside the hard, bony skull sits the relatively soft brain which is divided into 6 parts: telencephalon, diencephalon, cerebellum, mesencephalon, pons, and medulla oblongata. A schematic of the human brain is shown in Figure 2.2.

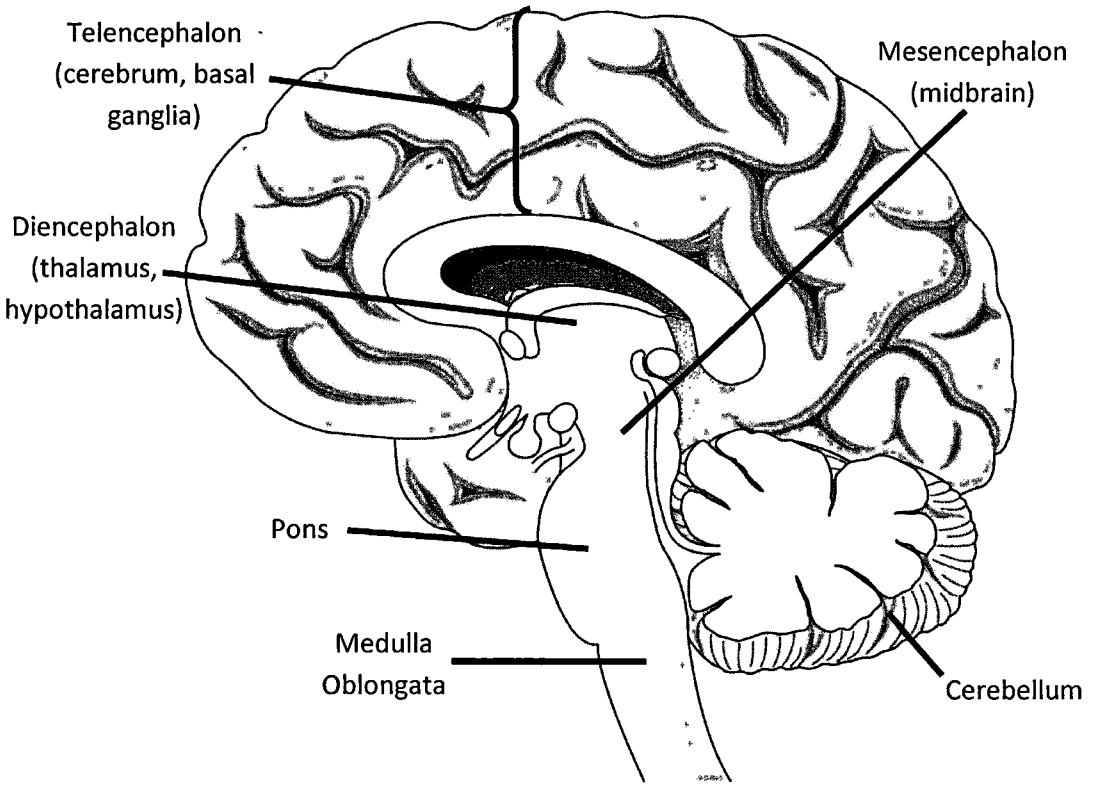

Figure 2.2. Midsagittal section of human brain. Used with permission LifeART image copyright 1998 Lippincott Williams & Wilkins. All rights reserved.

The largest division, the telencephalon, is comprised of the cerebral hemispheres and the basal ganglia. The cerebral hemispheres account for the majority of the brain volume in mammals (Withers 1992). The outer layer of the cerebral hemisphere, the cortex, is primarily composed of cell bodies, while the inner layer is made up of myelinated axons (Liebman 1991). The telencephalon has a large mass of axons that stream into and out of the cerebral cortex and connect it with other regions, including the corpus callosum, the

major pathway for communication between the hemispheres. The corpus callosum is often a site of injury for traditional TBI and blast TBI (Risling 2010, Park 2008).

To increase the surface area and thus the amount of cortex relative to its volume, the cerebrum has gyri (convolutions) and sulci (grooves) in humans and other mammals (Brodal 2004). Although gyri and sulci are present in almost every gyrencephalic brain, no two brains have exactly the same pattern in humans (Liebman 1991). To obtain accurate strains and stresses in brain tissue using finite element models, detailed gyri and sulci must be used (Cloots 2008, Ho 2009). Consequently, to accurately assess the human injury risk for brain tissue from a blast exposure, the model for the brain should include gyri and sulci.

Inside the cerebral hemispheres is the diencephalon which is divided into the thalamus and hypothalamus. The thalamus consists of many cell bodies and acts as a relay station for information from the lower part of the central nervous system to the cerebral cortex. It is also a relay station in the visual pathway. The hypothalamus is responsible for autonomic nervous system control (Brodal 2004).

Dorsal to the brainstem is the cerebellum. It represents only about 10% of the central nervous system by volume, but it contains roughly 50% of all of the neurons in the central nervous system in humans (Ransom 2003a). The cerebellum is mainly involved in the execution of movements. It has three large bundles of white matter called peduncles, which connect the cerebellum to the spinal cord and cerebral cortex. Like the cerebrum, the cerebellum has a layer of gray matter covering white matter, but it also has another region of gray matter enclosed in the white matter. The cerebellar surface is also extensively folded, forming folia that are predominantly oriented transversely (Brodal

2004). After blast exposure, hemorrhages, injured axons, and increased activity of microglia are often found in and around the cerebellum (Bauman 1997, 2009, Knudsen 2003, Saljo 2008, Kaur 1995).

The mesencephalon, or midbrain, is a relatively short section of the upper brainstem. At the base of the midbrain there is a pair of huge fiber bundles, the crus cerebri, that descend from the cerebral cortex to the brainstem and spinal cord (Liebman 1991). The midbrain also contains groups of neurons that are involved in hearing and vision (Ransom 2003a), which have also demonstrated degenerated fibers after exposure to blast (Petras 1997).

Caudal to the mesencephalon and the next part of the brainstem is the pons. It is involved in hearing and equilibrium. The large pontine nuclei receive input from the cerebral cortex and send their axons to the cerebellum (Brodal 2004). The pontine region has also been a site for hemorrhaging after a blast exposure in whales exposed to explosives (Knudsen 2003).

The remaining division of the brainstem is the medulla oblongata. It becomes continuous with the spinal cord at the foramen magnum. The respiratory and cardiac centers are also located in the medulla (Liebman 1991). The medulla contains ascending and descending fiber tracts that are similar to the other parts of the brainstem. Immediate post blast apnea which has been seen in blasted subjects with thoracic protection, with minor or no injuries to the respiratory system (Krohn 1941, Clemedson 1953) may involve injury to the medulla.

In addition, the brain is enclosed in three membranes, called the meninges. The innermost layer, the pia mater, is very vascular, and attaches directly to the brain and

closely extends into the sulci and fissures. The next membrane, the arachnoid, extends across the depressions, fissures, and sulci, unlike the pia mater. In between the pia mater and the arachnoid is the subarachnoid space (Liebman 1991). This space is filled with cerebrospinal fluid which provides a protective cushion from impacts to the head (Liebman 1991). The largest space, or cistern, is the cisterna magna, located posterior to the medulla below the cerebellum (Brodal 2004).

As a further means of protection there are fibrous filaments known as the arachnoid trabeculations, which extend from the arachnoid to the pia mater and help anchor the brain to prevent it from excess movement in cases of sudden acceleration (Liebman 1991). The subarachnoid space also contains the cerebral arteries and veins. The subarachnoid space is also a common site of hemorrhage after an exposure to blast (Kaur 1995, Knudsen 2003, Saljo 2008, Cheng 2010).

The outermost layer, the dura mater, is a thick strong layer of connective tissue that adheres to the inner surface of the skull. The space between the dura mater and the arachnoid is called the subdural space. In some instances, the dura restricts the movement of the brain within the skull. Large movements can damage vessels and nerves connecting the brain and the skull, and the increased pressure from the damaged vessels and nerves can cause additional harm to the brain (Brodal 2004). The subdural space is another common site of hemorrhage after a blast exposure (Knudsen 2003, Saljo 2008).

Finally, there are four main ventricles in the brain as shown in Figure 2.3. The ventricles of the brain make up a series of interconnected compartments where the cerebrospinal fluid is produced. The lateral ventricles are the largest and are located

within the cerebral hemispheres. The third ventricle is located in the midline between the thalami. The fourth ventricle is located in the brainstem and is continuous with the central canal of the spinal cord. It is from the fourth ventricle that the cerebrospinal fluid enters the subarachnoid space (Ransom 2003b). The ventricles, filled with the cerebrospinal fluid, have different acoustic impedance than the surrounding brain tissue (Evans 2006). This difference may contribute to injuries at the ventricle and brain interface after an exposure to blast.

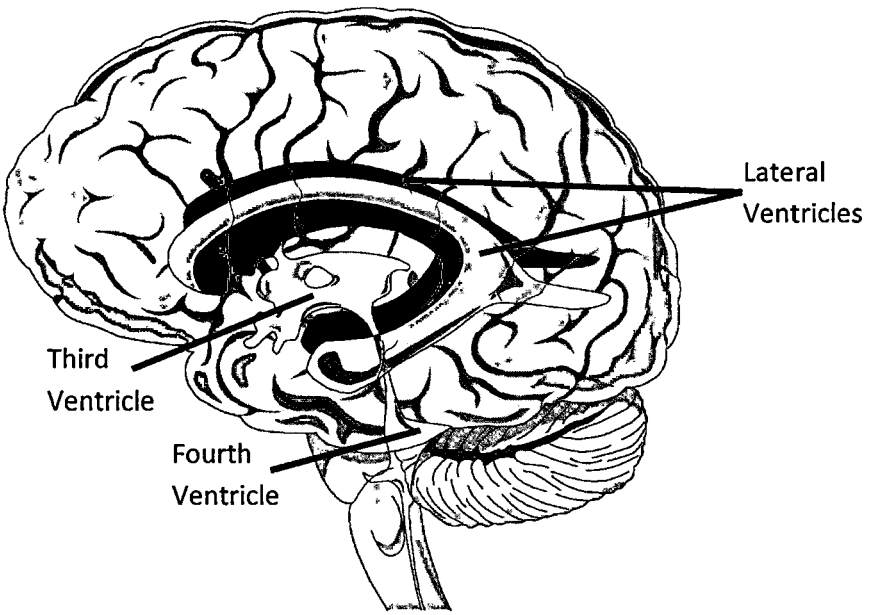

Figure 2.3. The ventricles of the brain. Used with permission LifeART image copyright 1998 Lippincott Williams & Wilkins. All rights reserved.

2.2 Blast Waves

Blast waves are shock waves that are generated from the rapid expansion of gas from an explosive that immediately compresses the surrounding air. The blast front, or the leading edge of the blast wave, which propagates supersonically, increases the density of the air through which is passes, raising its temperature (Iremonger 1997). Behind the blast front, the expanding gas from the explosive and the decompression of the high

density region of the gas creates a region below ambient pressure. The pressure profile of the blast front for a classic free field wave, or Friedlander wave, measured from a stationary point is shown in Figure 2.4. Other waveforms include complex waves which may be combinations of blast shocks and/or superposition of waves arriving from different directions. Complex waveforms are encountered frequently and may produce more severe pulmonary injuries to humans (Axelsson 1996, Stuhmiller 1997, Gruss 2006). These waveforms, however, are difficult to analyze and not well understood. The analysis in this study is generally limited to simple blast waves.

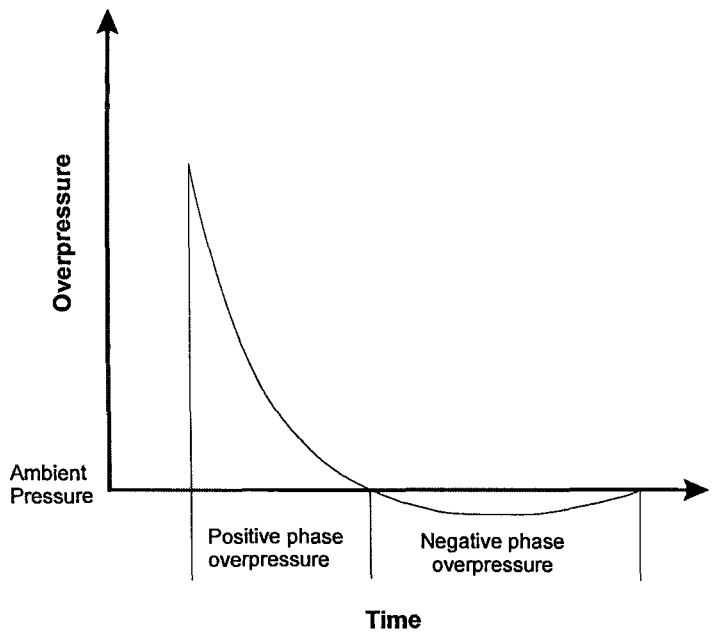

Figure 2.4. Ideal Blast Wave (adapted from Glasstone 1977)

For simple waveforms, pressures are generally measured in two ways. First is an incident or side-on pressure, measured with the sensing surface parallel to the direction of propagation of the blast wave. Second is the reflected pressure, measured with the sensing surface perpendicular to the direction of propagation of the blast shock. The risk function analysis in this study will be performed for each pressure measurement.

Detonating high explosives generates shock waves, but an air driven shock tube can be used as an alternative. The shock tube has been shown to be a valuable tool in studying the biological effects of primary blast (Cassen 1950, Celander 1955, Richmond 1961, Yang 1996, Dodd 1997, Elsayed 1997, Cernak 2001a, Gorbunov 2005, Bass 2008, Rafaels 2010b). The maximum pressure, impulse and positive phase duration can all be specifically designed outputs. In our laboratory, the blast overpressure time history generated from a live explosive was replicated as seen in Figure 2.5. Previous unpublished work demonstrated that the injuries seen in shock tube exposures are similar to those seen in high explosive tests, at least for the lung (Figure 2.6). Use of a shock tube eliminates complications from fragments or debris, hot gases and toxic fumes while investigating biological effects of primary blast.

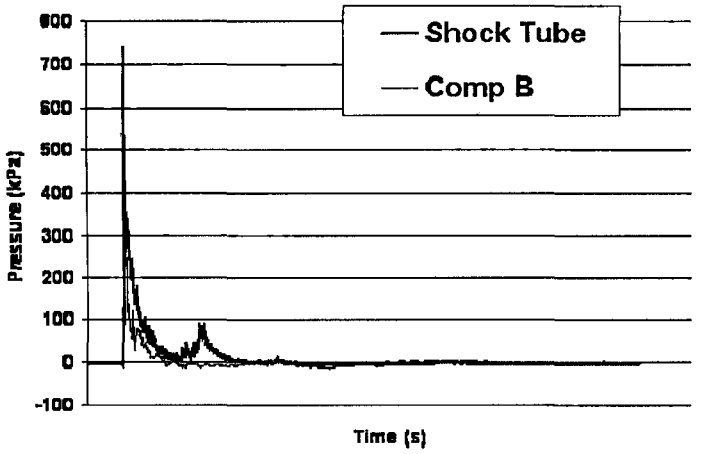

Figure 2.5. Comparison between shock tube and one pound of Composition B high explosive pressures (unpublished work).

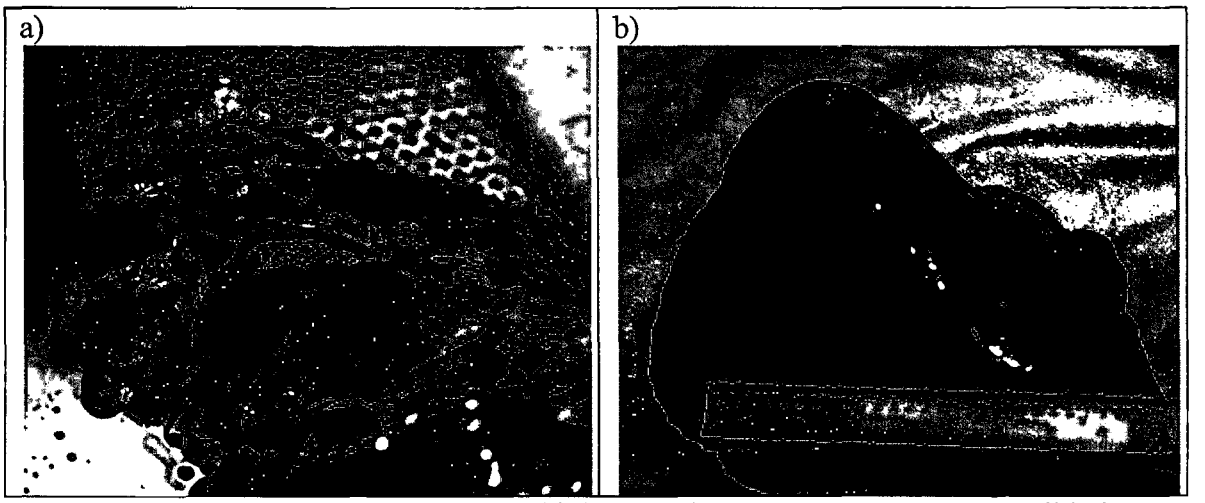

Figure 2.6. Pulmonary injuries from a high explosive exposure were reproducible in a shock tube exposure of a similar magnitude. a) High explosive exposure. b) Shock tube exposure. (unpublished work)

2.2.1 Blast Wave Interactions with the Body

When the blast wave encounters the body, it is reflected from, diffracted around, and transmitted into the body (Iremonger 1997). The load resulting from the reflected static overpressure and diffraction is unlikely to cause injury in short duration or low impulse events as the speed of the wave and the time of loading do not subject the body to substantial momentum transfer (United States 1996). The source of the remaining loads on the body is produced by the transmission of the blast wave into the body.

When transmitted into the body, blast waves generate compressive stress waves and shear stress waves (cf. Cooper 1997). The compressive stress waves are longitudinal pressure waves that are thought to injure tissues in a number of ways. First, the compressive waves may cause a pressure differential across delicate structures in the body (Horrocks 2000). For example, in blast lung injuries, the gas within the alveoli is compressible compared to the fluid containing tissues and vasculature surrounding it. When considering short duration blasts, which are the focus of this study, the blast wave

may create a pressure differential between the vascular system and the alveoli which may cause hemorrhaging (White 1960). Second, they may cause spalling at interfaces of tissue that have varying acoustic impedances. The reflection from the relatively stress free interface produces a region of tension when the decompression waves interact (Antoun 2003). Tearing of alveolar walls is likely due to this mechanism (Stein 1999). Third, the compressive waves may also cause cavitation by compressing a gas containing structure causing it to implode, or as the wave enters into rarefaction, the forceful re-expansion damages the structure (Horrocks 2000).

Shear waves, on the other hand, are transverse waves resulting from the deformation of the bodywall and compression of the structures within. The shear waves may also result from the conversion of volumetric stresses to deviatoric stresses in the tissue, itself. Tissues with different inertia can tear due to their asynchronous movements. In other words, when organs of different densities are accelerated at different relative rates, the tissue can experience local stresses and shearing forces (White 1960). Shear waves are thought to be responsible for injuries to the solid abdominal viscera, mesenteries, and the large bowel (Horrocks 2000).

2.3 Blast Loading vs. Blunt Trauma Loading

Human tissues are viscoelastic. Biological soft tissues, such as ligaments, have strong rate-dependent material properties (Lucas 2009). When loads are applied quickly, the tissue may experience large stresses and can fail both structurally and functionally, especially for localized application of forces. On the other hand, loads that are applied slowly to biological tissues may produce reduced damage from enhanced stress distribution (LaPlaca 2007). Traumatic brain injury (TBI) has mostly been studied for

conventional forms of brain injury such as motor vehicle accidents or falls, which have strain rates on the order of 1-10 s^{-1}. Although the exact strains involved in blast injuries are unknown, they are believed to be on the order of 100-1000 s^{-1} (Prevost 2010). Figure 2.7 demonstrates the loading curves for an automotive impact and a blast wave impact. For the same peak load, the impulses are vastly different. For the automotive condition, five ribs were fractured (Viano 1989); for the blast case, the probability of thoracic injury is nearly zero (Bass 2008). However, if the impulse of the blast condition were made the same as the automotive case, then the blast is almost certainly fatal (Bass 2008). Furthermore, when the higher strain rates are applied, injuries may become more localized. Despite the fact that there are similarities to conventional brain injury and some translation between the injuries, blast brain injury is distinct and must be investigated separately.

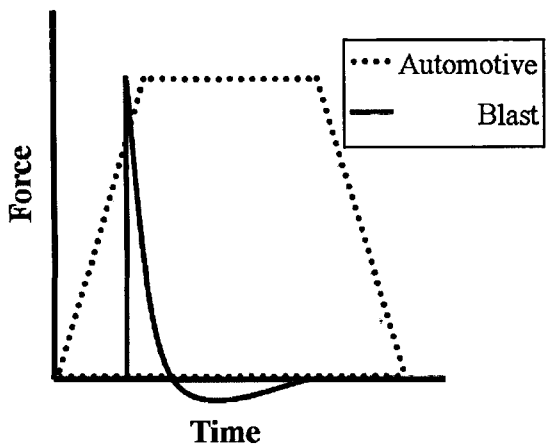

Figure 2.7. Force vs. Time plots comparing automotive to blast impacts. Automotive load adapted from Viano *et al.* (1989). Blast load is the calculated load from 5 kg trinitrotoluene (TNT) at a range of ~6.5 m using ConWep, a computer program for calculating weapons effects (Hyde 2004).

2.4 Blast Brain Injuries

With current knowledge, it is difficult to determine a unique clinical description of blast TBI because of its overlap of symptoms with post traumatic stress disorder (PTSD) and traditional TBI. To make matters worse, patients often have other serious injuries beyond TBI that may mask the symptoms or even the presence of TBI (Ling 2009). Most importantly, the increasing number of people with suspected blast brain injury along with the long term costs and consequences associated with TBI have added urgency to blast brain research. Therefore, it is necessary to examine blast TBI by itself and eliminate other causes of injuries that may cloud the etiology or presenting signs of blast TBI.

The correlation between impaired mental abilities and blast exposure with no outward trauma was first documented by British Army physician Sir Frederic W. Mott as far back as the First World War (Mott 1916). Yet he ultimately attributed the behavioral changes associated with "Shell Shock" to psychiatric illness and discarded the possibility of significant organic pathology (Bell 2008). However, recent clinical studies suggest that blast exposure may have significant and lasting cognitive effects, in addition to the behavioral changes (Trudeau 1998, Okie 2005, Hoge 2008).

Although TBI resulting from a blast exposure shares clinical features with PTSD and traditional TBI, it also has unique aspects. One unique characteristic of severe blast TBI is how commonly and rapidly patients develop diffuse cerebral edema, hyperemia, and delayed vasospasm (Ling 2009). A Defense and Veteran Brain Injury Center study using diffusion tensor imaging, an advanced MRI technique, showed that individuals with blast TBI had significantly decreased fractional anisotropy values and decreased apparent diffusion coefficient values compared with the control groups of impact only TBI and

healthy military controls (Cassels 2009). Additionally, PTSD patients with a history of blast concussion have demonstrated significantly different electroencephalographic (EEG) patterns when compared to matched controls (Trudeau 1998).

Current research on these blast induced, nonimpact closed head injuries includes very basic level work to study the damage inflicted by each component of the blast, including, heat, light, electromagnetic pulses (EMP), and pressure wave. Several theories currently exist for the mechanism behind blast brain injuries. One theory pinpoints EMP as a culprit (Singer 2008). Another theory postulates that blast waves that have entered through the torso travel up to the brain through the major blood vessels (Bhattacharjee 2008). Finally, there is the theory that the blast injury comes from the pressure wave directly through the skull (Chavko 2007).

2.4.1 Electromagnetic Field Transmission

An explosion can produce electromagnetic (EM) fields in several ways, most of which are too small to be considered major contributors to blast brain injuries. First, the initial explosion generates a flash of EM radiation six orders of magnitude below the Federal Communications Commission's (FCC) limit for occupational or general population exposure limits (FCC 1999). Further, these fields are reduced in the brain by an additional factor of about 10^5 at the neurologically important kHz frequencies (Lee 2010). Additionally, the shock front can ionize particles in the gas or other materials it passes through, but again, these resulting fields are orders of magnitude below safety limits for typical explosive threats in air (FCC 1999). The blast front can also polarize particles, which can lead to large electric fields for large blasts such as nuclear explosions, but negligible fields for the current blast threats (Lee 2010). Finally, EM

fields can be generated by polarizing piezoelectric skull. Even though the fields produced are short range, the proximity of the skull to the cerebral cortex may make the fields relevant (Lee 2010). However, the likely neurological effects from such an exposure would only lead to short term cortical function alterations (Wagner 2006). Exposure to EM fields cannot explain the edema, contusions, diffuse axonal injury, hematomas, hemorrhages, vasospasms, mood disturbances, or retrograde amnesia that have been observed after a blast injury (Hicks 2010).

2.4.2 Blast Wave Transmission

2.4.2.1 Vascular Transmission

The theory of vascular transmission of the blast wave to the brain was first proposed by Stewart *et al.* in 1941. Stewart formulated this theory for blast brain injuries to explain the extensive hemorrhaging seen in the brain of a pheasant that had been exposed to blast based on his experiences as a neurosurgeon (Stewart 1941). To demonstrate this theory, Young (1945) performed some experiments in which he exposed dogs to high pressures on the body using broad canvas bands. As a result of this exposure, hemorrhages and signs of neuronal damage were seen throughout the brain tissue, as well as lung hemorrhaging. However, the loading mechanism produced large displacements of the thoracic and abdominal tissue at slow rates for a relatively long duration compared to blast loading.

Although very large increases in pressure on the body can cause injuries to the central nervous system tissue, the mechanism of injury in Young's experiments may not be the same mechanism seen in air blast exposures, at least for short duration exposures. In fatal air blast exposures on rabbits, thoracic displacements did not exceed 20 mm

(Clemedson 1969), and for velocities of displacement less than 4.5 m/s, no lung injuries were seen (Jonsson 1979).

Alternatively, Cramer *et al.* (1949) believed that the blast wave is applied to the body wall, and that the force is transmitted to the cerebrum via the venous lakes comprised of the jugular veins and the spinal veins and spinal fluid. However, Clemedson showed that although a pressure wave can propagate to the brain when the head is protected, the magnitude and frequency content of the pressure wave is considerably less than the pressure wave that is directly transmitted into the skull. It should be noted that the study was performed on dead rabbits. It is unknown how normal hemodynamic conditions would affect the pressure wave transmission through the blood vessels, but it is unlikely that it would overcome the direct transmission of the wave as the largest contributor to pressure in the brain (Clemedson 1956b).

More recently, Cernak (1997, 2001a) has also argued that the shock wave may enter the brain via the large blood vessels based on results from experiments in which rats were exposed locally to the thorax. The results demonstrated similar effects on the central nervous system as whole body exposures. However, with a larger animal study, Saljo *et al.* (2008) showed contrary results. When the exposure was localized to the abdomen of their porcine specimens, only 3% of the peak pressure was seen inside the skull. Further, this peak pressure could also be explained by residual pressure transmitted in the air outside the local region of pressure application.

2.4.2.2 Direct Transcranial Transmission

There have been several studies that investigated the transmission of the blast wave into the cranial vault. The first study was performed by Clemedson and Pettersson

(1956a) on deceased rabbits due to the size of the pressure transducer. The pressure transducer was placed in the brain through the orbital for the left eye which was removed. The orbit was filled with clay to seal the cavity. Another pressure transducer was placed just outside of the head in the air for comparison. The pressure pulse changed very little during the passage through the skull as demonstrated in Figure 2.8. The principle change observed inside the skull was that the high frequency content was reduced compared to the pressure wave measured in the air. Additionally, in most cases, the peak pressure measured inside the skull was slight increased, while the negative phase of the pressure pulse was reduced (Clemedson 1956a). Similar results were shown by Romba *et al.* (1961) in deceased monkeys.

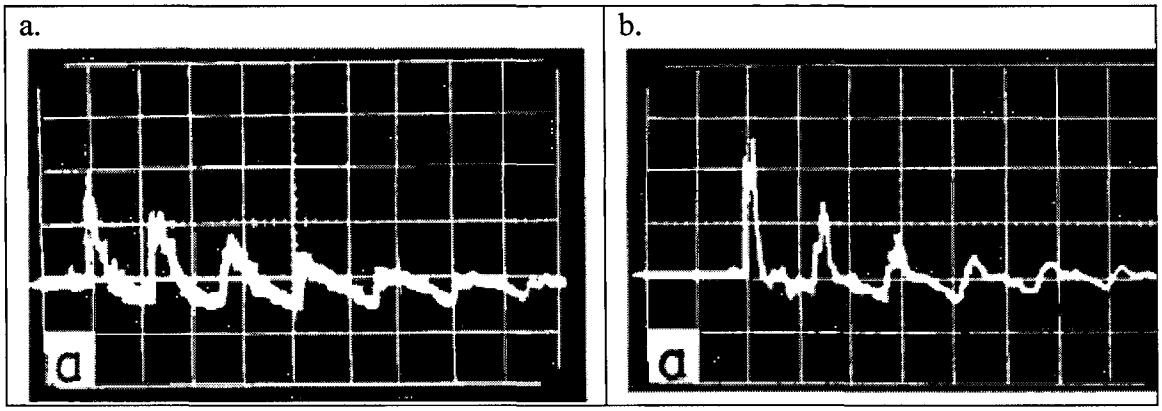

Figure 2.8. Pressure recordings demonstrating direct transcranial transmission of the blast wave in rabbits. Time scale for both graphs is 5 ms between vertical lines. The pressure scale is 0.35 kp/cm^2, or ~ 34 kPa, between the horizontal lines. a.) Pressure recording in air outside of skull. The multiple peaks are due to a repeated reflection of the blast wave against the end walls of the blast chamber. b.) Pressure recording in the skull. The pressure recording is higher inside the skull because the pressure transducer inside the skull was measuring a reflected pressure whereas the air pressure transducer was measuring incident pressure (Clemedson CJ, Pettersson H. Am J Physiol. 1956a, used with permission from Am Physiol Soc).

More recently, because of advanced technology allowing for smaller transducers, pressure waves have also been measured in live animal subjects. Chavko *et al.* (2007) placed small fiber optic pressure sensors into the cerebral ventricle of a rat. The sensor (0.9 mm diameter) was inserted into a guide cannula (1 mm diameter) that was secured in place using cranioplastic cement and screws. The surgical wound was closed with Vetabond surgical glue and sutures. Another pressure transducer was placed in the air for comparison. In this study, the specimens were exposed in two different orientations: a prone position with the head facing the blast, or a prone position perpendicular to the axis of the shock tube with the right side exposed to the blast. As shown in figure 2.9, the

peak overpressures were nearly the same inside the skull as in air, but the durations were longer inside the brain. In fact, the decay from the peak overpressure displayed a dependence on orientation (Chavko 2007). The increased duration of the initial overpressure peak in the frontal position may possibly be explained through diffraction loading, whereas the increased overpressure on the second peak for the lateral position may be due to reflections of the wave inside the skull. Additionally, the pressure measurements are directional. The exact orientation of the pressure transducer inside the skull is not known, so the pressure loading that was recorded may not be truly incident like the transducer in air outside of the skull.

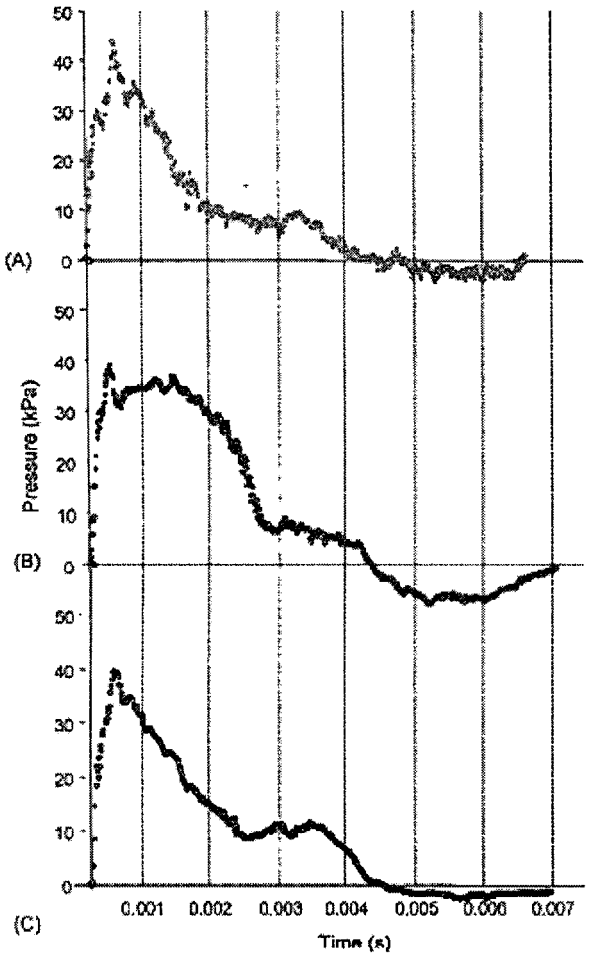

Figure 2.9. Pressure recordings demonstrating direct transcranial transmission of the blast wave in rats. a) Pressure recording in air outside of skull. b) Pressure recording in the skull from the rat placed in the frontal position. c) Pressure recording in the skull from the rat placed in the lateral position. "Reprinted from Journal of Neuroscience Methods, Vol. 159, Issue 2, Chavko M, Koller WA, Prusaczyk WK, McCarron RM, Measurement of blast wave by a miniature fiber optic pressure transducer in the rat brain, Pages 277-281, Copyright (2007), with permission from Elsevier."

In another recent study, Saljo *et al.* (2008) also measured intracranial pressures in a living animal model. Here, hydrophones were inserted under the dura in the right fronto-parietal region, 10 mm from the midline, of porcine brains. A 9 mm diameter hole was

drilled into the skull and an incision was made in the dura to allow for the introduction of the sensor. The hydrophone, which was covered with black rubber, fit tightly into the hole and was glued to the skull bone. For local shock tube exposures to the head, the peak pressure in the air was 22.4 kPa, compared to only 9.3 kPa in the brain (Saljo 2008). This reduction may be due to the attenuation across the skull and brain tissue. Another explanation for the decreased pressure may be improper sealing of the skull, which may not allow for accurate measurements of intracranial pressure (Del Cengio Leonardi 2009). However, for fast rising overpressures of short durations, like the ones used in the Saljo *et al.* study, there is not enough time nor is the vent area large enough for the pressure to flow out of the vent and significantly change the peak pressures measured (White 1960).

For occupational simulations of weapons firing, the pressures in air and in the porcine brain for the various weapons have been investigated and can be seen in Figure 2.10. The pressures in the brain for the howitzer exposure, most closely matched the pressures seen in air. The bazooka and automatic rifle did not follow as closely (Saljo 2008). Similar to the results shown by Clemedson and Pettersson (1956a), the high frequency components of pressure wave have been reduced in the brain as compared to air. However, the differences seen between the air and brain measurements in the weapons simulations may relate to the position of the "gunner" in relation to the firing portion of the weapon, as well as the firing mechanism of the weapon itself.

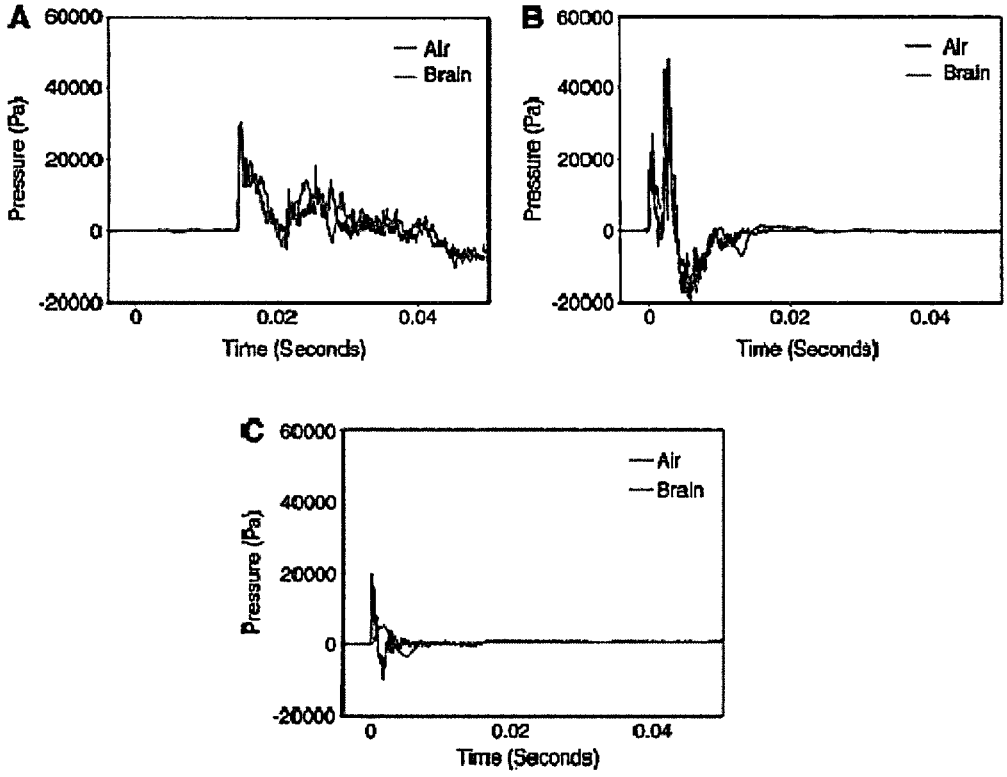

Figure 2.10. Pressure recordings demonstrating direct transcranial transmission of the blast wave in pigs. The pressure waves recorded in air outside of the head are in blue, and the waves recorded in the brain are red. a) Howitzer 30 kPa. b) Bazooka. c) Automatic Rifle. (Reprinted with permission from JOURNAL OF NEUROTRAUMA (Vol. 25, Issue 12, Pages 1397-1406) published by Mary Ann Liebert, Inc. New Rochelle, NY)

2.4.3 Blast Brain Injury Studies

Blast brain injury may have first been described in accounts from Napoleonic times that suggested the possibility of brain injury arising from cannon fire close to the head (Denny-Brown 1945). But the correlation between impaired mental abilities and blast exposure with no outward trauma was definitively suggested by British Army physician Sir Frederic W. Mott in the First World War (Mott 1916), though he later reconsidered

his original position on the organic source of blast (Bell 2008). Although experiments with animals exposed to blast presented with cognitive deficits, there were frequently no visible lesions (Krohn 1941, Clemedson 1953). Any macroscopic evidence for a physical injury was often dismissed as carbon monoxide poisoning or traditional blunt injury (Denny-Brown 1945). These controversies, as well as research into the more visible and life threatening pulmonary aspect of blast injuries, put blast brain injury research on the back burner, so to speak, for fifty years, though limited study continued throughout the 20th century.

During and following World War II, British and Swedish researchers investigated blast brain injuries specifically and propagation of blast waves through the body (Krohn 1941; Clemedson 1953, 1956a, 1956b). Research into blast brain gained some momentum in the 1990s to elucidate the reasons behind a large increase in the cases of "late onset" post traumatic stress disorder from veterans of the Vietnam War being seen in the US Veterans Affairs system. Additionally, at the same time, physicians were seeing electrocortical dysfunction and cognitive deficits in blast victims from the war in the former Yugoslavia (Cernak 1999a). The latter half of the current decade has seen an explosion of blast brain injury research owing to large numbers of anecdotal reports of blast associated brain injuries from the conflicts in Iraq and Afghanistan. According to the Defense Veterans Brain Injury Center and a study of US Army combat infantry soldiers, approximately 2,700 U.S. troops have suffered a TBI or presented with TBI-like symptoms and potentially hundreds of thousands more may have suffered a mild TBI, perhaps as a result of IED blast waves (Glasser 2007; Hoge 2008).

2.4.3.1 Macroscopic Blast Brain Injuries

One of the difficulties in assessing blast brain injuries is that, anecdotally, the injuries may occur without clinically obvious damage. However, macroscopic injuries do occur in experimental animal models. One of the most common macroscopic findings is hemorrhaging or contusions on the brain. A summary of the studies that presented with hemorrhages are shown in Table 2.1. However, this macroscopic injury typically occurs at severe blast levels, levels that are likely to cause fatalities from pulmonary injuries. As demonstrated in Table 2.1, the majority of the studies in which a hemorrhage is present exposed the specimens at or above the estimated 50% pulmonary fatality levels for the overpressures and durations of that particular study. The Kaur *et al.* (1995) study did not report the blast wave parameters. Massive subarachnoid hemorrhages were found in only 2 of the 22 specimens in that study. That group also published additional work, with similar reported test conditions, and did not find this injury in any of those tests, making the incidence less than 3% at this test condition (Kaur 1996, 1997a, 1997b). The results from Saljo *et al.* (2008) also demonstrated subdural hemorrhaging at lower than expected blast levels. However, this study exposed the porcine specimen to multiple exposures with nonidealized blast waves. Therefore, the 50% pulmonary fatality risk displayed may not be the appropriate value for these test conditions. It is already known that the tolerance of biological tissue decreases after exposure to multiple and complex blast waves (Stuhmiller 1996). These hemorrhagic types of blast brain injuries, although very severe and life threatening, are not difficult to diagnose with modern imaging techniques, such as computed tomography (CT), or magnetic resonance imaging (MRI) and have an accepted treatment course.

Table 2.1. Summary of blast brain injury studies presenting with hemorrhages. The column "P50 for pulmonary" stands for the approximate peak pressure that would result in a 50% risk for fatality from pulmonary injuries under the test conditions in the study. (HE = high explosive)

Study	Animal	Exposure	Orientation	Peak Pressure and Duration	P50 for pulmonary	Region(s) of Brain	Macroscopic Findings
Krohn 1941	Rabbit	HE, specimen in iron tube, head exposed		607-1124 kPa, NA	200 kPa	Olfactory and occipital lobes	Cerebral lesions
Kaur 1995	Rat	HE, specimen inside blast chamber		~10^1 kPa, NA	200 kPa	Temporal cortex, roof of 4th ventricle	Massive subarachnoid hemorrhages
Bauman 1997	Rat	Compressed air shock tube	Perpendicular to blast	129 kPa, NA	200 kPa	Meninges, cerebrum, cerebellum	Mild to moderate multifocal hemorrhages
Knudsen 2003	Whale	HE	Harpoon and grenade inside body	NA, NA	233 kPa	Cortical surface, midbrain, brainstem, peduncular cisterns, thalamus, cerebellum	Extensive subdural, subarachnoid, intraventricular hemorrhages
Nakagawa 2003	Rat	Underwater shock wave, laser generated	Applied directly to dura	10,000 kPa, NA	250 kPa	Parietal section under application site	Subarachnoid and intraparenchymal hemorrhages
Kato 2007	Rat	Underwater shock wave generated with microexplosive	Applied directly to dura	12,500 kPa, NA	250 kPa	Cortical and subcortical regions	Intracerebral hemorrhage, contusional lesion
Saljo 2008	Pig	3 shots from Howitzer, Bazooka, or Automatic rifle	Positioned as the user of the weapon	30 kPa, 5.1 ms - howitzer; 42 kPa, 1.9 ms - bazooka; 23 kPa, 1.2 ms - rifle	225-550 kPa depending on exposure condition	Parietal, occipital lobes, cerebellum, brainstem	Small subdural and subarachnoid hemorrhages
Svetlov 2009a	Rat	Shock tube	Directed at head	358 kPa, 10 ms	200 kPa		Intracranial hematomas, edema
Long 2009	Rat	Compressed air shock tube, specimens both w/ and w/o Kevlar vest	Perpendicular to shock tube	147 kPa, NA	200 kPa	Bilateral, more pronounced on ipsilateral side	Hemorrhaging, necrosis
Cheng 2010	Rat	HE, specimen in aluminum box, head exposed	Dorsal aspect of head exposed	200-400 kPa, 0.25 ms for 400 kPa	200 kPa	Diffuse in cortex, obvious in frontal and parietal lobes	Contusions, diffuse subarachnoid hemorrhages, edema

2.4.3.2 Microscopic Blast Brain Injuries

In addition, studies have seen cognitive deficits resulting from blast exposure without observable macroscopic injuries to the brain (Bogo 1971; Cernak 2001a, 2001b; Risling 2002). Microscopic brain injuries that result from blast may be investigated using histology, electron microscopy, and modern immunohistochemical techniques. By providing specific visualization of a localized injury, they can promote an understanding of particular injury mechanisms.

Traditional histology and electron microscopy can demonstrate the structural and/or morphological changes that occur from blast loading. Similar to traditional traumatic brain injury, neurons from brains exposed to blast demonstrated mitochondrial swelling, vacuolated cytoplasm, glial swelling, and darkened dendrites (Farkas 2007; Cernak 2001a, 2001b; Kaur 1995, 1996, 1997a, 1997b; Dietrich 1994; Saljo 2001; Long 2009; Kato 2007; Moochhala 2004). These morphological changes indicate neuronal necrosis. In ischemic brain injury, these neuronal changes have been associated with membrane pump failure; however, it is likely that other factors associated with direct mechanical perturbation are important for blast (Farkas 2007). These potential mechanisms are not yet well understood.

Morphological changes associated with microglial activation have also been seen after blast exposures (Kaur 1995, 1997b, Saljo 2001). Additionally, chromatin condensation and axoplasm shrinkage has been observed, which is linked with apoptosis in traditional TBI (Cernak 2001b, Kaur 1996, Farkas 2007). Morphological changes for reorganization and repair have also been seen in blast exposed brains, such as

disorganization of the endoplasmic reticulum (Cernak 2001b, Kaur 1995, 1996, 1997b, Farkas 2007).

In addition to these neuronal injuries, diffuse axonal injury also occurred in both mild and severe blast conditions and in many areas of the brain, including the brainstem, cerebellum and hippocampus (Petras 1997, Cernak 2001b, Long 2009, Garman 2009, Bauman 2009, Svetlov 2009a, Cheng 2010). These axonal injuries, that often appear as axonal bulbs, likely result from reactive axonal changes rather than actual transsection of the axon (Farkas 2007). These structural and/or morphological changes can occur in both mild and severe blast loading conditions. They can also occur without any macroscopic injuries present. These diffuse types of changes indicate that blasts may activate cellular cascades that contribute to the overall blast brain injury.

Moreover, immunohistochemical techniques provide a window into those processes that are otherwise difficult to investigate. Mild blast brain injuries may cause little visible damage, but instead incite biochemical pathways that can cause damage after the initial insult has occurred. Table 2.2 lists the immunohistochemical techniques and other biomarkers that have been used for blast brain and their studies. The majority of the markers that have been used for the blast exposed brain are related to the immune response. The immune response of the brain plays a dual role after an injury has occurred: guiding both regeneration and degeneration of neurons and glia (Streit 2000). Not surprisingly then, the majority of the studies reported increases in the presence and activity of these markers (Kaur 1995, 1996, 1997a, 1997b, Saljo 2001, Tompkins 2008, Svetlov 2009a, Garman 2009, Bauman 2009). It is not clear whether the presence or activation of many of these markers is for regeneration or degeneration of the brain

tissue. Consequently, we cannot gain a full understanding of the immune responses in the brain resulting from a blast exposure and whether we should be suppressing or promoting it for therapeutic strategies. Additionally, the immune response is active in the brain before an injury occurs, that in some cases, the injured specimens cannot be distinguished from the controls (Kaur 1996, Garman 2009).

Other common markers that have been used in blast brain injury studies are those for apoptosis, or programmed cell death. Apoptosis prevents harmful intracellular molecules from damaging neighboring cells. Necrotic cells, however, lyse and spill their contents before they can be sequestered. It is believed that necrosis and apoptosis lie on opposite ends of the cell death spectrum, with necrosis being a result of incomplete apoptosis. Often, cell death is somewhere between the two extremes (Leist 1998). The severity and cause of injury may determine where in the spectrum the cell death pathway occurs. Additionally, the balance between anti- and pro-apoptotic signals determines if the injured neuron will continue along the apoptotic pathway or survive (Farkas 2007). Some of the genes and proteins involved in apoptosis and necrosis and their byproducts have been shown to increase after a shock wave exposure, even at overpressures as low as 20 kPa (Saljo 2002a, 2002b, Moochhala 2004, Kato 2007, Park 2008). These injury markers, although useful, do not provide the mechanism behind the injuries, nor do they discriminate among neurons that do not go on to complete the apoptotic pathway.

Aside from the markers for apoptosis and necrosis, other markers for cellular damage have been investigated for blast injury. Markers for damage in and resulting from the neurons, oligodendrocytes, and astrocytes have increased after blast exposure (Saljo 2003, Tompkins 2008, Svetlov 2009a, Bauman 2009, Cheng 2010). The usefulness of

many of these markers is their ability to be sampled in the cerebrospinal fluid (CSF) or blood to determine damage, but some problems still exist. Neuron specific enolase, which at first was thought to be strictly neuronal, has been found in blood and platelets, making it susceptible to cross-contamination. Additionally, S100β, predominantly found in glial cells, is expressed outside of the brain, again clouding its origins in collected samples.

These immunohistochemical techniques have also demonstrated axonal injury after primary blast exposure (Saljo 2000a, 2002, Svetlov 2009a, Bauman 2009). Axons span different areas of the brain, crossing the grey-white matter interface, running along ventricles or near blood vessels which can create stress concentrations at these boundaries (Smith 2000). Moreover, within their own structure, myelinated axons can have stress concentrations at nodes of Ranvier. In fact, the structure at nodes of Ranvier has been shown to become disrupted in stretch injuries (Maxwell 1996). Myelin degeneration byproducts were increased in the serum and the tissue after blast exposure (Svetlov 2009a, Bauman 2009). Axonal transport was also found to be disrupted (Saljo 2000, 2002a). Staining for phosphorylated neurofilament subunit proteins showed conformational changes to the cytoskeleton, indicative of axonal degeneration (Saljo 2000). The expression of β-amyloid precursor protein (β-APP), one of the most sensitive markers in traditional traumatic axonal injury (Bain 2001), was also increased after blast exposure (Saljo 2002a). For both of the axonal transport studies, there were no immunopositive stains in the control (unblasted) cases (Saljo 2000, 2002a). These results show that these markers can distinguish between blast injured cells and uninjured cells. Moreover, several researchers have reported β-APP accumulation in axonal swellings as

early as 2 hours post injury and have seen axonal responses dependent on injury severity (McKenzie 1996, Pierce 1996, Bramlett 1997, Stone 2000, Ai 2007). Because of the high sensitivity and early time course of β-APP, it was used in this study to determine when blast brain injury has occurred and to help determine severity.

Table 2.2. Biomarkers used in blast brain injury studies.

Biomarker	Function and use	Study	Peak Pressure	Duration	Findings
OX-42	Binds to surface receptor found on immune cells – Microglial/ macrophage marker	Kaur 1995	~10^1 kPa		Increase in positive cells as early as 1 day, lasting almost 4 weeks. In both grey and white matter. More apparent in grey. Specifically located in subpial region of temporal cortex, cerebellar cortex, hypothalamus, pineal gland, and neuropophysis.
		Kaur 1996	~10^1 kPa		Increase in positive cells beginning on day 7, lasting almost 4 weeks. Found in epiplexus cells.
		Kaur 1997b	~10^1 kPa		Increase in positive cells beginning on day 7, lasting almost 4 weeks. Found in pineal gland.
		Saljo 2001	154 or 240 kPa	1.7 or 2 ms	Increase in positive cells as early as 2 hours for 240 kPa, lasting 3 weeks, and as early as 18 hours for 154 kPa, lasting almost 3 weeks. Found in superficial layer of cerebral cortex and hippocampus, hypothalamus, and lateral septal nucleus.
OX-18	Antigen on MHC class I molecules, binding degraded cystolic proteins – T-cell marker	Kaur 1995	~10^1 kPa		Between 1 and 14 days, positive cells were ubiquitous, weakly stained by days 21 and 28.
		Kaur 1996	~10^1 kPa		Increase in positive cells beginning on day 7, lasting almost 4 weeks. Found in epiplexus cells.
		Kaur 1997b	~10^1 kPa		Increase in positive cells beginning on day 7, lasting almost 4 weeks. Found in pineal gland, often clustered.

Biomarker	Function and use	Study	Peak Pressure	Duration	Findings
OX-6	Antigen on MHC class II molecules, binding degraded extracellular proteins – T-cell marker	Kaur 1995	~10^1 kPa		Positive cells present 1-14 days. Uneven distribution. Fewer positive cells than OX-42 or OX-18.
		Kaur 1996	~10^1 kPa		Increase in positive cells beginning on day 7, lasting almost 4 weeks. Found in epiplexus cells.
		Kaur 1997b	~10^1 kPa		Increase in positive cells beginning on day 7, lasting almost 4 weeks. Found in pineal gland, often clustered.
ED-1	Antigen on macrophages that have been transformed from microglia – Microglial/ macrophage marker	Kaur 1995	~10^1 kPa		Negligible positive cells.
		Kaur 1996	~10^1 kPa		Increase in positive cells beginning on day 7, lasting almost 4 weeks. Found in epiplexus cells.
		Kaur 1997b	~10^1 kPa		Increase in positive cells beginning on day 7, lasting almost 4 weeks. Found in pineal gland, often clustered.
		Garman 2009	241 kPa	4 ms	Some foci of positive cells.
p-NFH (phos-phorylated heavy neuro-filament protein)	Antigen on structural element of axon – Axonal damage	Saljo 2000	154 or 240 kPa	1.7 or 2 ms	Increase in positive cells as early as 18 hours, returning to normal by 3 weeks. Found in neuronal perikarya of layers II-IV in temporal cerebral cortex and other cortical regions, most pronounced on ipsilateral side. Also found in cingulate cortex, CA1 pyramidal cells of hippocampus and granule cells of dentate gyrus (DG). Increased frequency and intensity of positive cells for 240 kPa.

Biomarker	Function and use	Study	Peak Pressure	Duration	Findings
GFAP (glial fibrillary acidic protein)	Protein found mostly in glial cells, but also in other tissue like bones, skin, liver. Highest in astrocytes – Astrocytic activation	Saljo 2001	154 or 240 kPa	1.7 or 2 ms	Increase in positive cells as early as 18 hrs, lasting 3 wks. Dense networks seen 7-21 d. Found in cerebral cortex, mossy fiber region, region sup. and inf. of the hippocampus. Outlined capillaries in cerebral cortex, DG, and CA1-4 pyramidal cell layer.
		Tompkins 2008			Increased at 24 hrs post-injury.
		Svetlov 2009a	358 kPa	10 ms	Accumulated substantially in hippocampus and to a lesser extent the cortex 24 hrs post, persisting for 30 d. In blood, GFAP content increased at 24 hrs, followed by a decline and later increase in the CSF.
		Bauman 2009		~12 ms	At 2 wks, astrocytosis evident in ipsilateral cortex, alveus and hilus, and the stratum radiatum, and the molecular layer of the dentate gyrus. Protein expression in extracts from ipsilateral frontal cortex increased 3-fold.
		Garman 2009	241 kPa	4 ms	Not increased compared to sham.
c-Fos	Protein that forms part of a transcript-ion factor that activates many genes, including ones for the late stages of apoptosis – Apoptosis	Saljo 2002a	154 or 240 kPa	1.7 or 2 ms	Increase in positive cells as early as 2 hrs, lasting 3 wks. Found in neurons in layers II-VI in the grey matter of the temporal, cingulate, and piriform cortices in the neuronal cytoplasm, axons, and dendrites. Also found in CA1-3 pyramidal cell layer of the hippocampus and in the granule cells of the DG. Most pronounced on the blasted side. Both levels had similar staining.

Biomarker	Function and use	Study	Peak Pressure	Duration	Findings
c-Myc	Transcription factor that activates many genes, including ones for apoptosis – Apoptosis	Saljo 2002a	154 or 240 kPa	1.7 or 2 ms	Increase in positive cells as early as 2 hours, lasting 7 days. Found in neurons and astrocytes throughout layers II-VI in the grey matter of the temporal, cingulate, and piriform cortices, and in the CA1-3 pyramidal cell layer of the hippocampus and in the granule cells of the DG. Most pronounced on the ipsilateral side. Both levels demonstrated similar staining.
β-APP (Beta-amyloid precursor protein)	Membrane protein expressed in many tissues and concentrated in the synapses of neurons. Travels down axon through fast transport – Axonal damage	Saljo 2002a	154 or 240 kPa	1.7 or 2 ms	Increase in positive cells as early as 6 hours, lasting 3 weeks. Found in neuronal perikarya of the temporal, cingulate, and piriform cortices, and in the thalamus, the CA1-3 pyramidal cell layer of the hippocampus and in the granule cells of the DG. Axons in the white matter also showed immunoreactivity. Both levels demonstrated similar staining.
c-Jun	Gene and protein that forms part of a transcription factor that activates many genes, including ones for apoptosis – Apoptosis	Saljo 2002b	154 or 240 kPa	1.7 or 2 ms	Increase in positive cells as early as 2 hours, lasting 3 weeks. Found in neurons throughout layers II-VI in the grey matter of the temporal, cingulate, and piriform cortices and in the CA1-3 pyramidal cell layer of the hippocampus and in the granule cells of the DG. Both levels demonstrated similar staining.

Biomarker	Function and use	Study	Peak Pressure	Duration	Findings
TUNEL (Terminal deoxy-nucleotidyl transferase dUTP nick end labeling)	Detects DNA fragmentat-ion – Apoptosis	Saljo 2002b	154 or 240 kPa	1.7 or 2 ms	Increase in positive cells as early as 6 hours, lasting 7 days. Found in neurons in layers II-VI in the grey matter of the temporal, cingulate, and piriform cortices and in the CA1-3 pyramidal cell layer of the hippocampus. Half the immunoreactivity as c-Jun. Both levels demonstrated similar staining.
		Moochhala 2004	2.8 or 20 kPa		Cerebral cortex displayed over 50% positive area in the sampled tissue areas. Aminoguanidine application improved area to just under 25%. No positive cells for 2.8 kPa
		Kato 2007	1,000 or 12,500 kPa		Increase in positive cells as early as 4 hours, max at 24 hours, and back down at 72 hours at both levels. Dispersed throughout the area around the contusional lesion. Changes not significant for 1,000 kPa.
		Park 2008	20 or 51 kPa	0.59 or 0.48 ms	The periventricular region had the greatest concentration of TUNEL-staining at 24 hours, followed by the corpus callosum, cerebral cortex, and hippocampus. Positive cells also seen at 72 hours.

Biomarker	Function and use	Study	Peak Pressure	Duration	Findings
NSE (Neuron Specific Enolase)	Enzyme mainly found in cytoplasm of neurons, but also in platelets and erythrocytes – Neuronal damage	Saljo 2003	154 or 240 kPa	1.7 or 2 ms	CSF levels increased. For epidural sampling, it was significant for both levels for at least 10 hrs. For external sampling, a significant although transient increase was only found at 240 kPa.
		Svetlov 2009a	358 kPa	10 ms	Levels in blood were significantly elevated within 24 and 48 hrs.
		Bauman 2009		~12 ms	Levels greatly elevated in serum at 6, 24, and 72 hrs.
		Cheng 2010	100 or 200 kPa		Levels in serum peaked at 1 d, then decreased until 5 d where it returned to normal values for 200 kPa. For 100 kPa, levels in serum increased early, but decreased rapidly back to normal values by 2 d. Levels in cortex neurons decreased. For 200 kPa, they peaked at 2 d. For 100 kPa, they peaked at 1 d.
S-100B	Protein that is glial specific, primarily expressed in astrocytes – Astrocytic damage	Saljo 2003	154 or 240 kPa	1.7 or 2 ms	CSF levels increased. For epidural sampling, it was significant for both levels. For external sampling, a significant although transient increase was only found at 240 kPa.
		Tompkins 2008			At 1 hr, present mainly in astrocytes. At 24 hrs, it was evenly divided between neurons and astrocytes. By 3 wks, the tissue was markedly positive.
Caspase 3	Protease that plays an essential role in apoptosis, necrosis, and inflammation – Apoptosis	Kato 2007	1,000 or 12,500 kPa		Significant increase in ipsilateral cortex of 12,500 kPa. Dispersed throughout the area around the contusional lesion.

Biomarker	Function and use	Study	Peak Pressure	Duration	Findings
COX-2 (cyclooxy-genase)	Enzyme important in immune response – Macrophage marker	Tompkins 2008			Elevated at 24 hours.
HMGB1 (high-mobility group protein B1)	Protein that acts as a cytokine when released by necrotic and inflammatory cells – Immune response	Tompkins 2008			Elevated at 3 weeks, primarily localized on oligodendrocytes.
4-HNE (4-Hydroxy-nonenal)	Produced by lipid peroxidation in cells – Cell damage	Tompkins 2008			Observed at 24 hours predominantly in neurons. By 3 weeks, it was found in neurons and astrocytes.
CNPase (2', 3'-cyclic nucleotide 3'-phospho-diesterase)	Present almost exclusively in oligodendryte and Schwann cell – Myelin degeneration	Svetlov 2009a	358 kPa	10 ms	Accumulated substantially in hippocampus and to a lesser extent the cortex 24 hours post, persisting for 30 days.
UCH-L1 (Ubiquitin carboxy-terminal hydrolase L1)	Gene whose expression is highly specific to neurons. Role in removal of proteins – Neuronal marker	Svetlov 2009a	358 kPa	10 ms	In blood, content was increased at 24 hours, followed by a decline. In the CSF, increased levels persisted throughout 14 days and varied significantly in individual rats.
Iba1 (ionized calcium binding adaptor molecule 1)	Protein specifically expressed in macrophages/ microglia – Microglial/ macrophage marker	Garman 2009	241 kPa	4 ms	Not increased compared to sham.

Biomarker	Function and use	Study	Peak Pressure	Duration	Findings
MBP (Myelin basic protein)	Protein important in myelination – Myelin degeneration	Bauman 2009		~12 ms	Levels were greatly elevated in serum at 6, 24, and 72 hours. Increase in MBP was much larger and more sustained than increase in NSE.

2.4.3.3 Blast Brain Injury Studies from Direct Transcranial Transmission

Previous blast research has long suggested that, at least for fatalities, that the brain is more tolerant to blast loading than are the lungs or the gastrointestinal tract (e.g. Hooker 1924). With increased protection to the thorax and abdomen used in current conflicts, it is necessary to examine the brain separately from the lungs. Few studies have focused solely on blast injury restricted to the cranium with respect to ensuing brain pathology. A summary of the findings of these studies are shown in Table 2.3. Isolated blast injury to the brain requires the necessary preparatory steps to protect the thorax from the primary blast wave. Krohn *et al.* (1941) tested 21 rabbits using freefield blast tests, with five specimens having their thorax enclosed in either an iron box or plaster. Three of the five specimens survived these blasts, which were at levels considered lethal for pulmonary injuries (>600 kPa). One of the fatalities was most likely due to a broken neck. Many of the specimens were immediately apneic with no signs of thoracic damage. Some specimens presented with lesions or contusions, while others appeared to have no macroscopic damage. Clemedson and Pettersson (1953) evaluated the blast wave impact of plastic explosive containing 3-4 grams of Pentaerythritol tetranitrate at a standoff distance of 110 cm (~1000 kPa) upon 18 rabbits with thoracic protection from a steel cylinder. All specimens survived blast injury and the authors concluded that blast

loading caused no cerebral concussions. Again, short-lasting apnea was seen in most specimens without any lung injury. More recently, Cheng *et al.* (2010) placed rats in aluminum boxes with only their heads exposed to a free field blast. Thirty rats were exposed to levels that were well above the 50% lethality risk for pulmonary injury for small animals (White 1961), 400 kPa compared to 200 kPa. Twenty-one of those specimens survived. Sixty more rats were exposed at levels near the 50% lethality risk for pulmonary injury or lower (200 or 100 kPa), with all of the specimens surviving. The majority of the rats in this study presented with immediate apnea. The higher the input pressure level was, the more likely the incidence of apnea. Further, seizures were seen for all of the tested blast levels, and hemorrhaging, contusions, and edema were seen in the 400 and 200 kPa blast levels. Microscopically, the intercellular and vascular spaces in the cortex were enlarged, the nerve fibers were tattered, and the cortex neurons had signs of damage (Cheng 2010).

In an effort to determine fatal blast levels from a blast exposure to the head, Rafaels *et al.* (Rafaels 2010b) exposed 12 rabbits with their thoraces and abdomens protected by a steel cylinder, to various blast overpressures and durations ranging from 170 kPa to 1085 kPa and 3.1 to 6.4 ms. Figure 2.11 displays the risk of fatality determined in that study. For the blast conditions tested, the overpressure needed to produce a 50% risk of fatality from an exposure to head (750 kPa) was more than twice the 50% risk for pulmonary lethality (305 kPa). For all of the tests, no pulmonary injuries were observed; however, apnea was present in the specimens exposed to overpressures above 600 kPa.

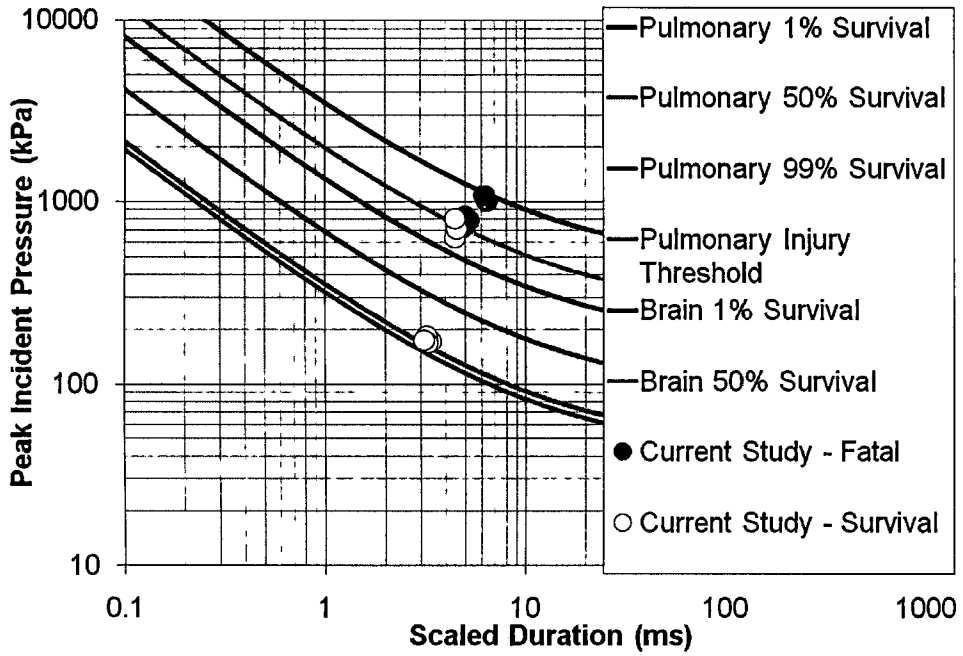

Figure 2.11. Risk of fatality from an isolated blast exposure to the head. (Rafaels 2010b)

Other studies have protected only the thorax and parts of the abdomen from the blast wave, similar to the coverage of the vests for the current troops. In two recent studies, rats wore "vests" that were fashioned from Kevlar and wrapped around the thorax and upper abdomen (Long 2009, Garman 2009). The vest, although not as protective as the iron or steel boxes, did provide protection from lung injury. Without the vest, nearly 50% of the specimens at the blast levels tested did not survive 24 hours. However, with the vest, at the same blast levels, all of the specimens survived (Long 2009). At the most severe blast condition, hemorrhaging and extensive necrosis was common, as was cortical cell loss and gliosis. In the moderate condition, the only injury that could be seen was axonal degeneration (Long 2009). The second study which exposed the specimens wearing vests to higher levels of blast, just above the 50% lethality risk from pulmonary injury, had approximately 75% of the specimens survive (Garman 2009). Axonal

degeneration and microglial/macrophage activity was present. Apnea was seen in all of the specimens from the Long *et al.* (2009) study, and approximately 25% of the specimens from the Garman *et al.* (2009) study.

In another study, pigs were dressed in a lead and foam lined vest that covered the chest and upper abdomen (Bauman 2009). The blast levels tested in this study were just below the 50% lethality risk for pulmonary injury for large animals (Rafaels 2010a). All of the specimens survived; however, unlike the previously mentioned studies with similar blast severity levels, this study did not find any specimens with immediate apnea. Although other signs of brain injury did exist, such as axonal degeneration, vasospasm, gliosis, and neuronal degeneration (Bauman 2009), nonetheless, existing research strongly suggests that the fatality level for brain injury is higher than that for pulmonary injury. Therefore, the body must be protected to evaluate the full spectrum of blast brain injuries.

Table 2.3. Summary of blast brain injury studies with an isolated exposure to the head. (HE = high explosive)

Study	Animal	Exposure	Protection	Orientation	Peak Overpressure	Duration	Findings
Krohn 1941	Rabbit	HE	In iron tube, head unprotected		607-1124 kPa		Cerebral lesions, neurological deficit, apnea, thorax and abdomen uninjured
Krohn 1941	Rabbit	HE	Thorax in plaster of Paris tube, head unprotected		703 kPa		Immediate apnea, heart rate dropped, no thoracic injury
Clemedson 1953	Rabbit	HE in blast chamber	In steel tube, head unprotected		981-1324 kPa		Apnea, no cerebral concussions, no lung damage
Cheng 2010	Rat	HE	In aluminum box, head exposed	Dorsal aspect of head exposed	100-400 kPa	0.25 ms for 400 kPa	69% experienced apnea. 73% experienced seizures. Brain contusions, lacerations, hemorrhages, and hematomas at higher blast levels. Edema seen at all levels. Enlarged intercellular and vascular spaces in cortex. Increased permeability of cortex neurons.
Rafaels 2010b	Rabbit	Compressed air shock tube	In steel tube, head unprotected		170-1085 kPa	3.1-6.4 ms	Apnea present at levels >600kPa. Fatal at levels >725kPa. Brain hemorrhaging present in all fatal cases.
Long 2009	Rat	Compressed air shock tube	With and without Kevlar vest	Body perpendicular to shock tube	114-147 kPa		Immediate apnea for all specimens. Bradycardia and hypotension for all levels, however, improved with vest. Cortical cell loss, gliosis, hemorrhage and necrosis at highest blast level. Axonal degeneration for all but the lowest blast level. Cognitive deficit.

Study	Animal	Exposure	Protection	Orientation	Peak Overpressure	Duration	Findings
Garman 2009	Rat	Compressed air shock tube	Kevlar vest	Body perpendicular to shock tube	241 kPa	4 ms	Apnea, axonal degeneration, neuronal degeneration, macrophage production
Bauman 2009	Pig	Explosive driven shock tube	Lead and foam lined vest	Body perpendicular to shock tube, for EEG only head was placed in shock tube	172 kPa	~12 ms	Transient EEG power shift, constricted cerebral arteries, axonal degeneration, gliosis, increased neuronal permeability, myelin injury

2.4.3.4 Clinical Tools for Blast Brain Injuries

Many survivors of blast exposures may appear outwardly unscathed, but subsequently experience headaches; disturbances of vision, memory, and concentration; and behavioral changes (Trudeau 1998, Okie 2005, Hagerman 2008). These symptoms can be attributed to TBI, but also to PTSD. This overlap of symptoms and the lack of definitive selection criteria diagnosing blast brain injury make it difficult to distinguish between blast TBI and a psychiatric disorder (Ling 2009). The correct diagnosis is important because it affects the treatment strategy, medical costs, and stigma associated with the disability.

While histology and immunohistochemistry are important research tools, they may are not equally useful in clinical settings for they require tissue samples for examination. Therefore, it is important to discover a clinically relevant technique to determine if a correlation exists between the microscopic results and the clinical tool.

As mentioned in Section 2.4.3.2, serum and cerebrospinal fluid markers can be an effective tool for triaging and managing injuries. However, the biological mechanisms, and consequently, the biomarkers for blast brain injury are still unknown. The current markers available from traditional TBI do not appear to be specific or sensitive enough even for traditional TBI (Svetlov 2009b).

Medical imaging techniques can provide structural, functional, and metabolic information about the brain to the physician. Computed tomography (CT) imaging is sensitive to fractures, edema, and large collections of blood (Laughlin 1998). Additionally, CTs are useful for finding fragments and shrapnel that have been buried in the body from the blast. However, CT scanners expose patients to radiation and have not been shown to clinically diagnose mild TBI. Positron Emission Tomography (PET) has

been used for over 30 years to image glucose metabolism in the brain, which is thought to parallel synaptic function; although for traditional mild TBI, it has not produced consistent results. Research into new radioligands may provide useful biomarkers for imaging TBI (van Boven 2009).

Magnetic resonance imaging (MRI) has been used extensively for brain imaging. Like the CT, traditional MRI techniques are good for fractures and large areas of bleeding, but show enhanced contrast for soft tissues relative to CT. Specialized MR sequences do show some promise. They have been shown to have increased sensitivity for nonhemorrhagic contusions and shearing injuries, and detect cerebral microhemorrhages (Benzinger 2009). However, these measures have had little correlation to long term outcomes in traditional TBI (Hughes 2004). Diffusion tensor imaging (DTI) and functional MRI (fMRI) have shown the most promise as effective imaging techniques for blast brain injuries. DTI assesses white matter tract lesions, which have been associated with changes in cognitive speed (Benzinger 2009). Several studies with DTI and blast TBI have preliminarily shown that DTI can distinguish between blast TBI and traditional TBI (Benzinger 2009, Cassels 2009); however, other studies saw no significant differences (Levin 2009, 2010).

fMRI measures the changes in blood flow during task-driven cortical activation or evaluates spontaneous connections between various cortical regions when the brain is at rest. Although some studies are in progress with this technique (Carr 2009), no results have been published. Though some of these MRI techniques have great promise, there are currently no MRI scanners available in field hospitals, and victims who have been

exposed to fragments and shrapnel, a likely occurrence for a blast victim, cannot use these MRI techniques.

In contrast, measuring the electrical activity of the brain is a promising, relatively inexpensive, noninvasive clinical tool for blast brain injuries. The temporal resolution of the brain activity using electrophysiological techniques is vastly superior to PET and fMRI (Arciniegas 2005). Patients with a history of blast concussion have demonstrated electroencephalographic (EEG) changes (Trudeau 1998, Cernak 1999b), perhaps suggesting a mild TBI. Furthermore, animal studies have also displayed EEG signal changes after a blast exposure (Krohn 1942, Cramer 1949, Clemedson 1956c, Axelsson 2000, Bauman 2009). These studies show that blast can affect the brain's normal electrical activity.

Sensory evoked potentials (EPs), specific techniques of measuring the brain's electrical activity, can reflect the neurophysiologic processing along the sensory pathways from sensation to primary sensory cortex. One significant advantage of short-latency EPs over other electrophysiological measures is that they can be performed on subjects in many states of wakefulness: awake, under anesthesia, or in a coma (Arciniegas 2005). Changes in the EP signals can indicate an injury along the sensory pathway being tested. Amplitude changes in the signals can result from damage to the nerve structures (Bartl 1982). Latency changes can result from defects or injuries to the myelin or from damaged axons (Bodis-Wollner 1982), as is found in blast brain (Saljo 2000, 2002a, Bauman 2009, Svetlov 2009a). After a blast exposure, the hearing and visual sensory systems are frequently impaired. In a study of 62 patients with blast-related TBI, 85% of the patients had sensory impairment in either hearing or vision (Lew

2009). Histological studies of rats exposed to blast demonstrated significant pathologic changes along the optic tract and visual pathways (Petras 1997). Injuries along the auditory pathway have also been demonstrated by delays in peak latencies and temporary and permanent threshold shifts in brainstem auditory evoked potentials (BAEPs) after blast exposure (Pratt 1985). Additionally, the occipital lobe and the brainstem are frequent areas of hemorrhaging after blast (Krohn 1941, Bauman 1997, Knudsen 2003, Saljo 2008). The types of injuries that induce changes to EPs result from injuries to the visual and auditory systems that are already seen in blast exposures. Therefore, visual evoked potentials (VEPs) and BAEPs will be used in this study to compare the results from the clinical tool to the pathological and immunohistological results, hopefully to help differentiate physical from psychological brain injury.

2.5 Injury Thresholds/Risks

Injury risk values or functions provide a useful tool for designing protective equipment, producing test methodologies and surrogates for injury risk, and researching injury mechanisms. The risk assessments define a magnitude of loading which produces a specific type of injury severity and/or risk.

2.5.1 Injury Thresholds/Risks for Brain Injury

The most widely used assessments for blunt head injury risk are the Gadd Severity Index (GSI) (Gadd 1966) and the Head Injury Criterion (HIC) (Versace 1971). These criteria are based on the Wayne State Tolerance Curve (WSTC) (Lissner 1960) which was based on animal concussions and cadaveric skull fractures from an impact with a flat, rigid surface. These injury criteria are based on linear acceleration alone and cannot distinguish between the different types of head injuries that can occur, such as skull

fractures, subdural hematomas, or diffuse axonal injuries (Deck 2008). Although the Generalized Acceleration Model for Brain Injury Threshold (GAMBIT) combines linear and rotational accelerations to determine threshold injury (Newman 1986), a more sophisticated criterion that represents the rate of change of kinetic energy, which includes linear and rotational accelerations, was created called the head impact power (HIP) (Newman 2000). However, HIP does not predict injuries from rotational injuries well (Kleiven 2007). Although criteria exist for pure angular rotation (Ommaya 1971), it is unlikely that real life loading conditions are strictly translational or rotational (King 2003). Moreover, the current head injury criteria also use global measures of head acceleration, whereas the high rates and relatively low momentum transfer of blast waves produce more localized injuries, at least for pulmonary blast injuries (Bass 2008). The accelerations alone may not be an adequate parameter to correlate with blast brain injury. Figure 2.12 illustrates the data used to generate the WSTC, as well as injurious high rate impacts that fall well below the head injury tolerance curves. In order to compare the high rate impacts with the relatively slow rate impacts on the WSTC, the bulk accelerations of the high rate impacts were used, which may not be appropriate. Finite element modeling of a blast exposure to the head produced much higher peak accelerations of the head (~1200 g) than are represented on Figure 2.12 (Panzer 2010). The accelerations resulting from a blast exposure, however, are more wavelike and do not act as a rigid body, which is assumed in the WSTC. No current blast brain injury criteria exist, and the currently available head injury criteria used for automobile and football impacts may not be appropriate for the loading conditions experienced in blast exposures.

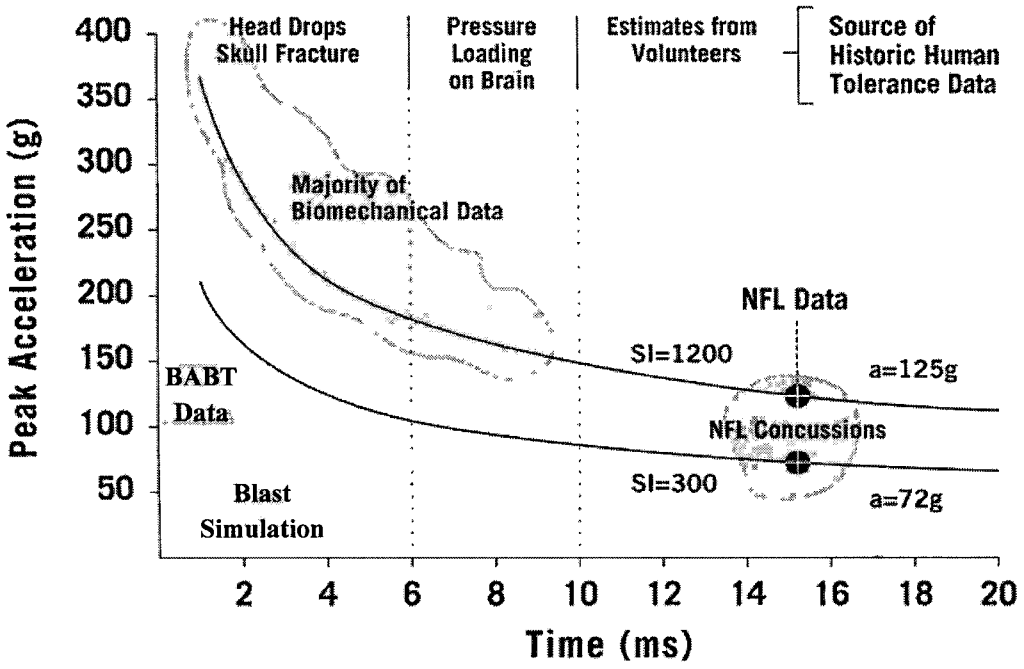

Figure 2.12. WSTC for head injuries (adapted from Pellman 2003). The tolerance curve is based on peak head acceleration and impact duration for the head impacts. The plot includes high rate injury data points from behind armor blunt trauma (BABT) cases (Bass 2003), and from a simulated blast brain injury study (Moss 2009).

2.5.2 Injury Thresholds/Risks for Blast Injury

Injury risk values or functions provide a useful tool for designing protective equipment, producing test methodologies and surrogates for injury risk, and researching injury mechanisms. The risk assessments define a magnitude of loading which produces a specific type of injury severity and/or risk. Development of an injury risk function for blast lung injury was essential since it has long been considered the chief concern of primary blast. Several injury risk functions have been determined for pulmonary blast injury (Bowen 1968, Dodd 1990, Axelsson 1996, Stuhmiller 1997, Bass 2008, Rafaels 2010a) and for ear drum rupture (Richmond 1989).

Bowen's curves (1968) are a widely used and generally accepted technique for theoretical and experimental blast lung injury assessment. They were derived using a statistical analysis of the blast tolerance of small and large animals to estimate the blast tolerance of humans in several orientations relative to a simple blast field. As shown in Figure 2.13, each lethality curve is assumed to be based on a single, continuous curve valid from positive phase durations of less than a millisecond to more than five seconds.

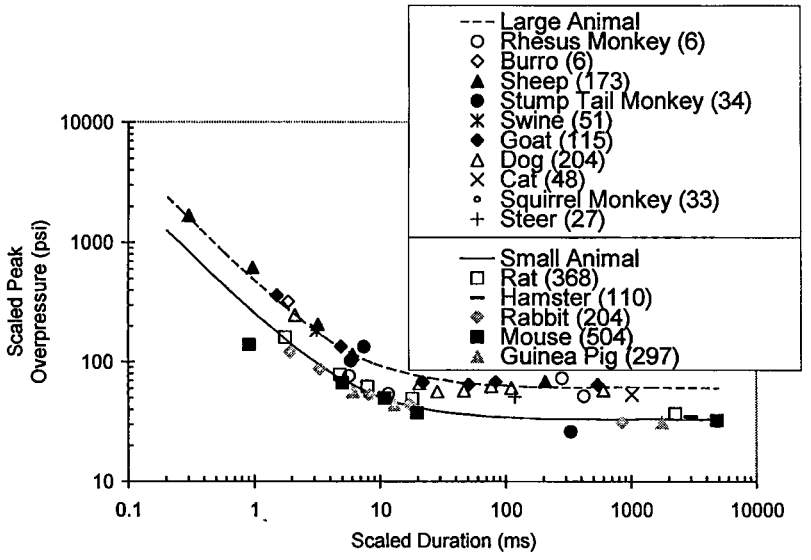

Figure 2.13. Bowen's injury risk curve (number of animals in parentheses) (adapted from Bowen 1968).

Bowen's injury risk curve plots peak overpressure against the duration of the peak pressure and was established using a Probit analysis on the lethality and injury of the animals. This curve gives a probabilistic assessment of the risk of injury for each combination of pressure and overpressure. The pressure/duration theoretical basis for Bowen's tolerance curve has been used by other investigators. For example, Dodd et al used peak pressure versus duration to predict lung injury for multiple exposures (Dodd 1990). Further, the currently held mechanism for lung injury is based on dynamic

pressure changes at tissue-density interfaces (DePalma 2005), which is the basis for Bowen's injury tolerance. Despite the general acceptance of Bowen's curves, there is substantial debate on its validity at short durations less than 14 ms (Richmond, unpublished manuscript 2002; Bass 2008).

In more recent work, Axelsson and Yelverton (1996) developed an injury predictor intended to assess injuries from both classic Friedlander waves and complex waves based on complex wave and free field blast experiments on 177 out of 255 sheep tested by Johnson *et al.* (1993). This model was found to have poor correlation with injury over a range of blast exposures. Later, a similar blast injury assessment model was developed by Stuhmiller *et al.* (1997) using the Lobdell model (1973), a simple, low rate model of thoracic motion with an uncertain validity at blast rates, combined with a cylindrical experimental blast assessment tool. The model includes relations for the stresses developed in the lung tissue owing to blast motion and correlates of the virtual work done by those stresses with observed lung contusion and damage. Stuhmiller *et al.* (1997) state that over 1100 animals were used in the development of the model; however, the range of input overpressure and duration are not explicitly stated. The authors recognize model limitations in internal wave propagation, interaction with internal organs, and viscoelastic forces. Moreover, the exact tensile strengths for lung tissue are assumed in this injury assessment and are still not known. Further, this model may have difficulty reproducing accurate thoracic responses across a wide range of pressure excitation frequencies, as the model does not account for the viscoelastic response of the human thorax (Kent 2003).

Two recent studies determined the risk of fatality from primary blast for short durations less than 30 ms and long durations greater than 10 ms in a similar fashion to

Bowen's injury criteria using existing animal experimental studies. The selected experiments were split into the two categories because they exhibit two different injury mechanisms. For a given injury risk, short duration blasts involve smaller momentum transfer and more localized pulmonary injury. In contrast, longer duration blasts produce more overall momentum transfer and more diffuse pulmonary injuries (Bass 2008). However, both analyses determined injury risk as a function of blast overpressure and duration. New curves were developed for risk of fatality and risk of pulmonary injury as shown in Figure 2.14. This assessment is limited to simple, Friedlander blast waves with peak pressure and positive overpressure phase duration as the independent variables. The models were found to be a good statistical fits to the animal experimental data (Bass 2008, Rafaels 2010a).

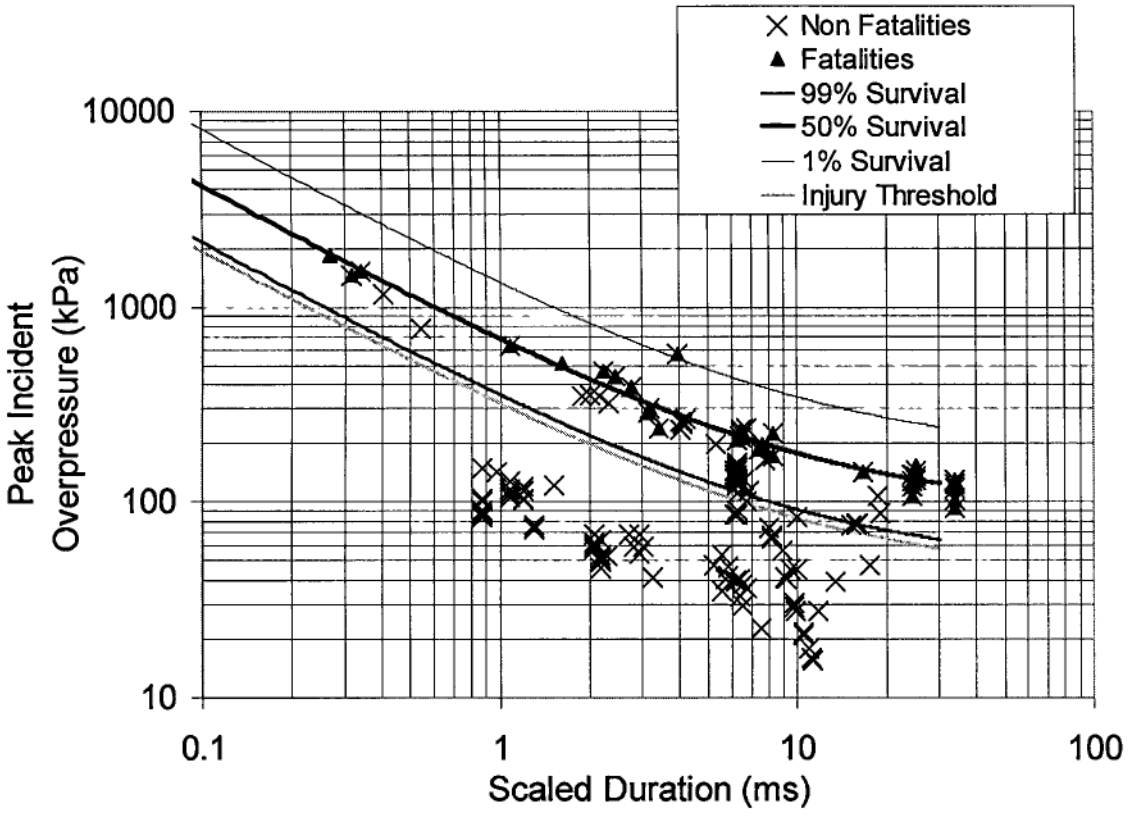

Figure 2.14. The re-evaluated pulmonary blast injury risk curves (Bass 2008).

Many researchers in the field recognize the importance of determining an injury threshold or risk function for blast brain injuries (Saljo 2000, Leung 2008, Moore 2008), but there is only one study available that addresses this issue (Rafaels 2010b). Rafaels *et al.* used a limited number of rabbit experiments to determine a fatality risk function from blast exposures to the head (Rafaels 2010b). While this study provided an upper bound for blast brain injury tolerance, it did not address mild traumatic brain injury. Therefore, the major goal of this work is to determine an injury risk function for blast using the overpressure and duration as has been done previously for pulmonary blast injuries.

Chapter 3. METHODOLOGY

3.1 Blast Wave Exposure

3.1.1 Generation of Shock Wave

A shock tube was used to simulate the explosive threats and to expose the specimen to the blast overpressure only. Bass *et al.* (2008) indicate that there is no statistical difference in injury outcome for the lungs between shock tube studies and free field studies for positive phase blast durations less than 30 ms. The shock tube uses a high pressure gas to create the shock wave as opposed to an explosive. The high pressure driver gases used in our shock tube are helium or air depending on the desired duration. The low pressure gas, or driven gas, is air.

A schematic of the shock tube can be seen in Figure 3.1. The shock tube consists of a horizontally mounted, 8 5/8-inch-diameter, circular steel tube. This tube is divided into a compression chamber, or driver section, separated from a 41-inch expansion chamber, or driven section, by a Mylar diaphragm (DuPont Co., Wilmington, DE, USA). The magnitude of overpressure at the end of the shock tube is determined based on the number of 0.010" thick membranes of Mylar. The duration can be varied by changing the length of the driver section and/or the high pressure gas used. The shock wave is initiated by filling the driver section of the shock tube with the high pressure gas until the Mylar diaphragm bursts. Once the diaphragm has ruptured, a compression wave enters into the driven gas, which then becomes a shock front. The shock wave continues to travel to the end of the tube. Three piezoelectric pressure gauges (Model 8530B, Endevco, San Juan Capistrano, CA, USA) are flush mounted at the end of the shock tube to measure the incident pressure of the shock tube.

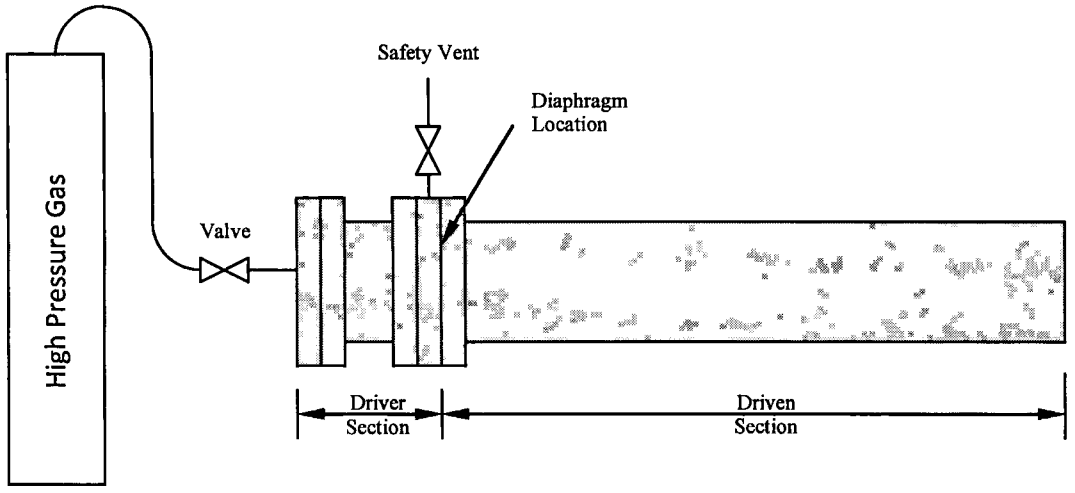

Figure 3.1. Schematic of shock tube.

3.1.2 Blast Brain Injury Model

A ferret model has been chosen for these blast experiments. The ferret model is similar to the human in the composition of the brain and its gyrencephaly. The gray to white matter ratio in the ferret neocortex and cerebellum are similar to those found in primates (Zhang 2000), which may be an important factor in the neurotrauma from blast effects. As stated in Section 2.4.3.4, many of the current diagnostic symptoms of mild TBI include cognitive and behavioral changes. Consequently, future work for blast brain injury must include neurobehavioral work, and the ferret learns tasks and behaviors readily without pretraining (Rabe 1985). In fact, for behavioral studies, the ferret model is preferred over felines, canines, and some primates (Baum 1988).

Another advantage to the ferret model is that the ferret's eyes have a fovea/area centralis. Previous reports indicate that abnormal oculomotor function can be found among persons who suffered a blunt injury resulting in moderate to severe TBI (Mulhall 1999, Suh 2006a, Suh 2006b, Glass 1995, Kraus 2007). The clinical data, including preliminary results from a clinician who treats blast TBI victims in a Veterans Affairs

hospital, suggests that abnormal oculomotor function may be a reliable marker of primary blast TBI (Capehart, personal communication). Therefore, an appropriate model of primary blast TBI should utilize an animal model in which this abnormal oculomotor function can be reproduced. Previous animal models that have been used for blast research including rabbits, pigs, and sheep are incapable of producing some of the visual and oculomotor disturbances seen clinically. These factors and its size, ease of animal care, and wide availability make the ferret the preferred model for blast brain injury when compared with rodents and rabbits.

3.1.2.1 Live Animal Tests

Sixty-seven (67) male ferrets (*Mustela Putorous Furo*) were used as blast specimens in this test series, and three ferrets were used as controls. The average ferret mass was 1.21±0.24 kg. Table 3.1 provides the body mass and head geometry for each ferret. Prior to testing, the experimental protocol was approved by the University of Virginia Animal Care and Use Committee. Ferrets were initially given glycopyrrolate (Robinul, Baxter Pharmaceutical, Deerfield, IL) (0.1 mg/kg body weight) subcutaneously as a pre-anesthetic to diminish build up of secretions in the pulmonary system. They were then anesthetized with an initial bolus intraperitoneal injection of urethane (Urethane, Sigma Aldrich, St. Louis, MO) (1.5 g/kg body weight of a solution containing 0.5g/ml urethane). A maintenance dose of about 1/10th the original dose was administered intravenously as needed based on jaw tension and/or toe pinch response. The specimens' heart rate, pulse oximetry, and electrocardiogram were continuously monitored, with the exception of approximately 5 minutes surrounding the blast exposure. During the blast, only the electrocardiogram was monitored. Body temperature was controlled using

heating pads or blankets. Venous lines were placed in the cephalic veins and/or tail vein to facilitate the drawing of blood at various stages of the experiment and to provide locations for the administration of medications. Additionally, an endotracheal tube was inserted into each specimen to allow for easy airway access should the specimen become apneic. In the event of post blast apnea, supportive therapy included supplemental oxygen, ambubag ventilation and one or more administrations of doxapram (Dopram-V, Ft. Dodge, Overland Park, KS) 2 mg/kg as a respiratory stimulant.

Table 3.1. Mass and head geometry of live ferrets

Specimen #	Mass (kg)	Head Circumference (cm)	Head Length (cm)	Head Width (cm)
LF01	1.5	-	-	-
LF02	1.2	15.0	8.0	6.0
LF03	1.3	15.5	8.5	7.0
LF04	1.3	16.0	8.0	7.0
LF06	1.1	16.0	8.0	6.5
LF07	1.3	16.0	8.0	6.5
LF08	1.3	16.5	8.5	6.5
LF09	1.0	15.5	8.0	5.5
LF10	1.0	15.0	8.0	5.5
LF11	1.0	14.6	8.3	6.0
LF12	1.0	-	-	-
LF13	1.1	14.0	7.5	5.5
LF14	1.2	14.8	8.0	6.0
LF15	1.2	14.5	7.5	5.5
LF16	0.9	14.5	7.5	5.5
LF17	1.0	15.0	8.0	6.0
LF18	1.1	14.5	8.3	6.0
LF19	1.0	14.5	7.0	5.3
LF21	0.9	13.5	7.0	5.5
LF22	1.0	15.0	7.5	5.0
LF23	1.0	14.0	8.0	6.0
LF24	0.9	14.0	7.5	6.5
LF25	0.8	14.0	7.5	6.0
LF26	1.0	15.0	8.0	6.0
LF27	-	-	-	-
LF28	1.0	15.0	7.5	7.5
LF29	1.0	13.5	7.5	5.0

Specimen #	Mass (kg)	Head Circumference (cm)	Head Length (cm)	Head Width (cm)
LF30	1.1	14.0	8.0	6.0
LF31	0.9	14.0	7.5	6.5
LF32	0.9	14.0	7.5	6.0
LF33	1.0	14.5	9.0	5.5
LF34	0.9	15.0	7.5	6.5
LF35	1.0	14.5	8.0	6.5
LF36	0.9	14.5	7.5	6.5
LF37	1.0	14.5	8.0	6.0
LF38	0.9	15.0	7.5	5.5
LF39	1.0	14.0	8.0	5.5
LF40	1.1	15.0	8.0	6.0
LF41	1.4	16.0	8.0	6.5
LF42	1.4	16.0	7.5	7.0
LF43	1.4	16.0	7.5	7.3
LF44	1.5	15.5	8.0	7.0
LF45	1.4	16.0	8.3	7.5
LF46	1.4	16.0	7.5	6.0
LF47	1.4	14.5	7.5	6.0
LF48	1.4	14.5	8.5	6.5
LF49	1.4	15.5	8.0	7.5
LF50	1.2	15.0	8.0	6.5
LF51	1.1	15.5	8.0	6.0
LF52	1.3	15.5	8.0	6.5
LF53	1.3	16.0	8.0	6.0
LF55	1.3	16.5	8.5	6.5
LF56	1.5	16.3	8.5	7.5
LF57	1.5	15.5	8.0	6.5
LF58	1.6	16.5	8.5	8.0
LF59	1.4	16.0	8.5	7.0
LF60	1.4	17.5	8.5	7.5
LF61	1.5	17.0	8.5	8.0
LF62	1.4	16.0	9.0	6.3
LF63	1.6	16.5	8.5	7.0
LF64	1.6	16.0	8.0	6.5
LF65	1.7	16.0	8.0	7.0
LF66	1.5	17.0	835	7.5
LF67	1.6	16.0	8.0	7.0
LF68	1.6	17.3	8.0	7.5
LF69	1.5	17.0	8.5	7.0
LF70	1.6	17.5	8.0	6.5

Specimen #	Mass (kg)	Head Circumference (cm)	Head Length (cm)	Head Width (cm)
Controls				
LF05	1.2	16.0	8.0	7.0
LF20	1.0	14.0	7.5	6.0
LF54	1.4	15.5	8.0	7.0

3.1.3 Blast Wave Exposure to the Head

Since pulmonary and intestinal injuries occur at lower peak overpressures than brain injury as described in the Section 2.4.3.3, to examine the higher severity brain injuries from what would otherwise be fatal pulmonary or abdominal injuries, the thorax and abdomen must be protected. The fact that military personnel generally wear protective vests that decrease the blast threat to the thorax and abdomen provides further real world support for using an isolated exposure condition (cf., Wood 2010). Additionally, for the lower severity brain injuries, isolating the exposure to the head allows for the examination of the effects of the blast on the head without complications of referred effects from pulmonary or abdominal injury.

To isolate the blast exposure to the head, the thorax and abdomen was placed into a protective fixture. A schematic of the protective cylinder is shown in Figure 3.2. The protective cylinder that was used is ½-inch thick steel tubing with a diameter of 8 5/8-inch. Vinyl nitrile closed cell foam (America Mat™, Soundproofing America, San Marcos, CA, USA), 2-inches thick, was used to close the open end of the cylinder. The cylinder was secured to the test stand to prevent translation of the entire fixture. A piezoelectric pressure gauge (Model 8530B, Endevco, San Juan Capistrano, CA, USA) was flush mounted in the cylinder to determine the amount of pressure inside the

protective cylinder. The test fixture was then secured to prevent translation resulting from the blast exposure.

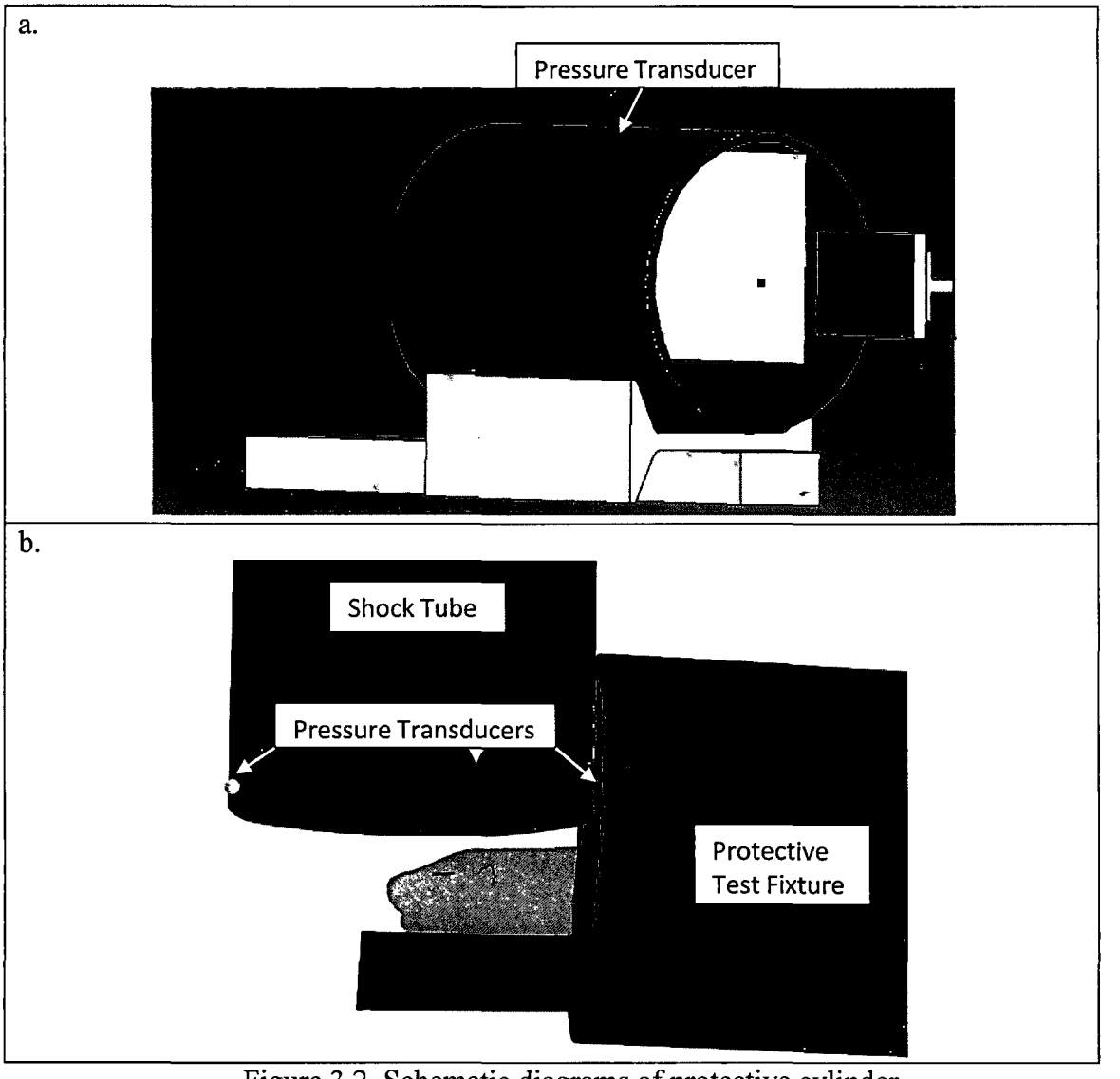

Figure 3.2. Schematic diagrams of protective cylinder.

In addition to isolating the blast wave exposure to the head, the global head motion must be reduced. Diffuse brain injuries can occur from inertial forces as a result of rapid head translational or rotational motions without direct impact (Ommaya 1975, Smith 2000). The blast wind that exits the shock tube can cause gross body motion which may include translational or rotational motions. These large motions can also create fatal neck

injuries for longer duration blast events, which would obscure the brain injuries being studied. Reducing global head motion is important for limiting the acceleration injuries that may result from the large momentum, blunt type injuries, allowing for an analysis of the blast brain injuries from the low momentum blast pressure wave that is unaffected by large amplitude rotation events.

To reduce global head motion, the head and neck were supported and secured. However, head motion cannot be entirely eliminated without the increased likelihood of the securing techniques themselves causing head injury. Therefore, the head support fixture used allows limited movement without much added weight or blast protective capabilities. A Kevlar (DuPont Co., Wilmington, DE, USA) collar was placed around the neck of the specimens to prevent neck motion and injury. The head was supported on a 5-inch-long head support extended from the protective cylinder to secure the head and prevent motion. The head was secured to the head support using a high tensile strength, waterproof and oil resistant medical tape (Kendall Wet Pruf ® Tape, Covidian, Mansfield, MA, USA). A schematic of the head and next supports are shown in Figure 3.3. The center of the head of the specimen was placed approximately 40 mm from the opening of the shock tube. High speed video (Redlake HG-100K, Tallahassee, FL, USA or Phantom v5.0, Wayne, NJ, USA) was taken to examine the amount of the head motion present in each test.

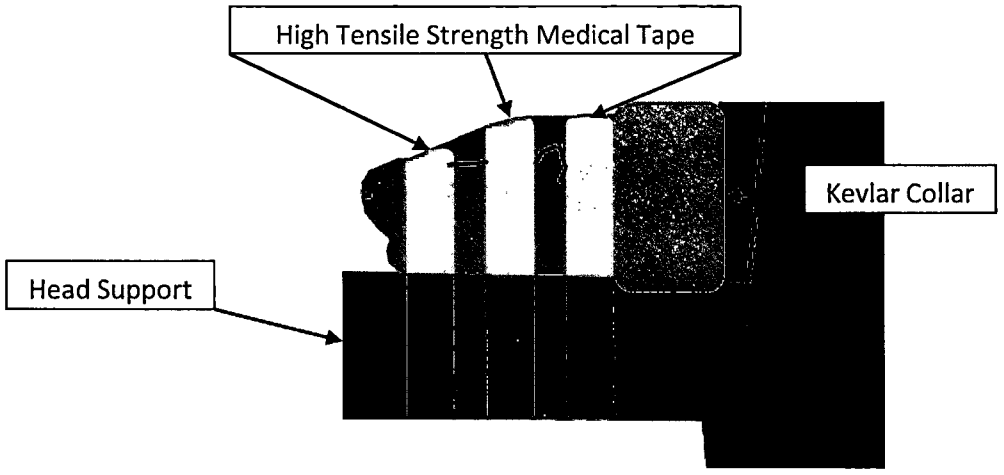

Figure 3.3. Schematic of the head and neck supports.

Owing to physical constraints, the ferret position relative to the tube entrance in the direction of the propagation of the shock had a standard deviation value of ±11 mm across the dataset. Since the blast wave decays as it moves farther away from the source, a correction to the measured overpressure and duration was made. Additionally, reflections from the test fixture and specimen often made the duration of the blast exposure difficult to determine, as shown in Figure 3.4. To correct for the effect of this variation on the incident overpressure and the reflection waves from the fixture and specimen, a finite element blast model was used to provide overpressure and duration relative to the end of tube conditions (Panzer 2010). The correction for this effect was small, averaging 0.6±0.4% of the measured incident peak overpressure and 8.0±5.1% of the measured positive phase duration, as seen in Figure 3.5.

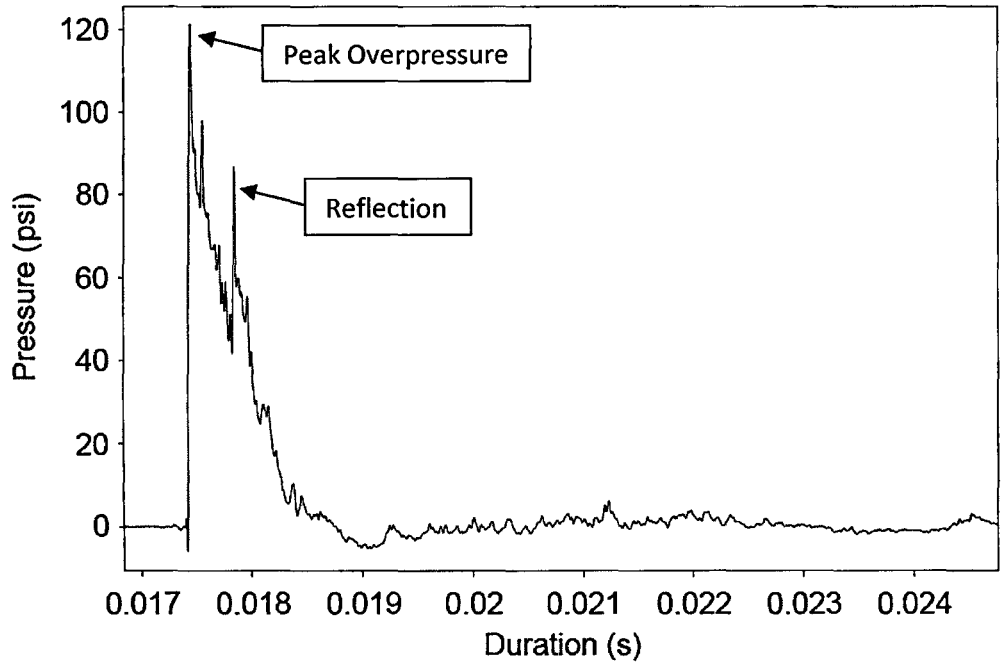

Figure 3.4. Pressure measurement from the end of the shock tube with a reflection wave from test LF70. The reflection results from the blast wave reflecting back from the test fixture and specimen.

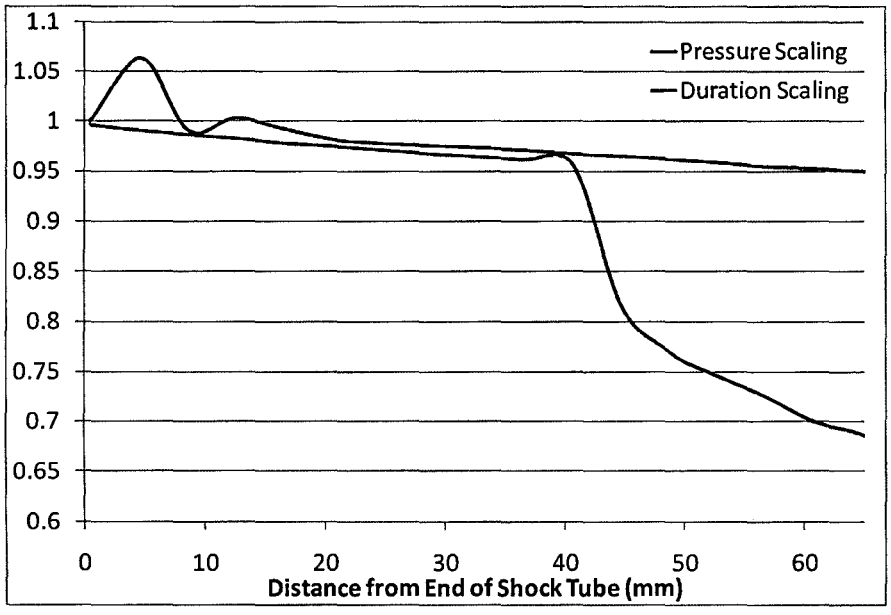

Figure 3.5. The correction to the measured pressures and durations at the end of the shock tube. The figure displays the percentage of the overpressure and duration that is maintained at various distances from the end of the shock tube.

3.2 Post-Mortem Examination of Live Animal Tests

Most specimens were euthanized five hours after exposure; however, if the specimen's clinical condition deteriorated despite resuscitation prior to the five hour time point, that specimen was euthanized at that time. The procedure used in euthanizing is as follows. First, to reduce clotting during the perfusion fixation technique, the specimen was injected with 500 units of heparin (Heparin sodium, APP Pharmaceuticals, LLC, Schaumberg, IL, USA). Then, a thoracotomy was performed to gain access to the heart after which the euthanasia solution (VirBac AH, Inc, Ft. Worth, TX, USA) was administered. From an incision in the left ventricle, a cannula was inserted into the ascending aorta, and the specimen was perfused with saline at physiological rates of flow out of the right auricle. Following the saline flush, the specimen was perfused with approximately 1 L of 0.1M phosphate buffer containing 4% paraformaldehyde (Electron

Microscopy Sciences, Hatfield, PA, USA). After perfusion fixation, the organs were examined macroscopically for gross changes and immersed in the paraformaldehyde solution for further fixation.

3.2.1 Evaluation of the Brain Tissue

3.2.1.1 Macroscopic Evaluation

A macroscopic analysis of the brain injury sustained by the blast included an evaluation of brain hemorrhaging. During the extraction of brain tissue, photographs were taken of the brain and cranial vault. The surface area of the hemorrhages and of the entire brain and cranial vault were calculated using ImageJ (Rasband). The area of the hemorrhages was divided by the total area of the brain and cranial vault to obtain a normalized area of hemorrhaging. The brains were then graded into four severity levels based on the normalized area of hemorrhaging: none (no visible bleeding), mild (< 3%), moderate (3% to 10%), and severe (> 10%).

3.2.1.2 Histological Preparation

To prepare the tissue for the various histology, the brains were immersed in the paraformaldehyde solution at 4°C for 7 hours in the first 8 eight specimens and for 16 hours in the remainder after perfusion fixation and extraction. They were then placed in 0.1 M phosphate buffer containing 20% sucrose also at 4°C. The sucrose solution was replaced the following day. The brains were shipped in the second sucrose solution within 7 days of extraction to FD Neurotechnologies, Inc. where the brains were rapidly frozen and stored at -75°C.

Serial sections were cut coronally on a cryostat through the whole cerebrum (approximately corresponding to the rat brain from bregma 5.64 mm to -9.00 mm , cf.

Paxinos & Watson 2007). Every 1st, 2nd, 3rd, 4th, 5th, 6th and 7th section of each series of 25 sections (interval: 1.0 mm) was collected separately in section storage solution (FD Neurotechnologies, Baltimore, MD, USA) to be processed according to the procedures outlined below. In addition, serial sections (2 sections per set, 7 sets per brain) were also collected from the brainstem and the cerebellum approximately at the levels corresponding to the rat bregma -10.20 mm and -10.80 mm, respectively. All free-floating sections were stored at -20°C before further processing.

The sections of the 1st set were processed to analyze neuronal death. They were mounted on gelatin-coated microscope slides and stained with fluoro-jade B (Histo-Chem, Jefferson, AR, USA). Fluoro-jade B is an anionic fluoroscein derivative that specifically stains degenerating neurons (Schmued 2000). It is considered a valuable tool for examining neuronal death in traditional TBI, and has been shown to be sensitive to the severity of the injury (Anderson 2005).

The sections of the 2nd set were processed to identify damaged axons with neurofilament alteration, using a monoclonal mouse anti-neurofilament-midsized antibody (clone: RM014.9, Invitrogen, Carlsbad, CA, USA, Cat. #34-1000). RM014 binds to the rod domain of the neurofilament medium chain when there has been a side-arm modification or loss (Marmarou 2005). First, the sections were incubated free-floating in 0.01 M phosphate-buffered saline (PBS, pH 7.4) containing 1% normal horse serum (Vector Lab., Burlingame, CA, USA), 0.3% Triton X-100 (Sigma, St. Louis, MO, USA) and the mouse anti-neurofilament antibody (1:500) for 42 hours at 4°C after inactivating the endogenous peroxidase activity with hydrogen peroxidase. Next, the immunoreaction product was visualized according to the avidin-biotin complex (ABC)

method of Hsu *et al.* (1981) with the Vectastin elite ABC kit (Vector Lab., Burlingame, CA, USA). The sections were incubated in PBS containing biotinylated horse anti-mouse immunoglobin G (IgG), Triton-X and normal horse serum for 1 hour and then in PBS containing avidin-biotinylated horseradish peroxidase complex for another hour. This was followed by incubation of the sections for 3 minutes in 0.05 M Tris buffer (pH 7.2) containing 0.03% 3',3'-diaminobenzidine (Sigma, St. Louis, MO, USA) and 0.0075% H_2O_2. All steps were carried out at room temperature except as indicated, and each step was followed by washes in PBS. After thorough rinses in distilled water, all sections were mounted on slides, dehydrated in ethanol, cleared in xylene, and coverslipped in Permount® (Fisher Scientific, Fair Lawn, NJ, USA).

The sections of 3rd set were processed for β-amyloid precursor protein (β-APP)-immunoreactivity, another marker of axonal injury, according to the method described by Stone *et al.* (2000). β-APP, along with other proteins travel from the neuron down the length of the axon via fast axoplasmic transport in an active, adenosine triphosphatase-(ATP) dependent process involving motor proteins (Ransom 2003a). If there is a disruption to the microtubules, the proteins can accumulate at the site of injury. Antibodies to β-APP have been shown to be a sensitive marker for visualizing the damage to the axonal transport system (Medana 2003). The brain tissue sections were processed for β-APP in the following manner. The sections were placed in 0.1 M citric buffer (pH 6.0) and microwaved at 45°C for 5 minutes after inactivating the endogenous peroxidase activity with hydrogen peroxidase. Following 20 minutes of cooling at room temperature, sections were pre-incubated for 40 minutes in 0.01 M PBS (pH 7.4) containing 10% normal goat serum (NGS, Vector Lab., Burlingame, CA, USA) and 0.3%

Triton X-100 (Sigma, St. Louis, MO). Sections were then incubated for 42 hours at 4°C in PBS containing 1% NGS and the rabbit anti-the C-terminus of the human β-APP (1:2,000, Invitrogen, Carlsbad, CA, USA, Cat. #51-2700). Next, the immunoreaction product was visualized according to the avidin-biotin complex method of Hsu *et al.* (1981) with the Vectastin elite ABC kit (Vector Lab., Burlingame, CA, USA) similar to the RM014 procedure. The sections were incubated in PBS containing a biotinylated goat anti-rabbit IgG, Triton-X and NGS for 1 hour and then in PBS containing an avidin-biotinylated horseradish peroxidase complex for another hour. This was followed by incubation of the sections for 4 minutes in 0.05 M Tris buffer (pH 7.2) containing 0.03% 3',3'-diaminobenzidine (Sigma, St. Louis, MO, USA) and 0.0075% H_2O_2. After thorough rinses in distilled water, sections were mounted on microscope slides, dehydrated in ethanol, cleared in xylene, and coverslipped in Permount® (Fisher Scientific, Fair Lawn, NJ, USA).

To visualize reactive gliosis, a common phenomenon in the central nervous system following tissue damage induced by trauma (Hausman 2000), three coronal sections were processed for glial fibrillary acidic protein (GFAP)-immunohistoreactivity. The three coronal sections were taken from three regions approximately corresponding to the rat brain through Bregma 5.64 mm, -3.72 mm and -7.56 mm (cf. Paxinos & Watson 2007). The sections were incubated free-floating in 0.01 M PBS containing 0.3% Triton X-100, 1% NGS and a rabbit anti-GFAP IgG (1:10,000; DAKO, Carpinteria, CA, USA) for 41 hours at 4°C after inactivating the endogenous peroxidase activity with hydrogen peroxidase. The immunoreaction products were then visualized according to the avidin-biotin complex method similar to RM014 and β-APP and 3', 3'-diaminobenzidine

(Sigma, St. Louis, MO, USA) as a chromogen. After thorough washes, all sections were mounted on microscope slides, dehydrated in ethanol, cleared in xylene, and coverslipped in Permount® (Fisher Scientific, Fair Lawn, NJ, USA).

For microscopic analysis of hemorrhage, several sections of the brain tissue was processed with hematoxylin and eosin (H&E) and leuco-patent blue (LPB) stains. H&E stains nuclei blue and eosinophilic, or mostly basic, structures pink or red. Cytoplasm is eosinophilic and red blood cells stain intensely red. Intense red staining outside of the blood vessels indicates a likely hemorrhage. LPB stains hemoglobin blue, both in red cells and pathologically elsewhere. If blue staining is found in the tissue outside of the blood vessels, it is a sign of hemorrhaging. Two mid-cortical and cerebellar/brainstem coronal sections were taken from eight brains and stained with H&E and LPB. The 40 μm free-floating sections from eight ferret brains were washed in 0.1 M phosphate buffer (pH 7.4) and mounted on 1"x3" Superfrost plus slides. Following defatting in xylene and graded ethanols, sections were stained with H&E and LPB. After dehydration, sections were cleared in xylenes and coverslipped with Permount® (Fisher Scientific, Fair Lawn, NJ, USA).

After the slides from all of the sections were prepared, they were visualized using several different pieces of equipment for microscopy. The sheer volume of slides made the organization of the slides essential; however, it also made blinding of the histological evaluation difficult. The slides with fluoro-jade B were examined with a fluorescence and confocal microscope. The fluorophore was excited by a blue laser and emitted light in the green spectrum on the confocal microscope. A fluoroscein isothiocyanate (FITC) filter was used on the fluorescence microscope. A Nikon TE 2000-E2 microscope

equipped with a Melles Griot Argon Ion Laser System and Nikon D-Eclipse C1 accessories was used to image these slides. Digital confocal images were acquired using a 20×/0.50 DIC M/N2 dry objective and Nikon EZ-C1 software (Nikon Instruments, Melville, NY, USA). All images were acquired using identical gain and aperture size settings on the confocal microscope. The remaining slides were first visualized under light microscopy and then digitally scanned at 40X magnification using an Aperio ScanScope CS slide scanning system (Aperio Technologies, Inc., Vista, CA, USA).

3.2.1.3 Histological Evaluation

The digitized histological slides were further evaluated to quantify the amount of positive staining present. As immunohistochemistry is based on enzyme-linked immunoreactivity, it can be quantitative, similar to enzyme-linked immunosorbent assay (ELISA) tests (Taylor 2006). Many studies have quantified immunohistochemistry by using segmentation or thresholding of grayscale or color images (Matkowskyj 2000). A similar technique was used in this analysis.

The scanned images were converted from the proprietary scanner format to the JPEG2000 format using ImageScope Software (Version 10.2.2.2319, Aperio Technologies, Inc., Vista, CA, USA). Once converted, the images could be loaded into MATLAB® (2009b or 2010a, The MathWorks, Natick, MA, USA). Due to the very large file size, images were loaded into MATLAB® in 3000 x 3000 pixel sections. An indexed image was determined for a section of an image that included positively stained tissue, negatively stained tissue, and no tissue for each stain type. The resulting color map was used for the rest of the analysis. By using an indexed image, the size of the image file was reduced to approximately one-third of the original size, decreasing the

computational time necessary to run any necessary algorithm. Another advantage of creating an indexed image is that it reduces the variation in perceptual color differences, by mapping all of the RGB (red, green, blue) color possibilities (over 16.7 million color variations per pixel) into the size of the map in the indexed image (in our case 100 or 50 color variations per pixel depending on the stain being analyzed).

For the quantitative study, the slice located approximately 8.00 mm inferior to the bregma was surveyed. This location was chosen because it displayed sections from both the cerebrum and brainstem. Also, during the macroscopic evaluation of the brain tissue, hemorrhaging was most frequently observed around the brainstem. Each slide stained for β-APP that was selected for the quantitative study was first analyzed using a MATLAB® code that selected possible injured axon regions within that section based on pixel color and region size and shape. Region size and shape were also included in the automated image analysis since it is considered to produce more reliable results than color or intensity alone (Rojo 2009). Regions of no tissue were also selected based only on pixel color. The areas of the no tissue regions were subtracted from the whole image to determine the total area of tissue in the section. Injured axonal area, as opposed to the number of individual injured axons, was chosen as the measure used in the quantitative study because the area of axonal staining for each axon increased with increasing blast severity levels. Additionally, individual axons may present with multiple positively stained areas. The code for the potential positive axonal areas is shown in Appendix A.

As there was significant false positive staining assessed manually throughout the tissue, the sections of tissue that were selected as having possible regions of injured axons were reanalyzed by hand. Another MATLAB® code was used with similar criteria

as the code used previously; however, the code could be modified to include regions with more or less strict criteria. Two figures were displayed: the first figure was the original, unmodified section; the second was a black and white image of the same section with the regions of possible injured axons highlighted. The figures were linked to allow for an easy examination of both images concurrently. The highlighted regions could be either selected or unselected to include in the final area calculation for the section. The final area selected represented the positively stained injured axons within that section. That axonal area was then divided by the total tissue area determined from the previous MATLAB® code for that section to determine the density of positively stained tissue. This process was repeated for all of the potential sections selected in the first MATLAB® code. To reduce the amount of error, adjacent sections to those sections that were found to contain positively stained axons were also analyzed in this manner.

To determine the approximate error in the evaluation of positively stained axons, three slices of brain were chosen for axonal area determination by hand. Manual evaluations of histology are considered the "gold standard" (Inman 2005). Consultations with a histologist were made during the initial manual evaluations to assure selections of correctly positive stained axons. For the error evaluations, one brain was selected from each of the severity groups: severe, moderate, and mild. The severity groups were chosen based on the density of positive axons. Each 3000 x 3000 pixel section of the three slices of brain was examined to determine the total amount of positive axon area. This total area was compared to the area of the abbreviated analysis to determine the error of the evaluation method for each slice. To provide a more general assessment of the error for the evaluation method, the remaining slices of evaluated brains were placed

in the different severity groups and were assumed to have the same error as the truly calculated error from their group. The errors were then averaged to determine the error of the evaluation method.

The sections of tissue that were stained for GFAP were analyzed using a MATLAB® code that selected positive tissue regions and regions of no tissue within that section based on pixel color. The areas of the no tissue regions were subtracted from the whole image to determine the total area of tissue in the section. The total area of positive staining was divided by the total tissue area to determine the density of activated glial cells in the tissue sample. The code is shown in Appendix A.

The sections of tissue that were stained for LPB were analyzed using a MATLAB® code that selected positive tissue regions based on pixel color and region size. The tissue areas that did not contain hemoglobin were faintly stained making the determination of the total area of tissue in the section difficult. The positive selected regions were reanalyzed by hand to eliminate regions of positive staining from red blood cells in vessels. These areas of hemorrhaging were then examined in the H&E slides for confirmation. The code can be found in Appendix A.

3.3 Evoked Potentials

Using protocols that follow the methods of Forester *et al.* (Forester 1987) and Kelly *et al.* (Kelly 1989), respectively, sensory evoked potentials for the visual and auditory system were taken both prior to and after the blast beginning with LF19. The evoked potentials were recorded with a Viking IV P quantitative electromyography/nerve conduction study system (Nicolet Biomedical, VIASYS Healthcare Inc., Madison, WI, USA).

3.3.1 Visual Evoked Potentials

Flash VEP was chosen as the method by which to record the visual evoked potentials. Although flash VEPs vary across subjects more than other methods of VEP, this method was chosen because it requires very little cooperation from the subject (Odom 2004). Flash VEP was also chosen because the potentials are generated from a larger retinal area (Sherman 1982), allowing for an increase in observable injured areas. Flash VEPs were recorded several times for each specimen. Since there is the potential for variation between subjects, the control VEP response was taken on each subject prior to blast exposure. The VEP was taken again at approximately one hour and four hours post blast to determine any effects on the VEP wave from the blast exposure.

To facilitate the placement of three needle electrodes, the animal's head was first shaved. The active electrode was then placed just anterior to the nuchal crest, the most posterior palpable portion of the skull, along the midsagittal plane. The reference electrode was placed along the midsagittal plane 35 mm anterior to the active electrode. The ground electrode was placed next, just medial of the ear. Figure 3.6 depicts the electrode placement. Finally, the electrode locations were marked so they could be placed at the same locations for subsequent tests.

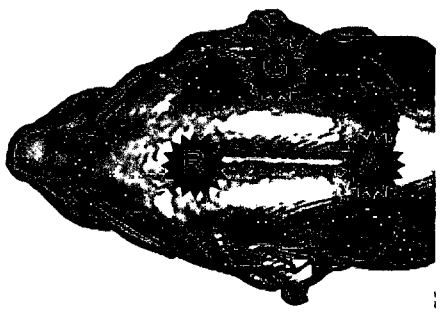

Figure 3.6. Electrode placement for visual evoked potentials test. A – active electrode. R – reference electrode. G – ground electrode.

To perform a test, a Grass Stimulator (Grass Technologies, West Warwick, RI, USA) was used to provide the trigger for a strobe light to flash at a rate of 1.1 Hz. The strobe light was placed at an equivalent-sized opening of a partial Faraday box. The specimen was placed in a prone position inside the box with the head near the opening to reduce unwanted electrical noise from adjacent test equipment. In addition to the mostly opaque box, the overhead lights in the room were turned off during the recording. Each eye was tested one at a time to reduce noise. A piece of opaque medical tape was placed over the untested eye, while the eye to be tested was taped open. After each eye was tested, a binocular VEP recording was performed.

Since evoked potentials have low amplitudes that are difficult to detect in the background wave pattern of an EEG, one hundred responses from the flash stimuli were averaged on the Viking system to obtain the VEP wave. This averaging allows the irregular background rhythms to cancel out so the evoked potentials can be clearly seen (FitzGerald 2007). The evoked potentials were recorded for 400 ms following the light stimulation. Three trials of one hundred averages were taken at each time point (pre blast, 1 hour post blast, 4 hours post blast). The saved waveform data was exported from the VikingDirect software and converted into decimal data for analysis. The converted data was plotted and the tests were randomized for blinded evaluation by a neurologist.

For the initial evaluation, the neurologist evaluated only the individual eye recordings and not the binocular tests. The neurologist identified the peaks associated with the PNP complex, a large positive-negative-positive section of the waveform, by hand. An example of a VEP waveform with the PNP complex identified is shown in Figure 3.7. Once the peaks were identified, the values for the peak amplitudes and latencies were

extracted. The effects of the blast on the positive peak and the width of the complex were examined.

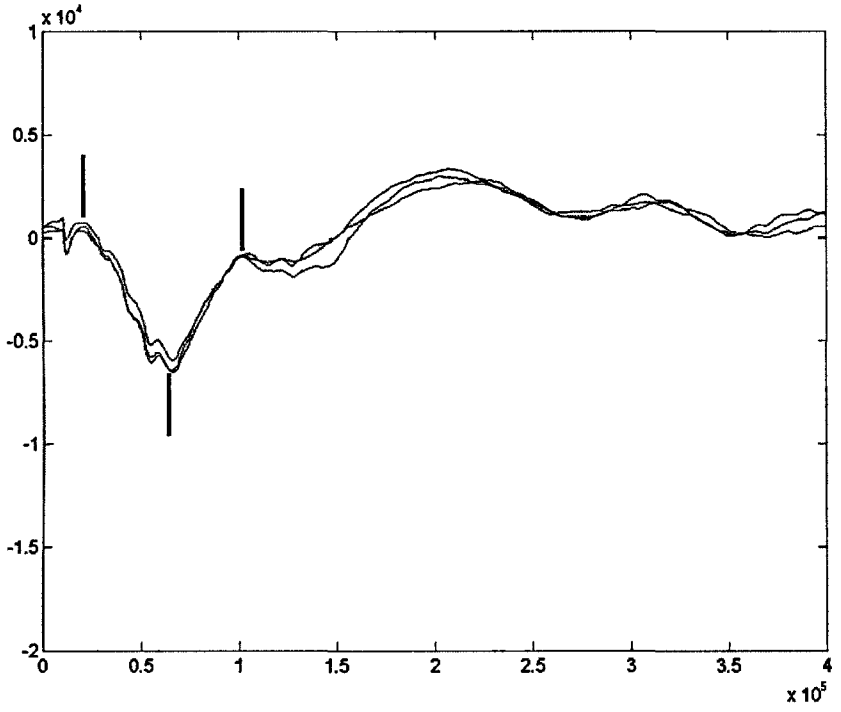

Figure 3.7. Example of flash VEP from this study. The PNP complex has been labeled.

3.3.2 Brainstem Auditory Evoked Potentials

Brainstem auditory evoked potentials follow the sequence of electrical events in the auditory pathway from the cochlea to the inferior colliculus, or, in other words, hearing impairment and brainstem dysfunction. BAEP abnormalities have been reported in traditional TBI and blast TBI patients (Abd Al-Hady 1990, Pratt 1985). BAEPs, like the VEPs, were recorded on each subject prior to blast exposure and again at approximately one hour and four hours post blast to determine any effects on the BAEP wave from the blast exposure.

To measure the BAEP, three electrodes were inserted into the head. The active electrode was placed on the mastoid process, or bony process behind the ear, of the ear to be tested. The reference electrode was placed on the mastoid process of the other ear. The ground electrode was placed at the vertex, or top of the head along the midline. Figure 3.8 depicts the electrode placement. The electrode locations were marked so they could be placed at the same locations for subsequent tests.

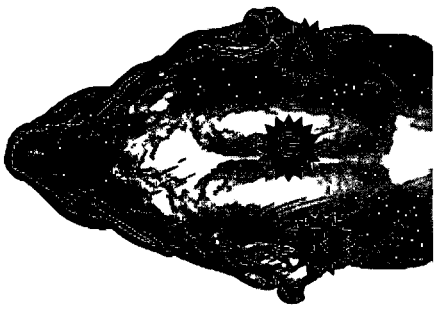

Figure 3.8. Electrode placement for brainstem auditory evoked potentials test. A – active electrode. R – reference electrode. G – ground electrode.

The Viking IV P quantitative electromyography/nerve conduction study system equipped with tubal insert phones (TIP 300, Cardinal Health, Madison, WI, USA) provided the interaural stimulus at a rate of 11.4 Hz. The foam eartips were placed in each ear and easily form-fitted to each subject. The eartips also helped to reduce extraneous noise. The stimulated ear received clicks at 85 dB, while the other ear received white noise at 45 dB. During the test, the specimen was in a prone position. Each ear was tested one at a time to reduce noise. After each ear was tested, a binaural BAEP recording was performed.

The auditory pathway is much shorter than the visual pathway. Consequently, it takes less time for the electrical signal to travel to the appropriate brain center. Therefore, the evoked potentials were recorded for 15 ms following the aural stimulation

compared to 400 ms in the VEP. The amplitude of the auditory signals is also smaller than the amplitude for the VEP, so three trials of one thousand averages were taken at each time point (pre blast, 1 hour post blast, 4 hours post blast). The saved waveform data was exported from the VikingDirect software and converted into decimal data for analysis. The converted data was plotted and the tests were randomized for blinded evaluation by a neurologist.

For the initial evaluation, the neurologist evaluated only the individual ear recordings and not the binaural tests. The neurologist identified the peaks associated waves I-V by hand. Waves I and II originate from the cochlear nerve and cochlear nucleus, respectively. Waves III, IV, and V originate from the superior olivary complex, lateral lemniscus, and inferior colliculus, respectively. An example of a BAEP waveform with the waves identified is shown in Figure 3.9. The auditory pathway with the origins of the signals is shown in Figure 3.10.

Once the peaks were identified, the values for the peak amplitudes and latencies were extracted. The effects of the blast on the amplitudes and latencies of each of the peaks were examined. Additionally, the latency difference between wave I and V was also examined, as that time interval is considered the "central conduction time" of the auditory pathway associated with the auditory pathway in the brainstem (Squires 1986).

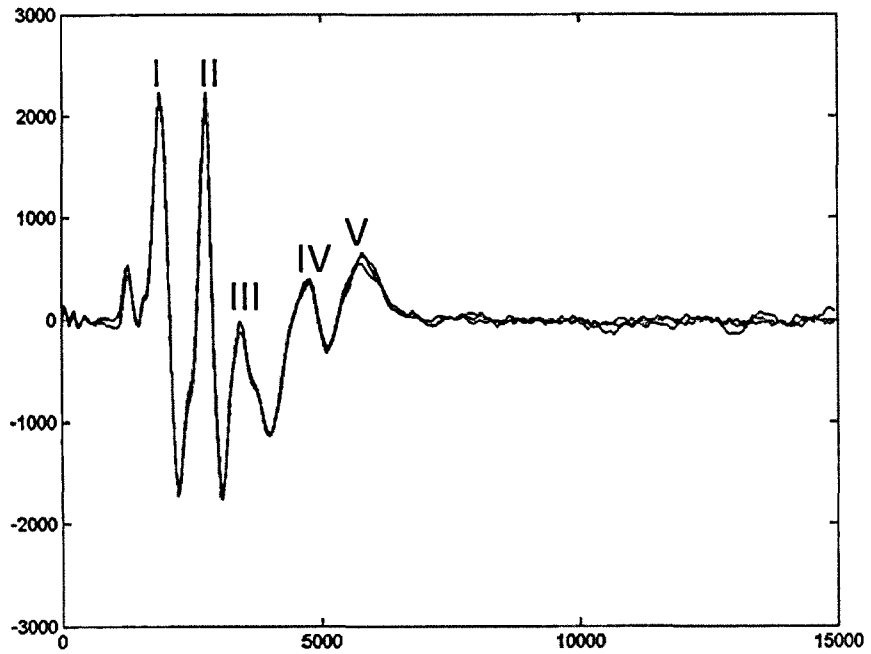

Figure 3.9. Example of BAEP from this study. Waves I-V have been labeled.

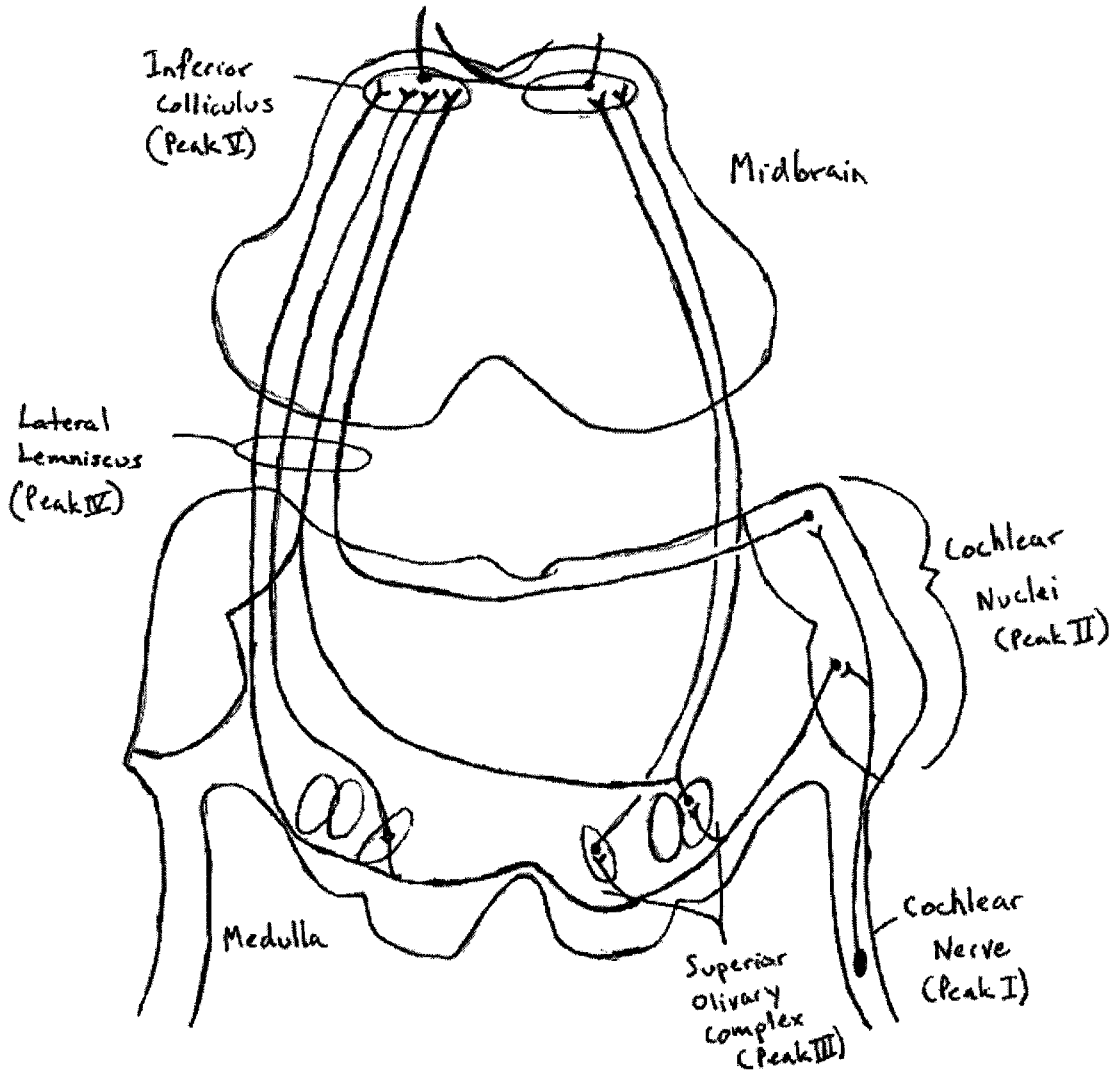

Figure 3.10. Diagram of the auditory pathway in humans with the wave origins labeled.

3.4 Statistical Methodology

3.4.1 Macroscopic Injuries

Three risk functions for the outcome measures of fatality, apnea, and hemorrhage (Equation 1, showing the example for fatality risk) were determined from experimental results by logistic regression (LogXact 8, Cytel Inc.). Each outcome variable, fatality, apnea, and hemorrhage, was modeling by adjusting for the peak overpressure (P) and the

duration (D) of the blast input. Equation 1 provides an example for the logistic regression model used for the three risk functions. The example uses fatality, but the presence of apnea or hemorrhage would be substituted in place of fatality for each of those models. The regression models' fit was assessed using the Hosmer-Lemeshow goodness-of-fit statistic (Hosmer 2004).

$$\log\left[\frac{\Pr(fatality|P_i, D_i)}{1-\Pr(fatality|P_i, D_i)}\right] = \beta_0 + \beta_1 D_i + \beta_2 P_i \qquad \text{Equation 1}$$

3.4.2 Histological Injuries

A linear regression model was used to determine the relationship between the positively stained area of brain tissue and the peak overpressure and duration of the blast test condition. The regression analysis was performed using PROC REG (SAS/STAT version 9.1.3, SAS Institute Inc., Cary, NC, USA) to determine the intercept and parameter coefficients in the model. Equation 2 displays the form of the regression used. The regression model fit was assessed by examining the residual plots for the parameters.

$$\ln(area) = \beta_0 + \beta_1 D_i + \beta_2 P_i \qquad \text{Equation 2}$$

3.4.3 Evoked Potentials

3.4.3.1 Visual Evoked Potentials

Two logistic regression models were used to determine the relationship between the VEP wave parameters and the blast test condition parameters. The first model investigated the risk of losing the PNP complex of the VEP trace after an exposure to blast. The second model investigated the risk of significantly delaying the latency of this complex by greater than a standard deviation of the distribution after an exposure to blast. The distributions used included all of the latencies collected for each individual eye or for

both eyes when evaluated together. The models were determined by adjusting for seven test condition parameters: the peak blast overpressure, the positive phase duration of the blast wave, the total anesthetic dose before the recording was performed, the timing of the last dose of anesthesia before the recording, the head length, the head width, and the head circumference of the specimen. Anesthesia parameters were considered because depth of anesthesia has been shown to have an effect on evoked potentials (Andel 2000, Fishback 1995, Keller 1992, Thees 1999); however, urethane was selected to diminish those effects (Hara 2002, Field 1993). The correlation between possible variables to include in the model was determined using the Pearson product-moment correlation coefficient in PROC CORR (SAS/STAT version 9.1.3, SAS Institute Inc., Cary, NC, USA). After the correlated variables were eliminated, a logrank test was performed to test for normality using PROC UNIVARIATE (SAS/STAT version 9.1.3, SAS Institute Inc., Cary, NC, USA). Using various transform functions such as taking the natural logarithm or the cube root of the variables, normal distributions could be achieved. Once the variables had a normal distribution, the regression model was evaluated with the test condition parameters using PROC LOGISTIC (SAS/STAT version 9.1.3, SAS Institute Inc., Cary, NC, USA). Significant test condition parameters were determined using stepwise regression in PROC LOGISTIC. Consequently, the regression models were evaluated with only the necessary parameters. The regression model fits were assessed using the Hosmer-Lemeshow goodness-of-fit statistic (Hosmer 2004).

3.4.3.2 Brainstem Auditory Evoked Potentials

As with the VEP, a logistic regression model was used to determine the relationship between the BAEP wave parameters and the blast test condition parameters. The absence

of wave V with or without the presence of earlier waves was modeled by adjusting for the same test condition parameters used in the VEP analysis. Again, using the same procedures in the SAS® software, the correlation between possible variables to include in the model was determined using the Pearson product-moment correlation coefficient. After the correlated variables were eliminated, the remaining non-normal variables were transformed into normally distributed variables. Once the variables had a normal distribution, the regression model was evaluated with the test condition parameters. Test condition parameters that were determined to be insignificant were removed, and the regression model was reevaluated with only the necessary parameters. The regression model fit was assessed using the Hosmer-Lemeshow goodness-of-fit statistic (Hosmer 2004).

Chapter 4. RESULTS

4.1 Blast Wave Exposure

4.1.1 Macroscopic Results

4.1.1.1 Pathophysiological Results

The specimen test conditions and a summary of the macroscopic assessments of apnea and hemorrhagic injury are listed in Table 4.1. There were seven fatalities in the dataset, concentrated among the more severe exposure levels for both short and long durations. The animals that did not survive five hours after the blast, despite mechanical ventilation and administration of doxapram (Dopram-V, Ft. Dodge, Overland Park, KS), demonstrated a similar clinical progression characterized by declining oxygen saturation levels prior to bradycardia that progressed to asystole. Intracranial hemorrhage, including subdural and subarachnoid hemorrhage (Figure 4.1), and cerebral contusions were found in nonsurvivors, often in the area on or around the brainstem. For all of the specimens that presented with a hemorrhage, the most frequent area of hemorrhaging was on or around the brainstem, followed by the ventral surface of the brain. The area around the dorsal junction of the cerebrum and cerebellum was also affected. Finally, petechial hemorrhages affected the frontal lobe in five specimens. Hemorrhaging occurred in 55 specimens; 13 were classified as severe, 15 were classified as moderate, and 27 were classified as mild. The percentage of hemorrhagic surface area ranged from 26% at the most severe to 0.13% for the mildest. Brains that were exposed to peak incident overpressures greater than 700 kPa received at least a moderate hemorrhage. The calvarium remained intact for all blast pressure and duration levels without any evidence of fracture on necropsy.

Table 4.1: Specimen test conditions/survival and injury assessment (OVP=overpressure)

Test #	Peak Incident OVP (kPa)	Scaled Dur. (ms)	Apnea	Brain Hemorrhage Grade	5 hr. Survival
LF01*	NA	NA	NA	NA	NA
LF02	98	2.1	No	none	Yes
LF03	600	3.8	No	moderate	Yes
LF04	226	9.8	No	mild	Yes
LF06	629	5.1	Yes	mild	Yes
LF07	98	2.1	No	none	Yes
LF08	598	3.7	No	mild	Yes
LF09	594	4.0	No	mild	Yes
LF10	600	5.0	No	mild	Yes
LF11	769	6.0	Yes	severe	Yes
LF12	818	6.3	Yes	severe	No
LF13	777	5.9	Yes	moderate	Yes
LF14*	NA	NA	NA	NA	NA
LF15	334	14.9	Yes	moderate	No
LF16	289	14.1	Yes	moderate	No
LF17	837	5.6	Yes	moderate	Yes
LF18	276	13.1	Yes	moderate	Yes
LF19	287	11.6	Yes	mild	Yes
LF21	327	13.8	Yes	severe	No
LF22	669	4.0	Yes	severe	No
LF23	759	4.3	Yes	severe	No
LF24	621	4.4	Yes	none	Yes
LF25	712	4.8	Yes	severe	Yes
LF26	625	4.0	No	none	Yes
LF27*	NA	NA	NA	NA	NA
LF28	816	4.6	Yes	severe	Yes
LF29	197	8.3	Yes	mild	Yes
LF30	225	8.8	No	moderate	Yes
LF31	291	11.3	Yes	severe	No
LF32	604	3.4	Yes	moderate	Yes
LF33	597	3.3	Yes	moderate	Yes
LF34	524	3.1	Yes	moderate	Yes
LF35	598	4.2	Yes	none	Yes
LF36	413	3.7	No	none	Yes
LF37	677	4.3	Yes	severe	Yes
LF38	734	4.4	Yes	severe	Yes
LF39	473	3.5	No	severe	Yes
LF40	385	3.4	No	moderate	Yes
LF41	446	4.0	No	mild	Yes

Test #	Peak Incident OVP (kPa)	Scaled Dur. (ms)	Apnea	Brain Hemorrhage Grade	5 hr. Survival
LF42	471	3.4	No	mild	Yes
LF43	545	3.4	No	mild	Yes
LF44	129	5.1	No	none	Yes
LF45	130	5.2	No	mild	Yes
LF46	234	2.6	No	none	Yes
LF47	198	2.5	No	mild	Yes
LF48	472	3.6	Yes	moderate	Yes
LF49	563	3.6	Yes	mild	Yes
LF50	335	2.9	No	none	Yes
LF51	320	3.0	No	mild	Yes
LF52	491	3.6	Yes	mild	Yes
LF53	524	3.6	Yes	mild	Yes
LF55	154	5.4	No	none	Yes
LF56	165	2.5	No	mild	Yes
LF57	421	4.0	No	moderate	Yes
LF58	327	2.7	No	mild	Yes
LF59	413	3.1	No	mild	Yes
LF60	519	3.4	No	mild	Yes
LF61	496	3.4	Yes	mild	Yes
LF62	520	3.5	No	moderate	Yes
LF63	384	2.8	No	mild	Yes
LF64	409	2.8	No	mild	Yes
LF65	410	2.8	No	mild	Yes
LF66	669	3.5	Yes	mild	Yes
LF67	440	3.0	No	mild	Yes
LF68	662	3.5	Yes	severe	Yes
LF69	703	3.7	Yes	moderate	Yes
LF70	753	3.6	Yes	severe	Yes
Controls					
LF05			No	none	Yes
LF20			No	none	Yes
LF54			No	none	Yes

*Died before blast exposure

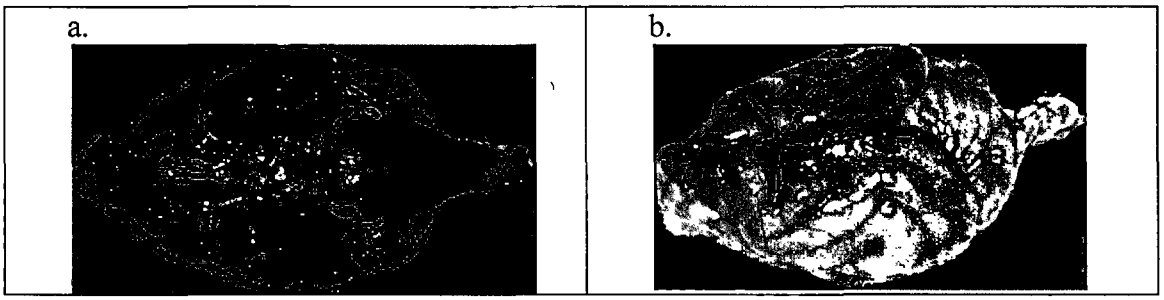

Figure 4.1. Subdural Hemorrhages. a.) Ventral View of Brain Excised from LF38 (severe injury). b.) Dorsal View of Brain Excised from LF29 (mild injury).

Seventeen specimens were apneic immediately after the blast exposure. Table 4.1 contains a summary of the apnea results. The occurrence of apnea was influenced by the duration of the blast positive pressure phase. For shock tube exposures with scaled blast durations less than 8.5 ms, all peak incident overpressures greater than 625 kPa resulted in immediate apnea, whereas all exposures to peak incident blast overpressures less than 418 kPa did not experience immediate apnea. For scaled blast durations greater than 8.5 ms, all peak incident pressures greater than 226 kPa experienced immediate apnea, but peak incident pressure below 197 kPa did not cause apnea. Spontaneous breathing was recovered in all of the specimens that survived for the duration of the experiment except LF70. The recovery times ranged from less than a minute to nearly an hour. In specimens exposed to peak incident overpressures greater than 700 kPa, spontaneous breathing did not resume within five minutes after the exposure.

The heart rate decreased after the blast exposure for all of the specimens that maintained ECG recording throughout the blast event. However, the heart rate typically recovered to normal values within ten minutes. The heart rate for eight specimens never returned to pre exposure values, although they did recover to normal ranges for a ferret within minutes of the blast (Fox 1988). Four of the eight specimens were exposed to

overpressures greater than 700 kPa. The other four specimens that were exposed to overpressures below 700 kPa were exposed to durations longer than 6 ms. Aside from the apnea, no trends were seen in the respiration rates after the blast exposure. If the specimen was able to recover from the apnea, the respiration rates returned to pre blast values.

For all of the recorded tests, the measured pressure inside the protective cylinder never exceeded 14 kPa. Although, the negative phase of the pressure pulse had a larger magnitude, it never went below -125 kPa, and the negative pressure was not associated with thoracic or abdominal injuries. In addition to keeping the pressure levels low, the protective cylinder also prolonged the rise time to the peak overpressure. Figure 4.2 shows the difference in magnitude between the blast overpressure and the pressure seen inside the protective cylinder.

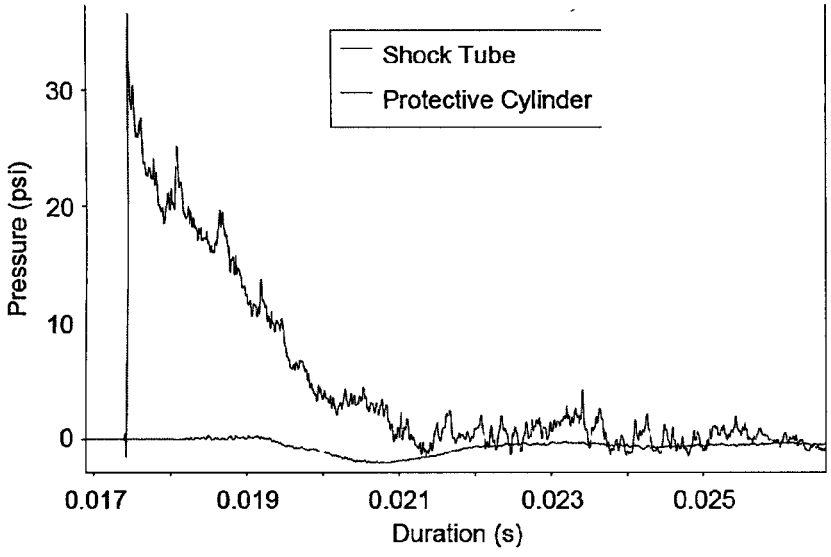

Figure 4.2. Pressure measurements for test LF30 from one of the pressure transducers at the end of the shock tube and the pressure transducer inside the protective cylinder. The data was filtered using a 40kHz, 8-pole Butterworth filter.

No serious pulmonary or gastrointestinal injuries were found during the necropsy, indicating that the thorax was suitably protected for the blast overpressure levels used in these tests. H&E stained tissue at the higher blast levels showed that seven ferrets had minor intraalveolar pulmonary hemorrhage. Thirteen ferrets demonstrated minor transmural, intramural, or submucosal hemorrhages in the trachea, five of which also demonstrated lung injury. Microscopic inspection of the liver, kidneys, stomach, spleen and gut did not reveal any pathologic findings. Very few injuries were seen in regions of the body that were protected. This finding likely indicates that there is limited blast wave transmission through the neck into the body.

4.1.1.2 Statistical Macroscopic Results

The logistic regression for the 50% risk of mild and moderate/severe subdural/subarachnoid bleeding for the ferrets in this study is shown in Figure 4.3. For reference, the pulmonary blast fatality and threshold injury assessments of Bass *et al.* (2008) are also included in the figures. Parameters for the regression model are shown in Table 4.2 with model statistics in Table 4.3. For mild bleeding, the coefficient for scaled duration ($p = 0.15$) was not statistically significant, so a second model was fitted without scaled duration dependence. In both models, the pressure coefficient was statistically significant ($p < 0.05$). For this model, the Hosmer-Lemeshow goodness-of-fit statistic indicates there is no evidence of a lack of model fit ($p > 0.2$). For moderate/severe subdural/subarachnoid bleeding, all model coefficients were statistically significant ($p < 0.01$). Further, the Hosmer-Lemeshow statistic for the model did not exclude a fit ($p > 0.8$).

The model for 50% risk of initial apnea is shown in Figure 4.4. The apnea model has statistically significant regression coefficients ($p < 0.01$). Further, the Hosmer-Lemeshow statistic for the model did not exclude a fit ($p > 0.7$), and the rescaled R^2 value of 0.63 shows that the model accounts for the majority of the variance. For the fatality model with ferrets, the pressure coefficient was only marginally significant ($p = 0.051$). A second fatality model was fitted with the addition of scaled rabbit fatality data acquired using the same test methodology (Rafaels 2010b). This model had statistically significant coefficients ($p < 0.01$), a good rescaled R^2 value of 0.61, and the Hosmer-Lemeshow statistic did not exclude a fit ($p > 0.7$).

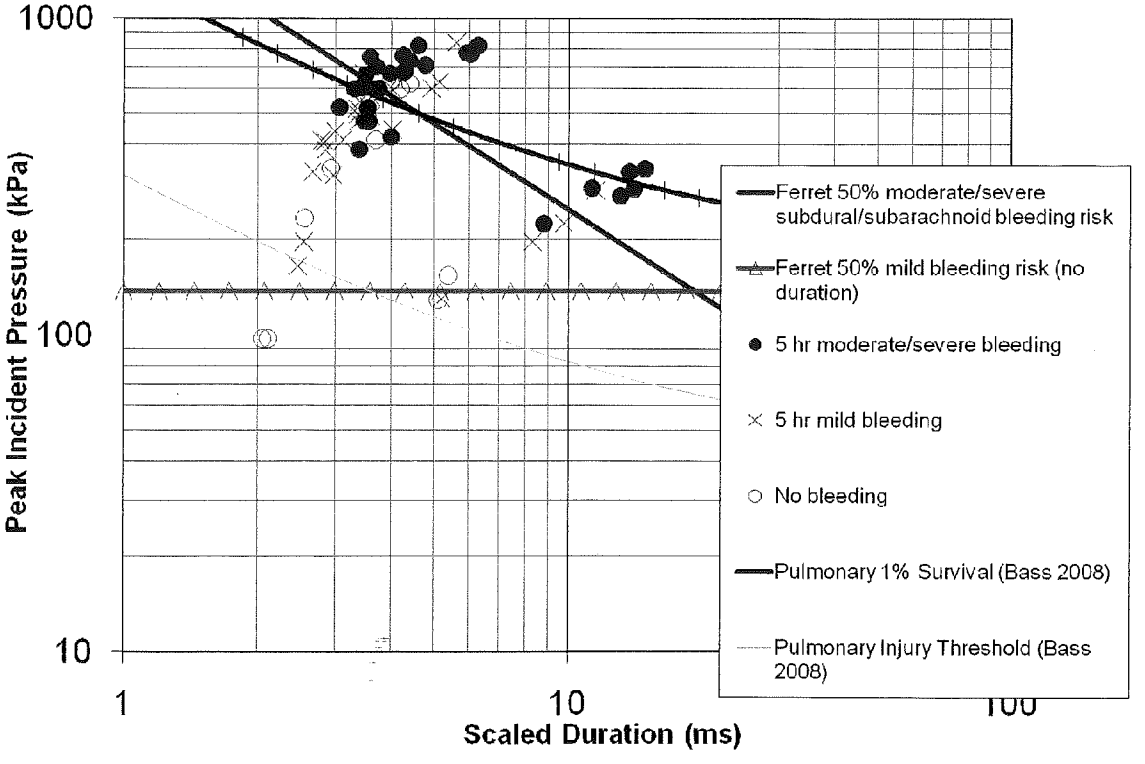

Figure 4.3. Logistic Risk Function (50%) for Mild and Moderate/Severe Meningeal Bleeding from Exposure to Primary Blast Waves

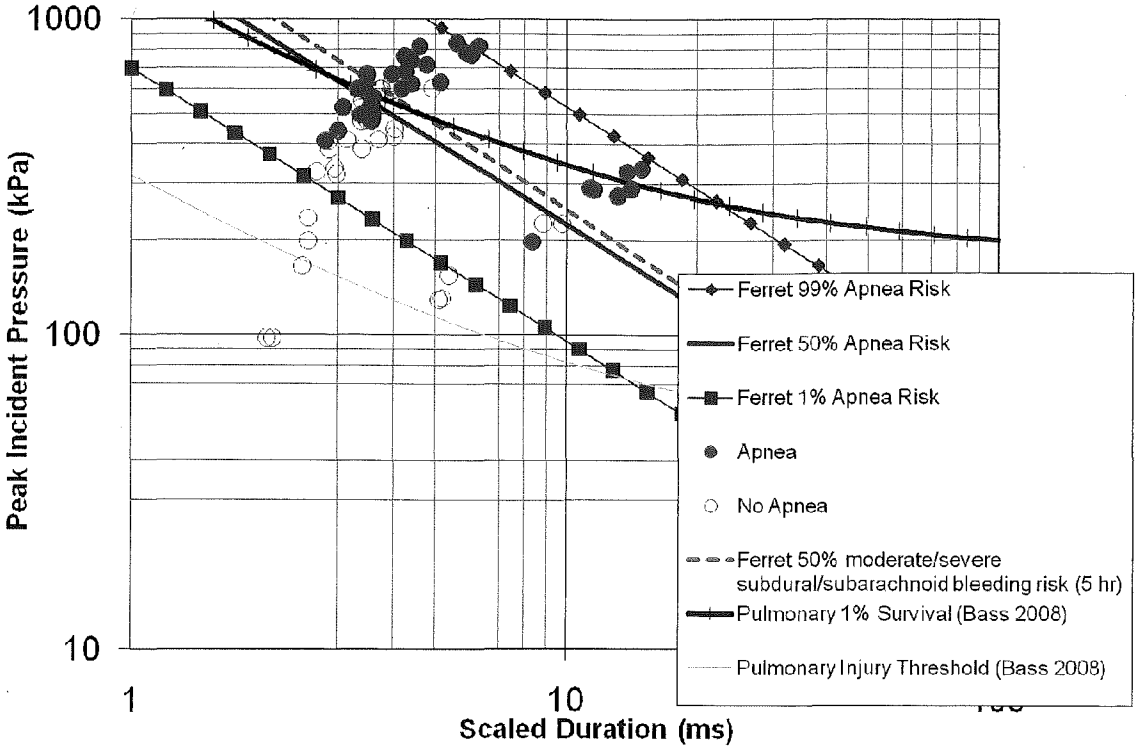

Figure 4.4. Logistic Risk Function (50%) for Initial Apnea from Exposure to Primary Blast Waves

Table 4.2: Logistic Regression Model Estimates (95% confidence limits)

Model	ln(Pressure)		ln(Duration)	
	Odds Ratio	p	Odds Ratio	p
Mild bleeding (no duration)	0.17 (0.05,0.60)	0.006	NA	NA
Mild bleeding (w/ duration)	0.17 (0.05, 0.64)	0.009	0.27 (0.05,1.64)	0.16
Moderate/severe bleeding	0.06 (0.01,0.38)	0.003	0.08 (0.02,0.39)	0.002
Apnea	0.005 (<0.001,0.09)	0.0004	0.01 (<0.001,0.13)	0.0005
Fatality	0.03 (<0.001,1.03)	0.05	0.004 (<0.001,0.164)	0.003
Fatality with rabbit data (Rafaels 2010b)	0.006 (<0.001,0.199)	0.004	0.002 (<0.001,0.067)	0.001

Table 4.3: Logistic Regression Model Fit Statistics

Model	Hosmer-Lemeshow	p
Mild bleeding (no duration)	11.8	0.23
Mild bleeding (w/ duration)	11.8	0.23
Moderate/severe bleeding	5.3	0.81
Apnea	3.2	0.96
Fatality	3.2	0.96
Fatality with rabbit data (Rafaels 2010b)	1.2	1

4.1.2 Histological Results

4.1.2.1 Qualitative and Quantitative Results

Positive results were obtained for visualizing damage to the axonal transport system using β-APP. Figure 4.5 shows light microscopy images of the β-APP stained brains from the same approximate location for a severe, moderate, and mild blast condition as well as the control. Although Figure 4.5d does not show any positively stained axons in the control image, there was some positive staining throughout the brains of the controls, albeit at a much smaller frequency than blasted specimens. The positive axons in the controls were always isolated and had a reduced intensity and size compared to those in blasted specimens. Positive staining for β-APP in the blasted specimens was seen throughout the cerebrum and brainstem. The positively stained axons were generally isolated surrounded by uninjured axons, as seen in Figure 4.5c, but were sometimes found in a cluster, as shown in Figure 4.5a. The latter case rarely ever occurred in the milder blast conditions. Figure 4.6 shows more examples of positive staining for the different blast conditions. Figure 4.7 shows the density of immunoreactive areas in the varying blast conditions for a posterior slide of the cerebrum. Some common areas of

positive staining included: the corpus callosum, the corona radiata, the hippocampus, the thalamus, the cerebellum, the sensory and motor tracts of the brainstem, cortical grey-white interface, and near the borders of ventricles. Examples of positive staining in these areas are shown in Appendix B. The intensity, size, and number of positively-stained axons appeared to increase with increased blast severity. The positively-stained axonal densities are shown in Table 4.4. Figure 4.8 shows the density of the positively stained axons as it relates to the peak incident overpressure and duration of the blast input.

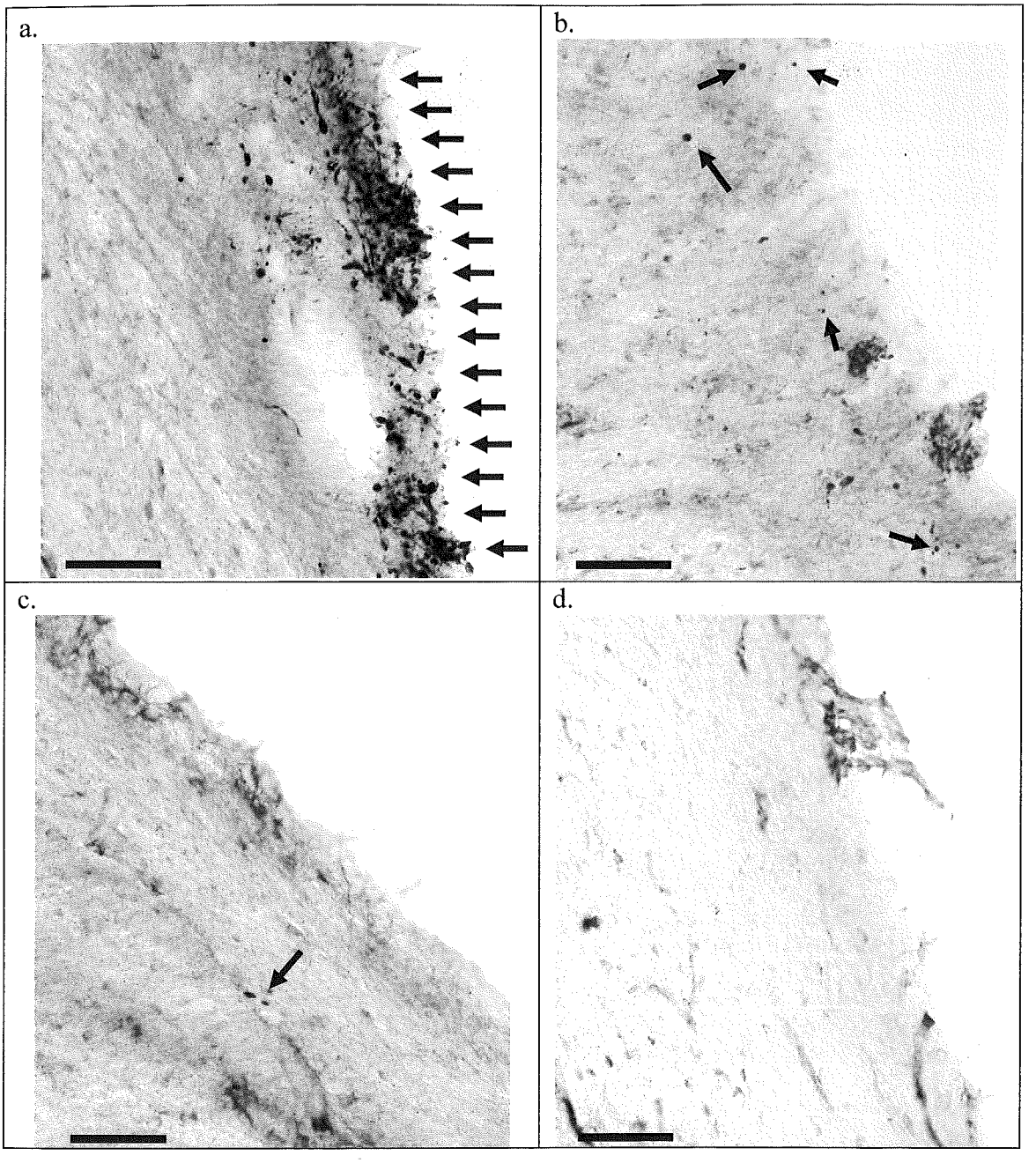

Figure 4.5. Positive β-APP stained tissue from coronal section on the external capsule of the lateral ventricle. The injured axons are highlighted by the black arrows. Black scale line = 50 μm. a.) LF11 (severe). b.) LF24 (moderate). c.) LF37 (mild). d.) LF54 (control).

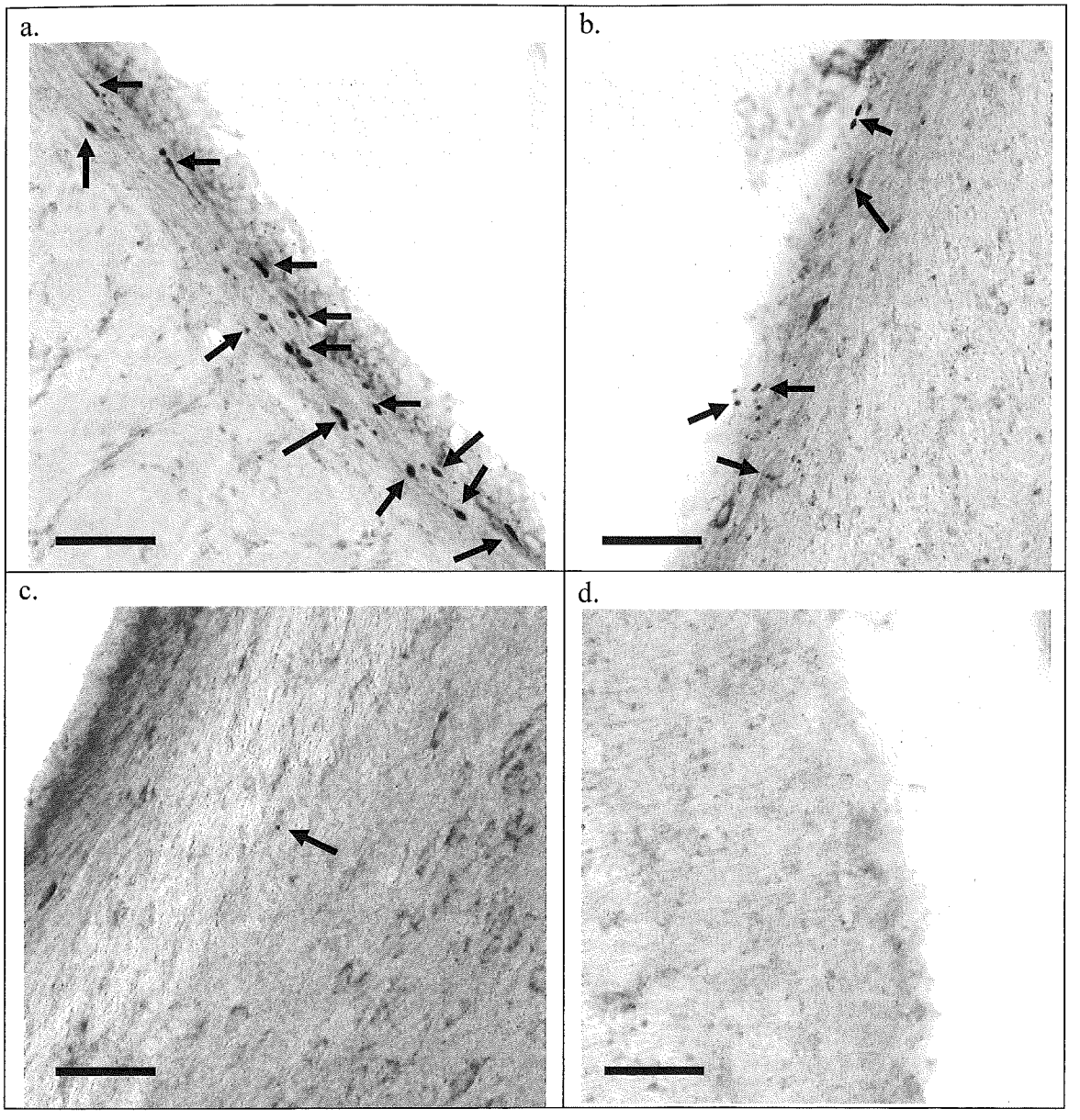

Figure 4.6. Positive β-APP stained tissue from coronal section on the external capsule of the lateral ventricle. The injured axons are highlighted by the black arrows. Black scale line = 50 μm. a.) LF13 (severe). b.) LF43 (moderate). c.) LF32 (mild). d.) LF20 (control).

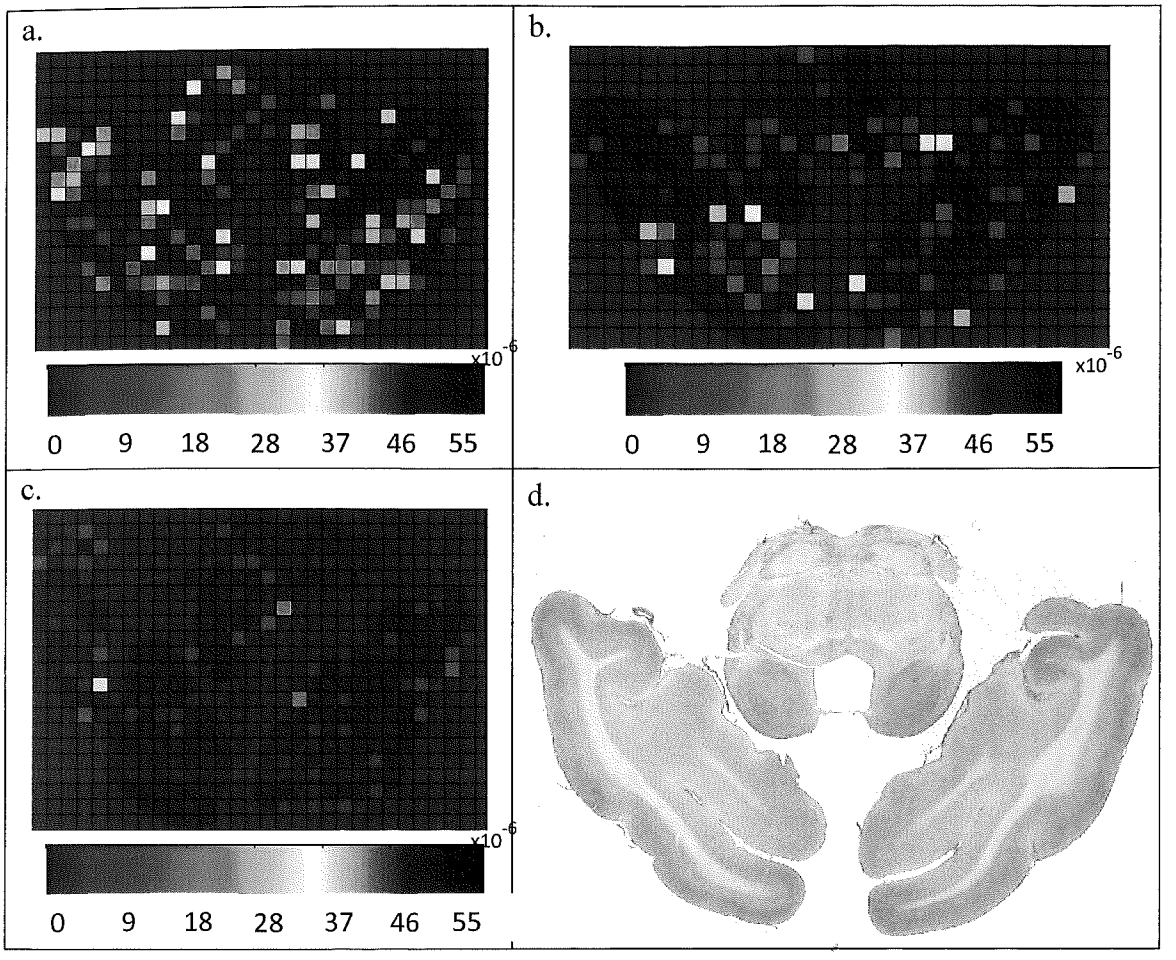

Figure 4.7. Density mapping of the positive β-APP stained tissue from the coronal slice at approximately bregma -8.00 mm. a.) LF11 (severe). b.) LF44 (moderate). c.) LF09 (mild). d.) LF11, unhindered view of tissue slice for better visualization of brain structures at this brain location.

Table 4.4: Specimen test conditions/positively stained axonal area assessment (OVP=overpressure)

Test #	Peak Incident OVP (kPa)	Scaled Dur. (ms)	Norm. Axonal Area ($x10^{-7}$)
LF09	594	4.0	9.34
LF11	769	6.0	252.93
LF13	777	5.9	181.19
LF17	837	5.6	136.18
LF18	276	13.1	130.62
LF19	287	11.6	162.48
LF24	621	4.4	35.13
LF25	712	4.8	22.01
LF28	816	4.6	211.55
LF29	197	8.3	43.61
LF30	225	8.8	25.99
LF32	604	3.4	18.95
LF34	524	3.1	16.68
LF35	598	4.2	79.23
LF36	413	3.7	9.89
LF37	677	4.3	19.76
LF38	734	4.4	30.47
LF39	473	3.5	17.62
LF41	446	4.0	9.57
LF42	471	3.4	15.62
LF43	545	3.4	32.20
LF44	129	5.1	28.07
LF45	130	5.2	15.89
LF46	234	2.6	16.03
LF47	198	2.5	5.30
LF70	753	3.6	234.87
Controls			
LF05			1.67
LF20			7.46
LF54			5.95

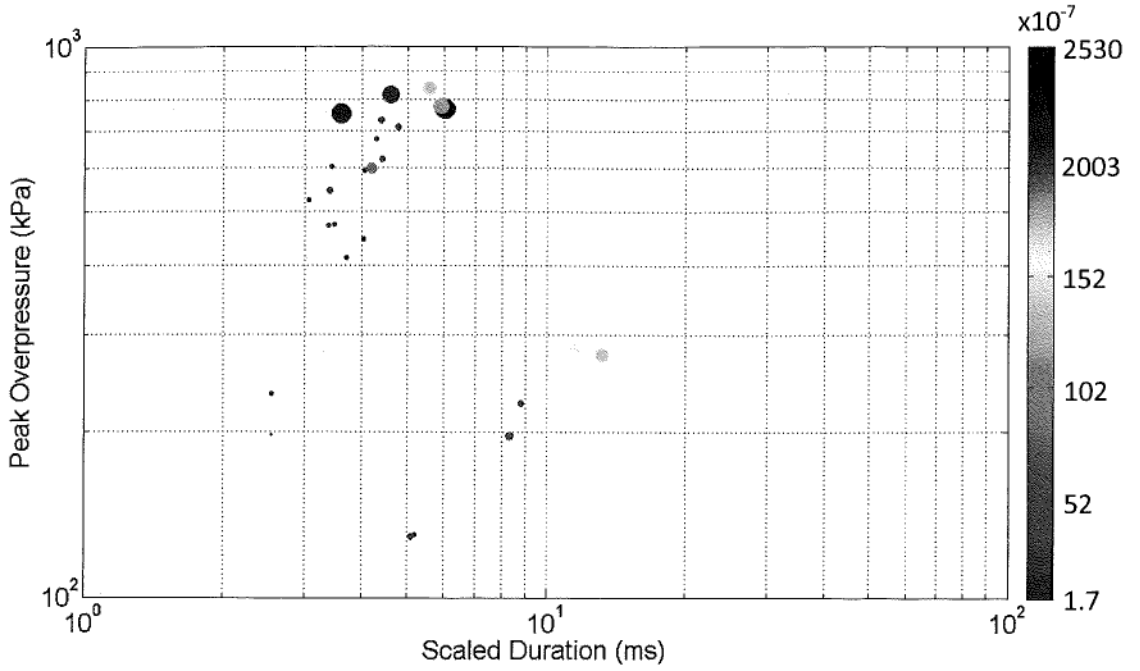

Figure 4.8. Positively-stained axon densities related to the input blast parameters. The size and color of the points on the plot correspond to the density of positively-stained axons at that overpressure and duration.

The error calculation for the β-APP semi-automatic quantification method is shown in Table 4.5. Using the methods described in Section 3.2.1.3, the weighted error for the entire evaluation method was 9.96%. The differences between the severity groups were sufficiently large such that the error bounds for each group do not intersect any other group.

Table 4.5: Error calculation of three slices of brain.

	Severe	**Moderate**	**Mild**
Specimen	LF11	LF24	LF46
Calculated Positive Pixels	73577	10642	4016
Total Positive Pixels	75521	13486	4395
Error	2.57%	21.09%	8.62%

Identifying damaged axons with neurofilament alterations obtained with RM014 stained brains was problematic. Figures 4.9 and 4.10 show light microscopy images of the RM014 stained brains from the same approximate location for a severe, moderate, and mild blast condition and the control. The staining intensity, number, and size of the positively-stained axons appeared to increase with increasing blast severity level. Longer duration exposures appeared to stain more axons with a higher intensity. Some common areas of positive staining included: the corpus callosum, the corona radiata, cortical grey-white interface, the cerebellum, the sensory and motor tracts of the brainstem, and the cerebellar and cerebral peduncles. Examples for positive staining in these areas are shown in Appendix C. However, there were very few definitive positively-stained axons within the samples. Several areas of the brain tissue, namely the cerebral and cerebellar peduncular regions, displayed a large amount of positive staining compared to the control specimens as shown in Figure 4.11. While this homogenous grouping of positive staining does not follow traditional staining patterns for this antibody, some possible explanations for this pattern of staining are offered in the discussion. Aside from these peduncular regions, the positively stained axons were generally isolated, surrounded by uninjured axons, as seen in Figure 4.9.

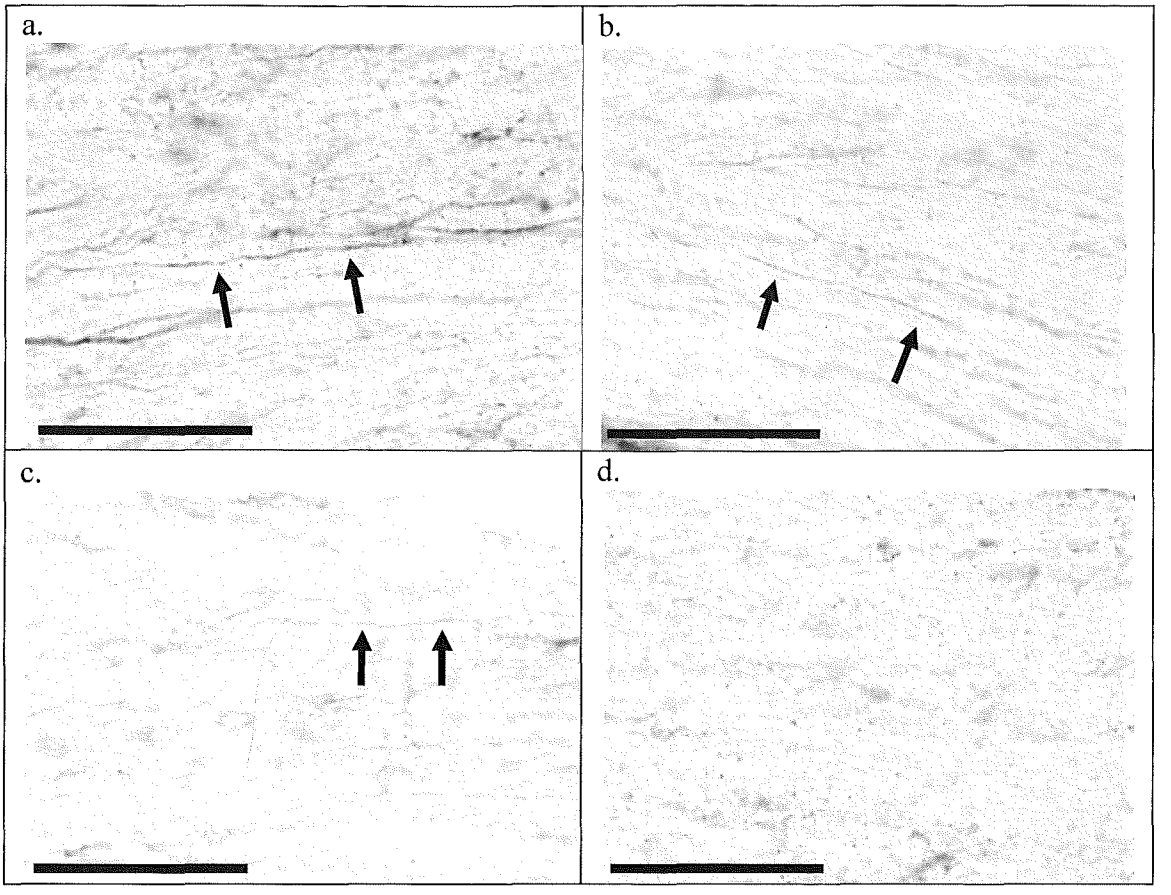

Figure 4.9. Positive RM014 stained tissue from coronal section of the corpus callosum. The injured axons are highlighted by the black arrows. Black scale line = 50 μm. a.) LF19 (severe). b.) LF30 (moderate). c.) LF45 (mild). d.) LF54 (control).

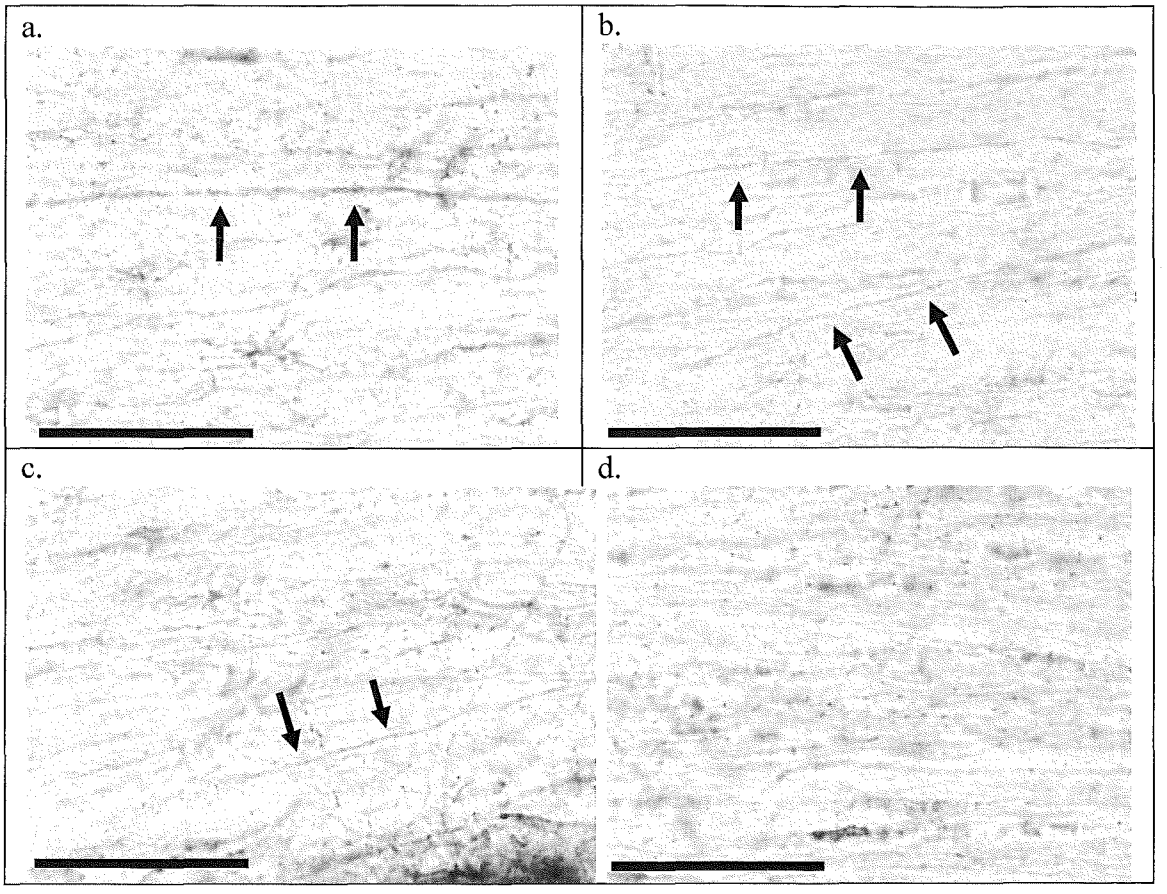

Figure 4.10. Positive RM014 stained tissue from coronal section of the corpus callosum. The injured axons are highlighted by the black arrows. Black scale line = 50 μm. a.) LF18 (severe). b.) LF29 (moderate). c.) LF41 (mild). d.) LF20 (control).

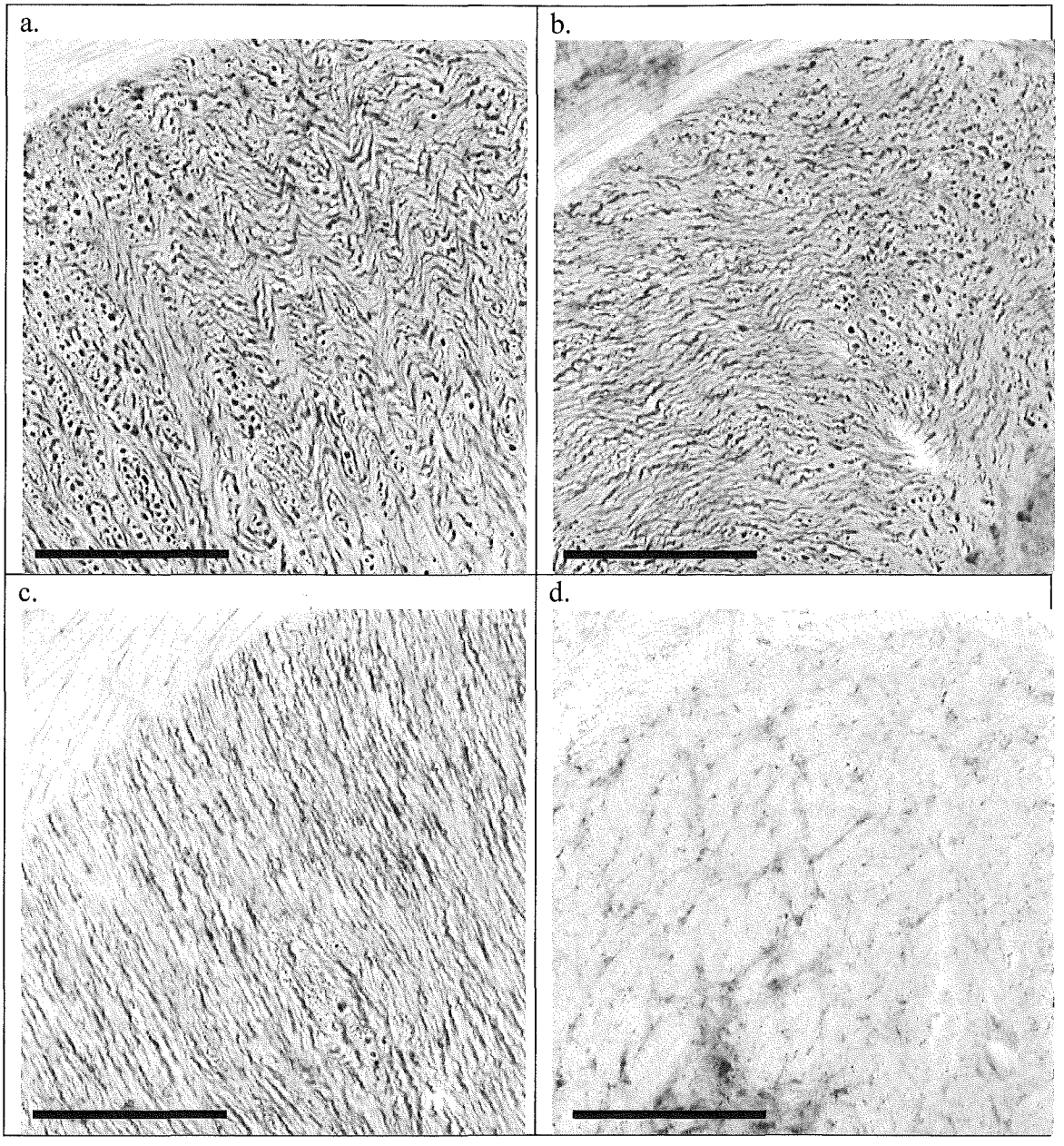

Figure 4.11. Positive RM014 stained tissue from coronal section of the cerebral peduncle. Black scale line = 200 μm. a.) LF18 (severe). b.) LF39 (moderate). c.) LF45 (mild). d.) LF54 (control).

Results from the GFAP stain to quantify reactive gliosis did not show any significant differences between a blasted specimen and a control at 5 hours post blast exposure.

Figures 4.12 and 4.13 show light microscopy images of the GFAP stained brains from the same approximate location for a severe blast condition and a control. The amount and intensity of the staining are similar in the brains. The computational quantitative analysis, summarized in Table 4.6, shows the lack of relationship between the amount of staining and the input blast condition. On the other hand, qualitatively, the severely blasted specimens demonstrate some of the morphological changes indicative of reactive gliosis, such as hypertrophic processes, increased cytoplasmic mass, and long, branching processes (Silver 2004). The banding of the hypertrophic processes of the reactive astrocytes can be seen in Figure 4.12a. Increased cytoplasmic mass and long, branching processes of the reactive astrocytes can be seen in Figure 4.13a. These areas of tissue also demonstrated positive staining for axonal injury.

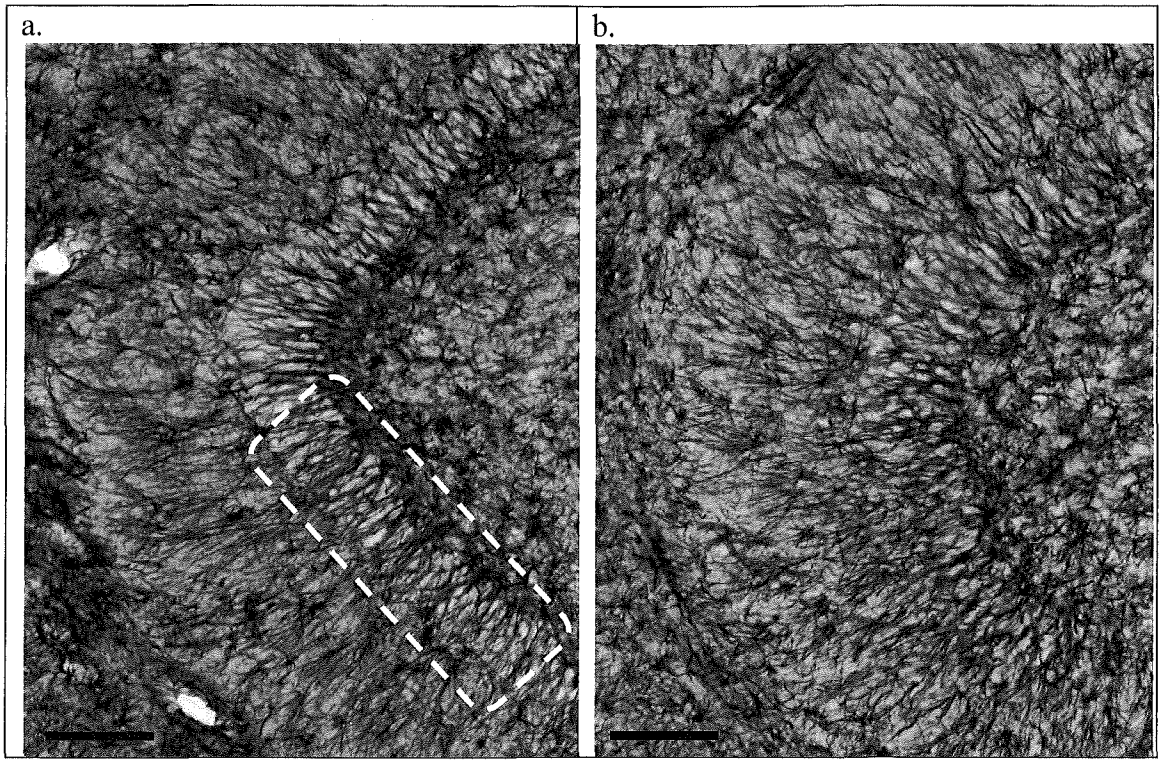

Figure 4.12. Positive GFAP stained tissue from a coronal section of the hippocampus. Black scale line = 100 μm. a.) LF11 (severe). A section of the reactive astrocytes is highlighted by the dashed white box. The astrocytes form an ordered band of cells in the formation of a glial scar. b.) LF05 (control).

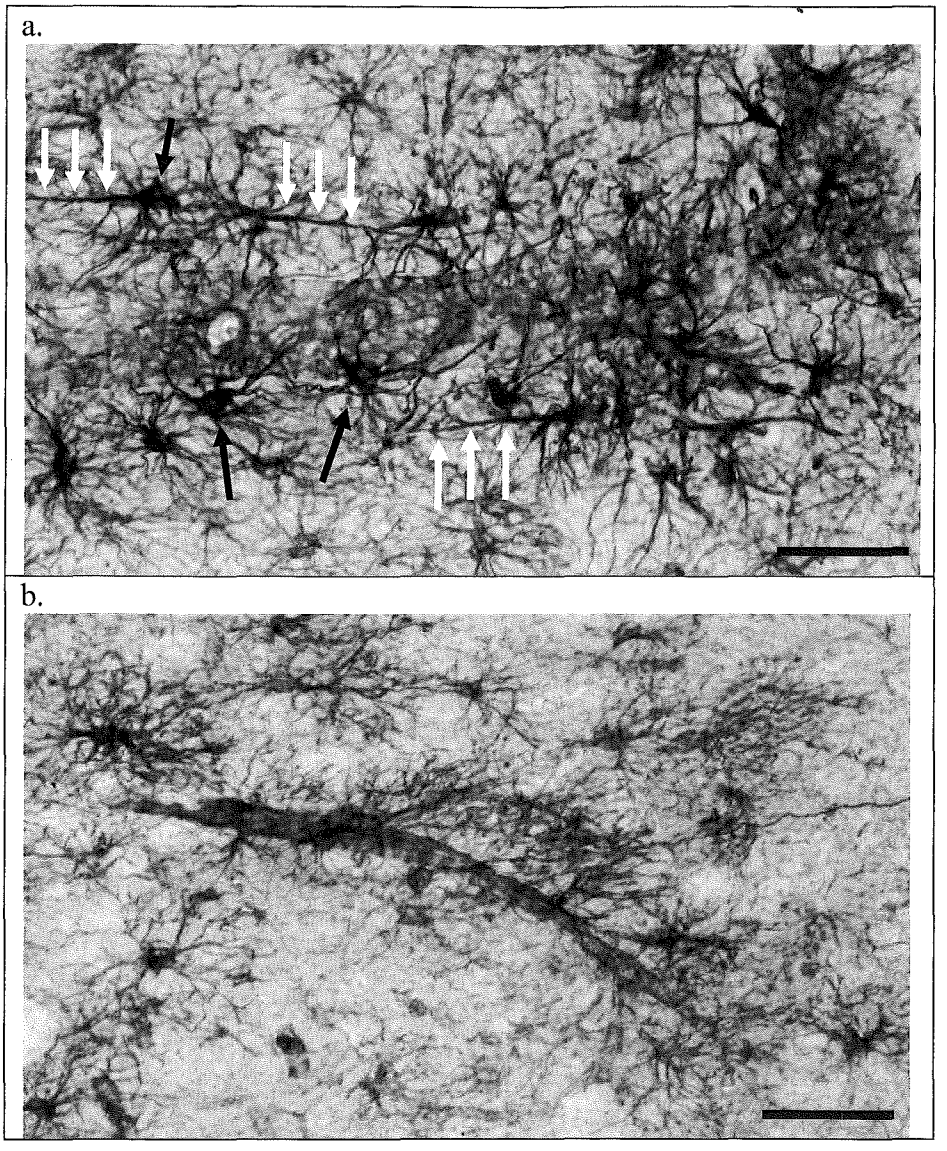

Figure 4.13. Positive GFAP stained tissue from a coronal section of the cerebral cortex at approximately bregma 5.64. Black scale line = 50 μm. a.) LF13 (severe). Some examples of the increased cytoplasmic mass are highlighted by black arrows. Examples of the long processes are highlighted by white arrows. b.) LF05 (control).

Table 4.6: Specimen test conditions/positively stained glial cell assessment

(OVP=overpressure)

Test #	Peak Incident OVP (kPa)	Scaled Dur. (ms)	Norm. Glial Cell Area
LF01*	NA	NA	NA
LF02	98	2.1	0.0163
LF03	600	3.8	0.0103
LF04	226	9.8	0.0116
LF06	629	5.1	0.0103
LF07	98	2.1	0.0095
LF08	598	3.7	0.0113
LF09	594	4.0	0.0145
LF10	600	5.0	0.0104
LF11	769	6.0	0.0085
LF12	818	6.3	0.0102
LF13	777	5.9	0.0216
LF14*	NA	NA	NA
LF15	334	14.9	0.0138
LF16	289	14.1	0.0098
LF17	837	5.6	0.0136
LF18	276	13.1	0.0055
LF19	287	11.6	0.0091
Controls			
LF05			0.0082
LF20			0.0118

*Died before blast exposure

The results obtained from the microscopic analysis of hemorrhaging using LPB and H&E stains are shown in Figure 4.14 which shows light microscopy images from the same approximate location for a severe blast condition. Intraparenchymal hemorrhaging occurred more frequently in the brainstem. The LPB stain often highlighted blood vessels within the tissue, but stained a darker shade of blue at more severe hemorrhage locations. Figure 4.14 highlights this darker staining at the hemorrhage site. The area in Figure 4.14a that stains the darkest blue corresponds to the area of accumulation of red

blood cells in Figure 4.14b. The computational quantitative analysis on a subset of specimens, summarized in Table 4.7, demonstrates that the hemorrhage area was larger in the cerebellum and brainstem than in the midbrain.

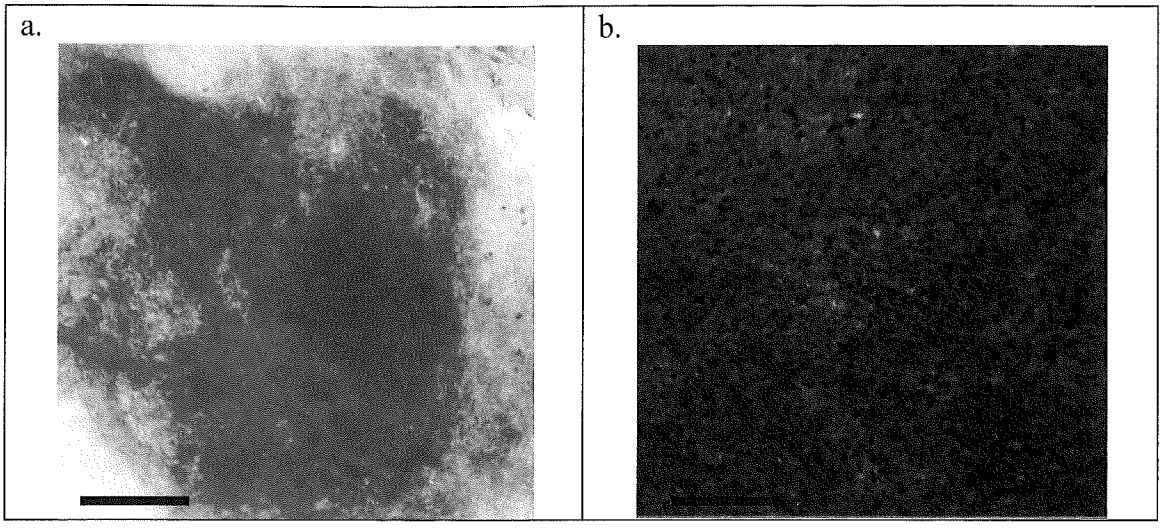

Figure 4.14. Evidence of hemorrhaging in the brain parenchyma from a coronal section of the cerebellum of LF70 (severe). Black scale line = 100 μm. a.) LPB stain. b.) H&E stain.

Table 4.7: Specimen test conditions/positively stained hemoglobin assessment

Test #	Peak Incident OVP (kPa)	Scaled Dur. (ms)	Hemorrhage Area of Midbrain (μm^2)	Hemorrhage Area of Cerebellum/ Brainstem (μm^2)
LF28	816	4.6	3.1×10^3	2.1×10^5
LF30	225	8.8	0	0
LF31	291	11.3	3.3×10^4	4.8×10^4
LF48	472	3.6	1.0×10^4	0
LF69	703	3.7	3.8×10^4	4.8×10^4
LF70	753	3.6	0	5.8×10^5
Controls				
LF20			0	0
LF54			0	0

The results on the fluoro-jade B stained tissue were limited due to the properties of the stain itself and the equipment available to visualize it. Figure 4.15 shows confocal microscopy images of the fluoro-jade B stained brains from the same approximate location for a severe blast condition and a control. Figures 4.15 a and b demonstrate similar edge artifact staining to that seen in the literature (Danzer 2010). These edge artifacts were seen throughout the brain tissue in control and blast exposed samples making the visualization of positively stained degenerating neurons difficult. The edge artifacts were much brighter than the surrounding tissue, disrupting the necessary gains and pixel dwells for visualizing the neurons. Since fluoro-jade B stains for degenerating neurons, it is likely that during the time for the perfusion process of the fixative, some of the neurons along the edge of tissue started degenerating before they were properly fixed. The staining also appeared to be nonspecific along the edges of the tissue. Edge artifacts were also seen in the GFAP stain and less so in the RM014 stain, perhaps suggesting improper fixation over antibody concentrations as the cause for the artifacts. However, some positively stained neurons were visible as shown in Figures 4.15 c and d. The amount of positively stained neurons and the intensity of staining did appear to be greater qualitatively in the severe blast exposure case compared to the control. An additional impediment to analyzing the fluoro-jade B stain was the low photostability of the fluorophore. Several minutes of being exposed to the fluorescent light would render the fluorescence no longer visible. Attempting to reduce the intensity of light exposure made it difficult to visualize the positively stained neurons. Consequently, the analysis on the fluoro-jade B stained tissue was limited.

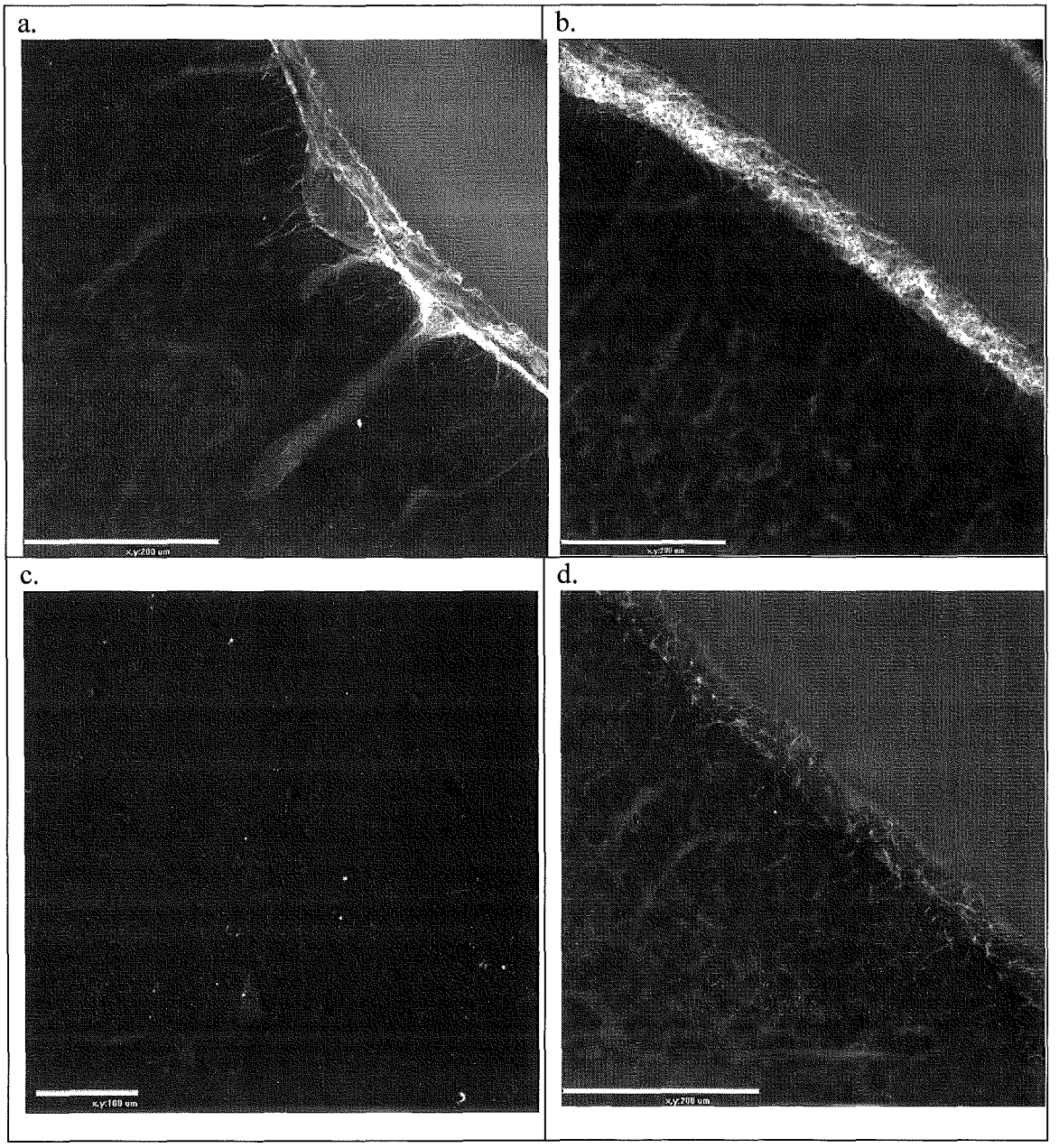

Figure 4.15. Positive fluoro-jade B stained tissue from coronal section of the retrosplenial region. a.) LF13 (severe) coronal section of the retrosplenial region. White scale line = 200 μm. b.) LF20 (control) coronal section of the retrosplenial region. White scale line = 200 μm. c.) LF13 (severe) coronal section of the cerebral cortex (approximately rat bregma -1 mm). White scale line = 100 μm. d.) LF20 (control) coronal section of the retrosplenial region. White scale line = 200 μm.

4.1.2.2 Statistical Results

Parameters for the regression model are shown in Table 4.8 for the peak incident overpressure coefficient (β_1) and scaled positive phase duration coefficient (β_2). For the injured axonal area, all of model coefficients were statistically significant ($p < 0.01$). Further, the residual plots for the model, shown in Figure 4.16, indicate a good model fit.

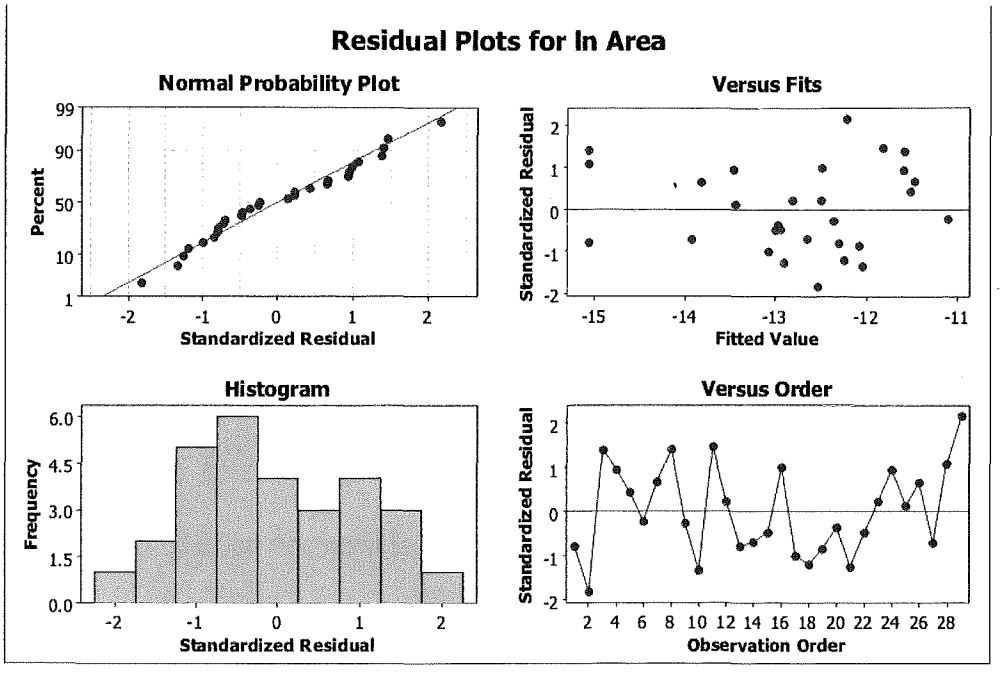

Figure 4.16. Residual plots for the axonal area regression.

Table 4.8: Regression Model Coefficients (±standard deviation values)

Model	Regression Coefficients				
	p	Pressure	p	Duration	p
ln(Axonal area)	<0.001	$2.6\text{x}10^{-3}$ $\pm 5.4\text{x}10^{-4}$	<0.001	$2.5\text{x}10^{-1}$ $\pm 4.9\text{x}10^{-2}$	<0.001

4.2 Evoked Potentials

4.2.1 Visual Evoked Potentials

Complete signal loss of the VEP occurred in three specimens after the exposure to blast, indicating a serious pathological injury along this sensory pathway. Figure 4.17 demonstrates the pre exposure and the one hour post exposure signal for the left eye of a specimen that lost its signal. When signal loss of the entire waveform occurred, it occurred in both the left and right eyes. Signal loss did not occur at blast overpressure levels less than 700 kPa. There were seventeen cases in which there was an atypical signal, making the peak amplitudes and latencies difficult to be reliably determined. Figure 4.18 demonstrates the pre exposure signal and the one hour post signal for the right eye of a specimen with an atypical waveform. These atypical morphologies occurred in both pre blast exposure and post blast exposure tests. If this type of waveform occurred, it often occurred in both eyes for that assessment time (6 assessment times, or 12 cases). The other five cases happened in just one eye of five different specimens, three in the left eye and two in the right.

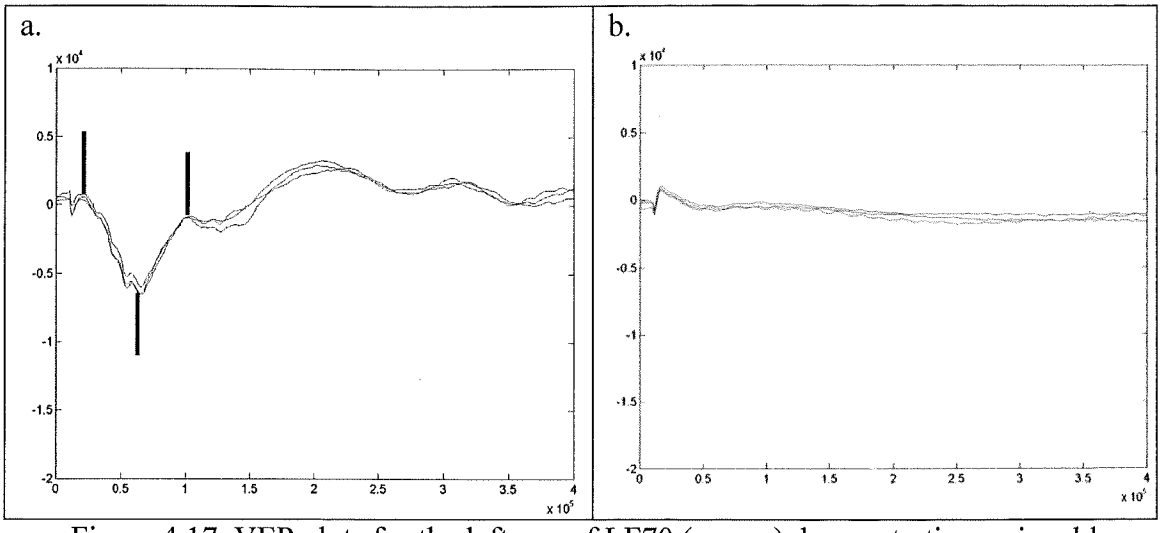

Figure 4.17. VEP plots for the left eye of LF70 (severe) demonstrating a signal loss after a blast exposure. The x-axis is μs. The y-axis is μV. a.) Pre exposure trace. The PNP complex is labeled. b.) Post 1 hour exposure trace. There is no PNP complex.

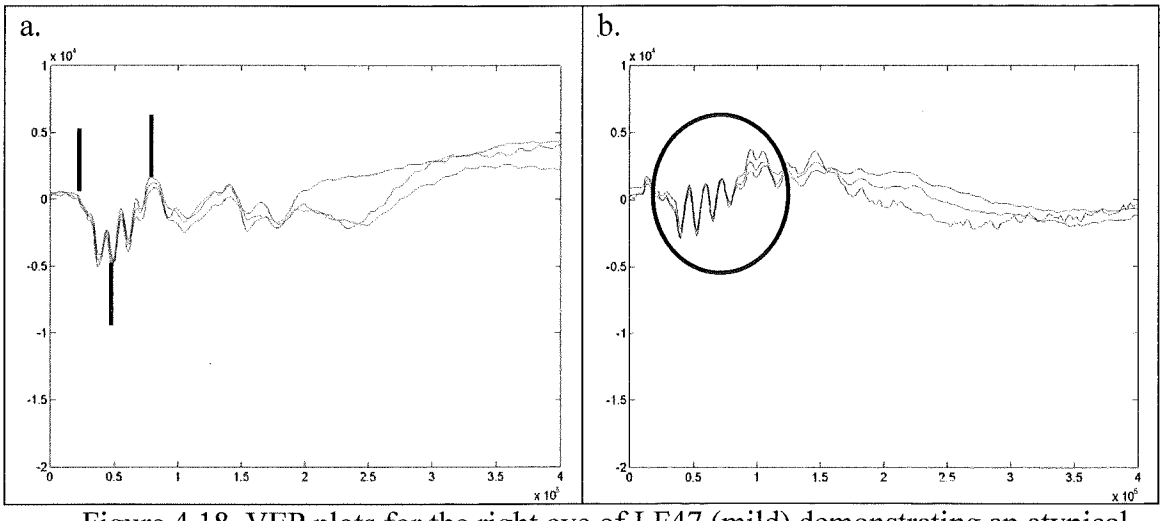

Figure 4.18. VEP plots for the right eye of LF47 (mild) demonstrating an atypical waveform. The x-axis is μs. The y-axis is μV. a.) Pre exposure trace. Although the signal has an atypical morphology, the overall shape of the PNP complex is present so the peaks can be labeled. b.) Post 1 hour exposure trace. The peaks of the PNP complex (circled) are difficult to extract from the multi-peaked waveform.

When signals were present, there was no statistically significant trend in values for the latencies and amplitudes of the waves. Tables with all of the calculated amplitudes

and latencies can be seen in Appendix D. There is an apparent increase in the average latencies for the one hour post exposure time point compared with the pre exposure values, as shown in Figure 4.19. However, the latency has no statistically significant dependence on the blast exposure or the assessment time after the exposure. Even grouping the specimens into similar blast severity levels also does not improve the variability. Similarly, there is an apparent decrease in the average amplitudes of the waves after the blast exposure compared with the pre exposure values, as shown in Figure 4.20. Again, however, there is no statistically significant dependence on the blast exposure, blast exposure level, or assessment time.

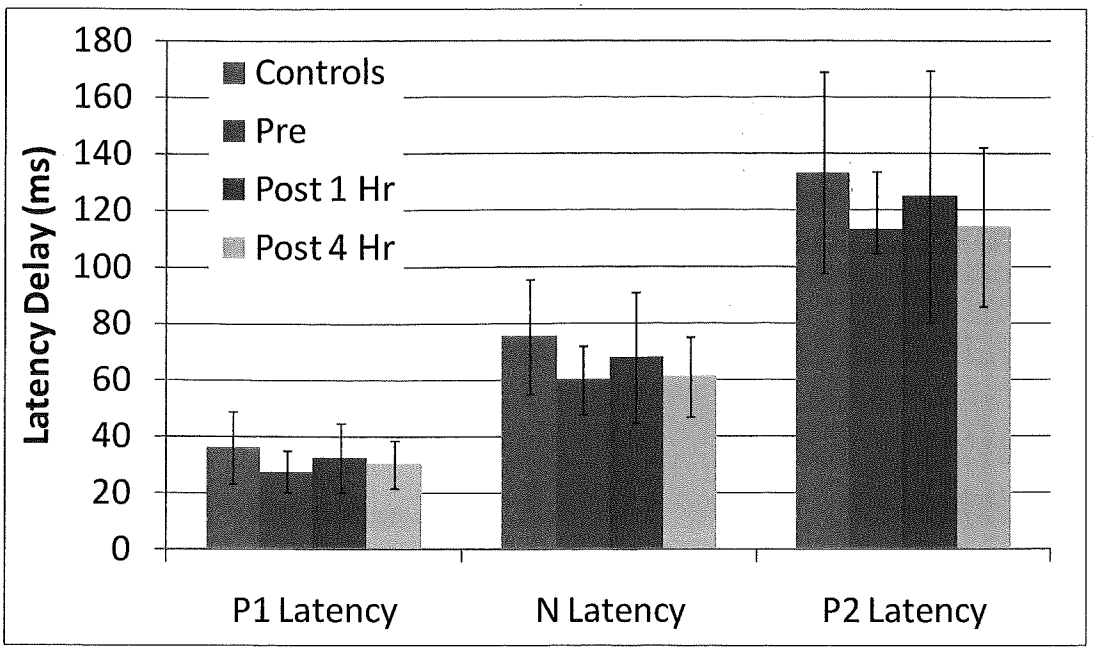

Figure 4.19. The latencies of the components of the PNP complex of the VEP traces for both eyes across all of the subjects at various time points (Pre = Pre blast exposure, Post = Post blast exposure). The data only reflects subjects in which the waveform was available. The data is presented as the mean latency ± the standard deviation. The n for the controls was 12. The n for the pre blast exposures was 100. The n for one hour post blast exposure was 86. The n for four hours post blast exposure was 78.

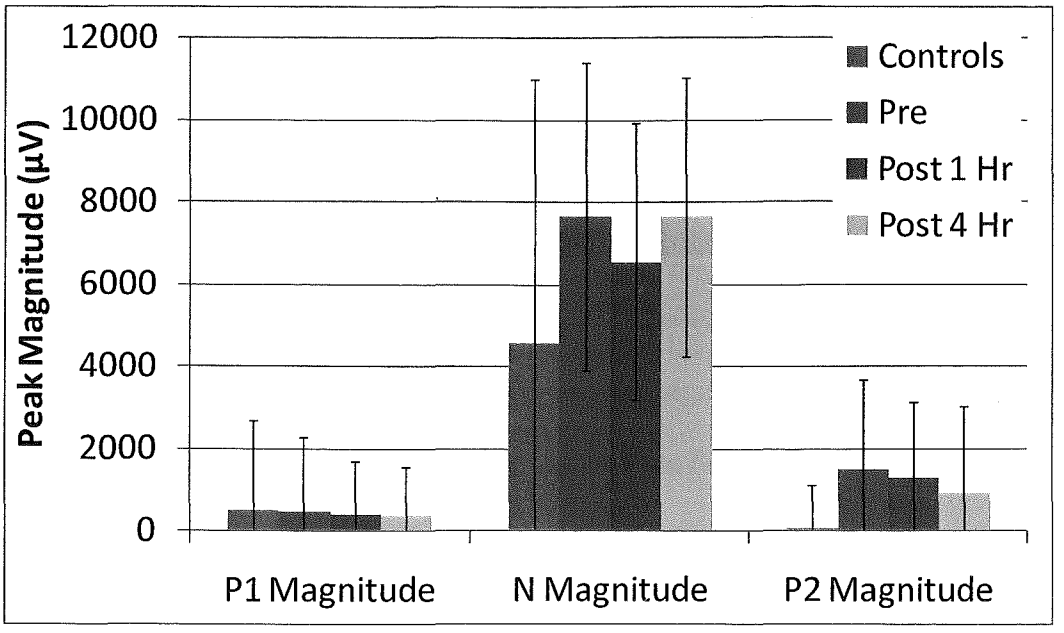

Figure 4.20. The magnitudes of the peaks in the PNP complex for the VEP traces for both eyes across all of the subjects at various time points (Pre = Pre blast exposure, Post = Post blast exposure). The data only reflects subjects in which the peak amplitude was available. The data is presented as the mean amplitude ± the standard deviation. The n for the controls was 12. The n for the pre blast exposures was 100. The n for one hour post blast exposure was 86. The n for four hours post blast exposure was 78.

4.2.1.1 Statistical Results

The results from the Pearson product-moment correlation coefficient showed that head width, length, and circumference were all correlated. Therefore, only head length was used for the remainder of the visual evoked potential analysis. Head length was chosen because the electrodes are placed along that axis of the head.

Duration and overpressure were the only significant parameters ($p<0.05$) in the logistic regression model when pressure, duration, head width, anesthetic dose, and the

time of the last dose were considered. Consequently, the remaining results only reflect the models that include pressure and duration.

The models for the 50% risk of VEP signal loss and significant latency delay are shown in Figure 4.21. Models for the signal loss and latency delays were calculated for each eye as well as both eyes together. Parameters for the regression model are shown in Table 4.9 with model statistics in Table 4.10. For the signal loss model, all of the eye models had statistically significant regression coefficients for peak incident overpressure and positive phase duration ($p < 0.05$). Additionally, the Hosmer-Lemeshow statistic did not exclude a fit for all of the models ($p > 0.06$).

For the latency delay model, the coefficient for the natural logarithm of duration was statistically significant in all of the models ($p < 0.05$). The coefficient for the natural logarithm of peak incident overpressure was not statistically significant for the right eye and both eye models. Although the Hosmer-Lemeshow statistic did not exclude a fit ($p > 0.1$), the rescaled R^2 values show that the models did not account for much of the variance (0.13- 0.17).

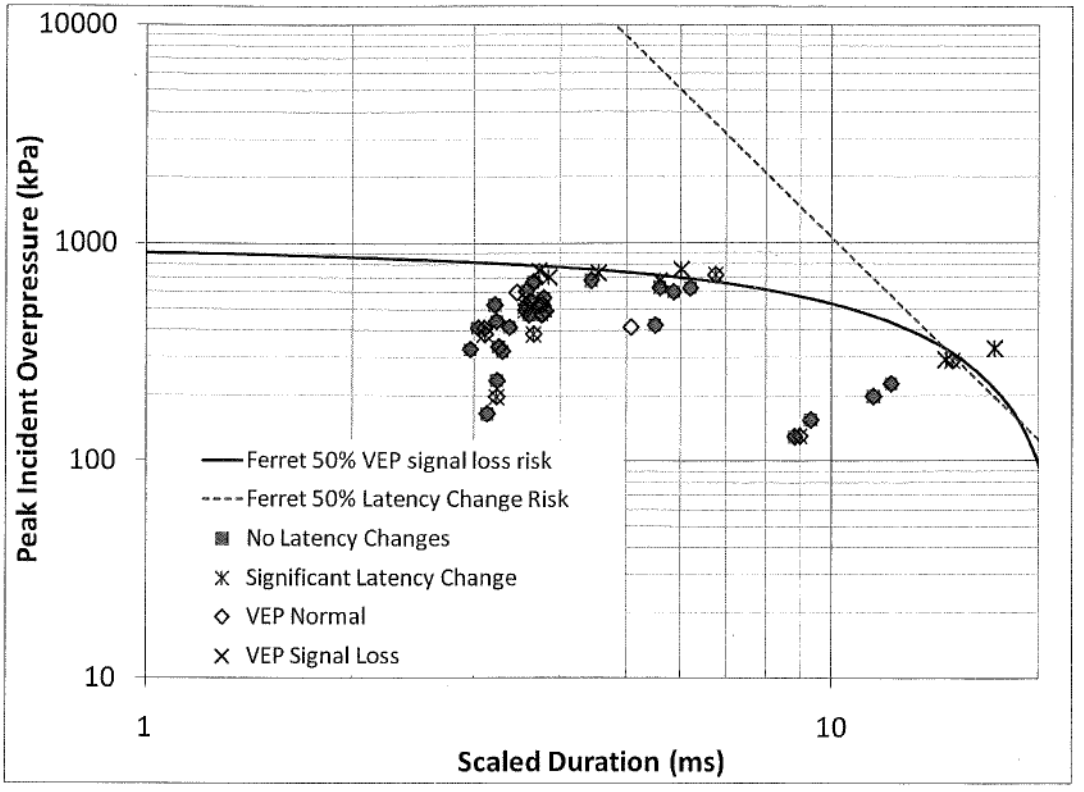

Figure 4.21. Logistic Risk Function (50%) for VEP Signal Loss and Significant Latency Change from Exposure to Primary Blast Waves

Table 4.9: Logistic Regression Model Estimates (95% confidence limits) for VEP

	Model	Pressure		Duration	
		Odds Ratio	p	Odds Ratio	p
Signal Loss	Left Eye Only	1.01 (1.00,1.02)	0.011	1.78 (1.17,2.73)	0.008
	Right Eye Only	1.01 (1.00,1.02)	0.011	1.78 (1.17,2.73)	0.008
	Left and Right Eye Together	1.01 (1.01,1.02)	0.0003	1.78 (1.32,2.41)	0.0002
	Model	**ln(Pressure)**		**ln(Duration)**	
		Odds Ratio	**p**	**Odds Ratio**	**p**
Latency Change	Left Eye Only	2.46 (0.55,10.96)	0.024	15.86 (1.10,228.91)	0.04
	Right Eye Only	1.20 (0.45,3.18)	0.72	9.82 (0.99,97.53)	0.05
	Left and Right Eye Together	3.04 (0.92,10.07)	0.07	13.67 (1.96,95.20)	0.008

Table 4.10: Logistic Regression Model Fit Statistics for VEP

	Model	Hosmer-Lemeshow	p
Signal Loss	Left Eye Only	7.4230	0.4918
	Right Eye Only	7.4230	0.4918
	Left and Right Eye Together	14.8460	0.0622
Latency Change	Left Eye Only	5.5445	0.6981
	Right Eye Only	6.9735	0.5395
	Left and Right Eye Together	11.8549	0.1054

4.2.2 Brainstem Auditory Evoked Potentials

The BAEP traces could generally be categorized into four groups for analysis. The first group contained traces with easily discernable waveforms, as shown in Figure 4.22a. These traces occurred in the control specimens, the baseline, or pre measurements, and the post exposure measurements for the blast exposed specimens. The second group contained traces where wave III was bifid, as shown in Figure 4.22b, making the

amplitudes and latencies for that peak difficult to measure. This group had the largest number of traces, accounting for 53% of all of the analyzed tests. The bifid appearance occurred in controls, baseline, and post blast exposure traces. The third group contained traces in which part of the waveform was missing, as shown in Figure 4.22c. For the purposes of this analysis, missing refers to waveforms that could not be separated from the noise. These missing waveforms likely indicate a lesion along the auditory pathway. The fourth group contained traces in which there was an absence of any wave components, as shown in Figure 4.22d, indicating a noisy signal, or more likely a severe injury. Injury is more likely than noise because the leads were functional both before and after the test, and there were positively stained axons for β-APP in areas along the auditory pathway.

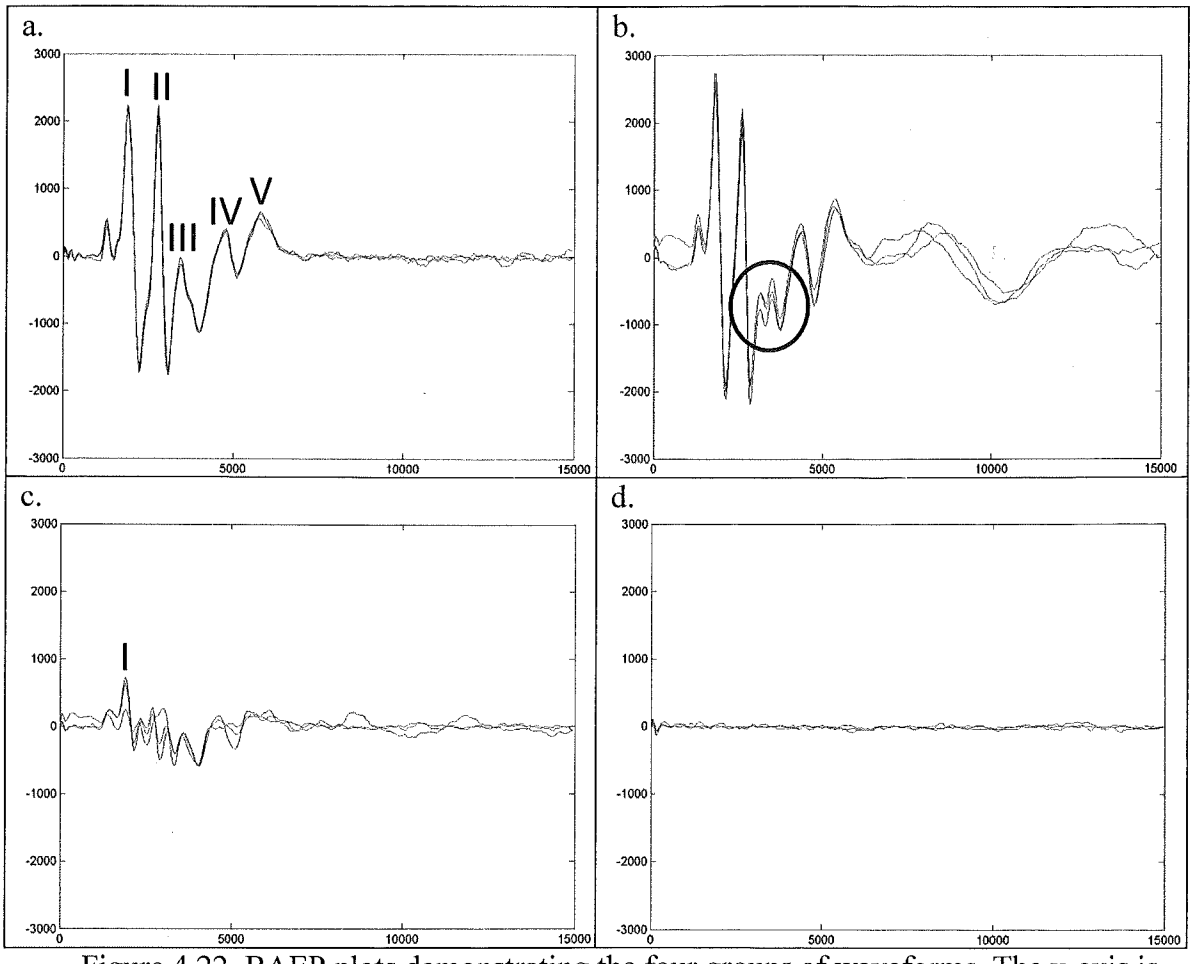

Figure 4.22. BAEP plots demonstrating the four groups of waveforms. The x-axis is μs. The y-axis is μV. a.) LF20 (control) right ear at 4 hours post sham exposure. Peaks I-V are identified. b.) LF59 (mild) right ear pre exposure. The bifid peak III is circled. c.) LF53 (mild) right ear at 1 hour post exposure. Peak I is labeled. The other peaks are considered missing. d.) LF41 (mild) right ear at 4 hours post exposure. No peaks are present.

Signal loss of the entire waveform occurred in both the left and right ears, slightly more frequently in the left ear, 14 times compared to 10 times. Signal loss did not occur at blast overpressure levels less than 400 kPa. The number of traces with missing waveforms occurred slightly more frequently in the right ear, 15 times compared to 10. Missing waveforms did not appear in the left ear at blast overpressure levels less than 330

kPa; however, they occurred at overpressure levels as low as 160 kPa in the right ear. Some trends in the missing waveforms are as follows. Figure 4.23 shows the percentage of the total possible signals at each physiological "transfer station" along the auditory pathway (refer to Figure 3.10 for the pathway), allowing the visualization of the signal loss related to the right side of the brain. Only the right ear lost wave II, while still maintaining wave I. Additionally, only the right ear lost wave III or wave V, while still maintaining all of the other waves. On eleven occasions, missing waveforms seen at one hour post blast exposure had recovered by the four hour post blast time point. However, the four hour latencies for wave V of these specimens were significantly delayed, except for the right ear of LF26. On sixteen occasions, the traces at four hours post exposure had additional or new missing waveforms compared to the traces at one hour post exposure. Generally, the latencies at the one hour time point for the same ear of these specimens were delayed. This phenomenon was always true when the right ear was the affected ear. However, for two of the specimens, there were no latency changes in the affected ear at the one hour time point, but there were latency changes in the opposite ear. Both of these two cases were in the left ear and lost waves III-V at the four hour post exposure time point. There were two exceptions to these latency delays, LF59 and LF32. Both of these specimens had no discernable signal at the four hour time point, but no significant latencies in either ear at the one hour time point.

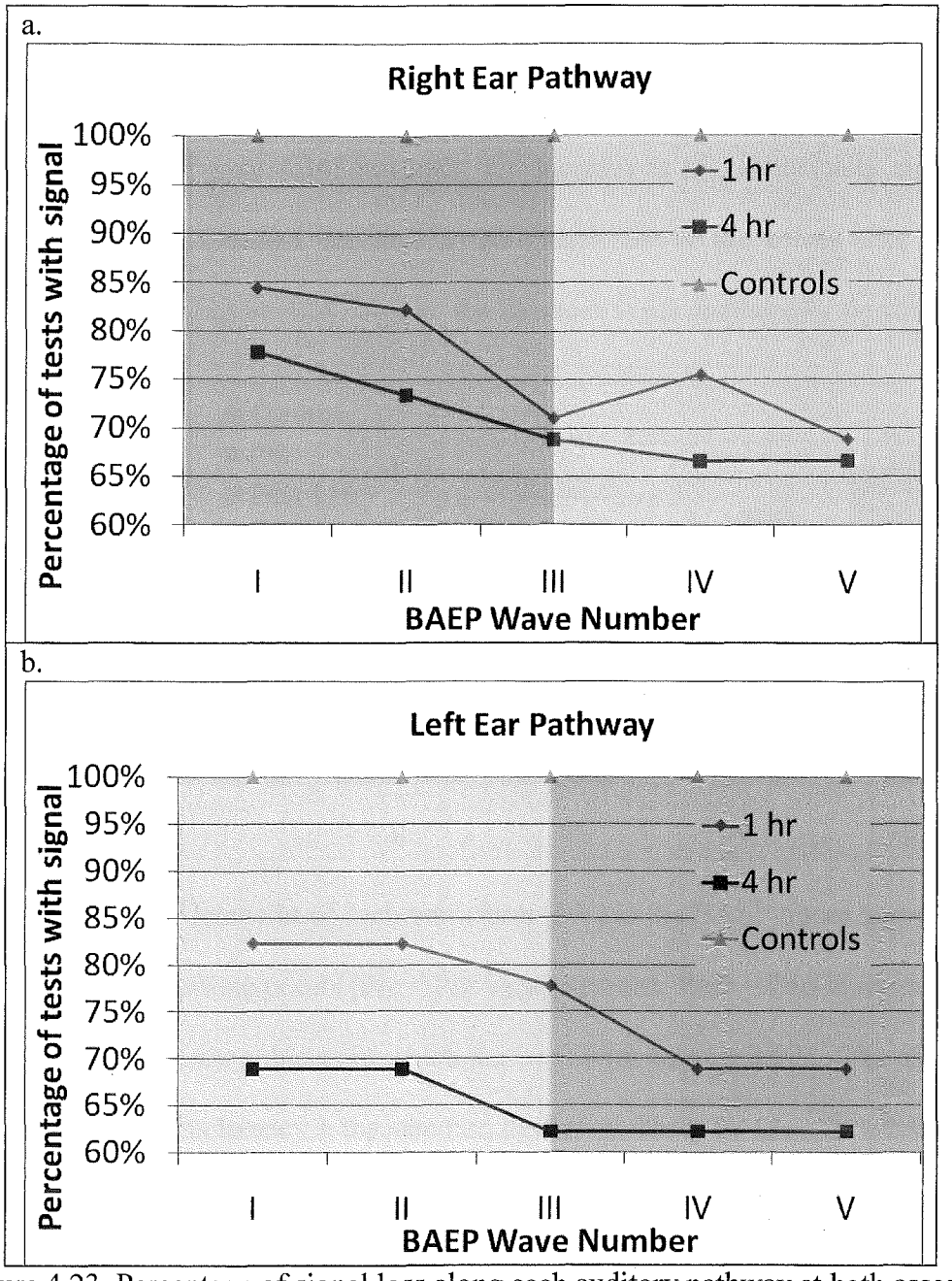

Figure 4.23. Percentage of signal loss along each auditory pathway at both assessment times after the blast exposure. The red and grey boxes signify the right and left sides of the body, respectively. At the superior olivary nucleus, wave III, the signal decussates to the opposite side of the head.

The actual values for the latencies and amplitudes of the waves, when present, showed no statistically significant trend with blast exposure, blast level, or assessment

time. Tables with all of the calculated amplitudes and latencies can be seen in Appendix D. There is an apparent increase in the latencies for the post exposure traces for all of the waves, as shown in Figure 4.24; however, the increase is not statistically significant. Similarly, there is an apparent decrease in the amplitudes of the waves after the blast exposure, as shown in Figure 4.25. Again, the decrease is not statistically significant.

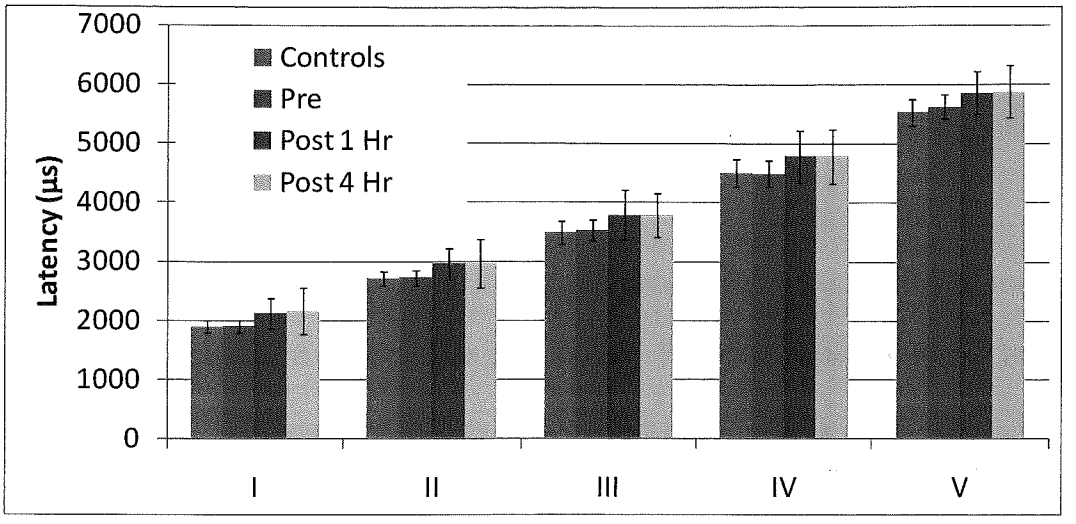

Figure 4.24. The latencies of each waveform (I-V) in the BAEP traces across all of the subjects at various time points (Pre = Pre blast exposure, Post = Post blast exposure). The data only reflects subjects in which the waveform was available. The data is presented as the mean latency ± the standard deviation. The n for the controls was 12. The n for the pre blast exposures was 100. The n for one hour post blast exposure was 71. The n for four hours post blast exposure was 62.

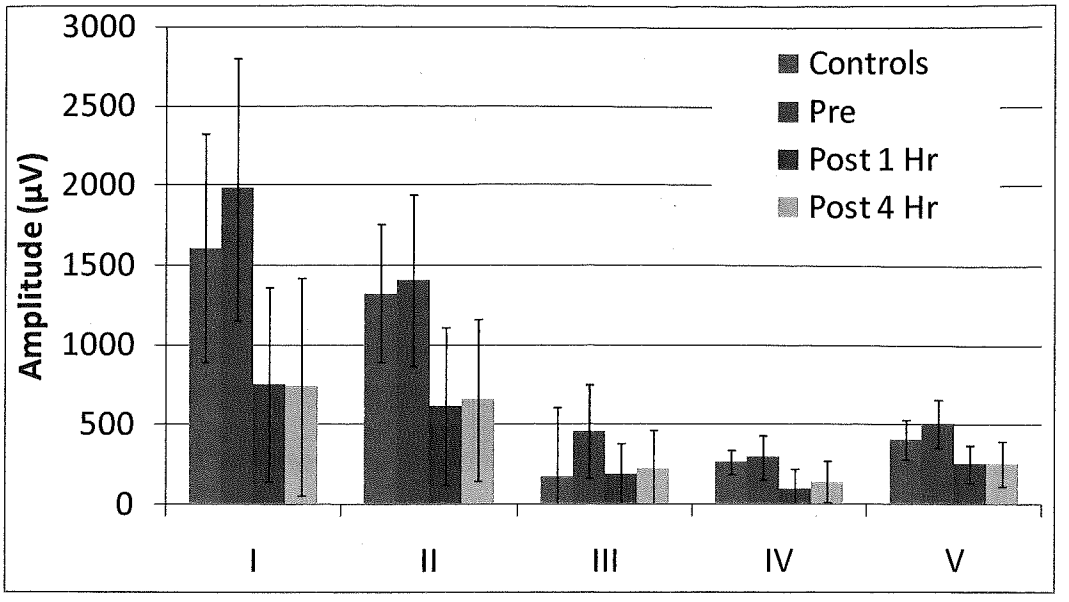

Figure 4.25. The magnitudes of the peaks for each waveform (I-V) in the BAEP traces across all of the subjects at various time points (Pre = Pre blast exposure, Post = Post blast exposure). The data only reflects subjects in which the peak amplitude was available. Peak III has a negative amplitude, but the magnitude of the amplitude is plotted here for ease of viewing. The data is presented as the mean amplitude ± the standard deviation. The n for the controls was 12. The n for the pre blast exposures was 100. The n for one hour post blast exposure was 71. The n for four hours post blast exposure was 62.

4.2.2.1 Statistical Results

Using the results of the Pearson product-moment correlation coefficient calculations mentioned in the VEP results, in which the head length, width, and circumference all correlated, the head width was chosen as the head anthropometry value to be used for the remainder of the brainstem auditory evoked potential analysis, since the electrodes are placed along that axis of the head.

Duration and overpressure were the only significant parameters ($p<0.05$) in the logistic regression model when pressure, duration, head width, anesthetic dose, and the time of the last dose were considered. Consequently, the remaining results only reflect the models that include pressure and duration.

The model for the 50% risk of BAEP signal loss is shown in Figure 4.26. Models for the signal loss were developed for each ear as well as both ears together. Parameters for the regression model are shown in Table 4.11 with model statistics in Table 4.12. The left ear and both ear models had statistically significant regression coefficients for pressure and duration ($p < 0.05$). The coefficient for the duration was not significant in the right ear model ($p > 0.05$). The model for the left ear was the only model that did not exclude a fit using the Hosmer-Lemeshow statistic ($p > 0.77$).

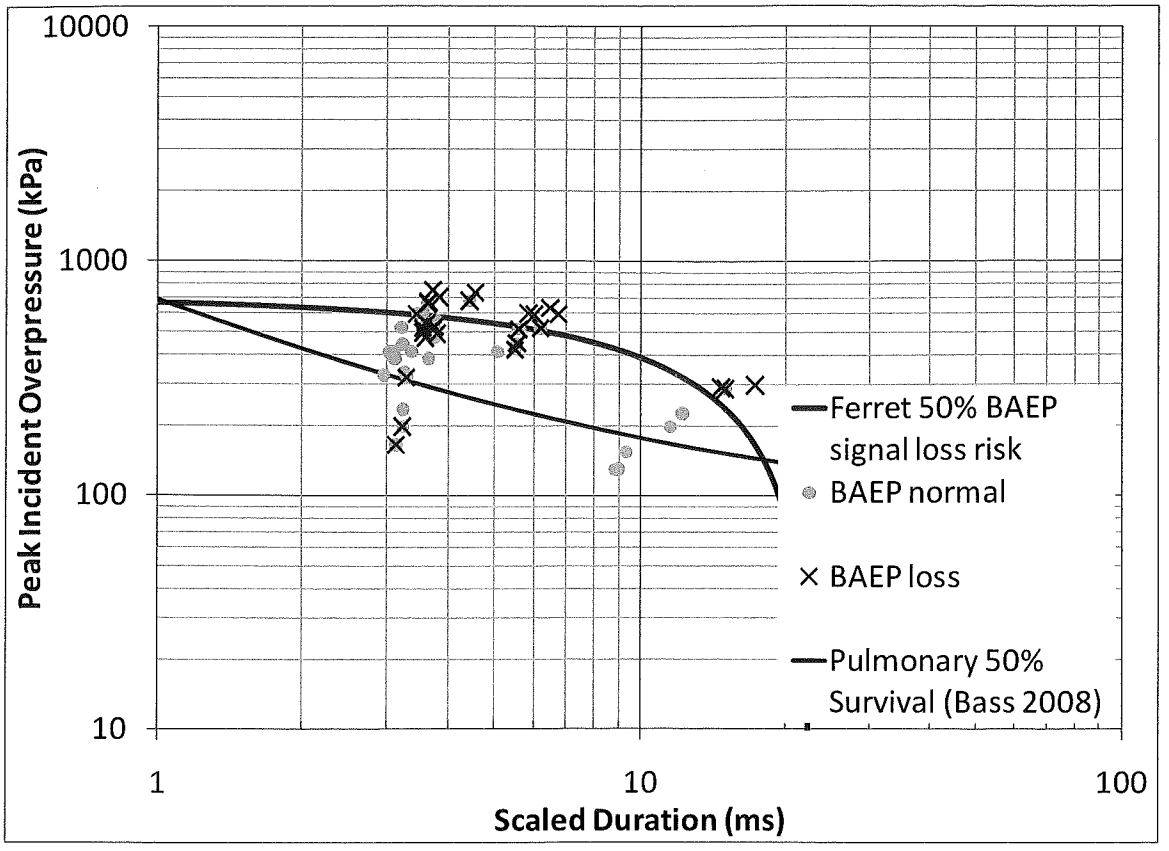

Figure 4.26. Logistic Risk Function (50%) for BAEP Signal Loss from Exposure to Primary Blast Waves

Table 4.11: Logistic Regression Model Estimates (95% confidence limits) for BAEP

	Model	Pressure		Duration	
		Odds Ratio	p	Odds Ratio	p
Signal Loss	Left Ear Only	1.02 (1.01,1.03)	0.0006	1.63 (1.18,2.23)	0.003
	Right Ear Only	1.01 (1.00,1.01)	0.008	1.23 (0.99,1.52)	0.06
	Left and Right Ear Together	1.01 (1.01,1.01)	<0.0001	1.34 (1.13,1.58)	0.0008

Table 4.12: Logistic Regression Model Fit Statistics for BAEP

	Model	Hosmer-Lemeshow	p
Signal Loss	Left Ear Only	4.8457	0.7739
	Right Ear Only	16.3192	0.0380
	Left and Right Ear Together	19.1329	0.0142

Chapter 5. DISCUSSION

The principal aim of the present study is to determine the injury risk of blast brain injuries from primary blast exposures. The study is divided into three parts. The first component was to create an appropriate model for a blast exposure to the head. The second component consisted of determining and measuring pathophysiological consequences to the blast exposure to be modeled in the risk functions. The final component established injury risk functions for the various clinical and nonclinical injury measures.

5.1 Blast Brain Injury Risk Functions

5.1.1 Macroscopic Injury Risk Functions

Typical injury metrics for unprotected blast have been based on pulmonary or gastrointestinal injuries. Previous blast research has long suggested that, at least for fatalities, the brain is more tolerant to blast loading than are the lungs or gastrointestinal tract (Hooker 1924). However, there were no previous risk functions for brain injury from primary blast. Several earlier studies had administered an isolated blast to the head while offering protection to the blast-sensitive thoracic and abdominal regions (Romba 1959, Clemedson 1953, Krohn 1941, Rafaels 2010b). These studies utilized blast pressure and duration levels that would have likely exhibited significant pulmonary injuries without protection. These results demonstrated little macroscopic evidence of brain injury, so research into blast brain injury and blast brain injury risks were not investigated.

However, the fact that blast exposure to the unprotected thorax and head will result in fatal pulmonary injury at pressure and duration levels below that required to produce

significant brain pathology, does not mean it is also true when the thorax and abdomen are protected. Comparing the peak incident overpressure and scaled duration of the tests in this study with the pulmonary injury risk assessment (Bass *et al.* 2008) shows the blast injury sensitivities of lung and brain are different. Using fatality as the endpoint for positive phase durations less than approximately 18 ms, the brain demonstrates a greater tolerance than lung for primary blast injury (Figure 5.1). In this study, the majority (73%) of blast brain cases that exceeded the 1% for pulmonary survival curve survived. The results of this study indicate that the blast brain injury fatality tolerance is much greater than the pulmonary fatality tolerance when the thorax and abdomen are protected from blast. At the lowest positive phase durations, the 50% fatality risk function for blast overpressure to the brain was more than twice the overpressure level for the same pulmonary lethality risk.

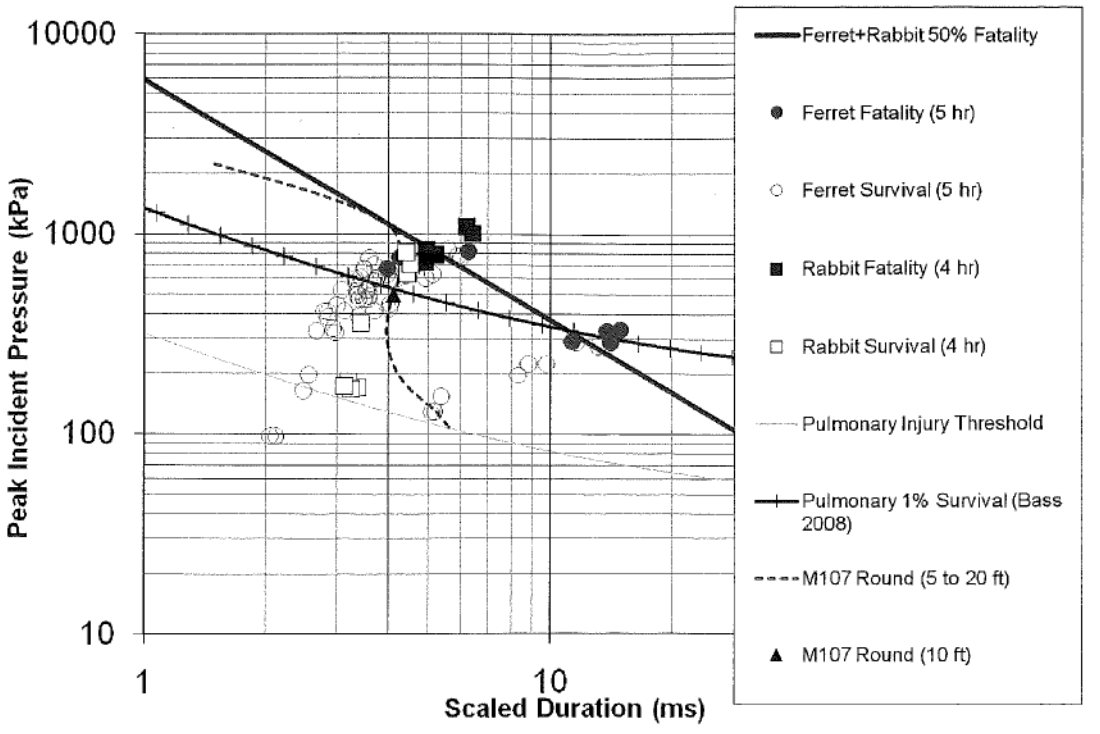

Figure 5.1. Logistic Risk Function (50%) for Fatality from Exposure to Primary Blast Waves with Scaled Rabbit Data (Rafaels 2010b)

On the other hand, for nonfatal injuries, the 50% injury risk for mild intracranial bleeding occurred at peak overpressure values comparable to those for low probability fatal and threshold pulmonary injury, especially at positive phase blast durations of 2 ms or less. This suggests that human brain injuries, especially brain injuries that might result in altered cognition and/or emotion, may occur at lower peak overpressure levels than that necessary for pulmonary fatalities. In current military conflicts, the almost universal use of body armor generally acts to increase the effective tolerance of the pulmonary system relative to the brain. Wood *et al.* (2010) found that ballistic protective vests with hard body armor decreased the overpressure applied to the torso by a factor of 50 or more, and decreased the overpressure rise time, with both effects substantially increasing the blast level required to create pulmonary injury. An available human epidemiological

primary blast injury case with a M107 round (Rafaels 2010b) is compared (Figure 5.2) to prior blast experiments with protected thoraces (Krohn 1941, Clemedson 1953). These prior data are consistent with both the case report and current fatality criteria reported in this study.

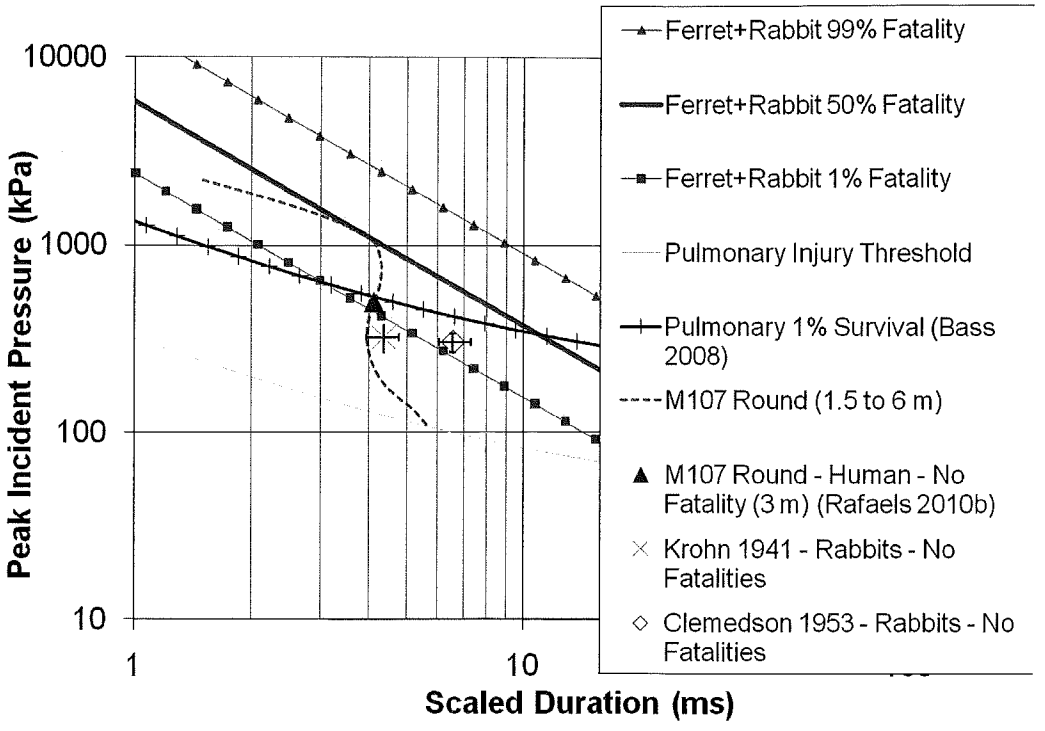

Figure 5.2. Previous Experiments, Epidemiology for Fatality from Exposure to Primary Blast Waves

5.1.2 Applicability to Humans

The principal unknown in the application of the injury risk functions to humans is the effect of body mass scaling. Realistically, it is impossible to test humans experimentally to determine the actual blast brain injury risk for man. Although animal models are the best models for studying blast brain injury, most animals are not the same size as humans, possibly making their risk different from a human's risk. Therefore, scaling must be performed to link the animal data with the human risk. Though there is

substantial evidence that body mass scaling is appropriate for blunt impact (cf. Eppinger 1984), its use in scaling blast injuries is not completely validated. Additional investigations on scaling for blast injuries are important as there is both histological and behavioral evidence of blast brain injury in rodents at incident overpressure levels below 20 kPa for very long scaled positive phase durations (Zhu 2010). In addition, there is a wide difference in the rodent animal model compared to the ferret, rabbit, or pig model. Other variables, such as the amount of gyrencephaly, the grey to white matter ratio, or the skull thickness may have to be taken into account in the scaling technique. In brief, more work needs to be performed to determine the best scaling method to assure greater confidence in the applicability of these risk functions to humans.

Aside from the scaling, the applicability of these risk functions is also limited to a single exposure from a freefield blast condition. The overpressure loading behind armor may not maintain the ideal blast wave. For the protected case, these curves can provide a conservative estimate for the injury risks to the brain, assuming the protective equipment reduces the peak overpressure. For the unprotected condition, these risk curves are directly applicable to freefield blast conditions. This unprotected condition would account for the majority of civilians and first-responders who are also at risk to blast exposures and do not wear or wear more limited personal protective equipment.

5.2 Pathophysiological Consequences

5.2.1 Cardiac and Respiratory Pathophysiological Measures

Heart rate decreases and apnea were present after isolated blast exposure to the head, in this study. Typically, bradycardia and apnea are found in blast injuries with blast exposures to the thorax (Guy 1998, Jaffin 1987, Clemedson 1949). Bradycardia often

occurs immediately after the thoracic exposure with a recovery to normal values within 15 minutes (Guy 1998, Irwin 1999). Apnea also occurs immediately after exposure and can recover within a few seconds or up to several hours later (Guy 1998, Clemedson 1949). The bradycardia and apnea in this study, however, may not follow the same injury pathway, as there were no remarkable lung injuries.

When there is injury to the lungs, previous research has linked the bradycardia and apnea seen after blast exposure to the vagal pathway (Irwin 1999, Cernak 1996). The vagal pathway begins in the medulla oblongata of the brainstem and travels down to the gut, branching off into several organs including the heart and lungs, slowing heart rate and constricting airways (McArdle 2001). It is believed that pulmonary congestion and edema in the interstitial space from the blast lung injury stimulates the nerve endings of vagus nerve. The signals then reach the brain causing a reflex response of increased cholinergic activity to induce the bradycardia and apnea (Irwin 1999).

However, in this study, no remarkable cardiac or pulmonary injures were present, yet bradycardia and apnea were. It seems that injury to the brain also causes downstream effects along the vagal pathway. Since the medulla oblongata lies very close to the foramen magnum of the skull, it is very susceptible to injuries from brain edema, hemorrhaging, or a pressure drop similar to flow across an orifice (Levy 1999). The pressure changes from any or all of these events may stimulate the vagus nerve and cause the bradycardia and apnea seen in this study.

Apnea itself is a common finding in traditional TBI. Since the duration of the apnea has been shown to be dependent on the amount of energy transmitted to the brain, apnea has been shown to be a better predictor for the outcome from TBI than the mechanism of

the brain injury itself (Atkinson 2000). As apnea is an easy clinical feature to measure, is a common occurrence in blast injuries, and can be a predictor of injury severity, it is a good pathophysiological measure of blast brain injury.

5.2.2 Macroscopic Pathophysiological Measures

In this study hemorrhagic lesions were commonly found around the brainstem and on the ventral surface of the brain. This finding is not surprising as the majority of the brain's blood supply passes through these points. Additionally, the foramen magnum, or the opening that the brainstem passes through, can act as an outlet for the shock wave and pressure pulse, increasing the forces and strains in that area. Fluid percussion injury models, which models brain injury resulting from a pressure pulse, also has subcortical axonal damage and brainstem pathologies (Melvin 2002), similar to the blast brain injury pattern seen in this study, providing some more evidence for the injury mechanism in this area.

Hemorrhages are volumetric injuries; however, this study only measured the surface area of the hemorrhages. Since the hemorrhages were most often surface, or meningeal hemorrhages, this approximation may be sufficient in this experiment. The intraparenchymal hemorrhages, which were evaluated using histology, were not common, nor did they account for a large area. In fact, the surface area calculations were used to grade severity rather than provide the actual amount of hemorrhaging. As such, the surface area of the hemorrhage did correspond to the blast severity level, providing some evidence that the surface area can be used to compare hemorrhage levels.

Moreover, hemorrhagic lesions can be a useful pathophysiological measure. First, subarachnoid hemorrhaging has been associated with poor outcomes after traditional TBI

(Servadei 2002). In addition, hemorrhagic lesion size has been related to the Glasgow Coma Scale, a measure for brain injury severity (Levin 1992). Finally, the hemorrhages can be easily measured on a living subject using CTs or MRIs. Advanced MRI techniques are now able to image microhemorrhages as well (Benzinger 2009). To sum up, the injury risk function for hemorrhage severity in this study is a better predictor for hemorrhage because it actually models hemorrhage risk, compared to traditional head injury criteria, such as HIC, which is derived from the risk of skull fracture (Viano 1988).

5.2.3 Histological Pathophysiological Measures

Injured axons were visualized in two different ways. The first type of injured axon demonstrated axons with impaired axonal transport using β-APP. The second type of injured axon was one in which the neurofilament had disrupted sidearms using RM014 antibody. Although the sections of tissue were only labeled with one antibody, similar sections of tissue from the same specimen were stained with the other antibody to investigate the co-localization of the two different types of injured axons. In general, the amount of axons with impaired axonal transport far outnumbered the axons with altered neurofilaments.

In addition to the number of axons with altered neurofilaments being fewer than the axons with impaired axonal transport, the areas with β-APP positive axons did not always correspond to the areas of RM014 positive axons. Figure 5.3 shows the common areas of staining for β-APP and RM014. For example, the hippocampus often had extensive staining for β-APP, but no positive staining for RM014. One explanation for this difference is the fact that smaller axons contain more microtubules for transport per unit area and larger axons contain more neurofilaments per unit area (Stone 2001, Marmarou

2006). The axons within the hippocampus are of a smaller caliber, so they would be more likely to show damaged axonal transport than neurofilament alteration (Papasozomenos 1987).

Another area in which the RM014 positive staining was more prevalent when compared to β-APP was the peduncular region of the cerebrum and cerebellum. In this case, the RM014 was much more prevalent. In fact, in the blasted specimens, the entire region demonstrated positive staining. The axons in the peduncular regions are some of the largest in the brain and therefore have more neurofilaments per unit area than other regions in the brain (Watson 1991). Despite the number of neurofilaments in this area, the staining in this region nonetheless appears to be artifactual. Typically, the RM014 axons stain positively in a more isolated fashion (Stone 2001, 2004; Marmarou 2005, 2006); however, in this region of tissue, the entire section stains positively. While a relationship between the staining and blast exposure cannot be excluded, a more likely cause of this type of staining would be an artifact from poor tissue sectioning since these regions are near the edge of the brain tissue. Another potential cause is poor perfusion of the fixative which can contribute to autolysis of the tissue, increasing the phosphatase activity thus increasing the staining pattern for RM014. These possible causes may have acted independently or in concert, to increase the staining of the tissue.

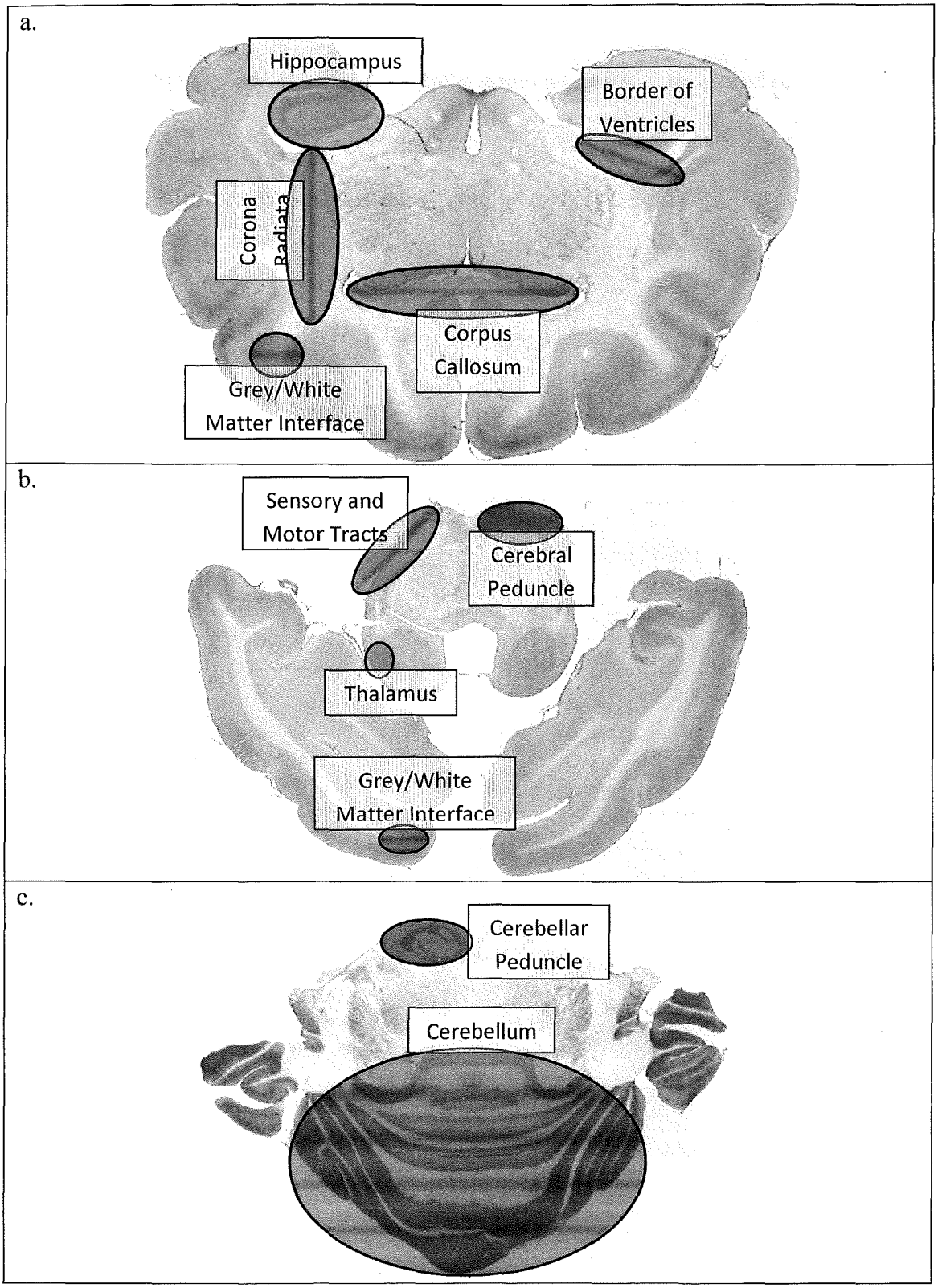

Figure 5.3. Frequent areas of positive staining for β-APP and RM014. The areas in which both stains were frequently immunopositive are colored both red and blue. The

areas in which only β-APP was frequently immunopositive are colored blue. And the areas in which only RM014 was frequently immunopositive are colored red. a.) Coronal section from the midbrain. b.) Coronal section from approximately 8 mm inferior to bregma. c.) Coronal section from the cerebellum.

In general, however, RM014 positive axons were more dependent on the duration of the blast exposure than the β-APP positive axons. Figure 5.4 shows the duration dependence for the positive staining of RM014 compared to β-APP. The theory behind this occurrence is that as the duration increases for a blast wave, the impulse, and consequently, momentum also increases. Generally, a short duration blast wave does not contain a lot of momentum; however, for longer duration blast waves, there is more momentum, and therefore, more deformation of the tissue (Cooper 1997). Estimates of the impulse conditions in this study using CONWEP demonstrate that the long duration exposures (>12 ms) match or exceed the impulses for even the highest pressure values, even though the pressures for the long duration conditions are just over a third of the magnitude. In traditional TBI, "ultrastructural compaction" of axons has been related to axonal stretching and dynamic deformation (Pal 2006). Similarly, the increased momentum for longer duration blasts may give rise to axonal stretching and dynamic deformation that would explain the increase in RM014 positive axons.

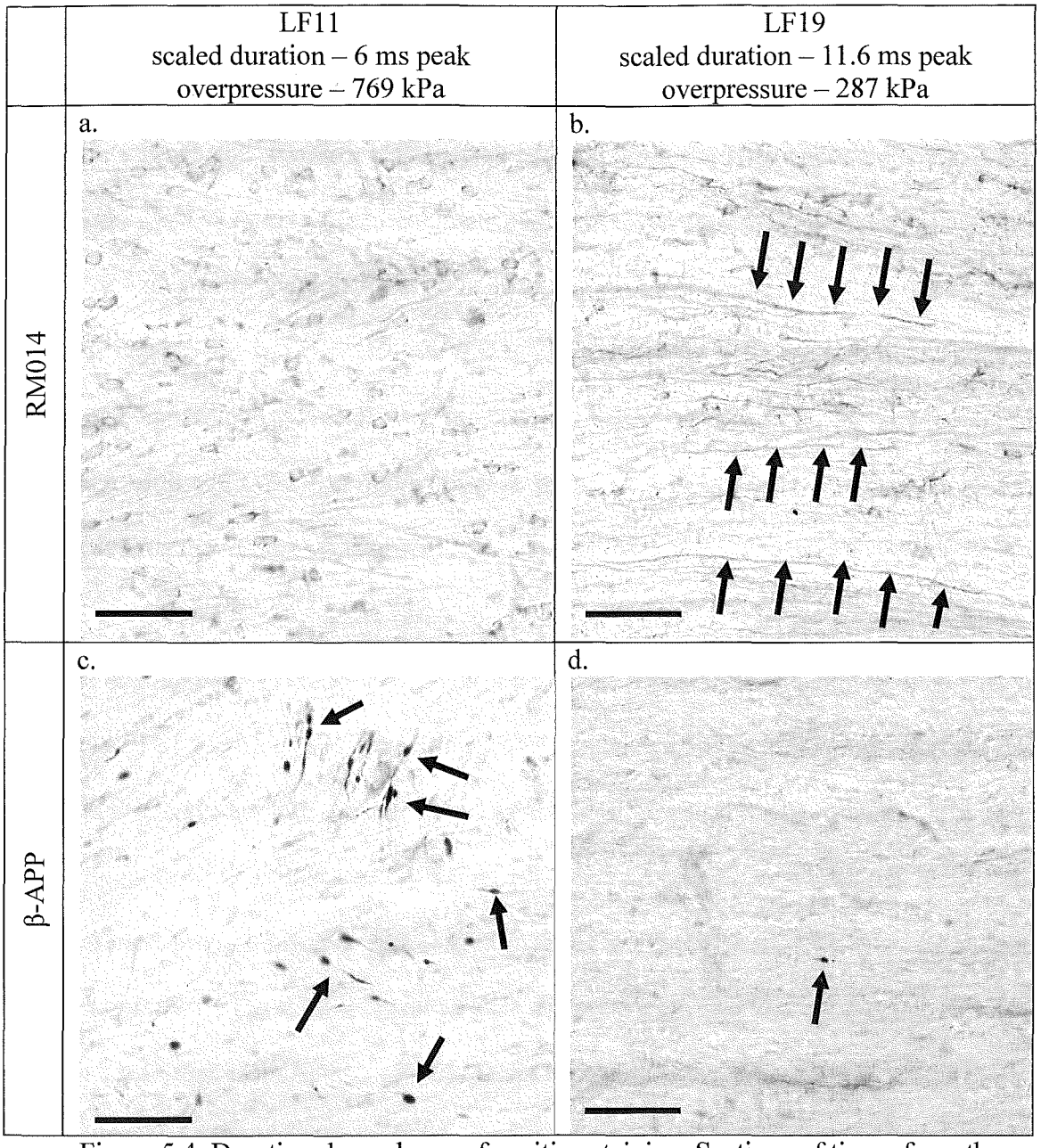

Figure 5.4. Duration dependence of positive staining. Sections of tissue from the corpus callosum. Black scale line = 50 μm. The black arrows highlight some of the positive axons. RM014 has more positive staining for longer durations (b) than shorter durations (a). β-APP has more positive staining for the higher overpressure (c) than the lower overpressure (d).

In this study, the antibody for GFAP did not demonstrate an increase in positive staining after an exposure to blast. However, other studies of blast brain injury did not visualize an increase in positive cells until 18 hours after the blast exposure (Saljo 2001, Tompkins 2008, Svetlov 2009a, Bauman 2009), perhaps suggesting that this study may not have had a long enough time point to measure the increases. On the other hand, Garman (2009) did not demonstrate any changes compared to the control specimens between 24 hours and 2 weeks after the blast exposure. Although no increased staining was seen with the GFAP antibody in this study, at 5 hours after the blast exposure, qualitative reactive gliosis was observed.

5.2.3.1 Traditional TBI vs. Blast TBI

The histological evidence suggests differences between the injury mechanisms in traditional TBI and blast TBI. Traditional TBI results from large momentum impacts that result in relatively large tissue deformations and motion. Blast exposure may cause brain injury with smaller strains and displacement when compared to traditional blunt TBI, perhaps indicating a different mechanism. When the brain is moving with an angular acceleration inside the skull from an impact, deviatoric stresses cause the axonal damage seen in traditional TBI (Adams 1984). Areas with high shear stresses, and consequently, higher amounts of positive axonal staining in traditional TBI, are the corpus callosum, the thalamus, and the midbrain (El Sayed 2008).

However, in blast TBI, the pressure wave causes volumetric stresses, as well as deviatoric stresses. The impedance mismatches between different structures in the brain, such as the grey/white matter and the CSF/tissue interfaces, provide a likely place for cavitation or spalling injury mechanisms that create volumetric stresses which also injure

the axons. Thus, in addition to increased numbers of injured axons at the high shear stress areas in traditional TBI, blast TBI also commonly has injured axons in the cerebellum, near the ventricles, and near the grey/white matter interfaces.

The higher prevalence of β-APP compared to RM014 also indicates that blast TBI is different from traditional TBI, where the amount of β-APP and RM014 positive staining is similar (Stone 2001, Marmarou 2006). Since there are more β-APP positive axons present in this study than RM014 positive axons, perhaps there is another mechanism for the increase in β-APP positive axons. It has previously been shown that the number of positively-stained β-APP damaged fibers is related to the brain's immune response, but the number of RM014 positive axons is not (Marmarou 2006). This may suggest that there is also an immune response component in the progression of these axonal injuries after blast exposure, in addition to the mechanical insult. In fact, measures for the immune response have already been shown to be increased after a blast exposure in previous studies (Kaur 1995, 1996, 1997b; Saljo 2001; Tompkins 2008).

Additional evidence for blast TBI having a different injury mechanism from traditional TBI is the pattern of staining throughout the brain tissue. The β-APP positive axons stained diffusely throughout the brain, while in traditional TBI the injured axons are generally found on the ipsilateral side (Bramlett 1997, Pierce 1996). This finding is similar to another study of blast brain injury where there appeared to be no regional difference of positive staining (Saljo 2002a). Most of the other biomarkers that have been used for blast have an association with the immune system, and no regional dependence has been noted (Kaur 1995, 1996, 1997b; Saljo 2001, Garman 2009, Tompkins 2008, Svetlov 2009a, Saljo 2003). However, not all reported biomarkers for

blast injury lack regional specificity. For example, another marker for neurofilament injury is more prevalent on the ipsilateral side to the blast exposure (Saljo 2000), as are markers for apoptotic transcriptional factors (Saljo 2002a, Kato 2007). The regional independence of the β-APP compared to traditional TBI may result from the blast wave impacting the whole head versus the focal impact region in a traditional blunt TBI. Additionally, the immune component to β-APP staining may contribute to its widespread immunoreactivity.

In other blast studies, GFAP staining has shown a higher amount of expression on the ipsilateral side (Bauman 2009). However, the GFAP staining in this study had qualitatively, but not statistically significant, positive reactivity on the side opposite of the blast for lower pressure conditions, while it was more diffuse for the higher pressure conditions as shown in Figure 5.5. The low pressures and long durations in this study may have caused the increased reactivity on the contralateral side because of the reflecting surface behind the head. This increase is similar to the contralateral side exhibiting more severe pulmonary injuries against a reflecting surface in a study by Bowen *et al.* (1968). Alternatively, the anatomy and structure of the ventral surface of the brain is markedly different from the dorsal surface, and may have contributed to this observed difference.

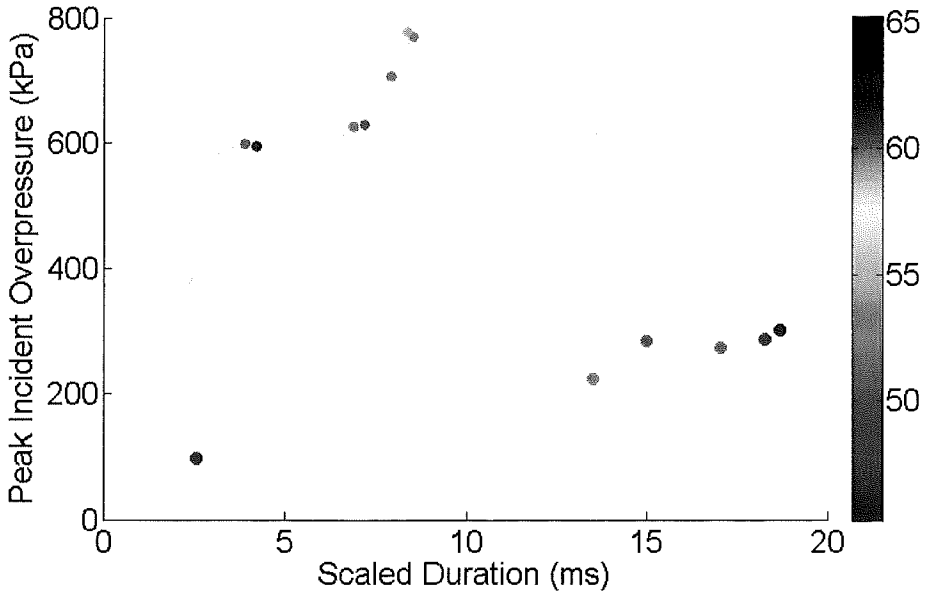

Figure 5.5. Regional distribution of GFAP positive staining after exposure to blast. The size and color of the points on the plot correspond to the percentage of positive staining for the contralateral side of the brain at that overpressure and duration.

5.2.3.2 Histological Injury Regression

The positive stained area for axonal injury visualized with β-APP was correlated with overpressure and duration levels of the blast exposure. As expected, as the pressure increased, the amount of positive area increased. Similarly, as the duration increased, the amount of positive area increased. Since the amount of positive axonal staining is correlated to the peak overpressure and duration of the blast exposure, as are the other injury risk functions, a relationship can be determined between the amount of injured axons and other injury metrics such as apnea and BAEP signal loss.

Interestingly, after performing a pathway analysis from pressure and duration to apnea through the axonal area, it was found that pressure and duration have direct and indirect effects on apnea following the path analysis described by Shipley (2000).

Pressure and duration directly affect apnea, but apnea was also affected indirectly, mediated by the axonal area. In other words, for a given change in pressure and duration, changing the axonal area and no other causal parents would affect the outcome on apnea. This finding makes sense biologically because if there are injured axons near the respiratory control center of the medulla oblongata, one can expect apnea.

Similarly, a pathway analysis was performed from pressure and duration to BAEP signal loss through axonal area. Again, it was found that the pressure and duration have direct and indirect effects on BAEP signal loss. This finding is consistent with the biology because one would expect to see injuries to the axons along the sensory pathway that was lost.

5.2.4 Clinical Pathophysiological Measures

The BAEP results have produced the most interesting findings for clinical measures. The right side of the head appeared to suffer more effects from the blast exposure than the left side of the head. First, portions of the BAEP waveform were lost more frequently and at lower overpressure levels for the right ear than for the left ear. Second, only the right ear ever lost wave II, while still maintaining wave I. Third, the right ear lost wave III, while still having all of the other waves at the one hour time point, whereas the left ear never did. Fourth, the right ear lost wave V, while still having all of the other waves at the one hour time point, whereas the left ear never did. Finally, the left ear lost waves III-V at the four hour time point with no previous indication of injury at the one hour time point in that ear; however, the right ear had latency delays at the one hour time point.

To understand these signal changes from the blast exposure, it is necessary to understand the anatomy of the auditory pathway (refer to Figure 3.10). The cochlear nerve, or wave I, travels from the internal acoustic meatus near the ear to the medulla oblongata of the brainstem. The cochlear nucleus, or wave II, is where the pathway enters the brainstem. The auditory pathway decussates, or crosses over to other side of the brain, after wave II. At wave III, or the superior olivary nucleus, the majority of the signal decussates and travels to the superior olivary nucleus on the opposite side before traveling up to the lateral lemniscus and inferior colliculus on the opposite side. The remaining signal stays on the original side and travels up to the lateral lemniscus and inferior colliculus on that side (FitzGerald 2007).

When the right ear loses wave II, but maintains wave I, the pathway is affected on the right side of the head. A lesion likely exists between the cochlear nerve and the cochlear nucleus. When wave III is lost and the other waves remain, the injury could result from the superior olivary nucleus on either side, as it gets inputs from both ears. However, in this study, when just wave III was lost in the right ear, the left ear either had no waves following wave III or no signal at the four hour time point. Waves IV and V from the left ear originate on the right side of the head after the signal has crossed over. When just wave V is lost, there could be minor damage along the beginning of the pathway to lose enough amplitude to not be distinguished from the noise. Wave V has been shown to be eliminated after cochlear pathology and no evidence of injury at the inferior colliculus (Hardie 1999). This finding would support an injury to the ear and not the central auditory system for a loss of wave V only.

An additional sign of injury to the right side of the head can occur with lost waveforms in the left ear trace. When the left ear lost waves III-V at the four hour time point with no indication of injury at the one hour time point in that ear, the right ear had latency delays at the one hour time point. As mentioned before, the auditory pathway decussates starting at wave III, so the origins for left ear waves III-V are on the right side of the head.

The BAEP trends suggest an increased incidence of injury to the right side of the head; however, this observation was not statistically significant. The logistic regression equation with the best fit and statistically significant parameters was for the left ear. The configuration for the blast exposure to the head was directed to the dorsal part of the head with neither the left nor right side of the head closer to the blast than the other. However, the right side of the head was facing the table holding the test fixture. Even though the right side of the head was approximately five-inches from the table, the blast wave could have reflected off of the table to provide a larger blast dose to that side than what was predicted to help explain the trends and the poorer fit for the right ear. Despite the evoked potential evidence for an increased injury to the right side of the head, the histology for β-APP and GFAP did not demonstrate increased immunoreactivity on the right side.

The VEP results did not provide any statistically significant correlation with the blast parameters. The logistic regression for loss of VEP signal had statistically significant parameters and a good fit, but the risk for signal loss of the BAEP signal requires a lower blast load, making it a more useful tool to distinguish milder injuries. The logistic regression for significant latency delays had statistically significant parameters for the

left eye only; however, the fit did not follow the data well. The signal loss and most cases of atypical morphology affected both eyes. The visual pathway seen in Figure 5.6 shows how both eyes use both the left and right pathways to relay the visual information. Since the light is not focused on either side of the visual field, some signal will likely be measured near the visual cortex even if there is an injury to one of the pathways. Only an injury to the optic nerve would eliminate the signal from a single eye. Future investigations should explore exciting only one hemifield of each eye at a time. In any case, the blast exposure in this model was not directed towards the optical system. The ventral location of the visual pathway contralateral to the blast wave exposure allows for a reduction of the blast loading on the interested structures, as the blast may be attenuated in the tissue before reaching the visual pathway. Additionally, the depth of the visual pathway in the tissue makes the VEP measurement a farfield measurement and, consequently, more susceptible to noise.

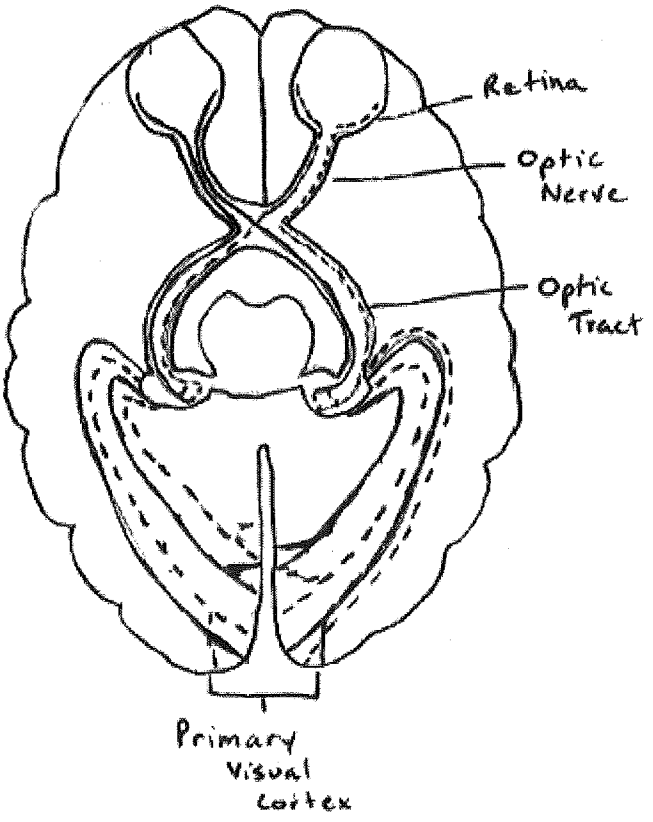

Figure 5.6. The visual pathway. Each eye uses a pathway on the ipsilateral side and the contralateral side to relay the visual information to the visual cortex.

Neither of the evoked potential tests provided any statistically significant correlation with the blast parameters when examining the amplitudes and latencies of the peaks. The determination of the descriptive values of the peaks is subject to interobserver and intraobserver variability when examined multiple times. Figure 5.7 demonstrates noisy traces alongside clear traces to illustrate the difficulty in reliably determining the amplitudes and latencies of the peaks for some waveforms. This difficulty may have contributed to the poor correlation of the amplitudes and latencies of the peaks with the blast parameters.

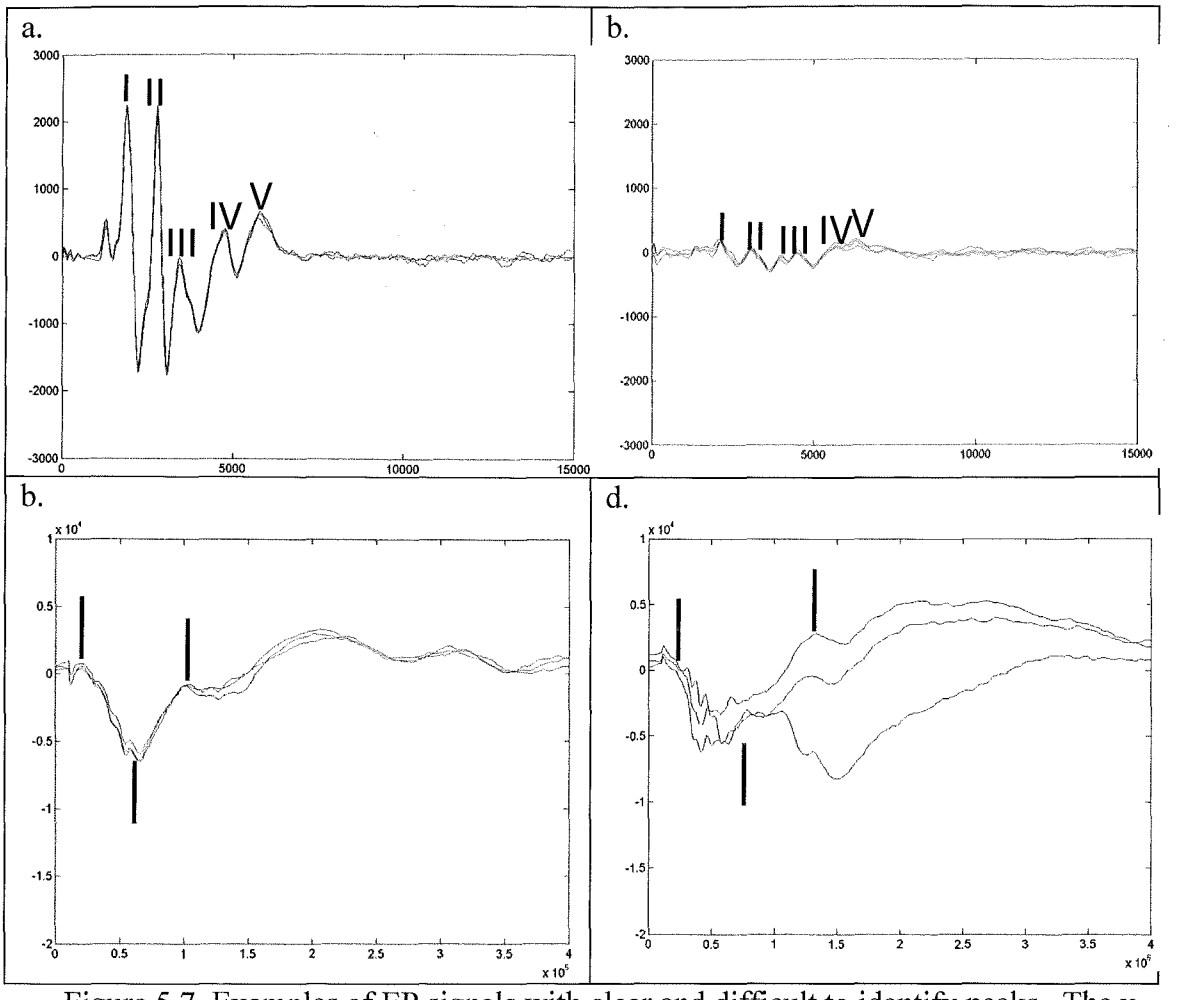

Figure 5.7. Examples of EP signals with clear and difficult to identify peaks. The x-axis is μs. The y-axis is μV. a.) BAEP for LF20 right ear at 4 hours post sham exposure. Example of easily identifiable peaks. b.) BAEP for LF53 left ear at 4 hours post blast exposure. Example of a trace with peaks that are difficult to identify. c.) VEP for LF70 right eye before the blast exposure. Example of an easily identifiable peak. d.) VEP for LF65 left eye at 1 hour post blast exposure. Example of a trace with a difficult peak to identify.

5.2.4.1 Evoked Potential Injury Risk Functions

The current injury metric for hearing loss is a risk for eardrum rupture (Richmond 1989). Although the eardrum acts to amplify the acoustical energy to the inner ear, it is

not needed to convert the mechanical energy to electrical energy for hearing. Consequently, although hearing loss is present with eardrum rupture, it does not eliminate hearing altogether (Hirsch 1968). The current BAEP signal loss injury risk curve is compared to the eardrum rupture tolerance in Figure 5.8. The 50% risk for eardrum rupture indicates that pressures above 100 kPa are likely to cause eardrum rupture. Although eardrum rupture was difficult to visualize in this study, every test condition exceeded the 50% risk for eardrum rupture, even though only a few of the specimens exposed to severe levels exhibited signs of eardrum rupture. One explanation for this difference in tympanic membrane rupture may be due to the different structure and anatomy of the ferret ear compared to the ears used in the study to determine the eardrum rupture risk (Hirsch 1968). The loss of at least wave V of the BAEP, the criteria used in this risk analysis, invariably signifies a poor prognosis from head trauma (Cant 1986). For short positive phase blast durations, the risk of significant head trauma, in the form of BAEP signal loss, lies below the 50% risk for apnea and the 1% survivability risk for pulmonary injuries. This finding suggests that brain injuries of a severe magnitude can occur at pressure levels that may be survivable without protection, but are even more survivable with protection to the thorax. Apnea is easy to diagnose and indicates that there is significant damage in the brain. In addition, the loss of BAEP signal may indicate severe damage at lower levels of blast that may not present with obvious outward symptoms.

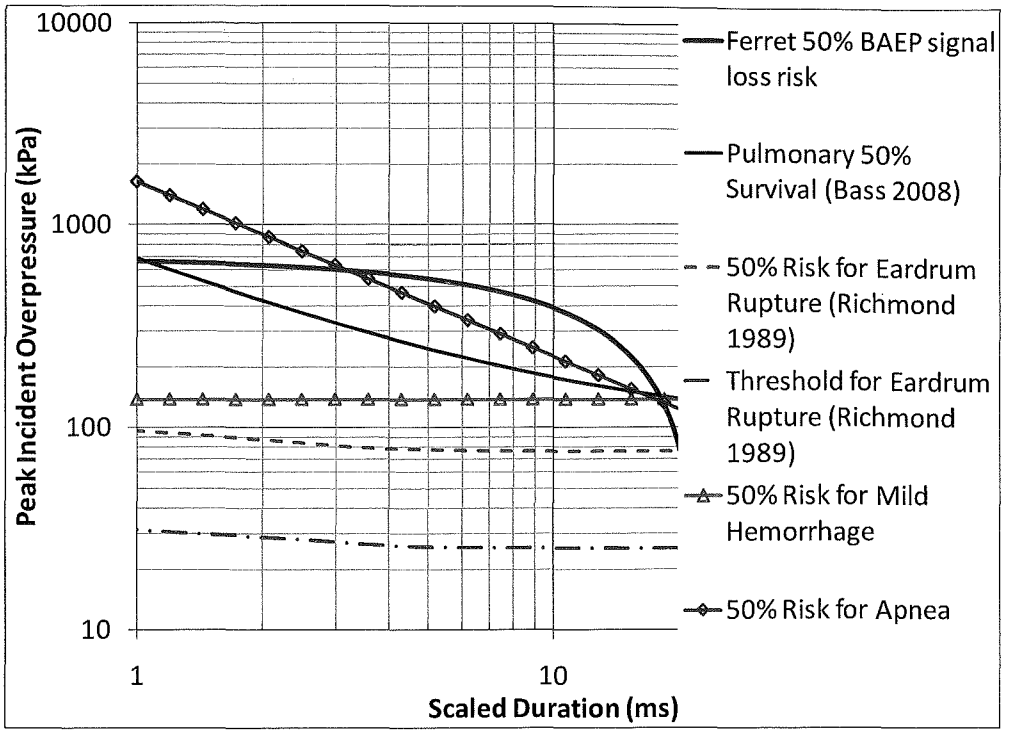

Figure 5.8. Eardrum rupture risk compared with the various injury risk functions determined in this study.

The risk for signal loss for VEP occurs at a greater overpressure than BAEP as demonstrated in Figure 5.9. Since the VEP is a farfield measure of the visual pathway and the signal for the flash of light would be transferred to the visual cortex along both sides of the brain, it is expected that a more severe injury would be required to lose the entire VEP signal. Although visual disturbances are seen clinically, and one of the goals of this study was to determine an injury risk based on visual system dysfunction, the flash VEP method employed may not be sensitive enough to discern mild injuries along the pathway.

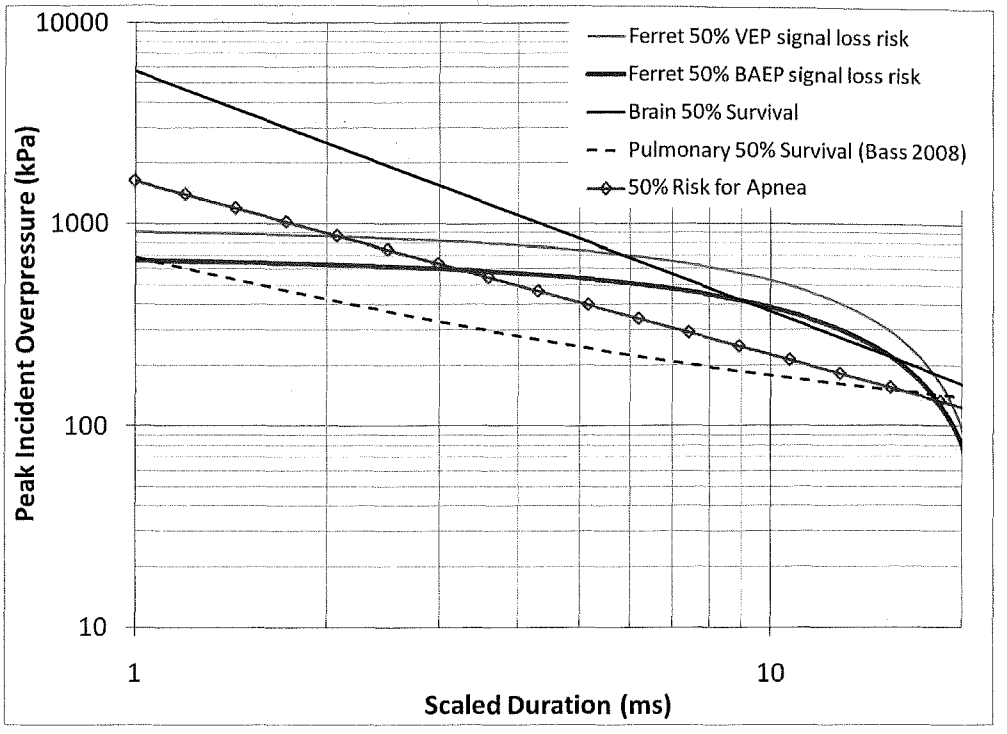

Figure 5.9. VEP signal loss risk compared to BAEP signal loss and fatality risk.

5.3 Laboratory Model for Primary Blast Brain Injury

5.3.1 Model for a Blast Exposure Isolated to the Head

The shock tube was able to recreate the overpressures and durations from a range of real explosives, as shown in Figure 5.10. The blast exposure conditions from this study can be compared to blast exposure conditions from current threats, which can be approximated by equivalent weights of TNT. Mortar rounds, such as M107, that are often used to produce IEDs which can cause blast injuries (Nelson 2008), for example, can be approximated with 7.3 kg of TNT. Additionally, the shock tube was able to replicate head injuries seen in animal and human cases produced from high explosives, namely hemorrhaging and apnea (Denny-Brown 1945).

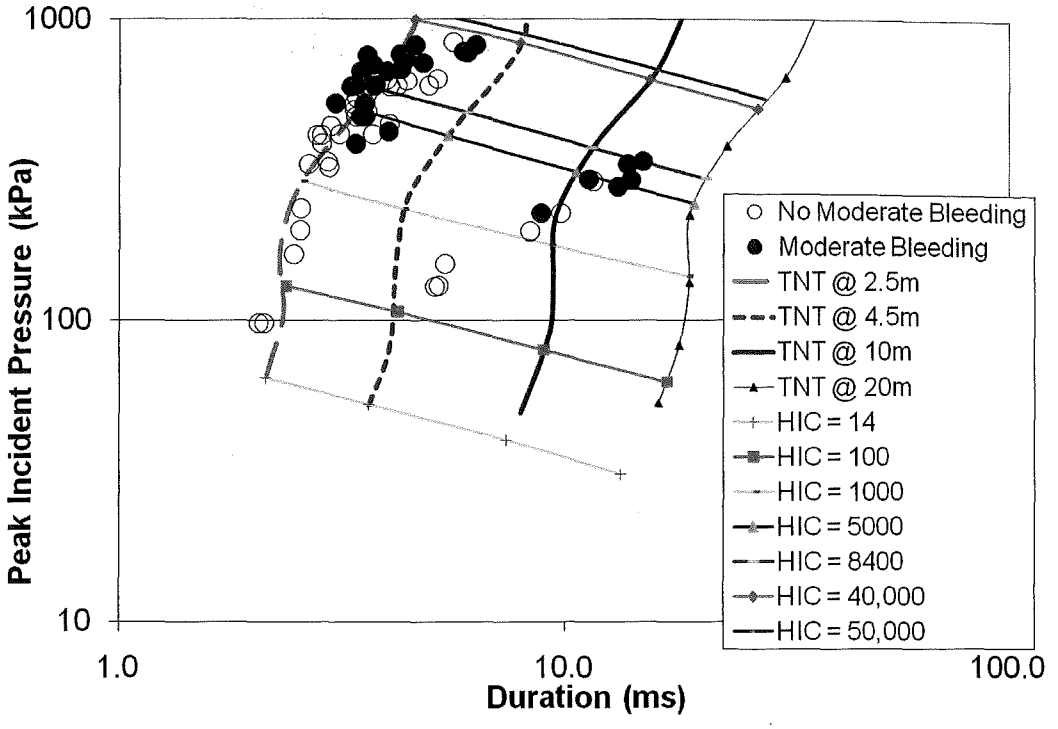

Figure 5.10. The blast exposure conditions from this study compared to 4 different standoff distances from various charge sizes of TNT. Seven iso-HIC lines are also represented on the chart to demonstrate how current injury metrics compare to the blast exposure conditions in this study.

Figure 5.10 also shows how HIC, a current injury risk function for head injury, compares to the blast loading scenarios in this study. A HIC value of 1000 is often specified as the level for onset of severe head injury in automobile impacts (NHTSA 1995); however, blast conditions with HIC values of 1000 did not result in even moderate level hemorrhage. Some of the disparities between the predicted injuries from HIC and the actual injuries seen in the experiments may be accounted for by the significant frequencies of automobile impacts compared to blast impacts. For automobile impacts, the head acceleration data is filtered with a cutoff frequency of 1650 Hz; however, the specimen response to blast has frequency content at significantly higher levels (40 kHz).

Additionally, HIC assumes the head and brain act as a rigid body, but this assumption does not hold for blast. For automotive impacts, the large deformations of the tissue can be approximated with rigid body motion, but not so for the smaller deformations of brain tissue in blast.

This study also provided very effective protection of the thorax and abdomen against the blast overpressure. The peak overpressures near the head were as low as 100 kPa or even as high as 820 kPa, while the peak overpressures near the thorax and abdomen never exceeded 14 kPa. These values were well below the threshold for pulmonary injury from a blast exposure as shown in Figure 5.11. In addition to reducing the peak overpressure, the protective cylinder also prolonged the rise time to the peak pressure, as was seen in Figure 4.1. Previous research indicates that injury tolerance is very dependent on rise times (Richmond 1959), with the body being better able to adapt to longer rise times (deCandole 1967). The protection was not as effective on the negative phase of the pressure wave as the pressure levels could get as low as -125 kPa. Despite the peak negative pressure having a higher magnitude, the duration of the negative pressure was less than 3 ms and the rate of establishment of the negative peak was relatively slow. No injurious effects have been seen with negative pressures resulting from a short duration blast (Clemedson 1960). Lethal effects begin to appear at durations greater than 100 ms in mice (Brown 1956).

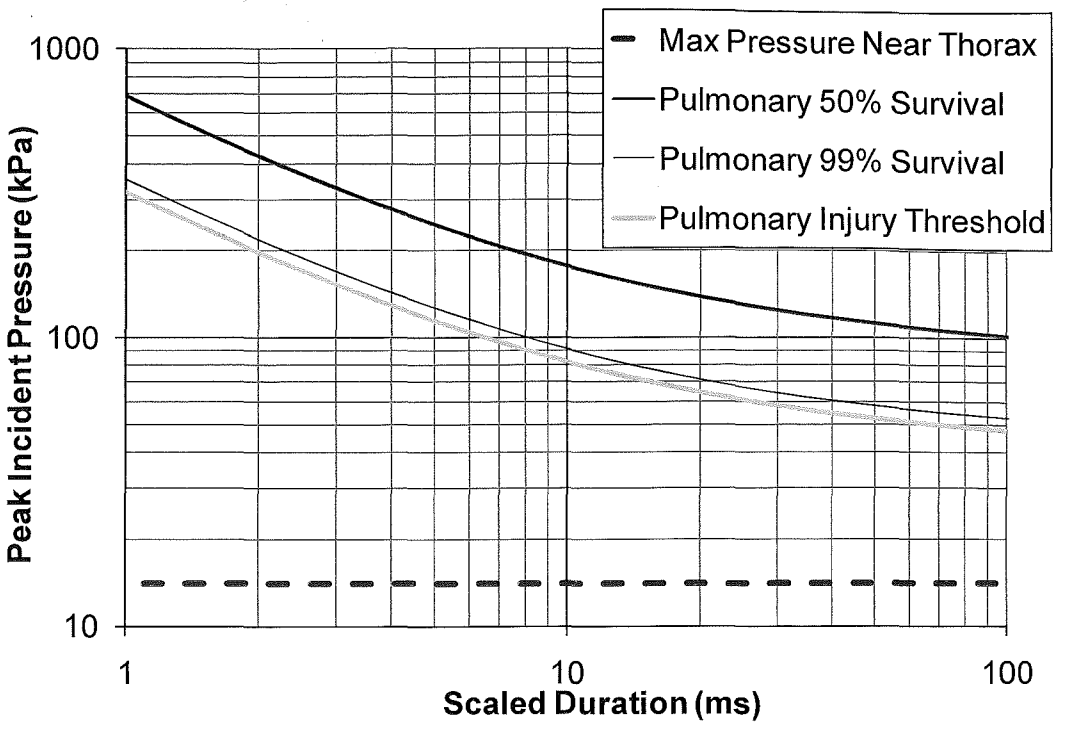

Figure 5.11. Maximum pressure value obtained from any test in this study near the thorax compared to the pulmonary injury risk curves from Bass (2008).

5.3.2 Animal Model for Blast Brain Injury

This work provides the baseline for future work into blast brain injuries using a model that has many advantages over the current rodent blast brain injury model. The rodent model, the most common blast brain injury model, has a relatively small size and modest cost, allowing for large scale studies; however, the lissencephalic nature of the rodent cortex does not allow for the appropriate modeling of the changes occurring in the gyri and sulci of brain injuries (Povlishock 1994). The next most prevalent model in blast brain injury studies has been the porcine model. This model has historically been chosen because of the larger size of the animal and the gyrencephalic brain, making this model more similar to humans (Saljo 2008). Unfortunately, neither the composition nor thickness of the rodent or porcine skull may be appropriate to model the blast wave

transmission into the calvarium (Bauman 2009). For traditional TBI, nonhuman primates most closely approximate the clinical manifestations of TBI (Povlishock 1994); however, the cost, size, technical limitations, and laboriousness of that animal model reduce its efficacy. This study has developed the ferret model as a model for blast brain injuries. The ferret model is both gyrencephalic as well as small and relatively inexpensive. Additionally, the skull thickness to the head length of the ferret is more similar to man than the rodent or pig. Aside from those factors, the model has been able to reproduce some of the injuries seen in human patients, including hemorrhaging (Ling 2009). Future work in blast brain injury should include behavioral studies, and the ferret may be a good model for those clinical measures as well (Rabe 1985). Thus, the ferret model is attractive in many ways and is recommended for further study into blast brain injuries.

5.4 Limitations

This study did not investigate the full spectrum of clinical measures for blast brain injury. Some of the key clinical features of blast brain injury are cognitive and behavioral (Ling 2009), but none of those changes were modeled here. While it is still uncertain how appropriate the ferret model or the shock tube exposure model is for studying the effects of blast brain injury, it is believed that the ferret will be a good model for the cognitive and behavioral changes that result from an exposure in the future because of its ease at learning tasks and behaviors (Rabe 1985).

Another limitation for the model was the length of time after the blast exposure. Physiological injuries need time for the injuries to progress and manifest. For hemorrhage, the amount of time after injury before death may affect the lesion size. It is possible for some of the more severe blast cases where there was a fatality before the 5

hour experimental period, the hemorrhagic areas were not as large as they could have been had the blood vessels continued to leak for a longer period of time. Immunohistochemistry positive staining also relies on a time course for the injuries to present themselves. In a study of blast brain injury, the levels of positive staining for β-APP were measured at 2, 6, and 18 hours and at 2, 7, and 21 days after the blast exposure (Saljo 2002a). The time point with the greatest positive staining occurred at the 18 hour time point, with the levels remaining high throughout the experiment. Immunoreactivity was detected beginning at 6 hours post blast. This study which evaluated injuries up to 5 hours post blast exposure, demonstrates the time dependence of the physiological pathways of injury. Perhaps extending the duration of the experiment would have increased the amount of positive staining in the milder blast conditions to more clearly define the lower levels of blast injury.

One of the clinical measures that was used in this study, VEP, had limitations that can be addressed in future investigations. First, flash VEP has been known to create large variability in the amplitude of the VEP signals (Squires 1986). The change in luminance between the light on and off creates this variability. Using a checkerboard pattern where the black and white squares alternate for the flash would keep the luminance the same throughout the test (Squires 1986). Second, visual half-fields should be used to isolate one visual pathway at a time to simplify the information in the resulting waveform. Additionally, a more robust electrode placement may help to reduce the variation between tests. Since the ferrets are hunters and tunnel diggers, the skin on the top of their heads has adapted to be thick and difficult to penetrate. Although great care was taken to place the electrodes in the same location for each test, there may have been slight

variations due to the difficulties in getting the electrodes through the skin. Finally, the test space in which the VEP tests were performed was affected by electrically noisy equipment in an adjacent room. Efforts to reduce this noise had limited success.

Finally, the limited range of blast overpressures and durations that were tested is a shortcoming that could be addressed in future tests. Although a range of blast exposure levels were investigated, there were levels that could not be reached with the current shock tube. High pressures at longer durations were difficult to achieve, as were durations less than 2 ms. Additional tests with a new shock tube configuration may be able to address those problems. Finally, the blast dose that is predicted for the ferret head may be smaller than was actually seen, especially for the right side of the head. A larger clearance between the table and the head support structure should be used in the future to eliminate any possible reflections. Additionally, perhaps a mesh netting should be used to support the specimen as opposed to the steel head support to prevent reflections for the long duration exposures. The increase in GFAP staining for the contralateral side of the head could be reduced with a different support system.

Despite these limitations, a reproducible model of blast brain injury was established, and clinical and histological evidence for blast brain injury was demonstrated. With this evidence, injury risk functions and relationships with blast overpressure and duration were determined for the first time.

Chapter 6. CONCLUSIONS

The most important contribution of this study is that it provides the first injury risk functions for mild and moderate to severe primary blast injuries to the brain in a gyrencephalic animal model for blasts with a broad range of severity. Logistic risk functions were developed for risk of mild and moderate to severe meningeal bleeding, initial apnea, and evoked potential signal loss from the application of a blast shock. In addition, a risk assessment was developed for fatality using data from the current study combined with previous rabbit data. Using length scaling, blast loads were comparable to free field blasts at standoffs of 2.5 to 20 m and charge sizes to approximately 800 kg-TNT. These risk assessments can be used in the design and assessment of protective equipment, as well as guiding the levels of blast exposure for future studies to elucidate the mechanisms of blast brain injury. The risk assessments predict various levels of injury severity so one can tailor their design or study for the appropriate risk.

Comparing the peak incident overpressure and scaled duration of the tests in this study with the pulmonary injury risk assessment (Bass *et al.* 2008) shows the blast injury sensitivities of lung and brain are different. For fatality, the brain demonstrates a greater tolerance than lung for primary blast injury, with the majority of blast brain cases that exceeded the 1% pulmonary survival curve surviving. In other words, the blast brain injury fatality tolerance is much greater than the pulmonary fatality tolerance when the thorax and abdomen are protected from blast. At the lowest positive phase durations, the 50% fatality risk function for blast overpressure to the brain was more than twice the overpressure level for the same pulmonary lethality risk. The thoracic and abdominal

protection worn by military personnel may allow these higher levels to be reached that would have otherwise been fatal.

When the scaled injury risk assessment was compared with the pulmonary injury risk along the same pressure/duration line, the blast level for 50% risk of mild brain bleeding was found to occur at approximately the same overpressure values as the 50% risk of unprotected pulmonary injury onset. This finding indicates that milder brain injuries that may alter cognition and/or emotion may occur at levels lower than those necessary to produce pulmonary fatalities. Nearly all of the military personnel use body armor which substantially increases the blast level required to create pulmonary injury (Wood 2010). For mild brain injuries, the 50% risk was found to be substantially below the injury tolerance levels associated with wearing ballistic protective vests with hard body armor, underscoring the need to protect the head against blast threats.

Another major contribution of this study was a characterization of injuries resulting from a primary blast exposure, which may shed some light on the injury mechanisms behind blast brain injury. For instance, the observed bradycardia and apnea may result from stimulation of the vagal pathway directly in the brain as opposed to stimulating vagus nerve endings in the lungs. Next, typical macroscopic injuries seen during the tests were associated with subarachnoid and subdural bleeding, and small contusions were seen throughout the brain. This injury pattern suggests a mechanism of small displacement, but rapid compression of the skull leading to intracranial bleeding, as skull fracture was not seen in any tests. In addition, the histological axonal injury results also support the small displacement injury mechanism, as there were fewer RM014 positive axons which are more susceptible to large strains and deformations in the tissue than β-

APP positive axons. The injury patterns demonstrated in this study differ from traditional blunt TBI, which can suggest a different injury mechanism for blast TBI than traditional blunt TBI. Finally, the histological results also may indicate an immune component to the blast brain injury manifestations.

The histological consequences from the blast exposure were quantified for an entire section of brain which has not been previously described. First of all, the density distribution of axonal transport was determined for a posterior level of the brain. Then blast brain injury was differentiated from traditional blunt TBI through the staining patterns for axonal injury. Finally, a correlation of the blast input to the injured axonal area was made which can hopefully be linked to clinical manifestations of blast brain injury in the future.

Another contribution of this study was an evaluation of a clinical technique for assessment of blast brain injuries. Correlations between the peak overpressure and durations of the blast exposure and the signal loss of the evoked potentials were made. The signal loss is a clinical indicator of a severe brain injury. However, indicators of more mild injuries, changes in peak amplitudes or latencies of the VEP and BAEP did not provide statistically significant correlations with the blast exposure, blast level, or assessment time. The EP techniques employed in this study may be made more sensitive to assess blast brain injury in future studies to reveal beneficial results in assessing blast brain injury. This study also demonstrates the applicability of apnea and hemorrhage as clinical measures for blast injury. As the amount of hemorrhage increases with blast severity level, imaging techniques such as CT or MRI may be used clinically to determine the injury severity.

Finally, a reproducible model of blast brain injury was established. This model includes the use of a shock tube as well as a protective mechanism to reduce the blast loading on the thorax to achieve blast levels on the head that would otherwise be fatal from pulmonary injury. The shock tube was able to replicate the blast waves from high explosives and munitions that are commonly seen in theater, and replicate some of the hemorrhaging and axonal injuries seen in brains with exposure to real high explosives. This research leads into future investigations which would validate the mass scaling principals used in this study and would investigate additional histological, physiological and behavioral injury criteria.

REFERENCES

Abbott WD, Due FO, Nosik WA. Subdural hematoma and effusion as result of blast injuries. J Am Med Assoc. 1943; 121(10):739-741.

Adams JH, Graham DI. "Diffuse brain damages in non-missile head injury." Recent Advances in Histopathology. Eds. RNM MacSween, PP Anthony. Edinburgh: Churchill Livingstone, 1984. 241-257.

Ai J, Liu E, Park E, Baker AJ. Structural and functional alterations of cerebellum following fluid percussion injury in rats. Exp Brain Res. 2007;177(1):95-112.

Andel H, Bayer GS, Ciovica R, Monsivais J, Basco M, Zimpfer M, Turkof E. Depressive effect of isoflurane on motor evoked potentials in the Nubian goat. Can J Anaesth. 2000;47(1):81-86.

Anderson KJ, Miller KM, Fugaccia I, Scheff SW. Regional distribution of fluoro-jade B staining in the hippocampus following traumatic brain injury. Exp Neurol. 2005;193(1):125-130.

Antoun T, Curran DR, Razorenov SV, Seaman L, Kanel GI, Utkin AV. Spall Fracture. New York: Springer, 2003.

Arciniegas DB, Anderson CA, Rojas DC. "Electrophysiological Techniques." Textbook of Traumatic Brain Injury. Eds. JM Silver, TW McAllister, SC Yudofsky. Washington DC: American Psychiatric Publishing, Inc., 2005. 135-157.

Atkinson JL. The neglected prehospital phase of head injury: apnea and catecholamine surge. Mayo Clin Proc. 2000;75(1):37-47.

Axelsson H, Yelverton JT. Chest wall velocity as a predictor of nonauditory blast injury in a complex wave environment. J Trauma. 1996;40(3):S31-S37.

Axelsson H, Hjelmqvist H, Medin A, Persson JK, Suneson A. Physiological changes in pigs exposed to a blast wave from a detonating high-explosive charge. Mil Med. 2000;165(2):119-126.

Bain AC, Raghupathi R, Meaney DF. Dynamic stretch correlates to both morphological abnormalities and electrophysiological impairment in a model of traumatic axonal injury. J Neurotrauma. 2001;18(5):499-511.

Bartl G. The effects of visual field changes and ocular hypertension on the visual evoked potential. Ann NY Acad Sci. 1982;388:227-242.

Bass CR, Boggess B, Bush B, Davis M, Campman S, Harris R, Rountree S, Eklund J, Monacci W, Ling G, Holborow G, Sanderson E. Helmet behind armor blunt trauma. NATO-RTO Specialists' Meeting on Personal Protection, Koblenz, Germany, 2003.

Bass CR, Rafaels KA and Salzar RS. Pulmonary injury risk assessment for short-duration blasts. J Trauma. 2008;65:604-615.

Baum MJ. "Use of the Ferret in Behavioral Research." Biology and Diseases of the Ferret. Ed. JG Fox. Philadelphia: Lea and Febiger, 1988. 315-323.

Bauman RA, Elsayed N, Petras JM, Widholm J. Exposure to sublethal blast overpressure reduces the food intake and exercise performance of rats. Toxicology. 1997;121:65-79.

Bauman RA, Ling G, Tong L, Januszkiewicz A, Agoston D, Delanerolle N, Kim Y, Ritzel D, Bell R, Ecklund J, Armonda R, Bandak F, Parks S. An introductory characterization of a combat-casualty-care relevant swine model of closed head

injury resulting from exposure to explosive blast. J Neurotrauma. 2009;26(6):841-860.

Bell MK. A standardized model is needed to study the neurological effects of primary blast wave exposure. Mil Med. 2008;173(6):v-viii.

Benzinger TLS, Brody D, Cardin S, Curley KC, Mintun MA, Mun SK, Wong KH, Wrathall JR. Blast-related brain injury: Imaging for clinical and research applications report of the 2008 St. Louis Workshop. J Neurotrauma. 2009;26(12):2127-2144.

Bhattacharjee Y. Shell shock revisited: Solving the puzzle of blast trauma. Science. 319(5862):406-408.

Bodis-Wollner I, Onorfrj M. System diseases and visual evoked potential diagnosis in neurology: changes due to synaptic malfunction. Ann NY Acad Sci. 1982;388:327-348.

Bogo V, Hutton RA, and Bruner A. The Effects of Airblast on Discriminated Avoidance Behavior in Rhesus Monkeys, Technical Progress Report, DASA-2659, Defense Nuclear Agency, Washington, D.C. March 1971.

Bowen IG, Fletcher ER, and Richmond DR. "Estimate of Man's Tolerance to the Direct Effects of Air Blast," Technical Progress Report, DASA-2113, Defense Atomic Support Agency, Department of Defense, Washington, D. C. October 1968.

Bramlett HM, Kraydieh S, Green EJ, Dietrich WD. Temporal and regional patterns of axonal damage following traumatic brain injury: a β-amyloid precursor protein immunocytochemical study in rats. J Neuropathol Exp Neurol. 1997;56(10):1132-1141.

Brodal P. The Central Nervous System: Structure and Function. New York: Oxford University Press, 2004.

Brown FW, Lee RH. Injury from the decompression component of an air-blast wave. Nature. 1956;178:490.

Cant BR, Hume AL, Judson JA, Shaw NA. The assessment of severe head injury by short-latency somatosensory and brain-stem auditory evoked potentials. Electroencephalogr Clin Neurophysiol. 1986;65(3):188-195.

Carr W. An fMRI Study of TBI Associated with Blast Injury. Technical Progress Report, A426105, Naval Medical Research Center, Silver Spring, MD. March 2009.

Cassels C. "AAN 2009: Imaging study shows blast injury may cause brain inflammation." Medscape Medical News. May 5, 2009.

Cassen B, Curtis L, Kistler K. Initial studies of the effect of laboratory-produced air blast on animals. J Aviat Med. 1950;21:38-47.

Celander H, Clemedson CJ, Ericsson UA, Hultman HI. The use of a compressed air operated shock tube for physiological blast research. Acta Physion Scand. 1955;33(1):6-13.

Cernak I, Savic J, Malicevic Z, Zunic G, Radosevic P, Ivanovic I, Davidovic L. Involvement of the central nervous system in the general response to pulmonary blast injury. J Trauma. 1996;40(3 Suppl):S100-S104.

Cernak I, Savic J, Lazarov A. Relations among plasma prolactin, testosterone, and injury severity in war casualties. World J Surg. 1997;21(3):240-246.

Cernak I, Savic J, Zunic G, Pejnovic N, Jovanikic O, Stepic V. Recognizing, scoring, and predicting blast injuries. World J Surg. 1999a;23(1):44-53.

Cernak I, Savic J, Ignjatovic D, Jevtic M. Blast injury from explosive munitions. J Trauma. 1999b;47(1):96-103.

Cernak I, Wang Z, Jiang J, Bian X, Savic J. Ultrastructural and functional characteristics of blast injury-induced neurotrauma. J Trauma. 2001a;50(4):695-706.

Cernak I, Wang Z, Jiang J, Bian X, Savic J. Cognitive deficits following blast injury-induced neurotrauma: possible involvement of nitric oxide. Brain Inj. 2001b;15(7):593-612.

Chavko M, Koller WA, Prusaczyk WK, McCarron RM. Measurement of blast wave by a miniature fiber optic pressure transducer in the rat brain. J Neurosci Methods. 2007;159(2):277-81.

Cheng J, Gu J, Ma Y, Yang T, Kuang Y, Li B, Kang J. Development of a rat model for studying blast-induced traumatic brain injury. J Neurol Sci. 2010;294(1-2):23-28.

Clemedson CJ. An experimental study on air blast injuries. Acta Physiol Scand. 1949;18(S61):1-200.

Clemedson CJ and Pettersson H. Genesis of Respiratory and Circulatory Changes in Blast Injury. Am J Physiol. 1953;174:316-320.

Clemedson CJ, Pettersson H. Propagation of a high explosive air shock wave through different parts of an animal body. Am J Physiol. 1956a;184(1):119-126.

Clemedson CJ. Shock wave transmission to the central nervous system. Acta Physiol Scand. 1956b;37(2-3):204-214.

Clemedson CJ. Blast injury. Physiol Rev. 1956c;36(3):336-354.

Clemedson CJ. Some blast studies with application to explosive decompression. JBIS. 1960;17:279-284.

Clemedson CJ, Frankenberg L, Jonsson A, Pettersson H, Sundqvist AB. Dynamic response of thorax and abdomen of rabbits in partial and whole-body blast exposure. Am J Physiol. 1969;216(3):615-620.

Cloots RJH, Gervaise HMT, van Dommelen JAW, Geers MGD. Biomechanics of traumatic brain injury: Influences of the morphologic heterogeneities of the cerebral cortex. Ann Biomed Eng. 2008;36(7):1203-1215.

Cooper GJ, Jonsson A. "Protection Against Blast Injury." Scientific Foundations of Trauma. Eds. G Cooper, H Dudley, D Gann. New York: Butterworth-Heinemann, 1997. 258-283.

Cramer F, Paster S, Stephenson C. Cerebral injuries due to explosion waves – "Cerebral blast concussion": a pathologic, clinical and electroencephalographic study. Arch Neurol Psychiatry. 1949;61(1):1-20.

Dal Cengio Leonardi A, Bir C, Ritzel D, VandeVord P. The effects of intracranial pressure sensor location and skull apertures during exposure of a rat model to an air shock wave. J Neurotrauma. 2009;26(8):A-18.

Danzer SC, He X, Loepke AW, McNamara JO. Structural plasticity of dentate granule cell mossy fibers during the development of limbic epilepsy. Hippocampus. 2010;20(1):113-124.

deCandole, CA. Blast injury. Can Med Assn J. 1967;96:206-214.

Deck C, Willinger R. Improved head injury criteria based on head FE model. Int J Crashworthiness. 2008;13(6):667-678.

Denny-Brown D. Cerebral concussion. Physiol Rev. 1945;25(2):296-325.

DePalma RG, Burris DG, Champion HR, Hodgson MJ. Blast injuries. N Engl J Med. 2005;352(13):1335-1342.

Dietrich ED, Alonso O, Halley M. Early microvascular and neuronal consequences of traumatic brain injury: a light and electron microscopic study in rats. J Neurotrauma. 1994;11(3):289-301.

Dodd KT, Yelverton JT, Richmond DR, Morris JR, Ripple GR. Nonauditory injury threshold for repeated intense freefield impulse noise. J Occup Med. 1990;32(3):260-266.

Dodd KT, Mundie TG, Lagutchik MS, Morris JR. Cardiopulmonary effects of high-impulse noise exposure. J Trauma. 1997;43(4):656-666.

Ellens DJ and Blumenfeld H. "EEG-fMRI in Animal Models." EEG-fMRI: Physiological Basis, Technique and Applications. Eds. C Mulert and L Lemieux. Berlin: Springer, 2010. 485-510.

Elsayed NM. Toxicology of blast overpressure. Toxicology. 1997;121(1):1-15.

El Sayed T, Mota A, Fraternali F, Ortiz M. Biomechanics of traumatic brain injury. Comput Mehods Appl Mech Engrg. 2008;197:4692-4701.

Eppinger R, Marcus JH, and Morgan R. Development of a Dummy and Injury Index for NHTSA's Thoracic Side Impact Protection Research Program, SAE Paper Number 840885, Society of Automobile Engineers, Warrendale, PA, 1984.

Evans DH. "Physical and Technical Principles." Handbook of neurovascular ultrasound. Ed. RW Baumgartner. Basel: Karger Publishers, 2006. 1-18.

Farkas O, Povlishock JT. Cellular and subcellular change evoked by diffuse traumatic brain injury: a complex web of change extending far beyond focal damage. Prog Brain Res. 2007;161:43-59.

Federal Communications Commission (1999). "Questions and Answers about Biological Effects and Potential Hazards of Radiofrequency Electromagnetic Fields." Washington, DC: OET Bulletin 56. Web. 4 Oct. 2010 < http://www.fcc.gov/Bureaus/Engineering_Technology/Documents/bulletins/oet56/oet56e4.pdf >.

Field KJ, White WJ, Lang CM. Anaesthetic effects of chloral hydrate, pentobarbitone and urethane in adult male rats. Lab Anim. 1993;27(3):253-269.

Fishback AS, Shields CB, Linden RD, Zhang YP, Burke D. The effects of propofol on rat transcranial magnetic motor evoked potentials. Neurosurgery. 1995;37(5):969-974.

FitzGerald MJT, Gruener G, Mtui E. Clincal Neuroanatomy and Neuroscience. Philadelphia: Saunders, 2007.

Forester GV, Peterson EA, Roy OZ. Effect of therapeutic level ultrasound on visual evoked potentials in the hypoxic cat. Ultrasound Med Biol. 1987;13(5):259-65.

Fox JG. "Normal clinical and biological parameters." Biology and Diseases of the Ferret. Ed. JG Fox. Philadelphia: Lea and Febiger, 1988. 159-173.

Gadd CW. Use of a weighted-impulse criterion for estimating injury hazard. Proceedings, Tenth Stapp Car Crash Conference. Warrendale, PA: Society of Automotive Engineers. 164-174.

Garman R, Jenkins LW, Bauman R, Swauger P, Parks S, Switzer R, Dixon CE, Clark RSB, Bayir H, Kagan V, Jackson EK, Kochanek PM. Blast overpressure injury in rats with body protection produces acute and sub-acute axonal, dendritic and synaptic neuropathology. J Neurotrauma. 2009;26(8):A-53.

Glass I, Groswasser Z, Groswasser-Reider I. Impersistent execution of saccadic eye movements after traumatic brain injury. Brain Inj. 1995;9(8):769-775.

Glasser R. A shock wave of brain injuries. Washington Post. 8 April 2007: B1.

Glasstone S, Dolan PJ. The Effects of Nuclear Weapons, Report ADA087568, U.S. Department of Energy, Washington, DC, 1977.

Goldberg MS. Death and injury rates of US military personnel in Iraq. Mil Med. 2010;174(4):220-226.

Gorbunov NV, McFaul SJ, Januszkiewicz A, Atkins JL. Pro-inflammatory alterations and status of blood plasma iron in a model of blast-induced lung trauma. Int J Immunopathol Pharmacol. 2005;18(3):547-556.

Graham T. "The explosive history of nitrogen." ChemMatters. Feb 2003:8-10.

Gruss E. A correction for primary blast injury criteria. J Trauma. 2006;60(6):1284-1289.

Guy RJ, Kirkman E, Watkins PE, Cooper GJ. Physiologic responses to primary blast. J Trauma. 1998;45(6):983-987.

Hagerman E. Shock to the system. Popular Science. September 2008:48-53,86-88.

Hara K, Harris RA. The anesthetic mechanism of urethane: the effects on neurotransmitter-gated ion channels. Anesth Analg. 2002;94(2):313-318.

Hardie NA, Shepard RK. Sensorineural hearing loss during development: morphological and physiological response of the cochlea and auditory brainstem. Hear Res. 1999;128(1-2):147-165.

Hausman R, Rieβ R, Fieguth A, Betz P. Immunohistochemical investigations on the course of astroglial GFAP expression following human brain injury. Int J Legal Med. 2000;113:70-75.

Hicks RR, Fertig SJ, Desrocher RE, Koroshetz WJ, Pancrazio JJ. Neurological effects of blast injury. J Trauma. 2010;68(5):1257-1263.

Hirsch FG. Effects of overpressure on the ear – A review. Ann NY Acad Sci. 1968;152(1):147-162.

Ho J, Kleiven S. Can sulci protect the brain from traumatic injury?. J Biomech. 2009;42(13):2074-2080.

Hofman MA. On the evolution and geometry of the brain in mammals. Prog Neurobiol. 1989; 32(2):137-158.

Hoge CW, McGurk D, Thomas JL, Cox AL, Engel CC, Castro CA. Mild traumatic brain injure in U.S. soldiers returning from Iraq. N Engl J Med. 2008;358(5):453-463.

Hooker DR. Physiological Effects of Air Concussion. Am J Physiol. 1924;67:219-274.

Horrocks C, Brett S. Blast injury. Curr Anaesth Crit Care. 2000;11:113-119.

Hosmer DW and Lemeshow S. Applied Logistic Regression. New York, NY: John Wiley and Sons; 1989.

Hsu S. M., Raine L. and Fanger H. Use of avidin-biotin-peroxidase complex (ABC) in immunoperoxidase techniques: a comparison between ABC and unlabeled antibody (PAP) procedures. J Histochem Cytochem. 1981;29:577-580.

Hughes DG, Jackson A, Mason DL, Berry E, Hollis S, Yates DW. Abnormalities on magnetic resonance imaging seen acutely following mild traumatic brain injury: correlation with neuropsychological tests and delayed recovery. Neuroradiology. 2004;46:550-558.

Hyde, D. ConWep 2.1.0.8 [Computer software]. US Army Engineer Research & Development Center, Vicksburg, Mississippi, 2004.

Inman CF, Rees LEN, Barker E, Haverson K, Stokes CR, Bailey M. Validation of computer-assisted, pixel-based analysis of multiple-colour immunofluorescence histology. J Immunol Methods. 2005;302(1-2):156-167.

Iremonger MJ. "Physics of detonations and blast waves." Scientific Foundations of Trauma. Eds. G Cooper, H Dudley, D Gann. New York: Butterworth-Heinemann, 1997. 189-199.

Irwin RJ, Lerner MR, Bealer JF, Brackett DJ, Tuggle DW. Cardiopulmonary physiology of primary blast injury. J Trauma. 1997;43(4):650-655.

Jaffin JH, McKinney L, Kinney RC, Cunningham JA, Moritz DM, Kraimer JM, Graeber GM Moe JB, Salander JM, Harmon JW. A laboratory model for studying blast overpressure injury. J Trauma. 1987;27(4):349-356.

Johnson, D.L., Yelverton, J.T., Hicks, W., and Doyal, R., Blast overpressure studies in animals and man, Report ADA280435, U.S. National Technical Information Service, Washington, 1993.

Jonsson A, Clemedson CJ, Sundqvist AB, Arvebo E. Dynamic factors influencing the production of lung injury in rabbits subjected to blunt chest wall impact. Aviat Space Environ Med. 1979;50(4):325-337.

Kato K, Fujimura M, Nakagawa A, Saito A, Ohki T, Takayama K, Tominaga T. Pressure-dependent effect of shock waves on rat brain: induction of neuronal apoptosis mediated by a caspase-dependent pathway. J Neurosurg. 2007;106(4):667-676.

Kaur C, Singh J, Lim MK, Ng BL, Yap EPH, Ling EA. The response of neurons and microglia to blast injury in the rat brain. Neuropathol Appl Neurobiol. 1995;21(5):369-377.

Kaur C, Singh J, Lim MK, Ng BL, Yap EPH, Ling EA. Studies of the choroid plexus and its associated epiplexus cells in the lateral ventricles of rats following an exposure to a single non-penetrative blast. Arch Histol Cytol. 1996;59(3):239-248.

Kaur C, Singh J, Lim MK, Ng BL, Yap EPH, Ling EA. Ultrastructural changes of macroglial cells in the rat brain following an exposure to a non-penetrative blast. Ann Acad Med Singapore. 1997a;26(1):27-29.

Kaur C, Singh J, Lim MK, Ng BL, Ling EA. Macrophages/microglia as 'sensors' of injury in the pineal gland of rats following a non-penetrative blast. Neurosci Res. 1997b;27(4):317-322.

Keller BP, Haghighi SS, Oro JJ, Eggers GW Jr. The effects of propofol anesthesia on transcortical electric evoked potentials in the rat. Neurosurgery. 1992;30(4):557-560.

Kelly JB, Kavanagh GL, Picton TW. Brainstem auditory evoked response in the ferret (Mustela putorius). Hear Res. 1989;39(3):231-40.

Kennedy JE, Jaffee MS, Leskin GA, Stokes JW, Leal FO, Fitzpatrick PJ. Posttraumatic stress disorder and posttraumatic stress disorder-like symptoms and mild traumatic brain injury. J Rehabil Res Dev. 2007;44(7):895-920.

Kent RW, Bass CR, Woods W, Sherwood C, Madeley NJ, Salzar R. Muscle tetanus and loading condition effects on the elastic and viscous characteristics of the thorax. Traffic Injury Protection. 4: 297-314, 2003.

King AI, Yang KH, Zhang L, Hardy W, Viano DC. Is head injury caused by linear or angular acceleration?. Proceedings, International Research Council on the Biomechanics of Injury (IRCOBI) Conference. Lisbon, Portugal, 2003.

Kleiven S. Predictors for traumatic brain injuries evaluated through accident reconstructions. Stapp Car Crash J. 2007; 51:81-114.

Knudsen SK, Oen EO. Blast-induced neurotrauma in whales. Neurosci Res. 2003;46(3):377-386.

Kraus MF, Little DM, Donnell AJ, Reilly JL, Simonian N, Sweeney, JA. Oculomotor function in chronic traumatic brain injury. Cogn Behav Neurol. 2007;20(3):170-178.

Krohn PL, Whitteridge D and Zuckerman S. The effect of blast on the heart and head. Preliminary note, RC 249, prepared for the Ministry of Home Security Civil Defence Research Committee, London, England, 1941.

Krohn PL, Whitteridge D and Zuckerman S. Physiological effects of blast. The Lancet. 1942;1:252-259.

LaPlaca MC, Simon CM, Prado GR, Cullen DR (2007). "CNS injury biomechanics and experimental models." Neurotrauma: New Insights Into Pathology and Treatment.

Ed. JT Weber. Amsterdam: Academic Press. ISBN 0444530177. http://books.google.com/?id=FyzEQPKUuPcC&pg=PP1&dq=neurotrauma. Retrieved 2008-11-10.

Laughlin S, Montanera W. Central nervous system imaging. When is CT more appropriate than MRI?. Postgrad Med. 1998;104(5):73-88.

Lee KY, Nyein MK, Moore DF, Joannopoulos JD, Socrate S, Imholt T, Radovitsky R, Johnson SG. Blast-induced electromagnetic fields in the brain from bone piezoelectricity. Neuroimage. 2010, doi:10.1016/j.neuroimage.2010.05.042.

Leist M, Nicotera P. Apoptosis, excitotoxicity, and neuropathology. Exp Cell Res. 1998;239(2):183-201.

Leung LY, VandeVord PJ, Dal Cengio AL, Bir C, Yang KH, King AI. Blast related neurotrauma: a review of cellular injury. Mol Cell Biomech. 2008;5(3):155-168.

Levin HS, Williams DH, Eisenberg HM, High WM Jr, Guinto FC Jr. Serial MRI and neurobehavioral findings after mild to moderate closed head injury. J Neurol Neurosurg Psychiatry. 1992;55(4):255-262.

Levin H, Wilde E, Troyanskaya M, Peterson N, Scheibel R. Diffusion tensor imaging of mild to moderate blast related TBI in relation to post-concussion and posttraumatic stress disorder symptoms. J Neurotrauma. 2009;26(8):A-69.

Levin H, Wilde E, Troyanskaya M, Peterson NJ, Scheibel R, Newsome M, Radaideh M, Wu T, Yallampalli R, Chu Z, Li X. J Neurotrauma. 2010;27(4):683-694.

Levy ML, Davis SE, Russell M. "Ballistics and Forensics." Traumatic Brain Injury. Eds. DW Marion. New York: Thieme, 1999. 201-214.

Lew HL, Garvert DW, Pogoda TK, Hsu PT, Devine JM, White DK, Myers PJ, Goodrich GL. Auditory and visual impairments in patients with blast-related traumatic brain injury: Effect of dual sensory impairment of Functional Independence Measure. J Rehabil Res Dev. 2009;46(6):819-826.

Liebman M, Tadmor R. Neuroanatomy made easy and understandable. Gaithersburg, MD: Aspen Publishers, Inc., 1991.

Ling G, Bandak F, Armonda R, Grant G, Ecklund J. Explosive blast neurotrauma. J Neurotrauma. 2009;26(6):815-825.

Lissner HR, Lebow M, Evans FG. Experimental studies on the relation between acceleration and intracranial changes in man. Surg Gynecol Obstet. 11:329-338.

Lobdell TF. Impact response of the human thorax. Proceedings of the Symposium on Human Impact Response, 1973.

Lockhart P, Cronin D, Williams K, Ouellet S. Investigation of head response to blast loading. J Trauma. 2010; DOI: 10.1097/TA.0b013e3181de3f4b.

Long JB, Bentley TL, Wessner KA, Cerone C, Sweeney S, Bauman RA. Blast overpressure in rats: recreating a battlefield injury in the laboratory. J Neurotrauma. 2009;26(6):827-840.

Lucas SR, Bass CR, Crandall JR, Kent RW, Shen FH, Salzar RS. Viscoelastic and failure properties of spine ligament collagen fascicles. Biomech Model Mechanobiol. 2009;8(6):487-498.

Marmarou CR, Walker SA, Davis CL, Povlishock JT. Quantitative analysis of the relationship between intra-axonal neurofilament compaction and impaired axonal

transport following diffuse traumatic brain injury. J Neurotrauma. 2005;22(10):1066-1080.

Marmarou CR, Povlishock JT. Administration of the immunophilin ligand FK506 differentially attenuates neurofilament compaction and impaired axonal transport in injured axons following diffuse traumatic brain injury. Exp Neurol. 2006;197(2):353-362.

Matkowskyj KA, Schonfeld D, Benya RV. Quantitative immunohistochemistry by measuring cumulative signal strength using commercially available software Photoshop and MATLAB. J Histochem Cytochem. 2000;48(2):303-312.

Maxwell WL. Histopathological changes at central nodes of Ranvier after stretch injury. Microsc Res Tech. 1996;34(6):522-535.

McArdle WD, Katch FI, Katch VL. Exercise Physiology: Energy, Nutrition, and Human and Performance. Baltimore: Lippincott Williams & Wilkins, 2001.

McKenzie KJ, McLellan DR, Gentleman SM, Maxwell WL, Gennarelli TA, Graham DI. Is β-APP a marker of axonal damage in short-surviving head injury? Acta Neuropathol. 1996;92(6):608-613.

Medana IM, Esiri MM. Axonal damage: a key predictor of outcome in human CNS diseases. Brain. 2003;126(Pt 3):515-530.

Mehdizadeh S, Khoshgoftar M, Najarian S, Farmanzad F, Ahmadi SAH. Comparison between brain tissue gray and white matters in tension including necking phenomenon. Am J Appl Sci. 2008;5(12):1701-1706.

Melvin JW, Lighthall JW. "Brain-Injury Biomechanics." Accidental Injury: Biomechanics and Prevention. Eds. AM Nahum, JW Melvin. New York: Springer, 2002.

Metz CE. Basic principles of ROC analysis. Semin Nucl Med. 1978;8:283-298.

Meyer K, Helmick K, Doncevic S, Park R. Severe and penetrating traumatic brain injury in the context of war. J Trauma Nurs. 2008;15(4):185-189.

Moochhala SM, Md S, Lu J, Teng CH, Greengrass C. Neuroprotective role of aminoguanidine in behavioral changes after blast injury. J Trauma. 2004;56(2):393-403.

Moore DF, Radovitzky RA, Shupenko L, Klinoff A, Jaffe MS, Rosen JM. Blast physics and central nervous system injury. Future Neurol. 2008;3(3):243-250.

Moss WC, King MJ, Blackman EG. Skull flexure from blast waves: a mechanism for brain injury with implications for helmet design. Phys Rev Lett. 2009;103(10):108702-1-4.

Mott FW. The effects of high explosives upon the central nervous system. Lecture I, II, III. Lancet. 1916; 4824, 4826, 4828: 331-338, 441-449, 545-553.

Moyes R. Explosive violence: The problem of explosive weapons. Landmine Action. 2009 August.

Mulhall LE, Williams IM, Abel LA. Bedside tests of saccades after head injury. J Neuroophthalmol. 1999;19(3):160-165.

Murthy JM, Chopra JS, Gulati DR. Subdural hematoma in an adult following a blast injury. Case Report. J Neurosurg. 1979;50(2):260-261.

Nakagawa A, Kusaka Y, Hirano T, Saito T, Shirane R, Takayama K, Yoshimoto T. Application of shock waves as a treatment modality in the vicinity of the brain and skull. J Neurosurg. 2003;99(1):156-162.

National Highway and Traffic Safety Administration. "Final Economic Assessment, FMVSS No. 201, Upper Interior Head Protection." Washington, D.C. June 1995.

Needham J. Science and civilization in China, Volume 5, Part 7. Cambridge: Cambridge University Press, 1986.

Nelson TJ, Clark T, Stedje-Larsen ET, Lewis CT, Grueskin JM, Echols EL, Wall DB, Felger EA, Bohman HR. Close proximity blast injury patterns from improvised explosive devices in Iraq: a report of 18 cases. J Trauma. 2008;65(1):212-217.

Newman J. A generalized acceleration model for brain injury threshold (GAMBIT). Proceedings of the International Conference on the Biomechanics of Impact (IRCOBI). 1986. 121-131.

Newman JA, Shewchenko N, Welbourne E. A proposed new biomechanical head injury assessment function – the maximum power index. Stapp Car Crash J. 2000;44:215-247.

Odom JV, Bach M, Barber C, Briqell M, Marmor MF, Tormene AP, Holder GE, Vaegan. Visual evoked potentials standard (2004). Doc Ophthalmol. 2004;108(2):115-123.

Okie S. Traumatic brain injury in the war zone. N Engl J Med. 2005;352(20):2043-2047.

Ommaya AK, Hirsch AE. Tolerance of cerebral concussion from head impact and whiplash primates. J Biomechanics. 1971;4:13-22.

Ommaya AK, Gennarelli TA. "Experimental head injury." Handbook of Clinical Neurology Injuries of the Brain and Skull: Volume 23. Eds. PJ Vinken, GW Bruyn. New York: American Elsevier Publishing Co., Inc., 1975. 67-90.

Owens BD, Kragh JF, Jr., Wenke JC, Macaitis J, Wade CE, Holcomb JB. Combat wounds in Operation Iraqi Freedom and Operation Enduring Freedom. J Trauma. 2008;62(2):295-299.

Pal J, Toth Z, Farkas O, Kellenyi L, Doczi T, Gallyas F. Selective induction of ultrastructural (neurofilament) compaction in axons by means of a new head-injury apparatus. J Neurosci Methods. 2006;153(2):283-289.

Panzer MB, Bass CR, Myers BS. Numerical study on the role of helmet protection in blast brain injury. Personal Armour Systems Symposium, Quebec City, QB, Canada, 2010.

Papasozomenos SC, Binder LI. Phosphorylation determines two distinct species of Tau in the central nervous system. Cell Motil Cytoskeleton. 1987;8(3):210-226.

Park E, Bell JD, Liu E, Gottlieb J, Baker AJ. Development of a model of primary blast brain injury: Shockwaves as a direct cause of brain injury. National Neurotrauma Symposium, Orlando, Florida. 2008.

Paxinos G and Watson C. Rat Brain in Stereotaxic Coordinates. London: Academic Press, 2007.

Pellman EJ, Viano DC, Tucker AM, Casson IR, Waeckerle JF. Concussion in professional football: reconstruction of game impacts and injuries. Neurosurgery. 2003;53(4):799-812.

Petras JM, Bauman RA, Elsayed NM. Visual system degeneration induced by blast overpressure. Toxicology. 1997;121(1):41-49.

Pierce JES, Trojanowski JQ, Graham DI, Smith DH, McIntosh TK. Immunohistochemical characterization of alterations in the distribution of amyloid precursor proteins and β-amyloid peptide after experimental brain injury in the rat. J Neurosci. 1996;16(3):1083-1090.

Povlishock, JT, Hayes RL, Michel ME, McIntosh TK. Workshop on animal models of traumatic brain injury. J Neurotrauma. 1994;11(6):723-732.

Pratt H, Goldsher M, Netzer A, Shenhav R. Auditory brainstem evoked potentials in blast injury. Audiology. 1985;24(4):297-304.

Prevost TP, Balakrishnan A, Suresh S, Socrate S. Biomechanics of brain tissue. Acta Biomater. 2011;7(1):83-95.

Rabe A, Haddad R, Dumas R. Behavior and neurobehavioral teratology using the ferret. Lab Anim Sci. 1985;35(3):256-67.

Rafaels KA, Bass CR, Panzer MB, Salzar RS. Pulmonary injury risk assessment for long-duration blasts: a meta-analysis. J Trauma. 2010;69(2):368-374.

Rafaels K, Bass CR, Salzar RS, Panzer M, Woods W, Feldman S, Cummings T, Capehart B. Injury Risk Assessment for Brain Injuries from Primary Blast. J Neurotrauma. (Submitted in 2010)

Ransom BR. "Organization of the Nervous System." Medical Physiology: A Cellular and Molecular Approach. Eds. WF Boron and EL Boulpaep. Philadelphia: Saunders, 2003a. 257-279.

Ransom BR. "The Neuronal Environment." Medical Physiology: A Cellular and Molecular Approach. Eds. WF Boron and EL Boulpaep. Philadelphia: Saunders, 2003b. 399-419.

Rasband, W.S., ImageJ, U. S. National Institutes of Health, Bethesda, Maryland, USA, http://rsb.info.nih.gov/ij/, 1997-2009.

Richmond, D.R., Taborelli, R.V., Sherping, F., *et al.* Shock Tube Studies of the Effects of Sharp-Rising, Long-Duration Overpressures on Biological Systems, Progress Report TID-6056, United States Atomic Energy Commission, Washington, D.C., March 1959.

Richmond DR, Clare VR, Goldizen VC, Pratt DE, Sanchez RT, White CS. Biological effects of overpressure. II. A shock tube utilized to produce sharp-rising overpressures of 400 milliseconds duration and its employment in biomedical experiments. Aerosp Med. 1961;32(11):997-1008.

Richmond DR, Yelverton JT, Fletcher ER, Phillips YY. Physical correlates of eardrum rupture. Ann Otol Rhinol Laryngol Suppl. 1989;98:35-41.

Risling M, Suneson A, Skold M, Lai LJ, Abo M, Chen Z, Bjelke B. Evaluation of diffuse brain injury with magnetic resonance imaging: technical report for the Swedish Defence Research Agency. Stockholm, Sweden: Defence Medecine, Experimental Traumatology, Swedish Defence Research Agency; 2002 December [accessed 2005 Feb 8]. Report No.: FOI-R—0756—SE. Available from: www2.foi.se/rapp/foir0757.pdf

Risling M, Plantman S, Angeria M, Postami E, Bellander BM, Kirkegaard, Arborelius U, Dividsson J. Mechanisms of blast induced brain injuries, experimental studies in rats. Neuroimage. 2010. doi:10.1016/j.neuroimage.2010.05.031

Ritenour AE, Baskin TW. Primary blast injury: Update on diagnosis and treatment. Crit Care Med. 2008;36 (7 Suppl):S311-S317.

Rojo MG, Bueno G, Slodkowska J. Review of imaging solutions for integrated quantitative immunohistochemistry in the Pathology daily practice. Folia Histochem Cytobiol. 2009;47(3):349-354.

Romba J and Martin P. "An Exploratory Study into the Effects of Low Blast Pressure on Behavior in Rhesus Monkeys," Technical Memorandum 11-59, Project No. TB1-1000, Human Engineering Laboratory, Aberdeen Proving Ground, MD. October 1959.

Romba JJ, Martin P, Dorsey W. "The Propagation of Air Shock Waves on a Biophysical Model," Technical Memorandum 17-61, Project No. 5B9520001, Human Engineering Laboratory, Aberdeen Proving Ground, MD. September 1961.

Saljo A, Bao F, Haglid KG, Hansson HA. Blast exposure causes redistribution of phosphorylated neurofilament subunits in neurons of the adult rat brain. J Neurotrauma. 2000;17(8):719-726.

Saljo A, Bao F, Hamberger A, Haglid KG, Hansson HA. Exposure to short-lasting impulse noise causes microglial and astroglial cell activation in the adult rat brain. Pathophysiology. 2001;8(2):105-111.

Saljo A, Bao F, Shi J, Hamberger A, Hansson HA, Haglid KG. Expression of c-Fos and c-Myc and deposition of β-APP in neurons in the adult rat brain as a result of exposure to short-lasting impulse noise. J Neurotrauma. 2002a;19(3):379-385.

Saljo A, Bao F, Jingshan S, Hamberger A, Hansson HA, Haglid KG. Exposure to short-lasting impulse noise causes neuronal c-Jun expression and induction of apoptosis in the adult rat brain. J Neurotrauma. 2002b;19(8):985-991.

Saljo A, Huang YL, Hansson HA. Impulse noise transiently increased the permeability of nerve and glial cell membranes, an effect accentuated by a recent brain injury. J Neurotrauma. 2003;20(8):787-794.

Saljo A, Arrhen F, Bolouri H, Mayorga M, Hamberger A. Neuropathology and pressure in the pig brain resulting from low-impulse noise exposure. J Neurotrauma. 2008;25(12):1397-1406.

Schmued LC, Hopkins KJ. Fluoro-Jade B: a high affinity fluorescent marker for the localization of neuronal degeneration. Brain Res. 2000;874(2):123-130.

Servadei F, Murray GD, Teasdale GM, Dearden M, Iannotti F, Lapierre F, Maas AJ, Karimi A, Ohman J, Persson L, Stocchetti N, Trojanowski T, Unterberg A. Traumatic subarachnoid hemorrhage: demographic and clinical study of 750 patients from the European brain injury consortium survey of head injuries. Neurosurgery. 2002;50(2):261-267.

Sherman J. Simultaneous pattern-reversal electroretinograms and visual evoked potentials in diseases of the macula and optic nerve. Ann NY Acad Sci. 1982;388:214-226.

Shipley B. Cause and correlation in biology. Cambridge, UK: Cambridge University Press, 2000.

Silver J, Miller JH. Regeneration beyond the glial scar. Nat Rev Neurosci. 2004;5(2):146-156.

Singer E. Brain trauma in Iraq. Technology Review. May/June 2008: 52-59.

Smith DH, Meaney DF. Axonal damage in traumatic brain injury. Neuroscientist. 2000;6(6):483-495.

Squires NK, Ollo C. "Human evoked potential techniques: Possible applications to neuropsychology." Experimental Techniques in Human Neuropsychology. Ed. HJ Hannay. New York: Oxford University Press, 1986. 386-418.

Stein M, Hirshberg A. Medical consequences of terrorism: The conventional weapon threat. Surg Clin N Am. 1999;79(6):1538-1552.

Stein J. Visual motion sensitivity and reading. Neuropsychologia. 2003;41(13):1785-93.

Stewart OW, Russel CK, Cone WV. Injury to the central nervous system by blast : Observations on a pheasant. 1941;1:172-174.

Stone JR, Singleton RH, Povlishock JT. Antibodies to the C-terminus of the β-amyloid precursor protein (APP): a site specific marker for the detection of traumatic axonal injury. Brain Res. 2000;871(2):288-302.

Stone JR, Singleton RH, Povlishock JT. Intra-axonal neurofilament compaction does not evoke local axonal swelling in all traumatically injured axons. Exp Neurol. 2001;172(2):320-331.

Stone JR, Okonkwo DO, Dialo AO, Rubin DG, Mutlu LK, Povlishock JT, Helm GA. Impaired axonal transport and altered axolemmal permeability occur in distinct

populations of damaged axons following traumatic brain injury. Exp Neurol. 2004;190(1):59-69.

Streit WJ. Microglial response to brain injury: A brief synopsis. Toxicol Pathol. 2000:28(1):28-30.

Stuhmiller JH, Phillips YY, Richmond DR. "The Physics and Mechanisms of Primary Blast Injury." Conventional Warfare. Ed. RF Bellamy, R Zajtchuk. Washington DC: TMM Publications, 1996. 241-270.

Stuhmiller JH. Biological response to blast overpressure: A summary of modeling. Toxicology. 1997;121(1)91-103.

Suh M, Kolster R, Sarkar R, McCandliss B, Ghajar J. Deficits in predictive smooth pursuit after mild traumatic brain injury. Neurosci Lett. 2006a;401(1-2):108-13.

Suh M, Basu S, Kolster R, Sarkar R, McCandliss B, Ghajar J. Increased oculomotor deficits during target blanking as an indicator of mild traumatic brain injury. Neurosci Lett. 2006b;410(3):203-207.

Svetlov S, Prima V, Kirk D, Atkinson J, Gutierrez H, Curley K, Hayes R, Wang K. Morphological and biochemical signatures of brain injury following head-directed controlled blast overpressure impact. J Neurotrauma. 2009a;26(8):A-75.

Svetlov SI, Larner SF, Kirk DR, Atkinson J, Hayes RL, Wang KKW. Biomarkers of blast-induced neurotrauma: Profiling molecular and cellular mechanisms of blast brain injury. J Neurotrauma. 2009b;26:913-921.

Sylvia FR, Drake AI, Webster DC. Transient vestibular balance dysfunction after primary blast injury. Mil Med. 2001;166(10):918-920.

Tanielian TL, Jaycox LH. Invisible wounds of war: psychological and cognitive injuries, their consequences, and services to assist recovery. Santa Monica, CA: RAND Corporation, 2008.

Taylor CR, Levenson RM. Quantification of immunohistochemistry – issues concerning methods, utility and semiquantitative assessment II. Histopathology. 2006;49(4):411-424.

Thees C, Scheufler KM, Nadstawek J, Pechstein U, Hanisch M, Juntke R, Zenter J, Hoeft A. Influence of fentanyl, alfentanil, and sufentanil on motor evoked potentials. J Neurosurg Anesthesiol. 1999;11(2):112-118.

Tompkins P, Tesiran Y, Lerner M, Brackett D, Lightfoot S. Whole body blast injury: Nervous system response. National Neurotrauma Symposium, Orlando, Florida. 2008.

Trudeau DL, Anderson J, Hansen LM, Shagalov DN, Schmoller J, Nugent S, Barton S. Findings of mild traumatic brain injury in combat veterans with PTSD and a history of blast concussion. J Neuropsychiatry Clin Neurosci. 1998;10(3):308-313.

United States (1996). "Effects of Nuclear Explosions". In NATO Handbook on the medical aspects of NBC Defensive Operations: Field manual 8-9, Washington, DC: Headquarters, Dept. of the Army.

Van Boven RW, Harrington GS, Hackney DB, Ebel A, Gauger G, Bremner JD, D'Esposito M, Detre JA, Haacke EM, Jack CR Jr, Jagust WJ, Le HB, Mathis CA, Mueller S, Mukherjee P, Schuff N, Chen A, Weiner MW. Advances in

neuroimaging of traumatic brain injury and posttraumatic stress disorder. J Rehabil Res Dev. 2009;46(6):717-757.

Versace J. A review of the severity index. Proceedings of the 15th Stapp Car Crash Conference. Warrendale, PA: Society of Automotive Engineers, 1971. 771-796.

Viano DC. Biomechanics of head injury – Toward a theory linking head dynamic motion, brain tissue deformation and neural trauma. Proceedings of the 32nd Stapp Car Crash Conference. Warrendale, PA: Society of Automotive Engineers, 1988. 1-20.

Viano DC. Biomechanical responses and injuries in blunt lateral impact. Proceedings of the 33rd Stapp Car Crash Conference. Warrendale, PA: Society of Automotive Engineers, 1989. 113-142.

Wagner M, Rihs TA, Mosimann UP, Fisch HU, Schlaepfer TE. Repetitive transcranial magnetic stimulation of the dorsolateral prefrontal cortex affects divided attention immediately after cessation of stimulation. J Psychiatr Res. 2006;40:315-321.

Warden D. Military TBI during the Iraq and Afghanistan wars. J Head Trauma Rehabil. 2006;21(5):398-402.

Watson D. Regional variation in the abundance of axonal cytoskeletal proteins. J Neurosci Res. 1991;30(1):226-231.

White CS, Richmond DR. "Blast Biology." Clinical Cardiopulmonary Physiology. New York: Grune and Stratton, 1960. 974-992.

White CS. Tentative biological criteria for assessing potential hazards from nuclear explosions, Technical Progress Report DASA-1462, DA-49-146-XZ-055, Defense Atomic Support Agency, Albuquerque, NM, December 1963.

Withers PC. Comparative Animal Physiology. Brooks Cole, 1992.

Wood GW, Panzer MB, Shridharani JK, Matthews KA, Bass CR. Attenuation of blast overpressure behind ballistic protective vests. Personal Armour Systems Symposium, Quebec City, QB, Canada, 2010.

Yang Z, Zhengguo W, Chenggong T, Youguo Y. Biological effects of weak blast waves and safety limits for internal organ injury in the human body. J Trauma. 1996;40(3):S81-S84.

Yelverton JT. "Blast Biology." Scientific Foundations of Trauma. Eds. G Cooper, H Dudley, D Gann. New York: Butterworth-Heinemann, 1997. 189-199.

Young MW. Mechanics of blast injuries. War Medicine. 1945;8(2):73-81.

Zhang K, Sejnowski TJ. A universal scaling law between gray matter and white matter of cerebral cortex. PNAS. 2000;97(10):5621-5626.

Zhu F, Mao H, Dal Cengio Leonardi A, Wagner C, Chou C, Jin X, Bir C, VandeVord P, Yang KH, King AI. Development of an FE model of the rat head subjected to air shock loading. Proceedings of Stapp Car Crash Conference, Scottsdale, AZ, 2010.

APPENDIX A. Histological Quantification MATLAB® Code

A.1 First pass MATLAB® code for quantifying positive reactivity for β-APP

```
function []=BAPP(filename)

%Function reads in Digital Slides and counts for Positively Stained
Axons
%written by Karin Rafaels
%filename is the name of the file to be analyzed

info = imfinfo(filename);
wide = info.Width;
high = info.Height;

%determine number of 3000 x 3000 pixel sections on slide

wlength = floor(wide/3000);
hlength = floor(high/3000);

%open color map

fid = open('BAPPmap100.mat');
CheckMatrix = repmat(['-'],wlength+1,hlength+1);
for w = 1:wlength
    wstart = (w-1)*3000 + 1;
    wend = w*3000;
     for h = 1:hlength
        hstart = (h-1)*3000 + 1;
        hend = h*3000;

%open 3000 x 3000 section

        image = imread(filename,'PixelRegion',{[hstart hend],[wstart
wend]});

%convert image to indexed image

        [indeximage] = rgb2ind(image,fid.map);

%exclude debris on slide that is black in color

        avgrgb = 1/3.*sum(image,3);
        logrgb = avgrgb < 30 & image(:,:,1) < 50;

%determine area of tissue

        air = ismember(indeximage, [5 10 11 13 14 15 22 23 24 25 26 33
69]);
        Ltissue = labelmatrix(bwconncomp(~air));
        tissstats = regionprops(~air,'Area');
        AreaTissue(w,h) = sum([tissstats.Area]);
        outfile = sprintf('TissueAreaMatrix-%s',filename);
        dlmwrite([outfile],AreaTissue)
```

```
        if AreaTissue(w,h) < 10000
            CheckMatrix(w,h) = 'N';
            areamat(w,h) = 0;
            quantmat(w,h) = 0;
            continue
        end

%select area of section that may be an axon using color, size, and
shape

        BWimage = ismember(indeximage,[0]);
        BWimage2 = bwareaopen(BWimage,5,4);
        L = labelmatrix(bwconncomp(BWimage2));
        stats = regionprops(BWimage2,'Area');
        idx = find([stats.Area] < 1000 & [stats.Area] > 5);
        BW2 = ismember(L, idx);
        L2 = labelmatrix(bwconncomp(BW2));
        statsellipses = regionprops(BW2,
'Area','MajorAxisLength','MinorAxisLength');
        idellipse =
find(([statsellipses.Area]./(pi.*([statsellipses.MajorAxisLength]/2).*(
[statsellipses.MinorAxisLength]/2)))>0.85);
        BWellipse = ismember(L2,idellipse);
        statsBWellipse = regionprops(BWellipse, 'Area');

%determine areas of section that may be blood vessels

         BWremoveblood = ismember(indeximage,[0 4 9 16 21 27 30 32 38
46 47 48 49 52 54 58 62 63 65 67 70 74 75 81 84 90 93 95 98 99]);
Lremoveblood = labelmatrix(bwconncomp(BWremoveblood));
BWremove = ismember(indeximage,[0 21 47 70 81 90]);
statsblood =
regionprops(BWremoveblood,'Area','Eccentricity','PixelList');
idline = find([statsblood.Eccentricity] > 0.975 & [statsblood.Area] >
250);
if length(idline) > 15
    CheckMatrix(w,h) = 'B';
end
BWblood = ismember(Lremoveblood,idline);
statsremove = regionprops(BWremove,'Area','BoundingBox','PixelList');
BWbloodpx = BWblood;
for k = 1:length(statsblood),
    px = statsblood(k).PixelList;
    px = sub2ind(size(indeximage),px(:,2),px(:,1));
    indexes = indeximage(px);
    dark = find(ismember(indexes, [0]));
    percentdark(k) = length(dark)/length(px);
    BWbloodpx(px) = (percentdark(k) < 0.025);
end
idremove = find([statsblood.Area] > 1000);
BWremove2 = ismember(Lremoveblood, idremove);
BWblood2 = BWremove2 & BWbloodpx;
BWpx = BWremove;
for k = 1:length(statsremove),
    px = statsremove(k).PixelList;
    px = sub2ind(size(indeximage),px(:,2),px(:,1));
```

```
    indexes = indeximage(px);
    dark = find(ismember(indexes, [0]));
    percentdark(k) = length(dark)/length(px);
    BWpx(px) = (percentdark(k) > 0.7);
end
Lrgb = L2(logrgb);
Lrgb(Lrgb <= 0) = [];
if isempty(Lrgb),
    BWrgb = zeros(3000,3000);
    BWrgb = BWrgb ~= 0;
else
    Lrgb = unique(Lrgb(:));
    BWrgb = ismember(L2,Lrgb);
end

%accept areas of tissue that are likely axons and not blood vessels

C = BWellipse & BWpx & ~BWblood2 & ~BWrgb;
        statsC = regionprops(C,'Area');
            areamat(w,h) = sum([statsC.Area]);
            if CheckMatrix(w,h) == 'B' & areamat(w,h) < 500
                areamat(w,h) = 0;
                quantmat(w,h) = 0;
            else
                areamat(w,h) = areamat(w,h);
                quantmat(w,h) = length([statsC.Area]);
            end
        outfile = sprintf('AxonAreaMatrix-%s',filename);
        dlmwrite([outfile],areamat)
        outfile = sprintf('AxonCountMatrix-%s',filename);
        dlmwrite([outfile],quantmat)
        outfile = sprintf('CheckMatrix-%s',filename);
        dlmwrite([outfile],CheckMatrix)
        disp(sprintf('%s Tile (%d,%d)',filename,w,h));
     end
     image = imread(filename,'PixelRegion',{[hend high],[wstart
wend]});
     [indeximage] = rgb2ind(image,fid.map);
        avgrgb = 1/3.*sum(image,3);
        logrgb = avgrgb < 30 & image(:,:,1) < 50;
      air = ismember(indeximage, [5 10 11 13 14 15 22 23 24 25 26 33
69]);
        Ltissue = labelmatrix(bwconncomp(~air));
        tissstats = regionprops(~air,'Area');
        AreaTissue(w,h+1) = sum([tissstats.Area]);
        outfile = sprintf('TissueAreaMatrix-%s',filename);
        dlmwrite([outfile],AreaTissue)
        if AreaTissue(w,h+1) < 10000
            CheckMatrix(w,h+1) = 'N';
            continue
        end
        BWimage = ismember(indeximage,[0]);
        BWimage2 = bwareaopen(BWimage,5,4);
        L = labelmatrix(bwconncomp(BWimage2));
        stats = regionprops(BWimage2,'Area');
        idx = find([stats.Area] < 1000 & [stats.Area] > 5);
```

```
        BW2 = ismember(L, idx);
        L2 = labelmatrix(bwconncomp(BW2));
        statsellipses = regionprops(BW2,
'Area','MajorAxisLength','MinorAxisLength');
        idellipse =
find(([statsellipses.Area]./(pi.*([statsellipses.MajorAxisLength]/2).*(
[statsellipses.MinorAxisLength]/2)))>0.85);
        BWellipse = ismember(L2,idellipse);
        statsBWellipse = regionprops(BWellipse, 'Area');
  BWremoveblood = ismember(indeximage,[0 4 9 16 21 27 30 32 38 46 47 48
Lremoveblood = labelmatrix(bwconncomp(BWremoveblood));
BWremove = ismember(indeximage,[0 21 47 70 81 90]);
statsblood =
regionprops(BWremoveblood,'Area','Eccentricity','PixelList');
idline = find([statsblood.Eccentricity] > 0.975 & [statsblood.Area] >
250);
if length(idline) > 15
    CheckMatrix(w,h+1) = 'B';
end
BWblood = ismember(Lremoveblood,idline);
statsremove = regionprops(BWremove,'Area','BoundingBox','PixelList');
BWbloodpx = BWblood;
for k = 1:length(statsblood),
    px = statsblood(k).PixelList;
    px = sub2ind(size(indeximage),px(:,2),px(:,1));
    indexes = indeximage(px);
    dark = find(ismember(indexes, [0]));
    percentdark(k) = length(dark)/length(px);
    BWbloodpx(px) = (percentdark(k) < 0.025);
end
idremove = find([statsblood.Area] > 1000);
BWremove2 = ismember(Lremoveblood, idremove);
BWblood2 = BWremove2 & BWbloodpx;
BWpx = BWremove;
for k = 1:length(statsremove),
    px = statsremove(k).PixelList;
    px = sub2ind(size(indeximage),px(:,2),px(:,1));
    indexes = indeximage(px);
    dark = find(ismember(indexes, [0]));
    percentdark(k) = length(dark)/length(px);
    BWpx(px) = (percentdark(k) > 0.7);
end
Lrgb = L2(logrgb);
Lrgb(Lrgb <= 0) = [];
if isempty(Lrgb),
    BWrgb = zeros(high-hend+1,3000);
    BWrgb = BWrgb ~= 0;
else
    Lrgb = unique(Lrgb(:));
    BWrgb = ismember(L2,Lrgb);
end
C = BWellipse & BWpx & ~BWblood2 & ~BWrgb;
        statsC = regionprops(C,'Area');
            areamat(w,h+1) = sum([statsC.Area]);
                        if CheckMatrix(w,h+1) == 'B' & areamat(w,h+1) <
500
```

```
                areamat(w,h+1) = 0;
                quantmat(w,h+1) = 0;
            else
                areamat(w,h+1) = areamat(w,h+1);
                quantmat(w,h+1) = length([statsC.Area]);
            end
        outfile = sprintf('AxonAreaMatrix-%s',filename);
        dlmwrite([outfile],areamat)
        outfile = sprintf('AxonCountMatrix-%s',filename);
        dlmwrite([outfile],quantmat)
        outfile = sprintf('CheckMatrix-%s',filename);
        dlmwrite([outfile],CheckMatrix)
        disp(sprintf('%s Tile (%d,%d)',filename,w,h+1));
end
    for h = 1:hlength
        hstart = (h-1)*3000 + 1;
        hend = h*3000;
        image = imread(filename,'PixelRegion',{[hstart hend],[wend
wide]});
        [indeximage] = rgb2ind(image,fid.map);
        avgrgb = 1/3.*sum(image,3);
        logrgb = avgrgb < 30 & image(:,:,1) < 50;
        air = ismember(indeximage, [5 10 11 13 14 15 22 23 24 25 26 33
69]);
        Ltissue = labelmatrix(bwconncomp(~air));
        tissstats = regionprops(~air,'Area');
        AreaTissue(w+1,h) = sum([tissstats.Area]);
        outfile = sprintf('TissueAreaMatrix-%s',filename);
        dlmwrite([outfile],AreaTissue)
        if AreaTissue(w+1,h) < 10000
            CheckMatrix(w+1,h) = 'N';
            continue
        end
         BWimage = ismember(indeximage,[0]);
        BWimage2 = bwareaopen(BWimage,5,4);
        L = labelmatrix(bwconncomp(BWimage2));
        stats = regionprops(BWimage2,'Area');
        idx = find([stats.Area] < 1000 & [stats.Area] > 5);
        BW2 = ismember(L, idx);
        L2 = labelmatrix(bwconncomp(BW2));
        statsellipses = regionprops(BW2,
'Area','MajorAxisLength','MinorAxisLength');
        idellipse =
find(([statsellipses.Area]./(pi.*([statsellipses.MajorAxisLength]/2).*(
[statsellipses.MinorAxisLength]/2)))>0.85);
        BWellipse = ismember(L2,idellipse);
        statsBWellipse = regionprops(BWellipse, 'Area');
  BWremoveblood = ismember(indeximage,[0 4 9 16 21 27 30 32 38 46 47 48
49 52 54 58 62 63 65 67 70 74 75 81 84 90 93 95 98 99]);
Lremoveblood = labelmatrix(bwconncomp(BWremoveblood));
BWremove = ismember(indeximage,[0 21 47 70 81 90]);
statsblood =
regionprops(BWremoveblood,'Area','Eccentricity','PixelList');
idline = find([statsblood.Eccentricity] > 0.975 & [statsblood.Area] >
250);
if length(idline) > 15
```

```
    CheckMatrix(w+1,h) = 'B';
end
BWblood = ismember(Lremoveblood,idline);
statsremove = regionprops(BWremove,'Area','BoundingBox','PixelList');
BWbloodpx = BWblood;
for k = 1:length(statsblood),
    px = statsblood(k).PixelList;
    px = sub2ind(size(indeximage),px(:,2),px(:,1));
    indexes = indeximage(px);
    dark = find(ismember(indexes, [0]));
    percentdark(k) = length(dark)/length(px);
    BWbloodpx(px) = (percentdark(k) < 0.025);
end
idremove = find([statsblood.Area] > 1000);
BWremove2 = ismember(Lremoveblood, idremove);
BWblood2 = BWremove2 & BWbloodpx;
BWpx = BWremove;
for k = 1:length(statsremove),
    px = statsremove(k).PixelList;
    px = sub2ind(size(indeximage),px(:,2),px(:,1));
    indexes = indeximage(px);
    dark = find(ismember(indexes, [0]));
    percentdark(k) = length(dark)/length(px);
    BWpx(px) = (percentdark(k) > 0.7);
end
Lrgb = L2(logrgb);
Lrgb(Lrgb <= 0) = [];
if isempty(Lrgb),
    BWrgb = zeros(3000,wide-wend+1);
    BWrgb = BWrgb ~= 0;
else
    Lrgb = unique(Lrgb(:));
    BWrgb = ismember(L2,Lrgb);
end
C = BWellipse & BWpx & ~BWblood2 & ~BWrgb;
        statsC = regionprops(C,'Area');
           areamat(w+1,h) = sum([statsC.Area]);
                       if CheckMatrix(w+1,h) == 'B' & areamat(w+1,h) <
500
               areamat(w+1,h) = 0;
               quantmat(w+1,h) = 0;
           else
               areamat(w+1,h) = areamat(w+1,h);
               quantmat(w+1,h) = length([statsC.Area]);
           end
        outfile = sprintf('AxonAreaMatrix-%s',filename);
        dlmwrite([outfile],areamat)
        outfile = sprintf('AxonCountMatrix-%s',filename);
        dlmwrite([outfile],quantmat)
        outfile = sprintf('CheckMatrix-%s',filename);
        dlmwrite([outfile],CheckMatrix)
        disp(sprintf('%s Tile (%d,%d)',filename,w+1,h));
     end
     image = imread(filename,'PixelRegion',{[hend high],[wend wide]});
     [indeximage] = rgb2ind(image,fid.map);
    avgrgb = 1/3.*sum(image,3);
```

```
    logrgb = avgrgb < 30 & image(:,:,1) < 50;
     air = ismember(indeximage, [5 10 11 13 14 15 22 23 24 25 26 33
69]);
        Ltissue = labelmatrix(bwconncomp(~air));
        tissstats = regionprops(~air,'Area');
        AreaTissue(w+1,h+1) = sum([tissstats.Area]);
        outfile = sprintf('TissueAreaMatrix-%s',filename);
        dlmwrite([outfile],AreaTissue)
        if AreaTissue(w+1,h+1) < 10000
            CheckMatrix(w+1,h+1) = 'N';
        else
         BWimage = ismember(indeximage,[0]);
        BWimage2 = bwareaopen(BWimage,5,4);
        L = labelmatrix(bwconncomp(BWimage2));
        stats = regionprops(BWimage2,'Area');
        idx = find([stats.Area] < 1000 & [stats.Area] > 5);
        BW2 = ismember(L, idx);
        L2 = labelmatrix(bwconncomp(BW2));
        statsellipses = regionprops(BW2,
'Area','MajorAxisLength','MinorAxisLength');
        idellipse =
find(([statsellipses.Area]./(pi.*([statsellipses.MajorAxisLength]/2).*(
[statsellipses.MinorAxisLength]/2)))>0.85);
        BWellipse = ismember(L2,idellipse);
        statsBWellipse = regionprops(BWellipse, 'Area');
  BWremoveblood = ismember(indeximage,[0 4 9 16 21 27 30 32 38 46 47 48
49 52 54 58 62 63 65 67 70 74 75 81 84 90 93 95 98 99]);
Lremoveblood = labelmatrix(bwconncomp(BWremoveblood));
BWremove = ismember(indeximage,[0 21 47 70 81 90]);
statsblood =
regionprops(BWremoveblood,'Area','Eccentricity','PixelList');
idline = find([statsblood.Eccentricity] > 0.975 & [statsblood.Area] >
250);
if length(idline) > 15
    CheckMatrix(w+1,h+1) = 'B';
end
BWblood = ismember(Lremoveblood,idline);
statsremove = regionprops(BWremove,'Area','BoundingBox','PixelList');
BWbloodpx = BWblood;
for k = 1:length(statsblood),
    px = statsblood(k).PixelList;
    px = sub2ind(size(indeximage),px(:,2),px(:,1));
    indexes = indeximage(px);
    dark = find(ismember(indexes, [0]));
    percentdark(k) = length(dark)/length(px);
    BWbloodpx(px) = (percentdark(k) < 0.025);
end
idremove = find([statsblood.Area] > 1000);
BWremove2 = ismember(Lremoveblood, idremove);
BWblood2 = BWremove2 & BWbloodpx;
BWpx = BWremove;
for k = 1:length(statsremove),
    px = statsremove(k).PixelList;
    px = sub2ind(size(indeximage),px(:,2),px(:,1));
    indexes = indeximage(px);
    dark = find(ismember(indexes, [0]));
```

```
    percentdark(k) = length(dark)/length(px);
    BWpx(px) = (percentdark(k) > 0.7);
end
Lrgb = L2(logrgb);
Lrgb(Lrgb <= 0) = [];
if isempty(Lrgb),
    BWrgb = zeros(high-hend+1,wide-wend+1);
    BWrgb = BWrgb ~= 0;
else
    Lrgb = unique(Lrgb(:));
    BWrgb = ismember(L2,Lrgb);
end
C = BWellipse & BWpx & ~BWblood2 & ~BWrgb;
        statsC = regionprops(C,'Area');
            areamat(w+1,h+1) = sum([statsC.Area]);
                        if CheckMatrix(w+1,h+1) == 'B' &
areamat(w+1,h+1) < 500
                areamat(w+1,h+1) = 0;
                quantmat(w+1,h+1) = 0;
            else
                areamat(w+1,h+1) = areamat(w+1,h+1);
                quantmat(w+1,h+1) = length([statsC.Area]);
            end
        outfile = sprintf('AxonAreaMatrix-%s',filename);
        dlmwrite([outfile],areamat)
        outfile = sprintf('AxonCountMatrix-%s',filename);
        dlmwrite([outfile],quantmat)
        outfile = sprintf('CheckMatrix-%s',filename);
        dlmwrite([outfile],CheckMatrix)
        disp(sprintf('%s Tile (%d,%d)',filename,w+1,h+1));
        end
     totcolrow = sum(areamat);
       AreaAxon = sum(totcolrow)
       totcolrowtis = sum(AreaTissue);
       TissueArea = sum(totcolrowtis)
       NormAxonArea = AreaAxon/TissueArea
```

A.2 Semi-automatic MATLAB® code for quantifying positive reactivity for β-APP

```
%Reads in 3000 x 3000 sections of image and through user-interface
counts for Positively Stained Axons
%written by Karin Rafaels

%open color map then 3000 x 3000 section

fid = open('BAPPmap100.mat');
image = imread('LF05-Slide10.jp2','PixelRegion',{[x1 x2],[y1
y2]});%{[hstart hend],[wstart wend]});
[indeximage] = rgb2ind(image,fid.map);
avgrgb = 1/3.*sum(image,3);
logrgb = avgrgb < 30 & image(:,:,1) < 50;
BWimage = ismember(indeximage,[0]);
BWimage2 = bwareaopen(BWimage,5,4);
```

```
L = labelmatrix(bwconncomp(BWimage2));
stats = regionprops(BWimage2,'Area');
idx = find([stats.Area] < 1000 & [stats.Area] > 5);
BW2 = ismember(L, idx);
L2 = labelmatrix(bwconncomp(BW2));
statsellipses = regionprops(BW2,
'Area','MajorAxisLength','MinorAxisLength');
idellipse =
find(([statsellipses.Area]./(pi.*([statsellipses.MajorAxisLength]/2).*(
[statsellipses.MinorAxisLength]/2)))>0.85);
BWellipse = ismember(L2,idellipse);
 BWremoveblood = ismember(indeximage,[0 4 9 16 21 27 30 32 38 46 47 48
49 52 54 58 62 63 65 67 70 74 75 81 84 90 93 95 98 99]);
Lremoveblood = labelmatrix(bwconncomp(BWremoveblood));
BWremove = ismember(indeximage,[0 21 47 70 81 90]);
statsblood = regionprops(BWremoveblood,'Area','PixelList');
statsremove = regionprops(BWremove,'Area','PixelList');
BWbloodpx = BWremove;
for k = 1:length(statsblood),
    px = statsblood(k).PixelList;
    px = sub2ind(size(indeximage),px(:,2),px(:,1));
    indexes = indeximage(px);
    dark = find(ismember(indexes, [0]));
    percentdark(k) = length(dark)/length(px);
    BWbloodpx(px) = (percentdark(k) < 0.025);end
idremove = find([statsblood.Area] > 1000);
BWremove2 = ismember(Lremoveblood, idremove);
BWblood2 = BWremove2 & BWbloodpx;
BWpx = BWremove;
for k = 1:length(statsremove),
    px = statsremove(k).PixelList;
    px = sub2ind(size(indeximage),px(:,2),px(:,1));
    indexes = indeximage(px);
    dark = find(ismember(indexes, [0]));
    percentdark(k) = length(dark)/length(px);
    BWpx(px) = (percentdark(k) > 0.7);
end
Lrgb = L2(logrgb);
Lrgb(Lrgb <= 0) = [];
if isempty(Lrgb),
    BWrgb = zeros(3000,3000);
    BWrgb = BWrgb ~= 0;
else
    Lrgb = unique(Lrgb(:));
    BWrgb = ismember(L2,Lrgb);
end
C = BWellipse & BWpx & ~BWblood2 & ~BWrgb;

%interactive figures with original image and image with selected areas
highlighted
%user can remove selections that are not axons
%user can also change first term in regionclick function to increase
selected areas
%output is the area of the selected regions

C = regionclick(BW2,image);
```

```
statsC = regionprops(C,'Area');
areamat = sum([statsC.Area])


%interactive function for selecting positive regions

function BW = regionclick(BW, Indexed)
    close all;
    [B,L] =bwboundaries(BW);
    HP = NaN(size(B));   %patch handles
      figure, imshow(Indexed);      hB=gca;
      figure, imshow(BW);
    hA= gca; hold on;  hfig = gcf; linkaxes([hA hB],'xy');

    for k=1:length(B),
       Border = B{k}(:,[2 1]);  %boundary of region corresponding to
region L
       plot(Border(:,1), Border(:,2), 'red');
       HP(k) = plot(Border(:,1), Border(:,2), 'g-'); hold on;
       set(HP(k), 'LineWidth',1, 'Parent', hA);
    end

    set(hfig, 'WindowButtonDownFcn',@clickfcn);
    uiwait(hfig); %wait for clicking to occur
    mode = '';
    close(hfig);

    function clickfcn(src,eventdata)
        btn = get(src, 'SelectionType');   %determine which kind of
click
        if strcmp(btn, 'extend'),
            mode = '';
            set(hfig, 'WindowButtonDownFcn','');
         %   close(hfig); %imshow(BW);
            uiresume(hfig);
        end
        pos = get(hA,'CurrentPoint');
        pos = pos(1,1:2);
        Lidx = [];
        for p=1:length(B),
            Border = B{p}(:,[2 1]);
            in = inpoly(pos,Border);  %inpoly code downloaded from
MATLAB® fileshare
            if in,
                Lidx = p;
                pHandle = HP(p);
                break;
            end
        end
        if isempty(Lidx),  return;  end;  %do nothing if no region
clicked
        switch btn,
            case 'normal',  %left click
                mode = 'discard';
                set(pHandle, 'Color', 'magenta');   %red to indicate
discard region
```

```
                LPos = ismember(L, Lidx);
                BW = BW & ~LPos;   %eliminate that region from tile
            case 'alt',   %right click
                mode = 'add';
                set(pHandle, 'Color','green');  %green to indicate
retain region
                LPos = ismember(L, Lidx);
                BW = BW | LPos;   %add that region back to tile
            case 'open',  %double click to follow last click
                switch mode,
                    case 'discard',    %set all regions to red
(discard)
                       set(HP,'Color','magenta');
                       BW = false(size(BW));
                    case 'add',         %set all regions to green
(keep)
                        set(HP, 'Color','green');
                        BW = (L ~= 0);
                end
        end

    end
close all;
end
```

A.3 MATLAB® code for quantifying positive astrocyte activity

```
function []=GFAP(filename)

%Function reads in Digital Slides and counts for Positively Stained
Glial Cells
%written by Karin Rafaels
%filename is the name of the file to be analyzed

info = imfinfo(filename);
wide = info.Width;
high = info.Height;
wlength = floor(wide/3000);
hlength = floor(high/3000);
fid = open('GFAPmap50.mat');
for w = 1:wlength
    wstart = (w-1)*3000 + 1;
    wend = w*3000;
     for h = 1:hlength
        hstart = (h-1)*3000 + 1;
        hend = h*3000;
        image = imread(filename,'PixelRegion',{[hstart hend],[wstart
wend]});
        [indeximage] = rgb2ind(image,fid.map);
        air = ismember(indeximage, [3 4 5 6 7 8 9 10 11 12 13 14 33 35
36 37 42]);
        Ltissue = labelmatrix(bwconncomp(~air));
        tissstats = regionprops(~air,'Area');
        AreaTissue(w,h) = sum([tissstats.Area]);
        outfile = sprintf('GFAPTissueAreaMatrix-%s',filename);
```

```
        dlmwrite([outfile],AreaTissue)

%select areas of section that are likely positive astrocytes using
color and size

        BWimage = ismember(indeximage,[0 21 30]);
C = BWimage;
        statsC = regionprops(C,'Area');
            areamat(w,h) = sum([statsC.Area]);
            if areamat(w,h) < 500
                areamat(w,h) = 0;
            else
                areamat(w,h) = areamat(w,h);
            end
        outfile = sprintf('GFAPAreaMatrix-%s',filename);
        dlmwrite([outfile],areamat)
        disp(sprintf('%s Tile (%d,%d)',filename,w,h));
     end
     image = imread(filename,'PixelRegion',{[hend high],[wstart
wend]});
     [indeximage] = rgb2ind(image,fid.map);
        air = ismember(indeximage, [3 4 5 6 7 8 9 10 11 12 13 14 33 35
36 37 42]);
        Ltissue = labelmatrix(bwconncomp(~air));
        tissstats = regionprops(~air,'Area');
        AreaTissue(w,h+1) = sum([tissstats.Area]);
        outfile = sprintf('GFAPTissueAreaMatrix-%s',filename);
        dlmwrite([outfile],AreaTissue)
        BWimage = ismember(indeximage,[0 21 30]);
C = BWimage;
        statsC = regionprops(C,'Area');
            areamat(w,h+1) = sum([statsC.Area]);
                        if areamat(w,h+1) < 500
                areamat(w,h+1) = 0;
            else
                areamat(w,h+1) = areamat(w,h+1);
            end
        outfile = sprintf('GFAPAreaMatrix-%s',filename);
        dlmwrite([outfile],areamat)
        disp(sprintf('%s Tile (%d,%d)',filename,w,h+1));
end
     for h = 1:hlength
        hstart = (h-1)*3000 + 1;
        hend = h*3000;
            image = imread(filename,'PixelRegion',{[hstart hend],[wend
wide]});
     [indeximage] = rgb2ind(image,fid.map);
        air = ismember(indeximage, [3 4 5 6 7 8 9 10 11 12 13 14 33 35
36 37 42]);
        Ltissue = labelmatrix(bwconncomp(~air));
        tissstats = regionprops(~air,'Area');
        AreaTissue(w+1,h) = sum([tissstats.Area]);
        outfile = sprintf('GFAPTissueAreaMatrix-%s',filename);
        dlmwrite([outfile],AreaTissue)
        BWimage = ismember(indeximage,[0 21 30]);
C = BWimage;
```

```
        statsC = regionprops(C,'Area');
            areamat(w+1,h) = sum([statsC.Area]);
                        if areamat(w+1,h) < 500
                areamat(w+1,h) = 0;
            else
                areamat(w+1,h) = areamat(w+1,h);
            end
        outfile = sprintf('GFAPAreaMatrix-%s',filename);
        dlmwrite([outfile],areamat)
        disp(sprintf('%s Tile (%d,%d)',filename,w+1,h));
    end
    image = imread(filename,'PixelRegion',{[hend high],[wend wide]});
    [indeximage] = rgb2ind(image,fid.map);
            air = ismember(indeximage, [3 4 5 6 7 8 9 10 11 12 13 14 33
35 36 37 42]);
        Ltissue = labelmatrix(bwconncomp(~air));
        tissstats = regionprops(~air,'Area');
        AreaTissue(w,h+1) = sum([tissstats.Area]);
        outfile = sprintf('GFAPTissueAreaMatrix-%s',filename);
        dlmwrite([outfile],AreaTissue)
        BWimage = ismember(indeximage,[0 21 30]);
C = BWimage;
        statsC = regionprops(C,'Area');
            areamat(w+1,h+1) = sum([statsC.Area]);
                        if areamat(w+1,h+1) < 500
                areamat(w+1,h+1) = 0;
            else
                areamat(w+1,h+1) = areamat(w+1,h+1);
            end
        outfile = sprintf('GFAPAreaMatrix-%s',filename);
        dlmwrite([outfile],areamat)
        disp(sprintf('%s Tile (%d,%d)',filename,w+1,h+1));
    totcolrow = sum(areamat);
      AreaAxon = sum(totcolrow)
      totcolrowtis = sum(AreaTissue);
      TissueArea = sum(totcolrowtis)
      NormAxonArea = AreaAxon/TissueArea
```

A.4 First pass MATLAB® code for quantifying LPB stain

```
function []=LPB(filename)

%Function reads in Digital Slides and counts for Positively Stained
Blood cells
%written by Karin Rafaels
%filename is the name of the file to be analyzed

info = imfinfo(filename);
wide = info.Width;
high = info.Height;
wlength = floor(wide/3000);
hlength = floor(high/3000);
fid = open('LPBmap.mat');
for w = 1:wlength
    wstart = (w-1)*3000 + 1;
```

```
    wend = w*3000;
     for h = 1:hlength
        hstart = (h-1)*3000 + 1;
        hend = h*3000;
        image = imread(filename,'PixelRegion',{[hstart hend],[wstart
wend]});
[indeximage] = rgb2ind(image,fid.map);

%select areas of section that are stained with LPB

BWlpb = ismember(indeximage,[0 13 17 29 30 35 43 46 47]);
BWblue = ismember(indeximage,[47]);
BWimage2 = bwareaopen(BWlpb,5,4);
C = BWimage2 & imfill(BWlpb,'holes');
L = labelmatrix(bwconncomp(C));
stats = regionprops(C,'Area');
idx = find([stats.Area] > 1000);
BW2 = ismember(L, idx);
blood = BW2 & BWblue;
statsblood = regionprops(blood,'Area');
areamat(w,h) = sum([statsblood.Area]);
                areamat(w,h) = areamat(w,h);
        outfile = sprintf('BloodAreaMatrix-%s',filename);
        dlmwrite([outfile],areamat)
        disp(sprintf('%s Tile (%d,%d)',filename,w,h));
        image = imread(filename,'PixelRegion',{[hend high],[wstart
wend]});
        [indeximage] = rgb2ind(image,fid.map);
BWlpb = ismember(indeximage,[0 13 17 29 30 35 43 46 47]);
BWblue = ismember(indeximage,[47]);
BWimage2 = bwareaopen(BWlpb,5,4);
C = BWimage2 & imfill(BWlpb,'holes');
L = labelmatrix(bwconncomp(C));
stats = regionprops(C,'Area');
idx = find([stats.Area] > 1000);
BW2 = ismember(L, idx);
blood = BW2 & BWblue;
statsblood = regionprops(blood,'Area');
areamat(w,h+1) = sum([statsblood.Area]);
                areamat(w,h+1) = areamat(w,h+1);
        outfile = sprintf('BloodAreaMatrix-%s',filename);
        dlmwrite([outfile],areamat)
        disp(sprintf('%s Tile (%d,%d)',filename,w,h+1));
     end
         for h = 1:hlength
        hstart = (h-1)*3000 + 1;
        hend = h*3000;
        image = imread(filename,'PixelRegion',{[hstart hend],[wend
wide]});
[indeximage] = rgb2ind(image,fid.map);
BWlpb = ismember(indeximage,[0 13 17 29 30 35 43 46 47]);
BWblue = ismember(indeximage,[47]);
BWimage2 = bwareaopen(BWlpb,5,4);
C = BWimage2 & imfill(BWlpb,'holes');
L = labelmatrix(bwconncomp(C));
stats = regionprops(C,'Area');
```

```
idx = find([stats.Area] > 1000);
BW2 = ismember(L, idx);
blood = BW2 & BWblue;
statsblood = regionprops(blood,'Area');
areamat(w+1,h) = sum([statsblood.Area]);
                areamat(w+1,h) = areamat(w+1,h);
        outfile = sprintf('BloodAreaMatrix-%s',filename);
        dlmwrite([outfile],areamat)
        disp(sprintf('%s Tile (%d,%d)',filename,w+1,h));
         end
         image = imread(filename,'PixelRegion',{[hend high],[wend
wide]});
         [indeximage] = rgb2ind(image,fid.map);
BWlpb = ismember(indeximage,[0 13 17 29 30 35 43 46 47]);
BWblue = ismember(indeximage,[47]);
BWimage2 = bwareaopen(BWlpb,5,4);
C = BWimage2 & imfill(BWlpb,'holes');
L = labelmatrix(bwconncomp(C));
stats = regionprops(C,'Area');
idx = find([stats.Area] > 1000);
BW2 = ismember(L, idx);
blood = BW2 & BWblue;
statsblood = regionprops(blood,'Area');
areamat(w+1,h+1) = sum([statsblood.Area]);
                areamat(w+1,h+1) = areamat(w+1,h+1);
        outfile = sprintf('BloodAreaMatrix-%s',filename);
        dlmwrite([outfile],areamat)
        disp(sprintf('%s Tile (%d,%d)',filename,w+1,h+1));
         end
```

A.5 Semi-automatic MATLAB® code for quantifying LPB stain

```
%Reads in 3000 x 3000 sections of image and through user-interface
counts for LPB stained areas
%written by Karin Rafaels

fid = open('LPBmap.mat');
image = imread('LF70-LPB.jp2','PixelRegion',{[39001 42000],[171001
174000]});%{[hstart hend],[wstart wend]});
[indeximage] = rgb2ind(image,fid.map);
BWlpb = ismember(indeximage,[0 13 17 29 30 35 43 46 47]);
BWimage2 = bwareaopen(BWlpb,5,4);
C = BWimage2 & imfill(BWlpb,'holes');
L = labelmatrix(bwconncomp(C));
stats = regionprops(C,'Area');
idx = find([stats.Area] > 1000);
BW2 = ismember(L, idx);
C2 = regionclick(BW2,image);
statsC2 = regionprops(C2,'Area');
areamat = sum([statsC2.Area])
```

APPENDIX B. Additional figures of Positive β-APP Staining

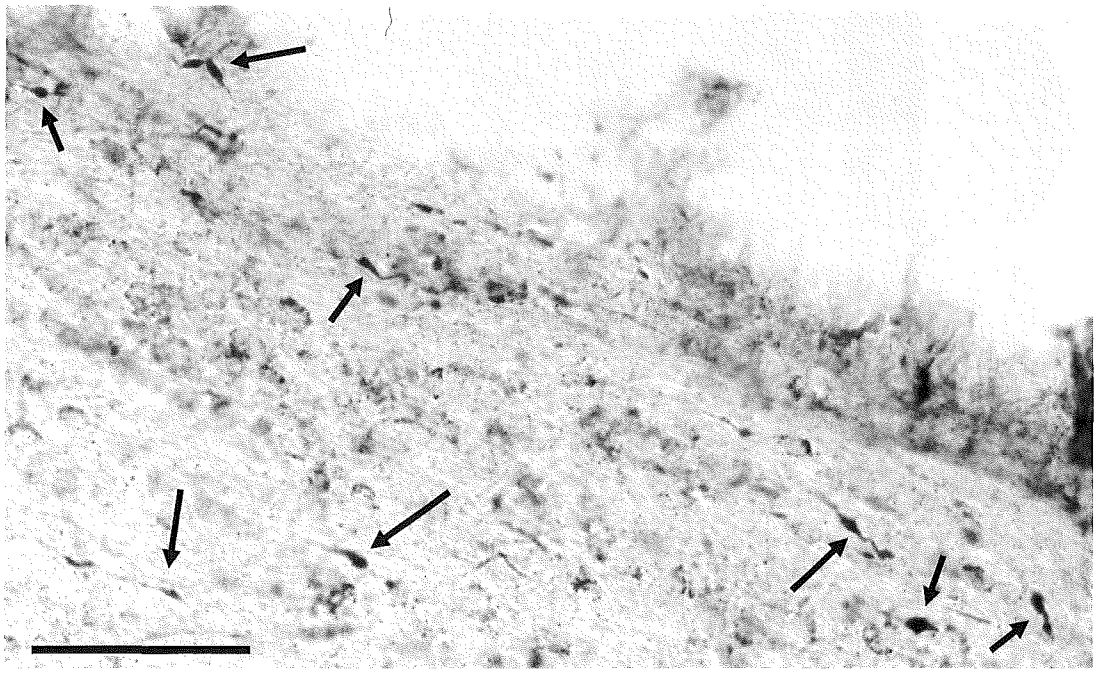

Figure B.1. Positive β-APP stained tissue from coronal section of corpus callosum from LF70. The injured axons are highlighted by the black arrows. Black scale line = 50 μm.

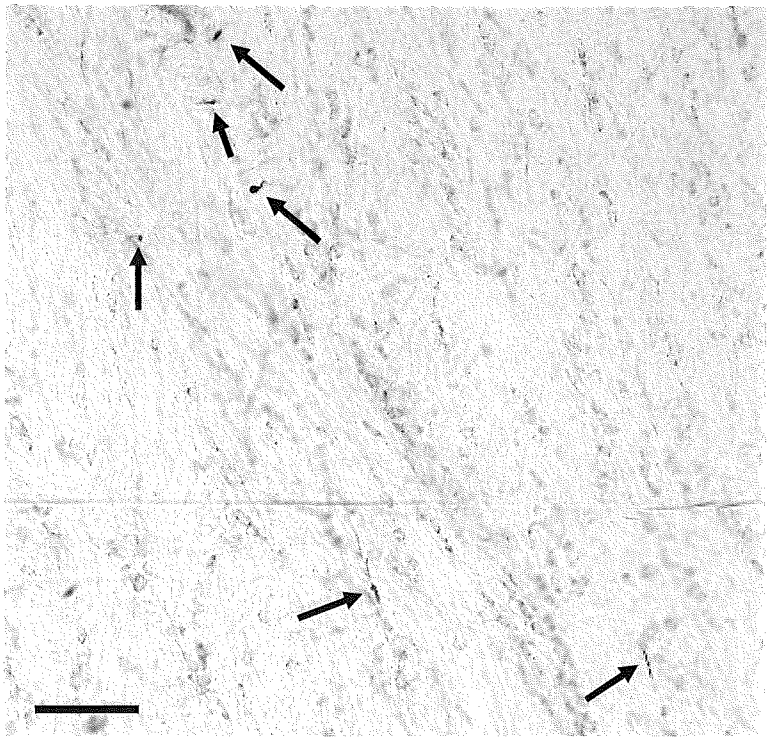

Figure B.2. Positive β-APP stained tissue from coronal section of corona radiata from LF70. The injured axons are highlighted by the black arrows. Black scale line = 50 μm.

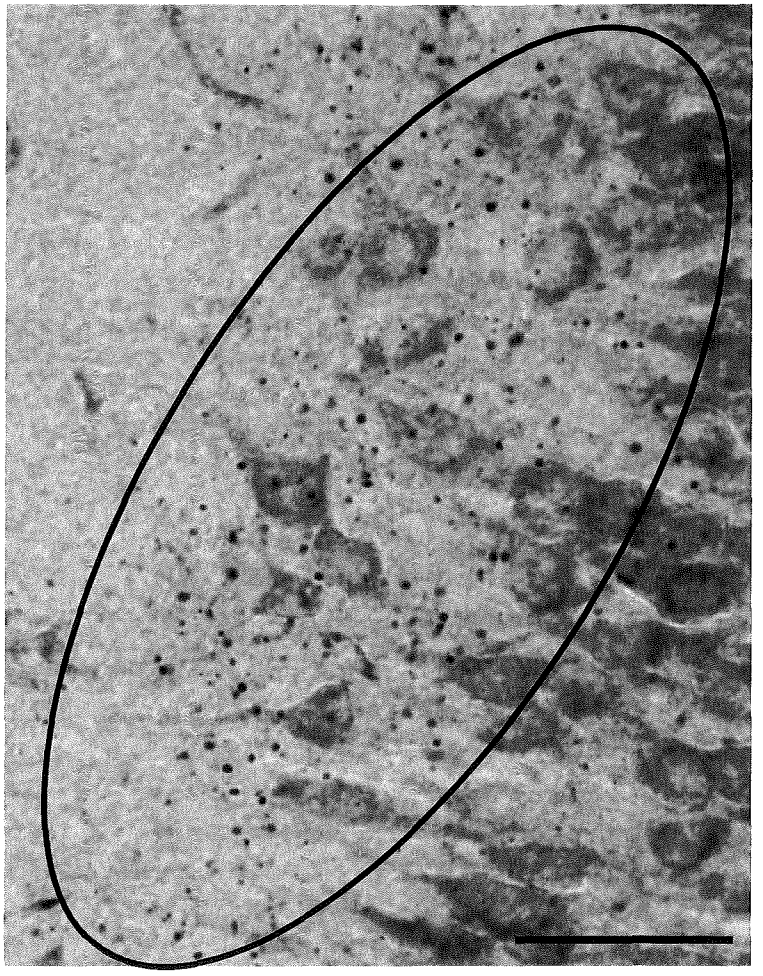

Figure B.3. Positive β-APP stained tissue from coronal section of hippocampus from LF19. Many of the visible injured axons are encircled. Black scale line = 50 μm.

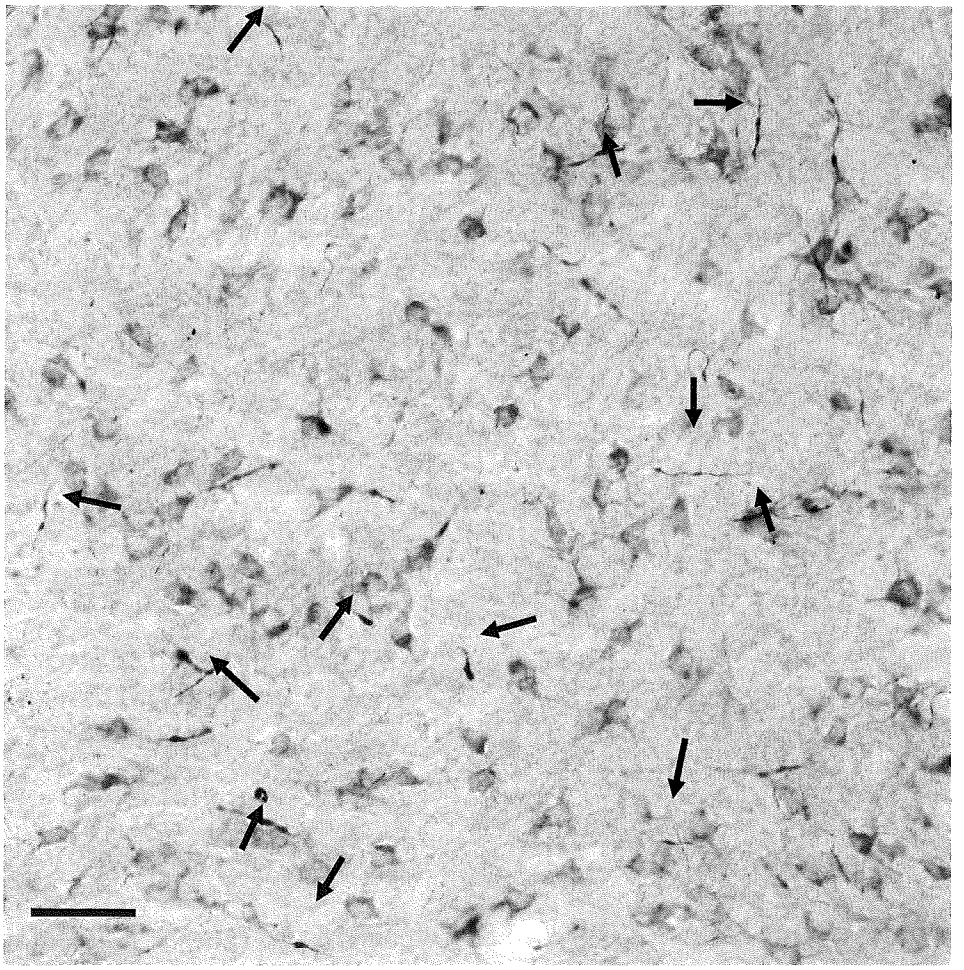

Figure B.4. Positive β-APP stained tissue from coronal section of the thalamus from LF11. The injured axons are highlighted by the black arrows. Black scale line = 50 μm.

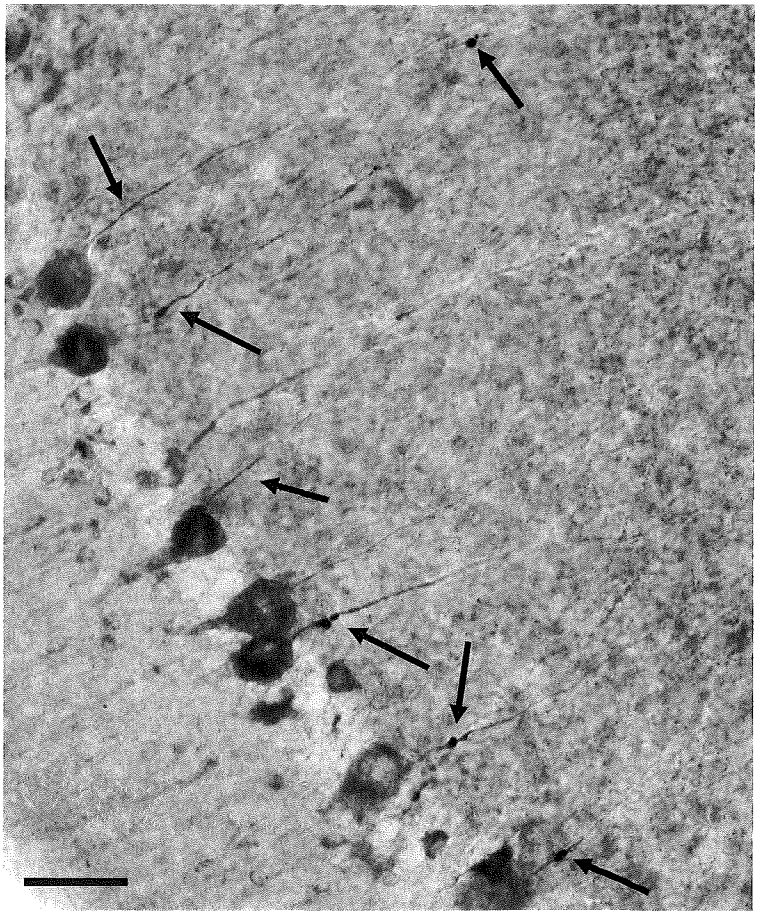

Figure B.5. Positive β-APP stained tissue from coronal section of the cerebellum from LF28. The injured axons are highlighted by the black arrows. Black scale line = 50 μm.

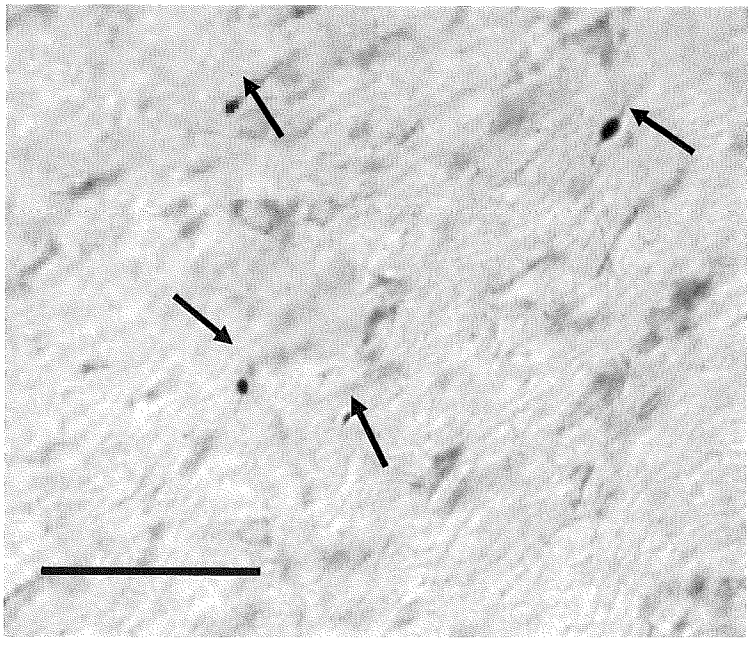

Figure B.6. Positive β-APP stained tissue from coronal section of the spinothalamic tract from LF11. The injured axons are highlighted by the black arrows. Black scale line = 50 μm.

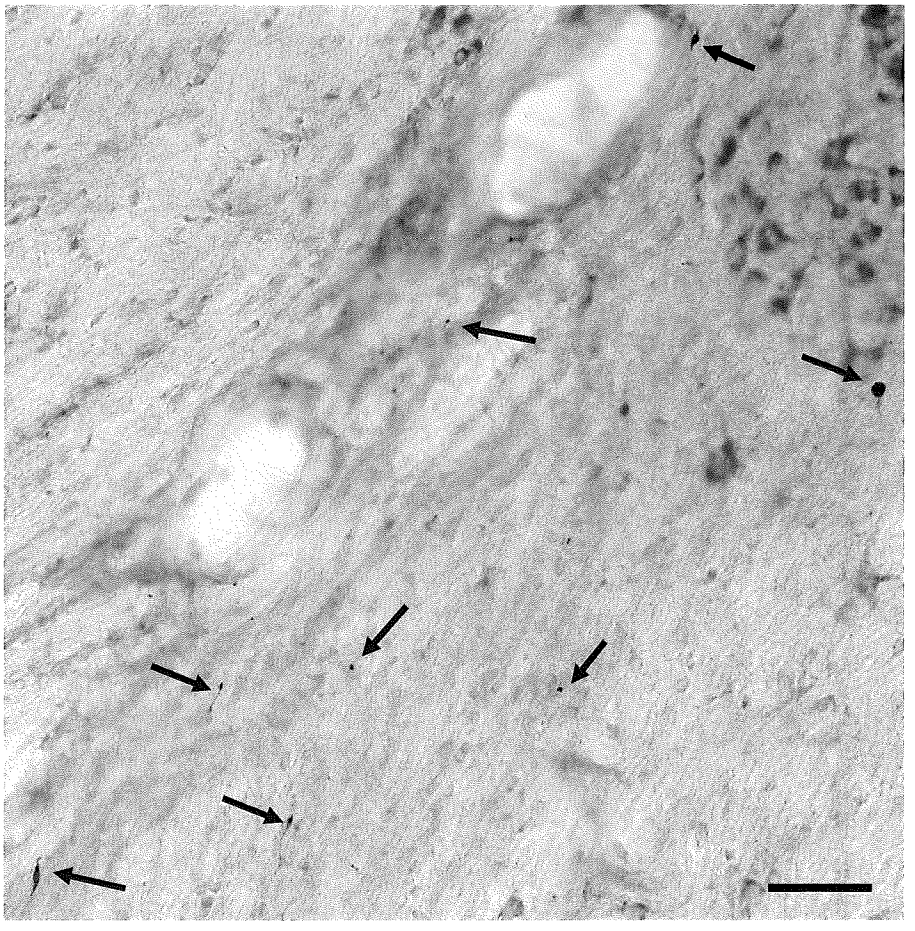

Figure B.7. Positive β-APP stained tissue from coronal section of the corticospinal tract from LF11. The injured axons are highlighted by the black arrows. Black scale line = 50 μm.

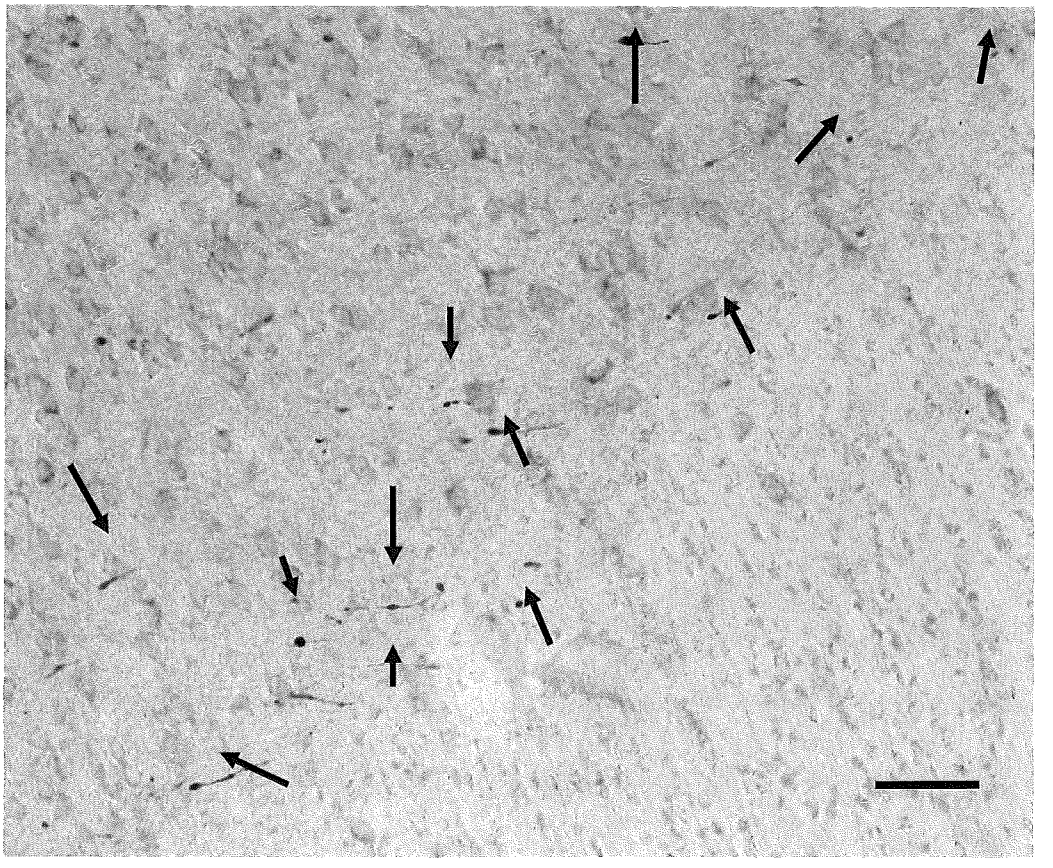

Figure B.8. Positive β-APP stained tissue at the interface between the grey and white matter in LF13. The injured axons are highlighted by the black arrows. Black scale line = 50 μm.

APPENDIX C. Additional figures of Positive RM014 Staining

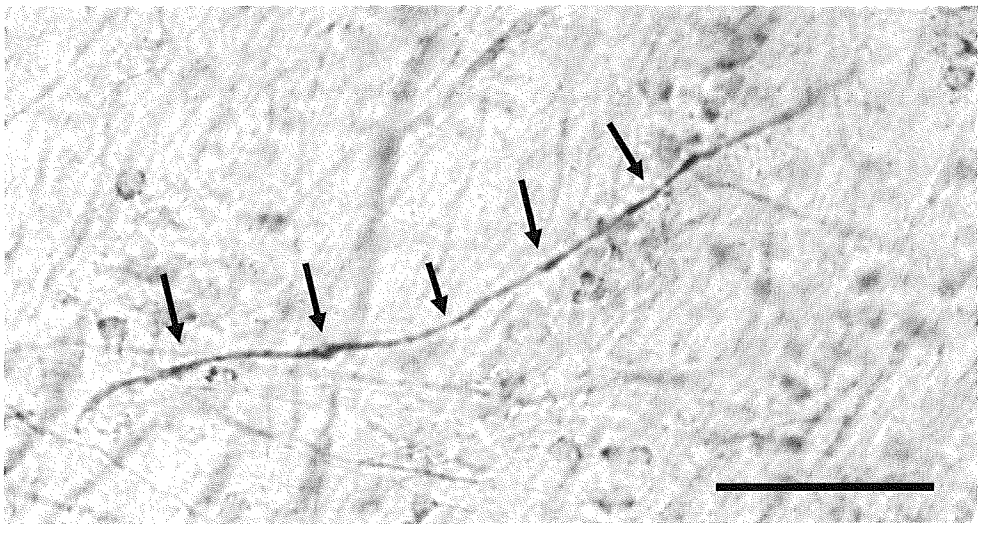

Figure C.1. Positive RM014 stained tissue from coronal section of corona radiata from LF19. The injured axon is highlighted by the black arrows. Black scale line = 50 μm.

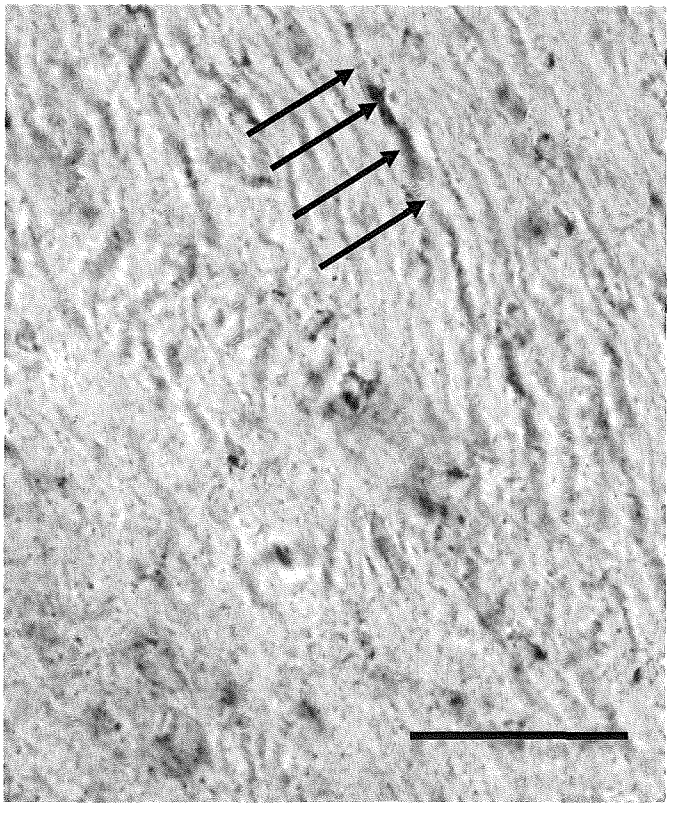

Figure C.2. Positive RM014 stained tissue at the interface between the grey and white matter in LF13. The injured axon is highlighted by the black arrows. Black scale line = 50 μm.

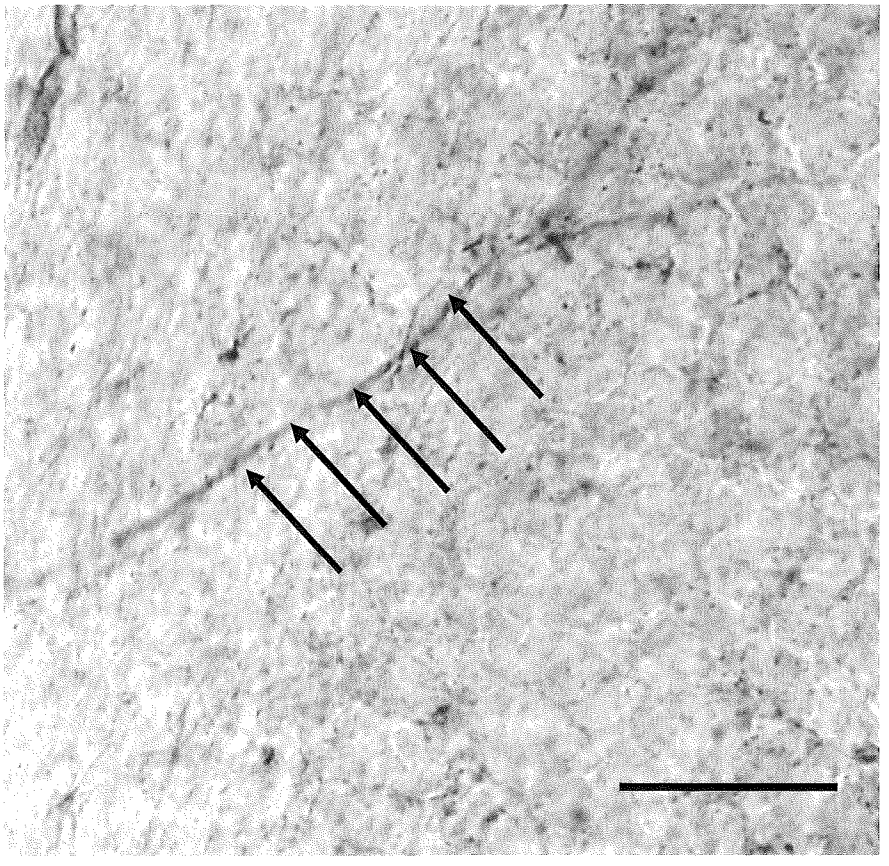

Figure C.3. Positive RM014 stained tissue from coronal section of the cerebellum from LF30. The injured axon is highlighted by the black arrows. Black scale line = 50 μm.

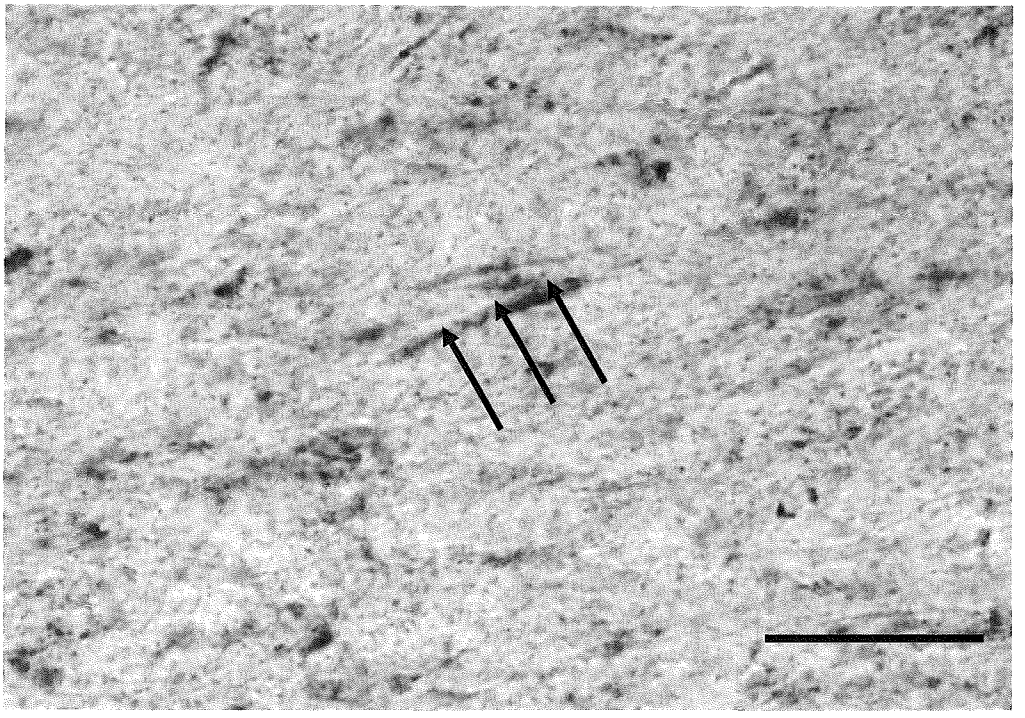

Figure C.4. Positive RM014 stained tissue from coronal section of the spinothalamic tract from LF30. The injured axon is highlighted by the black arrows. Black scale line = 50 μm.

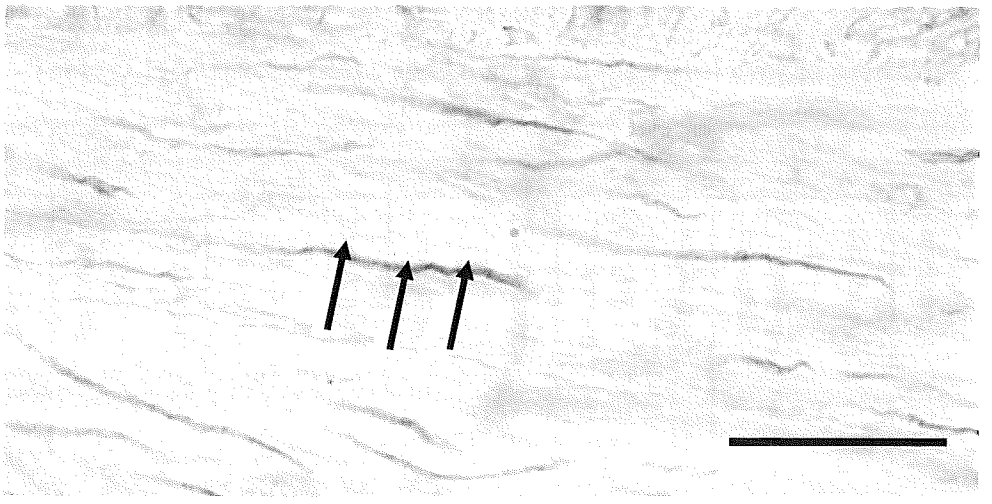

Figure C.5. Positive RM014 stained tissue from coronal section of the corticospinal tract from LF30. The injured axon is highlighted by the black arrows. Black scale line = 50 μm.

APPENDIX D. EP Data

Table D.1: Measured peaks and latencies of the visual evoked potentials.

		Right Eye						Left Eye					
		P1		N		P2		P1		N		P2	
Test #	Time Point	Amplitude (μV)	Latency (ms)	Amplitude (μV)	Latency (ms)	Amplitude (μV)	Latency (ms)	Amplitude (μV)	Latency (ms)	Amplitude (μV)	Latency (ms)	Amplitude (μV)	Latency (ms)
LF19	Pre	-52	20	-13160	61	6081	118	811	19	-9058	49	820	99
	Post 1 Hr	-1462	40	NA	114	-1333	213	-3916	41	NA	110	1	124
	Post 4 Hr	808	23	-4639	58	361	112	127	21	-4622	131	1200	284
LF21	Pre	183	26	-5869	55	2168	96	2042	37	-7361	63	1651	116
	Post 1 Hr	Died Post Blast											
	Post 4 Hr												
LF22	Pre	4960	21	-13610	57	4457	106	7551	30	-16270	50	4088	103
	Post 1 Hr	Died Post Blast											
	Post 4 Hr												
LF23	Pre	1634	26	-12140	62	1550	114	7220	22	NA	44	4849	108
	Post 1 Hr	Died Post Blast											
	Post 4 Hr												
LF24	Pre	5907	27	NA	66	1747	107	Atypical Morphology					
	Post 1 Hr	-378	28	NA	70	369	131	-321	36	-4846	56	374	81
	Post 4 Hr	763	29	-11380	52	2453	102	2578	31	-13280	57	6110	106
LF25	Pre	821	22	-5650	80	2481	125	765	24	-6839	57	2599	121
	Post 1 Hr	Atypical Morphology						Atypical Morphology					
	Post 4 Hr	902	60	-834	80	442	100	6	63	-1093	79	-245	91
LF26	Pre	-1226	52	-6623	91	27	146	Atypical Morphology					
	Post 1 Hr	4159	64	NA	111	4495	201	3084	50	-4037	83	4298	131
	Post 4 Hr	1585	32	NA	77	1502	125	269	31	NA	75	1426	115
LF28	Pre	726	36	-12830	65	8278	133	-477	32	-12060	66	6745	129
	Post 1 Hr	246	20	-1472	35	1595	65	1226	21	-604	36	3326	78
	Post	-73	17	NA	41	1545	74	188	26	NA	50	1929	77

	4 Hr												
LF29	Pre	406	19	-12980	61	3613	120	-1088	30	-14900	60	5345	144
	Post 1 Hr	279	23	-11750	62	1574	122	1617	31	-8213	58	1410	129
	Post 4 Hr	640	27	-9921	51	224	114	2468	30	-9476	52	42	112
LF30	Pre	1581	25	-10390	59	538	124	4300	26	NA	49	4109	96
	Post 1 Hr	1994	25	NA	56	-461	92	1447	29	-8944	47	-916	90
	Post 4 Hr	1990	31	NA	55	0	101	1742	30	NA	66	1171	132
LF31	Pre	815	14	-5396	56	2047	110	1256	22	-9181	58	1426	110
	Post 1 Hr	Died Post Blast											
	Post 4 Hr												
LF32	Pre	-1331	35	-6599	48	-1809	74	-1499	44	-4759	54	-1313	94
	Post 1 Hr	2264	33	NA	48	3279	88	498	24	-8346	44	3124	93
	Post 4 Hr	728	33	NA	49	-71	107	-709	26	-10360	44	1615	84
LF33	Pre	413	24	-13050	70	1241	148	-632	34	-12390	74	-486	156
	Post 1 Hr	-87	36	-11350	73	1875	150	-301	29	-11520	68	251	142
	Post 4 Hr	-944	32	-6750	47	-1483	64	-765	31	-8449	46	-982	62
LF34	Pre	Atypical Morphology						397	54	-8884	100	-483	159
	Post 1 Hr	-276	30	-5960	62	-114	137	1139	31	-8616	76	1333	130
	Post 4 Hr	3338	31	-2833	74	8982	174	4274	28	-3377	88	8347	180
LF35 *	Pre	325	28	-10470	73	-1608	108	1384	25	-10310	56	385	128
	Post 1 Hr	-485	22	-4883	72	0	144	-119	23	-9172	69	104	158
	Post 4 Hr	-1972	40	NA	76	433	131	-1280	32	NA	69	1292	140
LF36	Pre	163	30	NA	63	1109	97	692	41	NA	78	5107	133
	Post 1 Hr	-997	29	-6002	61	-2816	101	-156	32	-7444	70	-2703	119
	Post 4 Hr	681	26	NA	60	9	99	406	27	-8189	55	3366	101
LF37	Pre	332	25	NA	50	4072	128	86	29	NA	56	3489	131
	Post 1 Hr	724	24	NA	52	1693	107	722	22	NA	61	2672	114
	Post 4 Hr	2473	22	NA	80	796	138	786	29	-8168	61	1953	139
LF38	Pre	1229	25	-4971	39	1667	80	-561	39	-7699	72	436	114
	Post 1 Hr	575	27	-3764	39	695	76	646	24	NA	57	4191	105
	Post	No Signal						No Signal					

	4 Hr												
LF39	Pre	-149	32	-8700	72	-2348	117	-17	33	-9710	76	-1184	121
	Post 1 Hr	2182	34	-9169	70	1484	113	501	42	NA	96	1731	190
	Post 4 Hr	684	33	-7102	65	-364	110	-357	39	-7650	75	798	118
LF40	Pre	1063	23	-5820	63	2064	106	3136	24	-2460	42	4443	71
	Post 1 Hr	509	21	-14070	62	1812	117	691	30	-13710	58	3009	118
	Post 4 Hr	433	35	-9191	73	-664	115	1217	23	-8663	64	2022	109
LF41	Pre	Atypical Morphology						Atypical Morphology					
	Post 1 Hr	-365	28	-10270	68	364	130	-835	30	NA	54	317	94
	Post 4 Hr	-523	38	-10100	56	540	112	413	22	-10770	58	-1106	126
LF42	Pre	-273	38	-10100	64	4686	119	-47	36	-10080	61	-270	104
	Post 1 Hr	48	29	-9280	60	1400	108	1094	29	-4453	64	1513	104
	Post 4 Hr	-1323	28	-10930	57	-434	102	-1563	29	-11000	58	-1193	110
LF43	Pre	-220	34	-6155	84	3477	144	208	31	-8313	71	6232	144
	Post 1 Hr	-1969	59	-6618	90	-164	133	1519	80	-2472	106	238	145
	Post 4 Hr	90	45	NA	74	3333	120	925	39	-4078	73	435	102
LF44	Pre	-1089	30	-5563	66	-2461	102	-890	33	-8881	62	-2272	110
	Post 1 Hr	-2064	23	NA	104	5204	240	-240	45	-4423	128	1168	219
	Post 4 Hr	398	20	-6009	53	326	113	-993	23	-7916	57	303	109
LF45	Pre	-1055	27	-6652	55	1288	81	-691	34	-7092	53	942	90
	Post 1 Hr	-26	24	-3596	53	2442	96	1728	34	-3237	58	1326	100
	Post 4 Hr	Atypical Morphology						Atypical Morphology					
LF46	Pre	659	21	-6297	51	647	88	-624	25	-5641	57	1352	99
	Post 1 Hr	2834	38	NA	109	-63	232	2658	41	NA	112	-568	268
	Post 4 Hr	-833	24	-8565	72	92	107	1331	42	-5254	61	1078	97
LF47	Pre	-1317	31	NA	52	1629	80	Atypical Morphology					
	Post 1 Hr	511	28	NA	59	3314	98	1314	23	NA	48	1333	85
	Post 4 Hr	Atypical Morphology						Atypical Morphology					
LF48	Pre	273	24	-1040	62	954	132	1890	32	NA	58	NA	131
	Post 1 Hr	2945	36	NA	62	1736	143	1322	25	-8516	44	3190	90
	Post 4 Hr	1164	21	-17500	41	-4889	88	-1511	27	-16570	45	-2454	122

LF49	Pre	1010	25	-4176	52	2782	93	1544	24	-7720	46	2979	92
	Post 1 Hr	512	25	-12410	52	-593	98	1556	23	-9771	46	-19	97
	Post 4 Hr	-877	33	NA	69	-2039	113	1414	37	-10410	56	-1279	106
LF50	Pre	3399	28	NA	50	1790	81	42	34	-13770	72	-448	130
	Post 1 Hr	83	29	NA	66	-938	157	2420	30	-8906	68	-2197	115
	Post 4 Hr	-1222	38	NA	94	568	183	0	28	-8717	52	-243	115
LF51	Pre	1585	27	-6679	52	782	76	2388	20	-2380	52	3268	119
	Post 1 Hr	-612	24	-10670	64	504	127	-533	23	-8927	63	206	130
	Post 4 Hr	1006	22	-12560	55	1095	110	1861	20	-9909	59	2377	120
LF52	Pre	-379	24	-4539	53	-256	93	-68	28	-5971	43	2730	96
	Post 1 Hr	334	25	-3632	51	1226	92	1555	29	-2277	55	4723	91
	Post 4 Hr	491	28	NA	67	579	100	770	28	NA	55	2795	104
LF53	Pre	-2087	34	-7441	59	1254	118	-999	30	-8651	60	1489	124
	Post 1 Hr	808	38	-7473	59	2657	117	802	38	-7039	59	1115	124
	Post 4 Hr	657	37	-6109	63	2870	115	433	40	-5688	72	1788	122
LF55	Pre	1298	20	-7230	54	5931	124	1986	19	-8827	58	6498	126
	Post 1 Hr	-5	22	-8110	58	1772	119	980	21	-7747	64	386	123
	Post 4 Hr	968	23	-8718	53	2266	126	314	25	-10500	60	2988	120
LF56	Pre	-1059	26	-6126	53	-807	86	-75	24	-7485	53	-565	106
	Post 1 Hr	1825	24	-6796	44	58	90	1060	25	-7336	56	957	124
	Post 4 Hr	929	26	-4758	51	-402	84	782	30	-6998	54	1587	122
LF57	Pre	308	22	-5417	57	-373	102	220	26	-4733	58	49	107
	Post 1 Hr	457	31	-5829	49	-686	99	973	22	-6397	49	589	88
	Post 4 Hr	465	23	-7375	47	1056	100	-6	23	-7308	43	1336	96
LF58	Pre	-964	30	-7024	67	1040	134	909	32	-7208	68	425	126
	Post 1 Hr	896	32	-11380	63	8277	165	-1490	38	NA	111	272	206
	Post 4 Hr	344	29	-11170	65	3136	119	-84	34	-11630	66	-973	120
LF59	Pre	-1467	24	-4915	62	3254	124	-1335	29	-8844	64	1084	118
	Post 1 Hr	748	67	NA	126	5060	258	-1144	54	NA	140	2971	27
	Post 4 Hr	-201	30	-6264	68	-521	168	1800	25	-5064	59	1520	118
LF60	Pre	697	26	-4013	61	284	111	-601	38	-2267	84	-431	128

	Post 1 Hr	Atypical Morphology						1015	37	-2902	66	1066	115
	Post 4 Hr	-141	32	-3984	61	-405	114	654	49	-3341	79	-417	127
LF61	Pre	-135	23	-5458	54	486	131	34	22	-7657	46	-863	77
	Post 1 Hr	77	36	-3091	54	68	87	-145	27	-6125	44	-222	78
	Post 4 Hr	-116	28	-4552	46	547	105	-384	41	-3233	74	-1147	108
LF62	Pre	-533	27	-4723	60	1178	96	-1015	26	-8180	58	-1029	105
	Post 1 Hr	869	34	-4958	60	782	92	-1385	28	-6337	45	-142	82
	Post 4 Hr	164	31	-5059	60	-71	105	1096	32	-7345	58	3809	124
LF63	Pre	-323	30	-6634	58	-133	110	-1237	26	-5422	62	-134	124
	Post 1 Hr	Atypical Morphology						Atypical Morphology					
	Post 4 Hr	Atypical Morphology						Atypical Morphology					
LF64	Pre	-81	22	-8359	47	1021	113	-500	22	-9799	47	-1158	102
	Post 1 Hr	-1200	28	-6760	54	955	113	-526	26	-6493	53	499	116
	Post 4 Hr	-18	29	-7592	42	-391	92	885	26	-9603	39	-2647	80
LF65	Pre	819	18	-12980	50	1124	101	960	18	-13520	49	2402	102
	Post 1 Hr	821	21	NA	80	2384	127	-1229	27	-14780	60	5934	157
	Post 4 Hr	673	20	-11310	59	3127	104	-3414	34	-12530	51	3511	104
LF66	Pre	372	20	-7546	61	2800	99	-148	22	-7245	53	1835	100
	Post 1 Hr	-22	36	-3897	62	1980	108	821	45	-3201	78	3149	142
	Post 4 Hr	291	31	-3578	67	2413	112	1038	32	-5186	61	4138	109
LF67	Pre	814	19	-6458	56	771	104	-466	22	-8092	59	-336	107
	Post 1 Hr	324	26	-3875	63	-63	114	-524	24	-3962	62	-359	115
	Post 4 Hr	-48	28	-3848	45	339	112	-457	28	-4417	52	-1904	98
LF68	Pre	-868	21	-12730	55	1366	130	-1315	22	-11990	58	-1965	109
	Post 1 Hr	-1442	30	-4431	54	1862	102	438	24	-4763	56	1841	104
	Post 4 Hr	-947	27	-4362	63	-1183	102	-1426	32	-6368	60	1008	113
LF69	Pre	-1544	35	-5488	68	753	108	-1642	32	-6391	69	1331	120
	Post 1 Hr	-876	40	-5348	66	2380	129	-1	22	-2559	51	2732	105
	Post 4 Hr	No Signal						No Signal					
LF70 *	Pre	-1335	24	-7158	66	164	112	729	21	-6492	65	-815	102

	Post 1 Hr	No Signal						No Signal					
	Post 4 Hr	No Signal						No Signal					
		Controls											
LF20	Pre	2985	47	-2020	108	2387	183	5180	44	-4792	77	1253	170
	Post 1 Hr	707	51	NA	108	-1126	188	3080	52	-1818	105	243	182
	Post 4 Hr	540	52	NA	83	-1144	114	-2030	41	NA	62	-454	104
LF54	Pre	-720	22	10580	63	-192	104	-785	22	-8962	64	323	121
	Post 1 Hr	-1072	27	-8092	60	475	108	-1403	26	-7663	59	-766	106
	Post 4 Hr	669	26	-9958	60	673	105	-1004	24	-8564	57	-756	117

Table D.2: Measured peaks and latencies of the brainstem auditory evoked potentials from the left ear.

		I		II		III		IV		V	
Test #	**Time Point**	**Amplitude (μV)**	**Latency (μs)**	**Amplitude (μV)**	**Latency (μs)**	**Amplitude (μV)**	**Latency (μs)**	**Amplitude (μV)**	**Latency (μs)**	**Amplitude (μV)**	**Latency (μs)**
LF19	Pre	1111	1901	1378	2701	-34.2	3301	197.5	4551	452.5	5651
	Post 1 Hr	517	2101	750.3	3001	-73.8	3901	-4.3	4951	173.6	5901
	Post 4 Hr	349.9	2151	765	3001	176.9	3651	136.7	4951	330.9	6101
LF21	Pre	2939	1851	2191	2701	-763.9	3601	342.9	4651	770.4	5801
	Post 1 Hr	Died Post Blast									
	Post 4 Hr										
LF22	Pre	2102	2051	2287	2901	-548	3601	238.7	4701	355.9	5851
	Post 1 Hr	Died Post Blast									
	Post 4 Hr										
LF23	Pre	1807	1851	1287	2651		3301	121.5	4401	552.3	5301
	Post 1 Hr	Died Post Blast									
	Post 4 Hr										
LF24	Pre	1390	1851	1442	2751	-292.4	3551	566.4	4701	613.6	5801
	Post 1 Hr	No Signal									
	Post	No Signal									

	4 Hr										
LF25	Pre	1292	1951	593.5	2951		3901	310.9	5151	584.9	6201
	Post 1 Hr	No Signal									
	Post 4 Hr	No Signal									
LF26	Pre	3370	1901	1939	2701	-1056	3601	244.1	4651	820.9	5551
	Post 1 Hr	282.7	2201	279.9	3101	169.3	3601	Missing Waveform		Missing Waveform	
	Post 4 Hr	327.7	2151		3251	-251.7	4051		5051	173.1	6151
LF28	Pre	3538	1901	1733	2751	-34.7	4651	408.5	4651	734.1	5751
	Post 1 Hr	No Signal									
	Post 4 Hr	No Signal									
LF29	Pre	4304	1851	2730	2601	-966.8	3351		4201	587.6	5351
	Post 1 Hr	2445	1851	1823	2601	-91.7	3501	221.9	4301	517	5601
	Post 4 Hr	1608	2101	1607	2851		3701	523	4601		5651
LF30	Pre	1346	1901	1198	2751	-104.7	3601	60.8	4551	559.4	5851
	Post 1 Hr	928.3	2201	1068	3001	-74.9	3651	460.1	4801		6051
	Post 4 Hr		2101	754.1	2901	-328.8	3751	189.3	5151	699.9	6151
LF31	Pre	2442	1851	1827	2651	-555.6	3351	402	4451	587.6	5601
	Post 1 Hr	Died Post Blast									
	Post 4 Hr										
LF32	Pre	353.2	2201	437.8	3101	-401.5	4101		4901	224.6	5951
	Post 1 Hr	217	2251	371.1	3101	-223	4051	-5.4	4951	160.6	6001
	Post 4 Hr	No Signal									
LF33	Pre	2586	1851	1650	2701	-727.5	3351	468.8	4551	693.4	5701
	Post 1 Hr	1248	1951	1102	2901	-486.1	3601	129.7	4901		6251
	Post 4 Hr	367.8	2301	401.5	3401	-202.4	4201	75.4	5501	261	7051
LF34	Pre	268.2	1801	2193	2601	-39.6	3551	545.2	4401	671.7	5501
	Post 1 Hr	1153	1851	1157	2601		3351	402	4401		5501
	Post 4 Hr	474.2	1951	760.6	2801	-74.9	3851	50.5	4851	168.7	6451
LF35*	Pre	1839	1901	980.9	2801	-578.3	3801	262.6	4751		5901
	Post 1 Hr	No Signal									
	Post 4 Hr	No Signal									

LF36	Pre	1664	1851	949.4	2701	41.8	3301	378.1	4751	512.2	5801
	Post 1 Hr	967.3	1901	1052	2701	-261	3851	244.1	4751	347.2	6151
	Post 4 Hr	No Signal									
LF37	Pre	3634	1851	1225	2701	-1165	3651		4601	770.9	5651
	Post 1 Hr	453	2251	296.8	3051	Missing Waveform		Missing Waveform		Missing Waveform	
	Post 4 Hr	253.4	2251	204	3101	-170.4	3901	-73.8	5051	239.8	5951
LF38	Pre	2897	1901	2088	2701	-120.4	3351	269.1	4601	665.7	5601
	Post 1 Hr	No Signal									
	Post 4 Hr	No Signal									
LF39	Pre	3228	1851	1096	2651	-823.6	3551	43.4	4651	717.8	5701
	Post 1 Hr	1056	1901	793.2	2701	-435.7	3351	118.8	4701	339.6	5751
	Post 4 Hr	865.4	1901	679.3	2651		3351		4451	315.8	5651
LF40	Pre	3544	1851	1812	2701		3451	609.3	4601	640.2	5601
	Post 1 Hr	1737	1851	1240	2651	-67.3	3551		4401	450.3	5501
	Post 4 Hr	1769	1851	1286	2601		3351	361.3	4451	586	5401
LF41	Pre	2419	1851	1321	2701		3401	548	4701		5901
	Post 1 Hr	286.5	2201		2951	-183.4	3701	111.8	4751		5851
	Post 4 Hr	808.9	2151	-296.2	2951	-332.6	4751	207.8	4751		5751
LF42	Pre	289.2	2251	330.4	3051		3751		4701	143.8	5901
	Post 1 Hr	81.9	2451	112.3	3251	-57.5	4751	Missing Waveform		Missing Waveform	
	Post 4 Hr	35.81	2551		3251	Missing Waveform		Missing Waveform		Missing Waveform	
LF43	Pre	2091	1851	1371	2651	-435.1	3251	209.4	4351	438.9	5501
	Post 1 Hr	712.9	1901	696.1	2801	-103.6	3801	154.1	5151		6001
	Post 4 Hr	298.9	1901	70.5	2701		3651		4951	225.7	5601
LF44	Pre	1411	2101	1064	2901		3751	281.6	4601	323.9	5551
	Post 1 Hr	914.2	2101	866.4	2851		3651	97.7	4501	210.5	5401
	Post 4 Hr	646.2	2051	553.4	2751	-352.1	3551	189.9	4401	273.4	5351
LF45	Pre	2218	1801	1841	2551	-539.3	3501		4301	485.6	5351
	Post 1 Hr	2046	1851	1020	2551	-692.8	3601	-30.9	4101	423.7	5451
	Post 4 Hr	1463	1801	1510	2601	187.7	3251		4301		5401
LF46	Pre	2394	1851	1340	2651	-1018	3551	246.9	4501	542.5	5451

	Post 1 Hr	491.5	2201		3201		4101	3.8	5151	161.1	6351
	Post 4 Hr	229.5	2201	334.9	3201		3951	78.5	4901	168.9	6101
LF47	Pre	2150	1851	1152	2701	-894.6	3451	362.4	4501	534.4	5451
	Post 1 Hr	2940	1901	1603	2801	-766.6	3551	421.6	4651	576.7	5901
	Post 4 Hr	4270	1851	1465	3601	-1132	3501	256.1	4451	683.6	5651
LF48	Pre	3105	1851	2725	2601	-188.8	3551	315.8	4451	701.5	5451
	Post 1 Hr	267.8	1951		3001	-206.7	3851	117.2	4601	169.8	6201
	Post 4 Hr	No Signal									
LF49	Pre	2312	1851	2490	2751	-372.2	3701	344.5	4351		5501
	Post 1 Hr	1225	1901	1452	2801	-234.4	3801	124.8	4751	299.5	6001
	Post 4 Hr	1076	1851	1704	2651		3401	189.3	4301	234.4	5701
LF50	Pre	1529	1851	835	2601	-484.5	3451	270.7	4451	587	5401
	Post 1 Hr		1751		2951	-118.8	3501	68.4	4201	236	5501
	Post 4 Hr	97.1	4201	99.3	5351	Missing Waveform		Missing Waveform		Missing Waveform	
LF51	Pre	2225	1851	892.5	2651	-344.5	3501	164.9	4501	449.1	5551
	Post 1 Hr	1410	1851	712.9	2651	-124.8	3551	-56.4	4601	198	5601
	Post 4 Hr	1271	1801	1044	2551		3401	86.8	4051		5001
LF52	Pre	1817	1901	1623	2701	-654.8	3601	232.7	4551	437.8	5551
	Post 1 Hr	309.2	2001	175.2	2901	26.6	3951	Missing Waveform		Missing Waveform	
	Post 4 Hr	484.5	1901	329.9	2751		4151	391.2	5651	166.6	6501
LF53	Pre	1748	1851	1113	2651	-94.4	3551	404.7	4401		5601
	Post 1 Hr	122.6	2151	130.2	3201	-25	4651	97.1	5851	112.3	6651
	Post 4 Hr	196.4	2101	59.7	3051	-72.2	4001	114.5	5701	169.3	6351
LF55	Pre	1135	1851	841.5	2751	-410.7	3701	256.6	4601		5851
	Post 1 Hr	2580	1851	1481	2651	-427	3151	285.9	4201	285.4	5351
	Post 4 Hr	1986	1851	1671	2551	-241.4	3551	351	4251	307.1	5401
LF56	Pre	1735	1851	1315	2651		3401	497	4401	409.1	5501
	Post 1 Hr	1072	1901	1048	2701	-245.8	3351	77	4401	322.8	5751
	Post 4 Hr	740.6	1851	792.1	2651	-205.6	3501	170.4	4451	290.8	5651
LF57	Pre	3438	1851	2022	2601	-377.6	3451	473.6	4151	345.6	5301
	Post	113.9	3101	131.8	3851	Missing		Missing		Missing	

	1 Hr					Waveform		Waveform		Waveform	
	Post 4 Hr	No Signal									
LF58	Pre	2788	1801	1789	2501		3201	330.9	4151	445.4	5301
	Post 1 Hr	1151	2051	583.8	2751	-510	3701	14.1	4451		5751
	Post 4 Hr	1206	2001	593	2701	-310.9	3451	106.3	4301	332.6	5251
LF59	Pre	1581	1851	1451	2651	93.9	3051	251.2	4451		5851
	Post 1 Hr	394.4	1901	178	2701	-227.9	3551	66.2	4251		5401
	Post 4 Hr	No Signal									
LF60	Pre	2260	1901	1871	2701	-846.9	3651	137.8	4451	520.8	5551
	Post 1 Hr	No Signal									
	Post 4 Hr	No Signal									
LF61	Pre	1936	1851	1366	2651	-422.6	3551		4351	431.9	5401
	Post 1 Hr	703.1	1901	477.4	2701	-154.1	3301	-125.9	4501	217.6	5801
	Post 4 Hr	438.9	1851	395	2651	Missing Waveform		Missing Waveform		Missing Waveform	
LF62	Pre	2668	1851	2109	2651	-147	3601	444.9	4251	582.1	5401
	Post 1 Hr	1288	1901	1319	2651	-109.6	3551	-10.3	4651	336.4	5601
	Post 4 Hr	841.5	1851	619.6	2701		3301		4401		5651
LF63	Pre	1523	1901		2851	-182.3	3951	347.8	4501		5751
	Post 1 Hr	574	1901	269.1	2701	-222.4	3301	-25	4251	178.5	5701
	Post 4 Hr	287.5	2001	264.2	2801	-47.7	4251	39.6	4701		6051
LF64	Pre	504.6	2101	615.8	2951	-249	3501	92.2	4801	282.7	5851
	Post 1 Hr	321.2	2151	262.6	2951	-202.9	6401	44.5	4901		6251
	Post 4 Hr	325	2101	413.4	2851	-131.3	3401	68.9	4551	220.8	5651
LF65	Pre	2674	1851	1651	2601	-900.6	3251	20.1	4201	520.8	5351
	Post 1 Hr	521.9	2301	457.4	2801	-153	3551	86.3	4701	225.2	5601
	Post 4 Hr	544.7	1901	512.7	2751	-249.6	3551	123.7	4501	309.8	5401
LF66	Pre	2183	1851	1335	2651	-633.1	3601	417.8	4201	506.7	5551
	Post 1 Hr	241.4	2451	108.5	3201	-243.6	4351	61.3	5051		5951
	Post 4 Hr	No Signal									
LF67	Pre	1306	2051	1328	2851		3601	239.8	4551	392.8	5701
	Post 1 Hr	342.3	2201	201.8	3001	-316.3	3751		4801		5901

	Post 4 Hr	929.4	2101	918.5	2851	-404.2	3751	156.8	4651	249	5601
LF68	Pre	1702	1851	1496	2751		3451	492.1	4551	537.1	5551
	Post 1 Hr	1025	2801	-341.8	3451	114.5	4951				
	Post 4 Hr	551.2	2101	795.9	2901	20.1	4301	261.5	5501	236	6001
LF69	Pre	2746	1801	1971	2601		3401	524.6	4301	504.6	5501
	Post 1 Hr	No Signal									
	Post 4 Hr	1.628	3301	41.8	4151	17.4	5201	37.4	6501		
LF70*	Pre	2481	1851	1804	2701	-432.9	3651	462.8	4301	431.3	5501
	Post 1 Hr	No Signal									
	Post 4 Hr	No Signal									
Controls											
LF20	Pre	1148	1901	929.9	2751		3651	259.9	4751	422.1	5851
	Post 1 Hr	1570	1901	1495	2751	-607.6	3501	207.2	4701	473.1	5701
	Post 4 Hr										
LF54	Pre	2719	1851	1784	2651		3401	358.1	4301	593.5	5351
	Post 1 Hr	1737	1851	1402	2651		3401	180.7	4451	327.7	5351
	Post 4 Hr	1617	1851	1547	2601		3351		4251	297.9	5201

*Likely eardrum rupture

Table B.3: Measured peaks and latencies of the brainstem auditory evoked potentials from the right ear.

		I		II		III		IV		V	
Test #	**Time Point**	**Amplitude (μV)**	**Latency (μs)**	**Amplitude (μV)**	**Latency (μs)**	**Amplitude (μV)**	**Latency (μs)**	**Amplitude (μV)**	**Latency (μs)**	**Amplitude (μV)**	**Latency (μs)**
LF19	Pre	1653	1901	1150	2701	-287	3551	227.9	4551	357.5	5801
	Post 1 Hr	370.6	2151	900.1	3001	200.2	3701	68.2	4951	349.4	6001
	Post 4 Hr	No Signal									
LF21	Pre	2067	1901	1819	2701	-187.7	3301	233.3	4601	825.2	5751
	Post 1 Hr	Died Post Blast									
	Post 4 Hr										
LF22	Pre	2349	1901	1150	2751	-339.1	3301	73.8	4701	678.7	5751

	Post 1 Hr	Died Post Blast									
	Post 4 Hr										
LF23	Pre	1177	2051	681.4	2851	-283.2	3501	196.4	4551	377.1	5651
	Post 1 Hr	Died Post Blast									
	Post 4 Hr										
LF24	Pre	1941	1851	1553	2751	-221.9	3551	370	4651	625.5	5751
	Post 1 Hr	429.7	2351	326.6	3451	-131.3	4301	174.2	5801	290.8	7001
	Post 4 Hr	532.8	2751	379.2	3701	326.1	4651	Missing Waveform		Missing Waveform	
LF25	Pre	2918	1901	1748	2851		3751		4751	724.8	5951
	Post 1 Hr	No Signal									
	Post 4 Hr	No Signal									
LF26	Pre	654.3	2151	601.7	3101	-358.6	3851	155.2	5151	367.3	6201
	Post 1 Hr	749.8	2851	Missing Waveform		Missing Waveform		Missing Waveform		Missing Waveform	
	Post 4 Hr	661.4	2001	907.6	2901	-271.8	3801	-149	4801	183.9	5951
LF28	Pre	3053	1901	1636	2751		3401	219.2	4351	558.8	5701
	Post 1 Hr	No Signal									
	Post 4 Hr	No Signal									
LF29	Pre	3146	1851	2236	2601	-487.7	3451	281.6	4351	673.8	5401
	Post 1 Hr	2491	1851	1776	2601		3401		4301		5451
	Post 4 Hr	1672	2201	1592	3001	-642.4	3851	29.3	4701		6201
LF30	Pre	1380	1901	1406	2751	134	3601	341.3	4601	678.7	5851
	Post 1 Hr	665.7	2251		3051	-22.8	3651	124.8	5151	331.5	5901
	Post 4 Hr	817.6	2251	162.2	2951	-544.7	4151	296.2	5851	361.3	7051
LF31	Pre	1851	1851	1676	2651	-460.1	3501	174.2	4401	521.4	5551
	Post 1 Hr	Died Post Blast									
	Post 4 Hr										
LF32	Pre	354.8	2201	422.1	3101		3951	61.3	4951	196.9	5901
	Post 1 Hr	576.2	2101	707.5	3001	-429.7	3651	89	4851	243.6	5851
	Post 4 Hr	261	2301	410.7	3151	-108	3851	-66.7	4951	148.7	5951
LF33	Pre	2461	1851	1845	2701	-449.8	3551	593	4551	712.9	5601
	Post	228.9	2301	187.7	3251	-55.3	3901		5101		6451

	1 Hr										
	Post 4 Hr	No Signal									
LF34	Pre	2225	1851	1843	2651	-183.4	3501	398.8	4251	578.9	5551
	Post 1 Hr	1428	1851	1030	2601		3451	207.8	4201	286.6	5001
	Post 4 Hr	1553	1951	1466	2801	-497	3401	173.1	4951	279.9	6051
LF35*	Pre	2023	1901	1624	2751	-442.2	3501	293	4501	685.8	5901
	Post 1 Hr	No Signal									
	Post 4 Hr	No Signal									
LF36	Pre	1638	1901	876.7	2701	-5.4	3251		4401	437.3	5751
	Post 1 Hr	581.6	2201	423.2	3101	-204.5	3751	65.7	5201		6351
	Post 4 Hr	510	2201	620.1	3151		4051	60.2	5001	187.2	6351
LF37	Pre	1664	1851	1079	2701	-515.4	3401	237.6	4651	588.1	5751
	Post 1 Hr	475.3	2351	556.6	3151	-308.7	3951	57	5151		6151
	Post 4 Hr	314.1	2351	231.1	3301		4401	40.2	5351		6251
LF38	Pre	2278	1901	2205	2701		3601	341.8	4651		6001
	Post 1 Hr	No Signal									
	Post 4 Hr	No Signal									
LF39	Pre	2608	1851	1323	2651	-673.8	3601	202.9	4601	714	5701
	Post 1 Hr	1173	1901	1071	2701		3751	138.3	4651	336.4	5701
	Post 4 Hr	846.9	1851	1312	2651	-313	3601	263.7	4401		5601
LF40	Pre	1917	1901	1340	2701	-827.9	3601	256.1	4651	627.2	5651
	Post 1 Hr	223	2151	87.9	3051	-103.6	3901		4901	87.4	6301
	Post 4 Hr	607.6	2101	513.8	2951	-204	3901		4701	149.2	5751
LF41	Pre	1670	1851	1466	2701	-518.7	3501	200.2	4451	488.8	5601
	Post 1 Hr	164.9	2101	141.6	3001	20.6	4501		5751	Missing Waveform	
	Post 4 Hr	No Signal									
LF42	Pre	148.7	2251	315.2	3001	-8.1	3751	9.2	4751	90.1	6001
	Post 1 Hr	71.6	2551	71.6	3401				5151	45	6001
	Post 4 Hr	No Signal									
LF43	Pre	2928	1851	1093	2651	-833.9	3551	267.5	4501	530.1	5601
	Post 1 Hr	No Signal									

	Post 4 Hr	No Signal									
LF44	Pre	1421	2101	1106	2851	-510.5	3501	325	4451		5301
	Post 1 Hr	843.1	2101	938	2851	-206.7	3451	144.9	4401		4601
	Post 4 Hr	827.9	2251	853.4	2951		3651	345.6	4501	102.5	5701
LF45	Pre	2042	1801	1578	2551	-447	3401		4251	488.3	5301
	Post 1 Hr	595.7	2101	595.2	2901	-211	3451	-42.3	4751	215.4	5701
	Post 4 Hr	953.2	2101	760.1	2901	-415	3801	87.4	4801	223	5701
LF46	Pre	2389	1851	1389	2651	-712.9	3551	384.1	4501	512.7	5501
	Post 1 Hr	287.5	2251	256.6	3201	-299.5	3901	-11.4	5151	141.6	6251
	Post 4 Hr	255	2251	188.3	3151	-257.7	4101	-20.1	5201	143.2	6201
LF47	Pre	1750	1851	636.4	2701	-974.9	3451	199.7	4401	545.8	5551
	Post 1 Hr	788.8	2351	262	3351	76	4901	313	6101	Missing Waveform	
	Post 4 Hr		2101		2901	-573.5	3651	255.5	4601		5851
LF48	Pre	2624	1851	2003	2651		3401		4301	542	5501
	Post 1 Hr	319.6	2301	334.2	3201				5001	161.7	6151
	Post 4 Hr		2251	80.3	3301		4101	94.4	4951		6301
LF49	Pre	2465	1851	2339	2701		3501	409.1	4351		5601
	Post 1 Hr	1431	1951	1272	2801		3551		4651	276.7	6001
	Post 4 Hr	1138	1901	1470	2701	-269.6	3601	170.4	4451		5401
LF50	Pre	1356	1851	602.8	2651	-796.4	3501	262	4501	456.8	5401
	Post 1 Hr	131.8	2101	81.9	3001			10.9	4901	76	5951
	Post 4 Hr	435.7	2251	391.7	3051	-195.3	3601	91.1	4851		6151
LF51	Pre	1985	1851	890.8	2651		3501	62.9	4501	472	5551
	Post 1 Hr	647.2	2101	317.4	2951	-119.9	3651		4851		6151
	Post 4 Hr		2101		2851	Missing Waveform		Missing Waveform		Missing Waveform	
LF52	Pre	2352	1851	1833	2701		3451	335.3	4501	501.8	5451
	Post 1 Hr	572.4	2201	619.6	3051	-251.7	3651	-90.1	4851	269.6	5901
	Post 4 Hr	403.6	2201	480.1	3001	-114.5	3851	27.7	4701		5901
LF53	Pre	1291	2101	1360	2901	-457.9	3951	247.4	4701	301.7	5851
	Post 1 Hr	333.7	2251	462.2	3151	-311.4	4251	8.7	5101	178.5	5951
	Post	542	1901	Missing		Missing		Missing		Missing	

	4 Hr			Waveform		Waveform		Waveform		Waveform	
LF55	Pre	1062	1901	827.4	2751	-685.8	3601	275.6	4601		5701
	Post 1 Hr	902.8	2101	1126	2951	-488.8	3901	126.4	4751	402	5801
	Post 4 Hr	1190	2101	998.8	2901	-567	3901	193.1	4701	411.8	5651
LF56	Pre	1521	1851	1077	2651		3351	432.4	4401	353.7	5501
	Post 1 Hr	68.9	2301	207.2	3051	Missing Waveform		Missing Waveform		Missing Waveform	
	Post 4 Hr	62.4	2251	71.6	3001	15.7	3651	16.8	4901	69.4	6201
LF57	Pre	1259	1851	1591	2651	-143.2	3451	513.2	4301	418.3	5251
	Post 1 Hr	187.7	2351	193.1	3151	-213.8	3901	54.3	4901	129.7	5901
	Post 4 Hr	223.5	2201	311.4	3001	-259.3	3751	-0.54	4601	202.9	5751
LF58	Pre	2311	1801	1016	2551		3301	448.1	4101	515.9	5301
	Post 1 Hr	653.2	2151	540.4	2701	-203.5	3501	-15.2	4501	249.6	5601
	Post 4 Hr	585.4	2101	770.4	2651	-145.4	3401	60.2	4451		5601
LF59	Pre	2604	1801	2051	2601		3501	395.5	4351	754.1	5401
	Post 1 Hr	1496	1851	1675	2651		3401	308.2	4301	357	5501
	Post 4 Hr	1188	1851	1453	2601		3401	237.6	4201	251.7	5351
LF60	Pre	1142	1901	1200	2751	-609.8	3601	315.8	4401	416.7	5701
	Post 1 Hr	502.4	2051	541.4	2901	-109	3451	38.5	5001	127.5	5951
	Post 4 Hr	115.6	3451	Missing Waveform		Missing Waveform		Missing Waveform		Missing Waveform	
LF61	Pre	280.5	2201	283.2	3051		3851	25.2	4901	124.8	6001
	Post 1 Hr		2551	80.3	3401		4851		6001	Missing Waveform	
	Post 4 Hr	50.5	2401	92.8	3201	Missing Waveform		Missing Waveform		Missing Waveform	
LF62	Pre	991.2	2001	817.1	2751	-450.3	3451	256.1	4551	441.6	5601
	Post 1 Hr	83	2301	135.1	3251		4951	Missing Waveform		Missing Waveform	
	Post 4 Hr	131.8	2301	128	3101	-134	3851	0	4701	72.2	6151
LF63	Pre	2343	1851	1007	2601	-590.8	3551	167.6	4501	624.5	5451
	Post 1 Hr	1273	1901	1041	2701	-367.3	3701	178	4601	414	5501
	Post 4 Hr	1898	1851	1026	2551		3401	296.8	4201		5201
LF64	Pre	1898	1851	1577	2651	-349.4	3551	372.2	4401	379.2	5451
	Post 1 Hr	1165	1851	1044	2601	-307.1	3451	98.2	4351	357	5351
	Post 4 Hr	1530	1801	1291	2551		3201	299.5	3951	202.9	5251

LF65	Pre	2191	1851	1810	2601	-474.7	3451	149.7	4351	520.3	5301
	Post 1 Hr	252.2	2101	335.8	2951		3701		4601		6401
	Post 4 Hr	699.9	2101	395	2901	-122.1	3851	124.2	4651		5851
LF66	Pre	1603	1851	1036	2651		3501	230	4301	478	5501
	Post 1 Hr	89.5	2501	218.6	3301						
	Post 4 Hr	96.03	2351	113.9	3151	-178.5	3851		4801		6351
LF67	Pre	2586	1851	1093	2601		3351	179	4401	493.2	5501
	Post 1 Hr	373.8	2101	465	2901	-191.5	3551		4601	118.8	5601
	Post 4 Hr	611.4	2101	405.8	2901	-320.1	3651	25.3	4851		5851
LF68	Pre	1184	1851	1221	2751	-705.3	3601	265.3	4501	398.8	5451
	Post 1 Hr		2151	512.1	2901	-389	3801	-260	4401	308.7	5301
	Post 4 Hr	407.4	1901	144.9	2701	49.4	4151	304.4	5001	115	6401
LF69	Pre	2427	1851	1780	2601	-441.1	3301	423.2	4201	487.7	5601
	Post 1 Hr	No Signal									
	Post 4 Hr	No Signal									
LF70*	Pre	2527	1851	1811	2701	-538.7	3451	382.5	4301	442.2	5651
	Post 1 Hr	No Signal									
	Post 4 Hr	No Signal									
Controls											
LF20	Pre	1214	1901	974.9	2751		3651	288.6	4751	441.1	5801
	Post 1 Hr	156.8	1751		2501	312	3301	217.6	4251	247.4	5551
	Post 4 Hr										
LF54	Pre	925.6	1951	940.8	2751		3801	335.3	4451	333.7	5401
	Post 1 Hr	1635	1851	938	2651	-572.9	3551	229.5	4451	370	5401
	Post 4 Hr	2000	1851	812.7	2651	-342.3	3101		4201		5451

*Likely eardrum rupture